DOCTOR OF PHILOSOPHY

Coastal zone processes in the St. Andrews Bay region, Scotland

Lyons, M.G.

Award date:
1999

Awarding institution:
University of Wales, Bangor

COASTAL ZONE PROCESSES IN THE ST. ANDREWS BAY REGION, SCOTLAND

by

M.G. LYONS

A thesis submitted to the School of Ocean Sciences of the University of Wales, Bangor
for the degree of Doctor of Philosophy
September 1996

SOAEFD Marine Laboratory, Aberdeen
PO Box 101
Victoria Road
Aberdeen
AB11 9DB

Abstract

An investigation is carried out into the hydrography and circulation of the St. Andrews Bay region, at the mouth of the Firth of Tay. The amount of freshwater retained within the Bay is found to vary on a seasonal basis, modulated by the wind. The strong south-westerly winds typical of winter act to enhance stratification within the Bay, limiting freshwater to a thin surface plume and encouraging export of water. During the summer winds are weaker and freshwater is retained within the Bay.

Seasonal variations in the barotropic circulation of the Bay area are identified. Sub-tidal variability in the circulation of the local area of the SNSCZ is found to be principally determined by the balance between the longshore component of the wind stress and the opposing longshore pressure gradient which is set up be the wind. Flow in shallower waters near to the shore is aligned with the longshore wind while in deeper waters offshore of the Bay an opposing flow is generated by the longshore pressure gradient. During winter the stronger winds act to dominate the flow regime even in deeper waters.

The long-term mean circulation is baroclinic and to the south, induced by cross-shore density gradients. An onshore near bed flow is a consistent feature of the circulation of the Bay. Baroclinic flows around the headland of Fifeness at the southern boundary of the Bay are in approximate geostrophic balance throughout the year.

Seasonal fluxes of freshwater due to the mean circulation through the faces of a box encompassing the Bay are calculated assuming a mass balance. The results suggest that the majority of freshwater entering the Bay during the winter months leaves as a surface plume. This does not appear to be the case during the summer.

Acknowledgements

I would like to thank my supervisors Dr. Bill Turrell and Dr. Phil Balls for their considerable support and advice during the course of this work. I would also like to thank my supervisor at UCNW, Bangor, Dr. Ed Hill. This project was funded by the Scottish Office Agriculture, Environment and Fisheries Division.

Thanks to the staff of the Marine Laboratory, Aberdeen for their invaluable contributions to this project. In particular Dick Adams, Phil Gillibrand, George Slesser, Rodney Payne and Eric Henderson. Thanks must also go to the crew of the FRV Clupea.

I must also thank my colleagues at Westlakes Scientific Consulting, my present place of employment, for cajoling me, by means of numerous "witty" comments over the past three years, into finally revising and submitting this version of this thesis.

I would also like to thank Dr. Jack Blanton of the Skidaway Institute of Oceanography, Savannah for inspirational conversations during a conference at Woods Hole Oceanographic Institution in 1994 from which I received a great deal of encouragement.

Above all, I would like to thank and dedicate this thesis to my wife Kate who has put up with a lot during the seven years this study has taken to reach completion yet still managed to encourage me every step of the way. Thanks for everything.

Contents

List of Tables

List of Figures

Chapter 1

1. Introduction

The coastal zone forms the interface between the marine environment and the land. In the broadest sense it can be defined as the region extending from the coastline, the heads of estuaries and the lower reaches of rivers affected by tidal action, to the continental slope at the margin between shelf seas and oceans. In this study a more restrictive definition is adopted. The coastal zone is taken to be the strip of water in the vicinity of the coast within which the dynamics of circulation and mixing are dominated by the influence of freshwater inputs of riverine origin, shallow water processes and the presence of the coastal boundary.

As the interface between the land and sea the coastal zone is the initial marine destination of a wide range of anthropogenic discharges resulting from industrial processes, agricultural activities and the production of sewage. The eventual destination of contaminants in the marine environment is due, largely, to circulation and mixing processes within the coastal zone which act to transport and dissipate water within and beyond coastal regions. Circulation and mixing processes within British coastal waters are dominated by the action of the tides which act to transport water back and forwards along the coast over a twice daily cycle. The residual transport of water, that over longer periods than tidal, is however, largely governed by other forces. Dominant among these forces is the action of the wind, both directly due to friction with the surface of the sea and indirectly due to the generation of sea-surface gradients. In areas influenced by freshwater runoff and stratification density gradients can also induce significant flows. The sub-tidal circulation patterns generated by these factors, which are revealed by the filtering out of the dominant tidal signal in a time-series of Eulerian current velocity, are the principal subject of this thesis.

The programme of work reported on in this thesis forms part of a larger study which was funded by the Scottish Office in order to assess the influence of seasonal variations in circulation and hydrodynamic parameters on fluxes of nutrient into and through the Scottish North Sea Coastal Zone (SNSCZ).

In order to determine which region of the coastal zone was most appropriate for the intensive study programme that formed the basis of the investigation of nutrient dynamics of which the work reported on in this thesis is a part, a preliminary desk study was undertaken. The aim of the desk study was to investigate the relative significance of riverine nutrient inputs to various regions of the SNSCZ with the aid of riverine discharge and nutrient concentration data obtained from the various Scottish River Purification Boards (RPBs). The results of the study have been published by Lyons *et al,* (1993). On the basis of the findings of the preliminary study, the St. Andrews Bay region, which receives the discharge of the River Tay after it passes through the Firth of Tay, was identified as the most appropriate site for the year-long observational programme which was carried out during 1993. The location of the study area in relation to the Scottish coastline can be seen in Figure 1.1.

The choice of the St. Andrews Bay area as the principal focus of the nutrient transport study provided a challenge as regards the assessment of the main driving factors behind the coastal hydrodynamics due to the complexity induced in the local circulatory regime by the runoff from the Firth of Tay. As the recipient of the discharge from the largest single source of freshwater to the SNSCZ it is to be expected that the circulation of St. Andrews Bay will be strongly influenced by the presence of freshwater on a variety of spatial and temporal scales.

Over a semi-diurnal period the area of the Bay directly influenced by the estuarine plume changes as the plume is advected to the north and south with the tide. Circulatory patterns directly associated with the plume, such as frontal jets generated at the plume edges, may therefore also be expected to vary rapidly. This study is, however, largely concerned with the circulation of the Bay area over longer, sub-tidal, timescales. At frequencies longer than semi-diurnal, changes in the residual circulation in the vicinity of the Bay are likely to be dominated by variations in discharge from the Firth of Tay and by variations in the intensity and direction of the wind field, which will influence both the behaviour of freshwater within the Bay and the barotropic circulation of the Bay and the surrounding region of the SNSCZ.

The role of the wind as a major driving force behind coastal circulation and mixing is well established. A significant body of work exists within the literature describing the dynamics of the wind-driven coastal zone circulation and its coupling with the baroclinic

circulation induced by the presence of freshwater. This work is reviewed in this thesis and a range of the analytical methodologies developed to describe the coastal residual circulation are applied in the current study.

Although many papers and books exist describing coastal circulation in general very little work has been done on the SNSCZ. Chapter 2 includes a comprehensive review of the existing literature dealing with the hydrography and circulation of this area. No detailed description has previously been given of the dynamics of residual circulation within the SNSCZ and the influence of the Tay, one of the largest British rivers, on the adjacent coastal zone has remained unknown until the current study.

The aim of this thesis is to identify the Eulerian circulatory regime of the area of the SNSCZ chosen for study and the pattern of seasonal variations in that regime. It is intended that the principal forces governing the regional circulation be identified. The objectives of the study are fivefold:

- To collect and prepare for analysis a dataset suitable for the analysis of seasonal variations in the circulation of the St. Andrews Bay area.
- To describe seasonal variations in the hydrography of the St. Andrews Bay area and to determine the role of the local wind field in modifying that hydrography.
- To determine spatial and temporal variability in the extent of the role of the wind in forcing the circulation of the SNSCZ in the vicinity of St. Andrews Bay over both sub-tidal and seasonal timescales.
- To determine the depth-averaged longshore momentum balance of the SNSCZ and to assess the significance of a range of forcing factors to that balance.
- To determine the role of freshwater in the modification of the circulation of the St. Andrews bay area over sub-tidal and seasonal timescales.

The design of an observational programme sufficient to provide the necessary information to describe adequately both the semi-diurnal variability and dynamics of a shallow estuarine plume as well as the seasonal variation in the dynamics of the larger scale coastal circulation is difficult. The study described in this thesis is principally concerned with the analysis of the sub-tidal and seasonal dynamics of the area. The approach taken was to design a moored instrument grid capable of providing regular Eulerian current velocity, pressure, salinity and temperature measurements over the period of a year. This was supported by a number of hydrographic cruises, the main aim of which was to service

the moorings. The dataset resulting from such an observational regime is well suited to the analysis of larger scale coastal dynamics, however, due to their highly dynamic nature and typically small scale relative to the surrounding coastal zone, river and estuarine plume dynamics are not well described by such methods. A detailed analysis of the dynamics of the plume of the Tay does not, therefore, form a part of this thesis and would require a specifically designed observational programme. Advances in the measurement of coastal currents using HR radar (*e.g.* Prandle, 1987) would suggest this to be an ideal methodology for such a study.

The thesis is organised as follows:

Chapter 2 reviews the published literature pertaining to coastal hydrography and circulation processes in regions influenced by freshwater runoff. The direct and indirect role of the wind in generating barotropic circulatory patterns is described as is the generation of baroclinic flows by density gradients. The development of coastal frontal zones and stratification is discussed. The existing literature describing the hydrographic and circulatory regimes of the SNSCZ is assessed.

Chapter 3 details the observational program carried out in St. Andrews Bay during 1993. The locations of the moorings and hydrographic stations are given and the dataset is described. The initial analysis methodology, by which the raw data was filtered and divided into common periods for further analysis, is outlined.

In Chapter 4 the results of the analysis of the hydrographic observations are presented. Seasonal cycles in temperature and salinity are described. Seasonal variations in the freshwater content of the Bay are identified and the role of the wind in the retention of freshwater within the Bay is discussed.

An analysis of the time series data set is carried out in Chapter 5. A brief description of the local tidal regime is given prior to a full analysis of the low-pass filtered sub-tidal current records. The records are subjected to statistical analysis using the Empirical Orthogonal Function (EOF) technique. Aspects of the sub-tidal circulatory regime are identified and discussed. The relative roles of the wind and longshore pressure gradient in driving the barotropic sub-tidal circulation are analysed.

The longshore barotropic circulation is further analysed by the calculation of the terms of the longshore momentum balance in Chapter 6. The spatial and temporal variation over the year and relative significance of each term at a given location is assessed. The principal driving forces behind the longshore sub-tidal circulation are identified.

Chapter 7 concentrates on the baroclinic circulation of the Bay, calculating geostrophic flows by application of the thermal wind equation. A model of the baroclinic depth-dependant flow due to the cross-shore density gradient is used to confirm the relationship between the long-term mean circulation and the density-driven flow estimated using regression analysis. The mean flow around the headland of Fifeness is identified as being in approximate geostrophic balance throughout much of the year.

Chapter 8 applies the findings of the previous chapters to the estimation of fluxes of seawater and freshwater through the Bay using a mass balance approach. Seasonal variations in fluxes are identified. Shortcomings in the initial assumptions of the flux estimation methodology are identified and discussed.

Chapter 9 presents a summary of the conclusions reached and suggests areas for further work.

Figure 1.1. Geographical location of St. Andrews Bay in relation to the coastline of Scotland.

Chapter 2

2. Literature Review

2.1 What Drives the Coastal Circulation ?

Coastal zone circulation can be divided into two component parts, the barotropic and baroclinic modes. The barotropic circulation is that driven by external forces while the baroclinic mode is generated by density variations within the water itself. A further division is also possible on the basis of frequency. Energy within the coastal zone can be divided into high and low frequency bands, the obvious dividing line being the tidal frequency. Sub-tidal variability in the current signal is dominated by water movements generated by the action of weather systems and by freshwater runoff. Coupling between the barotropic and baroclinic modes and the various frequencies of movement exists, affecting the inter-relationship between the circulatory aspects in a variety of ways, for instance although long-term transport of water masses and associated contaminants is mainly accomplished by the residual (sub-tidal) flow, mixing within the water column principally occurs on tidal time scales due to the increased energy in the system at tidal frequencies.

Although it dominates the circulation at the semi-diurnal frequency, the tidal signal is less important than that generated directly or indirectly by the wind on longer time scales. To that end this review of circulatory processes will concentrate on sub-tidal variability, dealing only briefly with the tidal circulation of the St. Andrews Bay area.

2.1.1 Tidal circulation

The dominant feature in the dynamics of the North Sea is the tidal motion, which provides the driving energy for many of the mixing processes at work in the North Sea. The tides also give rise to a basic residual circulation pattern that, when combined with circulation induced by the action of the wind and that forced by baroclinic effects due to stratification and freshwater buoyancy input, results in a regime that determines the distribution of water masses and the transport of properties within the North Sea.

The tidal motion of the North Sea is dominated by the semi-diurnal M_2 (lunar) harmonic. The North Sea system was described in an early paper by Proudman and Doodson (1924)

as a system of cyclonically propagating Kelvin waves with three amphidromic points situated at the southern tip of Norway, the eastern tip of the Dogger Bank and near the entrance to the Southern Bight of the North Sea. This description has been confirmed many times since, both by observation and modelling. Tidal motion along the east coast of Scotland is largely governed by the northernmost amphidrome centred off the Norwegian coast which manifests within the SNSCZ as a southward travelling wave along the coast. South of the Firth of Forth, near the English border, the influence of the northern amphidromy is joined by that of the Dogger Bank system.

Non-linearity and asymmetry in the tidal cycle gives rise to a residual current which is proportional to the square of the tidal amplitude and which is therefore largest in the shallower regions of the sea near the shore, since the amplitude of a Kelvin wave is inversely proportional to water column depth. This tidally induced residual circulation is generally directed southward within the SNSCZ, the local velocity of the tidal current depending on the topography of the area, but ranging between 1 and 10 cm s^{-1}.

Headlands such as Fifeness modify the tidal flow, resulting in amplification of the tidal current rounding the headland and a weakening of tidal velocities in adjoining bays with associated large local variations in current velocity in response to tidal variation. Off promontories the result can be seaward tidal streaming, generating offshore residual flows. Residual circulation patterns are affected by the presence of a headland as vorticity generated at the promontory is transferred to the mean circulation (Pingree *et al,* 1977).

Within the Firth of Tay and St. Andrews Bay the interaction between the out of phase estuarine and seaward tidal current systems together with the effects of the topography lead to an asymmetric ebb and flood flow and complex residual circulations which, within the Firth of Tay, are further complicated by the presence of the Abertay Sands at the entrance to the Firth (Charlton, 1980). The tidal circulation that results leads to a modification of the classical tidal flushing action which in turn leads to an increase in the estuarine residual flushing rate, enabling freshwater and contaminants to be discharged more rapidly. Using a hydraulic model Charlton (1980) estimated that 60% of the volume of the estuarine ebb flow within the Tay is exchanged with the sea each tide. The main flow of the ebb tide at the mouth of the Firth of Tay is via the main channel and initially moves in a north-easterly direction on leaving the mouth, but is deflected southward just before low tide by the start of the flood tide moving southward down the coast from

Arbroath (Charlton *et al.*, 1975). The main tidal streams seaward of the entrance of the Firth of Tay flow approximately transversely across the mouth of the Firth with maximum tidal currents occurring near high and low tide. At the mouth and within the outer Firth the tidal motion is a quasi standing wave with slack water occurring at high and low water (Admiralty Chart no. 190). The southward flowing flood tide off the entrance to the Firth of Tay was described by Charlton *et al.*, (1975) as giving rise to a large eddy within the northern part of St. Andrews Bay which spills over Abertay Sands into the main channel giving rise to a saline wedge which extends as far as the Tayport narrows.

2.1.2 The wind-driven circulation

Wind blowing over the surface of the sea exerts a tangential stress due to friction between the air and water surfaces. The stress in a given direction is represented by

$$\tau = \rho_a C_D W_i W \qquad 2.1$$

where ρ_a is the density of air, W is the (scalar) wind speed (usually measured 10m above the water surface) and W_i the relevant component of the wind velocity. The drag coefficient C_D is dependant on the height at which the wind is measured, the stability of the air above the sea surface and the roughness of the sea surface (Bowden, 1983). Various formulations appear in the literature designed to take into account such factors as variable surface roughness, however Broche and Forget (1992) state that formulations of wind stress that specifically allow for the influence of surface waves are unnecessary. The value used in the present study is 1.2×10^{-3} after the formulation by Large and Pond (1981) for wind speeds below 11 m s^{-1}.

The wind stress gives rise to two components of drift within the surface layers. The Stokes drift arises due to a net forward movement of water after the passage of a wave and is caused by non-linearities in the orbits of water particles. The Stokes drift due to wind-generated waves is a high frequency phenomenon and as such is not well resolved by Eulerian measuring instruments such as current meters unless the instuments are configured specifically for such rapid sampling. The present study is directed towards the Eulerian component of the circulation and neglects the component due to Stokes drift.

As well as the drift due to the oscillatory wave motion the wind stress drives a steady movement of surface water. This movement is communicated through the water column

by internal shear stresses, weakening and veering to the right with increasing depth due to the Ekman transport. In deep water, classical Ekman theory (Ekman, 1905) predicts the mean flux of water in the wind driven layer to be at right angles to the wind direction and the surface current direction to be at 45° to the right of the wind if the steady state is reached, which will take approximately 28 hours at the latitude of St. Andrews Bay (Bowden, 1983). Ekman's work was revised by Madsen (1977) who found the surface current direction to be somewhat smaller, of the order of 10°, in line with observations. Madsen also found current velocities to reduce more rapidly with depth than predicted by Ekman resulting in a mean flux at an angle to the wind of far less than 90°.

In shallow water the mean transport may be expected to be at an angle even less than the 10° predicted by Madsen due to the effects of bed friction. In stratified conditions the effects of bottom friction may be partially negated due to the pycnocline acting as a low friction boundary. This results in reduced vertical eddy viscosity and the limiting of the Ekman spiral to the mixed layer above the thermocline, thus leading to an increase in the speed of the wind-driven surface current (Bowden, 1983).

In the vicinity of a coastline topographic steering dominates, the frictional effects of shallow water on the wind driven flow leading to the development of a coastal strip within which wind-driven transport can be regarded as being parallel to the coast at all depths. Beyond this coastal strip, the width of which is defined by bathymetry and the velocity of the longshore component of the wind, cross-shore transport due to coastal up/downwelling will increase in importance (Csanady, 1982).

2.1.3 Coastal upwelling and cross-shore pressure gradients

In the northern hemisphere a longshore wind blowing with the coast to its left will tend to advect surface water away from the coast due to Ekman transport. To preserve continuity of flow an onshore return flow is generated in the deeper layers leading to upwelling of bottom water near the coast. In deeper, stratified waters a corresponding rise in isopycnal surfaces towards the coast accompanied by the surface outcropping of the pycnocline may be associated with this. The onshore component of the near-bed return flow will turn to the right to run parallel to the shore as the water column gets shallower due to the action of the Coriolis force induced by the Earth's rotation, adding to the shallow-water wind-driven longshore flow previously described (Csanady, 1982). This leads to the

development of a convergence zone close to the shore in which material may be trapped and carried downwind (Blanton and Atkinson, 1983).

The offshore flux of surface water leads to a lowering of sea level near the shore. As a result of the cross-shore slope thus produced a geostrophic flow will be generated throughout the water column near the coast in the direction of the wind. For winds blowing with the coast on the right, favouring downwelling, the flow will be again in the direction of the wind (Blanton, 1991). This simple conceptual model assumes a level sea bed. For the more realistic case of a sloping bed Pingree and Griffiths (1980) stated that the increasing water depth offshore causes the pressure gradients set up in the shallower water by the wind to be of limited offshore extent. This results in the establishment of a return flow in the opposite direction to the coastal geostrophic flow in deeper water offshore.

Within the SNSCZ a wind from the south-west quarter, which approximates to the average wind direction, particularly in winter, for the British Isles (Pingree and Griffiths, 1980), could therefore be expected to promote the movement of surface waters offshore, leading to upwelling along much of the Scottish north-east coast and an associated offshore flux of nutrients carried into the coastal zone by runoff. It is, however, rare that a steady wind field will hold for long over Scotland as the British climate is governed by the effects of the passage of a series of atmospheric low pressure zones for much of the year leading to rapid variations in wind speed and direction. We would therefore expect coastal current systems to be subject to wind-driven reversals and changes in intensity and direction, particularly in those areas where the baroclinic component of transport is weak as compared to the component due to windstress.

Blanton (1981) observed a southerly flow along the Georgian coast in the south-eastern United States, induced by runoff and the similarly directed prevailing wind. Further work (Blanton and Atkinson, 1983) looked at the effect of reversals in direction of longshore windstress in the same area. The consequence of such reversals on the "trapping" of freshwater and associated contaminants against the shore was a marked reduction in the efficiency of the trapping mechanism due to reversals in current direction. It seems likely that a similar regime may exist along the north-east coast, which, in common with the Georgian coast is relatively straight with bathymetry parallel to the shore and with a number of important river inputs spread along the coast.

2.1.4 Storm surges

Coastal effects due to wind can occur not only as a direct effect of the local wind field, but also as a result of storm surges, which are defined as disturbances of sea level relative to tidal variations produced by a meteorological cause. Surges may be internal or external with respect to the North Sea, both are caused by a combination of atmospheric pressure gradients and strong winds to varying degrees. External storm surges that propagate into the North Sea are a consequence of meteorological disturbances to the north-west of Britain. The external surge moves southward from this area and travels down the east coast of Britain at approximately the same speed as the tide, having the form of a Kelvin wave (Dooley, 1971) and moving with speed $\sqrt{gh}$. The duration of a surge may range from a few hours to several days. An example of an internal surge in 1953 was recorded by Heaps (1967). The surge led to serious flooding in eastern England and was caused by a deep depression which tracked from north-west of Scotland south-eastward into the North Sea bringing with it intense northerly winds which were the primary cause of the surge. In this case wind stress effects were an order of magnitude greater than effects due to atmospheric pressure.

2.1.5 Longshore pressure gradients

Hill and Simpson (1988) found longshore pressure gradients to be an essential part of the description of the longshore dynamics of the circulation of the western Scottish coastal zone. Variability in the coastal current was found to be largely explained by pumping due to the sympathetic action of the local wind stress and longshore pressure gradients set up by the integrated effect of the non-local wind field associated with the passage of depressions to the north of Scotland. Longshore pressure gradients generated by the local wind field, which acts against bottom friction to produce a gradient with a positive slope in the same direction as the wind and which results in a downslope flow in the opposing direction, have been measured in many areas. Wang (1979) determined a mean annual longshore gradient along the coastal boundary of the Mid-Atlantic Bight to be generated by the mean wind field while both Chase (1979) and Pettigrew (1980) studied variability in the pressure gradient records in greater detail, Pettigrew in particular highlighting the relationship between the longshore wind and pressure gradient. The mechanisms leading to the development of the longshore pressure gradient are discussed further in Section 2.2.1.3.

2.2 Analysis of Mean Circulation in the Coastal Zone

Flow, as observed in shallow seas using tools such as current meters, is an essentially chaotic phenomenon due to its turbulent nature, variable in time and complex in spatial structure. The principal cause of this variability is that one of the main motive forces of ocean circulation, the wind field, is itself random in character and varies widely in both speed and direction even over short periods of time. In contrast flow measured over long periods, particularly by Lagrangian methods such as drogues, shows a greater appearance of order. Within a given geographical area consistent long-term circulatory patterns can often be identified, with variations in the long-term pattern being modulated on a seasonal basis.

The main driving forces in shallow seas are the winds and the tides. In coastal areas the effect of the tides is magnified as the amplitude of the Kelvin wave is inversely proportional to water column depth. An additional significant driving force in coastal areas is the cross-shore density gradient generated by freshwater runoff to the coast. Coastal zone circulation can therefore be divided into two parts, the barotropic and baroclinic modes. The barotropic circulation is that driven by external forces such as the wind and tides while the baroclinic mode is generated by density variations within the water itself.

It is well established that flow patterns at tidal and sub-tidal frequencies can be accurately replicated by application of the equations of motion simplified according to the hydrostatic and Boussinesq approximations. Numerical models using non-linear formulations of the equations of motion are commonly used in the prediction of flow fields generated by the tides and wind, see for instance Pingree and Griffiths (1980), Davies (1980, 1982). A steady state solution of these equations is often taken to be representative of the long term mean circulation, however it is unlikely that seasonal variations in the complex coastal flow field, influenced as it is by both barotropic and baroclinic forcing on a wide range of spatial and temporal scales, are adequately represented by such approaches (Csanady, 1976).

Csanady (1976) showed that it was possible to separate the various forcing factors leading to the generation of shallow water flow patterns when looking at the circulation over time scales that were long when compared with weather and tidal cycles. This was possible

because the statistical effects of higher frequency flow episodes were able to be parameterised into relatively simple terms such as linear boundary friction laws. In addition, the finding that horizontal salt transport could be attributed to tidal and storm mixing alone, with little contribution from the mean flow allowed the density driven flow to be decoupled from the barotropic components of the flow. On the basis of these findings Csanady (1976) developed a conceptual model of shelf sea circulation that was successfully applied to the problem of the circulation of the Mid-Atlantic Bight, allowing identification and analysis of the principal forcing factors driving the mean circulation of the region.

The mean circulation of the Mid-Atlantic Bight was found by Csanady to be driven by four principal elements, namely the longshore and cross-shore components of the windstress, the longshore pressure gradient and the cross-shore density gradient. Decoupling of the linearised equation allowed the contribution of each element to the flow field be derived independently, the actual flow at a given location being given by a simple summation of the individual terms.

Kundu *et al.* (1975) showed that it was possible to decompose the subtidal coastal velocity field into distinct barotropic and baroclinic modes by consideration of the theoretical dynamical equations describing the motion and by use of Empirical Orthogonal Function (EOF) analysis. Although the two modes showed evidence of coupling to some degree, it was assumed that the modes were decoupled for the purposes of the analysis. The method proved to be successful, allowing identification by use of correlation and EOF approaches, of the major forcing factors leading to variability within the flow field. It was found almost all the variance (91%) of the subtidal flow field off the Oregon coast could be accounted for by barotropic variability, with only 7% being associated with the baroclinic mode. A similar approach was used by Allen and Smith (1981) in an analysis of barotropic flows off the coasts of Oregon, Peru and north-west Africa. Adoption of this approach simplifies the problem of the analysis of current variability within an area subject to significant variations in runoff such as St. Andrews Bay considerably, allowing the barotropic and density driven circulations to be treated independently.

2.2.1 The depth-integrated barotropic momentum balance

The relative importance of the various terms in the momentum equation to the dynamics of circulation within the Coastal zone is best achieved by focusing on the depth-integrated barotropic momentum balance, which, for the subtidal circulation can be represented by

$$\begin{aligned} \frac{\partial u}{\partial t} - fv &= -\frac{1}{\rho}\frac{\partial p}{\partial x} + \frac{\tau_{sx}}{\rho h} - \frac{\tau_{bx}}{\rho h} \\ \frac{\partial v}{\partial t} + fu &= -\frac{1}{\rho}\frac{\partial p}{\partial y} + \frac{\tau_{sy}}{\rho h} - \frac{\tau_{by}}{\rho h} \end{aligned} \qquad 2.2$$

(Csanady, 1982; Marmorino, 1982). This formulation of the momentum equation neglects non-linear terms as being small in relation to other terms, an assumption shown by Csanady (1975) to be reasonable except very close to the shore in situations where, for instance, tidal rectification may result in a preferred direction for "first-order" (tidal) flow leading to a significant horizontal momentum flux term.

The relative importance of each of the individual terms of the equation to the subtidal circulation of the coastal zone varies from area to area, principally with depth of water (Allen and Smith, 1981). In many cases the cross-shore windstress and bottom friction terms are assumed negligible in comparison to other terms (Huthnance, 1983).

2.2.1.1 The balance between wind and bottom stress

Along open straight coastlines, such as the north-east coast of Scotland from Kinnairds Head to the Firth of Tay, barotropic flows can be regarded as reacting to direct wind forcing in a relatively simple way. Hickey and Hamilton (1980) proposed the relation

$$\frac{\partial u}{\partial t} = \frac{\tau_x}{h} - \lambda u \qquad 2.3$$

where τ_x represents the component of windstress parallel to the coast, h represents water column depth, λ is an empirically determined constant and u is the depth averaged longshore flow. For a constant wind and depth the solution of this equation is a constant flow velocity of magnitude $\tau_x / \lambda h$. In terms of the longshore momentum balance this would result in a steady-state balance between the windstress and bottom stress (here

parameterised as linearly dependant on velocity) terms and assumes no longshore pressure gradient.

The predictions of the conceptual model of the mean circulation derived by Csanady (1976) were compared with observations in the coastal zone off Long Island in 32 m of water (Scott and Csanady, 1976). The mean circulation pattern over a period of a month was successfully predicted from the sum of its individual components which were derived using the measured wind velocities over the study period. If a steady state is assumed with the longshore pressure gradient and cross-shore density gradient terms expected to change at a slower rate than the wind stress terms such that they can be assumed to be constant over a period of a month, the balance of depth integrated longshore momentum can be written as

$$\tau_{wx} - \tau_{bx} = \rho g h \frac{\partial \zeta}{\partial x} \qquad 2.4$$

where the left side contains wind and bottom stress along x and the right hand side the surface elevation gradient, which is assumed constant. Coriolis force is neglected as the integrated onshore flow is negligible close to shore and hydrostatic balance is also assumed. Although bottom friction is quadratic with velocity, the averaged form of the drag law in shallow waters dominated by tidal currents can be regarded as being linear with the mean velocity, being proportional to the friction velocity (Bowden *et al.*, 1959; Csanady, 1976). Thus

$$\tau_{bx} = \rho r \overline{u}_b \qquad 2.5$$

where r is a resistance coefficient of the dimension of velocity. Substitution of this into Equation 2.4 results in a linear relationship between the wind stress and mean velocity terms. Insertion of mean values of current velocity corresponding to longshore wind stress meaned for various classes of speed and direction into the equation allowed Scott and Csanady (1976) to confirm the linear relation was true for the Long Island coastal zone. From the relation thus derived it was possible to calculate appropriate local values for r and to estimate the longshore surface elevation gradient.

The steady state balance between wind and bottom stress of Equation 2.3 has been successfully used by a number of workers to explain much of the variance of the depth-integrated flow within the coastal zone. Gmitrowicz and Brown (1993), for instance,

applied the model to a region of strong density currents off the coast of north-east England and Prandle (1987), who incorporated a time lag to optimise the response of the model. A steady state approach incorporating the pressure gradient was used by Heathershaw (1982) in the identification of cross-shore near-bed compensatory flows resulting from wind induced coastal set-up.

2.2.1.2 The role of the Coriolis term in coastal regions

If a depth integrated approach is adopted for the wind-driven coastal circulation, and a straight coast is assumed with equal forcing along its length, from continuity the assumption of no cross-shore flow follows. In such a case the Coriolis term in the longshore equation is likely to be unimportant in shallow waters near to the shore. Such an approach was found to be appropriate in the study of a shallow coastal embayment by Heathershaw (1982) who found the circulation to be dominated by the action of wind stress, in contrast Murray (1975) found the Coriolis term to be significant even within 1 km of the coast.

As the depth-averaged cross-shore velocity v is typically derived in practise by averaging velocity measurements collected at a limited number of depths, significant errors can be expected to be associated with estimates of the longshore Coriolis term fv in the momentum balance. The errors associated with the derived value may be far larger than the actual signal itself (Lentz and Winant, 1986). This can make balancing the momentum equation difficult as the erroneous Coriolis term derived from the cross-shore velocity may dominate the momentum equation. Many studies have found the Coriolis term to be significant in the longshore momentum balance, but poorly correlated with other terms, for instance Allen and Smith (1981) in an analysis of the circulation off Oregon, Huthnance (1983) in a study of sub-tidal motion on the western Scottish shelf and Amin (1988) in a study of the circulation of the coastal zone of north-east England.

2.2.1.3 The Arrested Topographic Wave model

If the sub-tidal coastal circulation is assumed to have reached a steady state the acceleration term can be neglected as being small relative to other terms. In this case the depth-integrated longshore momentum equation takes on the following form

$$-fv = -\frac{1}{\rho}\frac{\partial p}{\partial x} + \frac{\tau_{sx}}{\rho h} - \frac{\tau_{bx}}{\rho h} \qquad 2.6$$

This formulation, for a barotropic fluid with a linear relation between bottom stress and longshore velocity, leads to the "arrested topographic wave" solutions (Csanady, 1978a). The travelling wave associated with a storm surge is effectively trapped within a coastal boundary layer, propagating along the coast and decaying. The conceptual model proposed by Csanady showed that it was possible for the slope set up by a steady wind to be sustained within a coastal region.

The mechanism by which such a slope could be sustained is fully described by the two-dimensional form of Equation 2.6 which is solved using the equation of continuity. In two-dimensions with the longshore pressure gradient is associated a cross-isobath geostrophic flow. As the cross-shore flow increases or decreases depth vorticity is generated which is balanced by the curl of the bottom stress. Under a steady forcing from the wind a flow pattern is created which, in equilibrium, can be represented by a half-open parabolic circulation cell hundreds to thousands of kilometres long which is accompanied by a pressure field trapped within a nearshore band a few tens of kilometres wide, a "shelf circulation cell" (Csanady, 1981). The longshore component of the circulation can be represented by Equation 2.6, however the field is in fact two-dimensional. In very shallow water the flow velocity diminishes as the bottom friction term becomes dominant while far from the coast transport is shoreward.

The conceptual model as described above applies to coastlines subject to wind forcing along their length. The north-east coast of Scotland however changes direction at the Firth of Forth and the Moray Firth. A longshore wind from the south-west along the north-east coast is therefore not longshore for other portions of the coast. The longshore pressure gradient may therefore only be expected to develop along the north-east coast itself, decaying to the north and having no input from the south under a south-westerly wind. In such a case, according to the arrested topographic wave model, the pressure gradient is developed by a reduction in sea level to the south due to offshore Ekman transport or vice-versa for a longshore north-easterly wind stress (Csanady, 1981).

The two-dimensional shelf circulation cell model was applied by Marmorino (1982) to the problem of sea level response along the West Florida shelf using real bathymetry. The model overestimated sea level responses to the wind. However, this is to be expected as the steady state assumed by the model is unlikely to be reached in nature before the wind

changes in speed and/or direction. Confirming the calculations of Csanady (1981) the response of coastal sea level to longshore wind was far greater than to the cross-shore wind. One of the most important conclusions of the work was that coastal sea level response to the wind was highly localised, varying with bathymetry and coastal orientation. This finding was further investigated during an observational programme (Marmorino, 1983) with reference to the effect of small-scale variations in sea level response on the longshore sea surface slope. It was found that the correlation between the longshore pressure gradient and longshore wind was not simple for a real coastline. The opposing pressure gradient predicted by the model for a long, straight coast was indeed observable over larger scales of the order of 150-300 km, however the response on smaller scales was variable in magnitude, being effected strongly by coastal orientation and bathymetry. Work by Blanton *et al.* (1989) found longshore pressure gradients imposed by non-local forcing to be altered in magnitude close to the shore, or even reversed under the influence of local winds and freshwater influxes.

2.3 Baroclinic Circulation

2.3.1 The influence of freshwater on the circulation of the coastal zone

Rivers and estuaries discharging freshwater to the SNSCZ give rise to a zone of coastal water of lower salinity than the offshore North Sea water. Even in mid-winter the lower temperature of the runoff is unlikely to offset the density reduction due to the reduced salinity, particularly after partial mixing with seawater has occurred within the estuary, so the low salinity zone is characterised by low density. Conceptually, due to the action of the Coriolis force, the offshore flux of water forced by the density gradient will be deflected to the right (in the northern hemisphere) to give a vertically sheared longshore flow in geostrophic balance. However, in most cases the frictional forces due to bed and wind stress play an important, and in many cases dominant, role in coastal zone dynamics as described previously, thus a flow in full geostrophic equilibrium may not form. However, in the absence of cross-shore windstress approximate geostrophic balance may dominate the energy considerations of the longshore flow in regions of significant runoff, resulting in a quasi-geostrophic balance.

In many areas freshwater discharge is the main driving force of coastal currents due to the geostrophic component of the longshore flow. Baroclinic currents of this type are not

uncommon and much research into their dynamics has been undertaken. Major examples include the Norwegian coastal current (Heaps, 1980), the Alaskan coastal current (Royer, 1979) and the winter current along the Chinese coast into the Taiwan Strait forced by flow from the Changjiang (Yellow River) (Shaw, 1992). In less dramatic cases where the influence of freshwater is weaker, such as is the case in the SNSCZ, variability in the balance between wind and baroclinic forcing can lead to significant modification of coastal flows (Blanton, 1981).

An investigation of the dynamics of the Scottish Coastal Current, a persistent low salinity flow moving northward along the west coast of Scotland with its origins in the brackish outflow from the Irish Sea supplemented by runoff from the Scottish coast, was carried out by Simpson and Hill (1986). The current was studied over a full seasonal cycle and observations were used as input for a quasi-geostrophic model. The flow was found to be largely driven by buoyancy input and strongly steered by the bottom topography due to the shallow nature of the sea on the Scottish west coast and the erosion of vertical structure by tidal mixing, which leads to an increased influence of bed friction on the flow. Atmospheric depressions passing to the north of the British Isles were found to induce fluctuations in the flow due to the pumping effect produced by the combined local wind-stress and longshore sea level gradients set up by both local and remote wind fields. The passage of smaller, secondary depressions to the south was found to induce a weaker, southward pulse within the current.

2.3.2 The Thermal Wind equation

Density gradients within the coastal zone typically vary with depth as well as in the offshore direction. This is particularly true in the case of plume fronts. The estimation of baroclinic flows in the vicinity of a front cannot therefore be done in a depth-averaged manner if accuracy is to hoped for and the vertical dimension must be explicit in the calculations. For areas of the coastal zone where the water column is vertically well mixed, typically away from the immediate vicinity of fronts, a depth averaged approach may be appropriate.

If a front is assumed to be in geostrophic balance it is possible to calculate the vertical velocity shear by use of the thermal wind equation, which for the longshore flow is given by

$$\frac{\partial u}{\partial z} = \frac{g}{\rho_0 f}\frac{\partial \rho}{\partial y} \qquad 2.7$$

In deeper waters it is often assumed that the velocity at the bed is zero, thus allowing a direct calculation of velocities by means of this model. In coastal regions this is unlikely to be true. However, if the baroclinic flow represented by the geostrophic shear is assumed to be decoupled from the barotropic flow, and the barotropic flow is well approximated by the vertically averaged flow, than any vertical variation in velocity from bed to surface can be ascribed to the baroclinic flow and is additive to the barotropic component, assuming a baroclinically generated shear of zero at the bed. Such a method was used by Munchow and Garvine (1993a, 1993b) in the estimation of longshore buoyancy fluxes in the Delaware Coastal Current.

As the geostrophic velocity is driven by the cross-shore density gradient the maximum velocities will occur in the vicinity of frontal zones and these velocities are likely to be confined to a relatively narrow "frontal jet". Although rapid, such jets are unlikely to be of great importance to the transport of freshwater and nutrients on sub-tidal time scales within the SNSCZ as the fronts which generate them are associated with an estuarine plume which will be advected back and forth with the tide resulting in the movement of and creation of the plume fronts on a semi-diurnal basis. Indeed in practical terms such jets are difficult to detect using Eulerian methods as moored current meters give only limited information on frontal behaviour since advection of the front by the tide will move the frontal interface across or away from the mooring position. Likewise long term averaged velocity records blur out the fine details of frontal circulation. Lagrangian methods of measurement following the movement of drogues in relation to a co-ordinate system that moves with the front can provide useful information, but are obviously more complex to use than fixed-position moorings.

More important to the transport of materials within and through the coastal zone is the mean geostrophic flow, both longshore and cross-shore, which is driven by the long term mean density gradient across the entire coastal zone.

2.3.3 Estuarine circulation

Mixing of freshwater and seawater starts in estuaries before the coastal zone proper is reached. In the case of the Tay, river water mixes to some extent with water from the sea

within the estuary. Before reaching the coastal zone the estuarine outflow must then pass through the Firth, where further mixing will occur. The extent to which water reaching the St. Andrews Bay is already mixed with seawater is largely determined by the riverine discharge. During high discharge periods the estuary and Firth will be stratified due to freshwater overlying more saline water of marine origin. Vertical mixing is inhibited by stratification and a distinct estuarine plume will be the result.

The most fundamental estuarine characteristic is the gravitational circulation driven by the longitudinal density gradient. In highly stratified estuaries this circulation, consisting of a seaward flow of low salinity water in the upper layers compensated by a landward flow of higher salinity water below it, will dominate observed current structures. In well mixed or partially stratified estuaries it may appear only as a residual flow, masked by wind or tidally-driven currents. In most estuaries the landward, bottom volume flux is nearly as large as the seaward surface flux and both are many times greater than the freshwater inflow rate (Garvine, 1986). This classical circulation is modified by the bottom topography of the estuary; where there is a deep channel the saline inflow will tend be confined to it with the seaward flow often extending to the bottom on either side of it. Within wider estuaries or Firths the Coriolis effect results in a sloping of the isopycnals within an estuary, with the lower density surface water tending to form a deeper layer to the right of the direction of seaward flow.

Other components of estuarine circulation can include local wind forcing and Stokes drift associated with tidal movements. These aspects were initially assumed to be less important than gravitational flow, but were later recognised as often major components of the estuary/shelf water exchange (Uncles and Jordan, 1979). A comprehensive treatment of estuarine circulation was given by Officer (1976).

Within the coastal zone the residual exchange flow between estuaries and the adjacent sea areas is of major importance. The estuarine circulation described previously is not confined to the estuaries themselves but is also an important mechanism in coastal zone circulation. The bottom return flow which is an important feature of estuaries is also a feature of coastal circulation, being generated by the cross-shore coastal density gradient, which also generates an offshore flow in the upper part of the water column.

An example of the extent to which the apparently localised effects of estuarine circulation can affect the circulation of a large area of the adjacent shelf was given by Norcross and Stanley (1967) who observed that bottom drifters released 70 km seaward of the mouth of Chesapeake Bay were drawn consistently toward the bay. Pape and Garvine (1982) found a similar result off Delaware Bay with a shoreward drift occurring within the estuary while Bumpus (1965) observed a drift rate of 1 km day^{-1} landward of the 60m isobath in the Middle Atlantic Bight. Landward drift in the coastal zone was modelled by Beardsley and Hart (1978) who predicted landward bottom flow towards estuaries on a large scale in agreement with the cited observations. The near bed landward drift within the coastal zone is readily measurable in the majority of areas and is well documented in the literature (eg Heaps, 1972), being in many cases more stable and therefore more important to the mean circulation than the theoretical longshore flow associated with the cross-shore density gradient or the upper layer offshore flow. This may be because the longshore flow generated by a cross-shore density gradient diminishes with depth (Csanady, 1982), its maximum occurring near to the surface and there being subject to masking by the effects of the wind, as is the, generally weak, upper layer offshore flow.

2.3.4 Estuarine plumes

Upon reaching the coastal zone the low salinity water from a river or estuary may form a surface plume which is separated from the surrounding water by a sharp frontal zone. The plume associated with large stratified or salt-wedge estuaries can often be detected many kilometres from the shore, with horizontal spreading being driven by the pressure gradient that arises as a result of the density contrast between the low salinity surface layer and the denser seawater. Mixed estuaries may form only a weak plume or no plume at all depending upon the level of mixing that has taken place within the estuary prior to the seaward flow reaching the coastal zone. In the case of a nearly homogenous outflow, spreading is mainly due to horizontal turbulence (Bowden, 1983). A partially mixed estuary such as the Tay (Charlton *et al.*, 1975) with a low salinity outflow many times greater than the freshwater input to the head of the estuary often gives rise to a surface plume of reduced salinity water that can spread over a large area (Bowden, 1983). A study of the behaviour of the plume of the Tees estuary by Lewis (1984) found the plume to form a broad area of low salinity water out to the 20m contour, beyond which the movement of the brackish layer was alongshore, governed by the residual coastal flow regime.

On reaching the coastal zone the plume is acted upon by the Coriolis force which will turn it to the right to flow along the coast. The extent to which the plume is affected by the Coriolis force depends, however, upon how well developed stratification within the plume is. The degree of influence can be parameterised (Garvine, 1986) by the Kelvin number

$$K = 2l/r_i \qquad 2.8$$

where

$$r_i = \left(g' H_m\right)^{1/2} / f \qquad 2.9$$

is the internal Rossby radius, l is the width of the estuary mouth, H_m is the depth of the brackish layer at the mouth, f is the Coriolis parameter and g' is the reduced gravity in the surface plume given by $g' = g(\rho_2 - \rho_1)/\rho_1$ with ρ_2 and ρ_1 being the densities of the upper and lower layers respectively. For $K<<1$ the effect of the Coriolis force on the plume will be unimportant, for $K = 1$ Coriolis is significant, while for $K>>1$ the Coriolis acceleration is a dominant force and is likely to produce flow near geostrophic balance.

The relative importance of the Coriolis acceleration, even in cases where $K>>1$, can be strongly enhanced or diminished by the effect of wind stress on the plume. The wind may in fact be the dominant force in determining the destination of plume water after leaving the mouth of the river or estuary. Bowman and Iverson (1977) cited the case of the Hudson River, which is diffuse and meandering in low wind conditions but hugs the coast to either the north or south of the river mouth depending on wind direction, giving rise to a coastal current in conditions of high wind.

Estuarine plumes may have differing characteristics depending on the extent of stratification of the plume on reaching the coast and on water depth. Plumes which do not extend to the bottom can be regarded as being purely buoyancy driven (if the wind is disregarded) and bottom friction can be regarded as being negligible. Such plumes typically occur in deep water and are exemplified by many of the major coastal currents. In contrast plumes which are full depth are strongly influenced by friction which acts to widen the plume as it travels along the coast, bottom friction acting to diffuse relative vorticity (Woods and Beardsley, 1988). Many of the smaller coastal currents which form from estuarine plumes and discharge into shallow coastal waters with depths of the order of one Ekman depth, exhibit both these cases to differing degrees depending upon

distance from source, extent of the freshwater discharge at a given time and wind direction. Examples of such currents are the Scottish Coastal Current (Simpson and Hill, 1986) and the Delaware Coastal Current (Munchow and Garvine, 1993a, 1993b). The Delaware coastal current was identified as having two dynamically distinct regions within it, which can be designated the plume and current regions. The plume region is characterised by distinct fronts and a current with a scale less than the internal Rossby radius. The current region has reduced lateral density gradients and a current wider than the Rossby radius. In both regions the flow was in near geostrophic balance with non-linear advection being significant only close to the mouth of the estuary where the plume turns anticyclonically.

2.4 Stratification, Frontal Zones and Mixing Processes

Stratification within the coastal zone results from coastal inputs of freshwater and from solar heating during summer. Near to the shore thermal stratification is broken down by vertical mixing, principally by the tides, resulting in a coastal strip of well mixed water which may be bounded at its seaward limit by a tidal mixing front. In areas influenced by freshwater runoff such as the St. Andrews Bay area buoyancy fronts may be formed at the boundaries between the two different water masses.

2.4.1 Tidal mixing fronts

Fronts of this type form in shallow shelf seas with strong tidal currents and sloping seabed. Many areas fitting this description are found in British waters and so tidal mixing fronts are an important feature of summer stratification around the British Isles (Pingree and Griffiths, 1978).

Tidal mixing fronts form as a consequence of turbulence generated by the motion of tidal currents over bottom topography. The intensity of tidal currents themselves being a function of the modifying effect of local topography and the shape of the sea basin on the general tidally forced motion of the waters. The turbulence generated by bottom shear acting on a tidal current will mix the water column to a distance above the sea bed largely dependent on the strength of the current. In shallow enough water this mixing may reach to the surface, but in deeper water the same energy input from the tidal current may not be sufficient to break down the pycnocline due to dissipation of the energy with increasing height above the sea bed.

The transition zone between stratified and vertically mixed regions is usually narrow and is generally referred to as a "tidal mixing front", the position of which can often be predicted approximately by application of the Simpson-Hunter criterion, h/u^3 (Simpson and Hunter, 1974), which relates the depth of the water column, h, and the amplitude of the tidal current u. Higher values of the parameter coincide with well stratified areas in summer months, while low values indicate areas that are vertically well-mixed throughout the year, the transition value being dependant on the heat input and other terms included in the full tidal mixing equation.

The tidal mixing front usually takes the form of a diverging pycnocline with the upper section curving to the surface and the lower part to the sea bed. Dooley (1971) recorded the formation of a such a front 10 km seaward of the north-east coast during August 1969 in approximately 50m of water. Between the front and the shore the water was observed to be homogenous with the temperature gradient across the front being noted to exceed 3°C. It was observed that the front was not a permanent feature during the period of stratification, but was subject to destruction by strong winds.

2.4.2 Buoyancy fronts

Buoyancy fronts occur at the boundary between two water masses of differing densities, the density contrast being due principally to salinity differences. The term includes estuarine and plume fronts (Garvine and Monk, 1974; Bowman and Iverson, 1977) as well as larger scale fronts that may form parallel to the coast due to runoff into inshore waters. Fronts of this type may extend from surface to bottom, often in an S-shaped curve due to the less dense water tending to flow seaward over the denser watermass, or may curve down to a horizontal pycnocline depending on the size and density of the watermasses and the bottom topography (Csanady, 1971).

The shallowness of plume fronts will free them from the influence of bottom topography, as long as stirring is weak and the water column deep enough to dissipate the turbulent mixing energy spreading upwards from the bottom. In contrast, estuarine fronts on reaching the coastal zone, may outcrop at both surface and seabed due to the extent of vertical mixing that has taken place both within the estuary and on reaching the coast. Mixing in plume fronts is considered to be due to downward entrainment of surface water (Garvine, 1974).

Garvine (1986) in observations of the Connecticut River plume found that fronts with very high horizontal gradients formed on the offshore boundary toward which tidal currents, running normal to the river mouth, were impinging as the plume was deflected with ebb and flood tides. Craig (1959) reported that the southern edge of the Tay plume can on occasion be defined to within about one metre when the ebb tide is running.

2.4.3 Thermohaline fronts

During the summer coastal fronts arising due to tidal mixing at the edge of the summer thermocline can be reinforced by buoyancy due to freshwater runoff. This leads to the formation of a thermohaline front which is more stable than the sum of its parts, due to enhancement of the density gradient. Such a frontal zone has been described off Islay on the west coast of Scotland by Hill and Simpson (1989). The Islay Front is a composite formed by the interaction of the buoyancy front which forms the offshore edge of the Scottish Coastal Current (Simpson and Hill, 1986) and a thermal front that develops in spring and summer and marks the boundary between mixed and stratified regimes. The relative locations of the two fronts change with the season. In winter only the buoyancy front is present but in summer the two interact giving rise to vertical haline stratification. Runoff in winter is typically colder than the seawater it flows into, thus offsetting to a greater or lesser extent the density difference between the two water masses. This results in a less stable frontal zone than would arise due to summer runoff (Mooers *et al.*, 1977).

Simpson and co-workers have developed the theory describing the location of tidal mixing fronts to include the effects of the wind and buoyancy inputs on the establishment and breakdown of stratification in Regions of Freshwater Influence (ROFIs), looking in detail at the variation in stratification on tidal time scales (Simpson *et al.*, 1990, 1991, 1993).

2.4.4 Mixing processes

Within the coastal zone the principal causes of mixing relate to the stirring effects generated by tidal stress on the sea bed and wind stress on the surface. Mixing downward from the sea surface is induced by friction between the wind and the sea surface. Kinetic energy is transferred from the wind to the upper layer of the sea by the creation of surface currents and surface waves. This energy is dissipated via the downward transfer of momentum which acts to induce turbulent mixing. In shallow water this energy may

reach the sea bed and mix the entire water column. In stratified regimes the upper layers are often mixed to the pycnocline by windstress.

Because of the shallow depth of most of the SNSCZ, in most areas the entire water column will fall within the upper, wind-mixed, boundary layer. Mixing processes and circulation within the coastal zone are therefore heavily influenced by the wind. The wind stress on the surface induces turbulence within the upper layers due to shear instabilities within the wind-driven current, which gives rise to diffusion. Wind-driven currents also advect water masses, promoting mixing on a larger scale. The role of waves in mixing shallow coastal waters is significant, although less important than that of wind shear, particularly in exposed stretches of coastline (Grant and Madsen, 1979).

In the lower levels of the water column tidal currents play a similar role to the wind, inducing turbulence due to bottom shear. Depending on bathymetry, the amplitude of the tidal current, the water depth and the degree of stratification in the water column this turbulence may mix only a section of the water column or reach to mix the entire column.

Kinetic energy inputs to coastal zones occur at a higher frequency than those to areas of the open ocean, largely due to the increased tidal energy, but also to the fact that weather systems input energy on a more rapid time scale in coastal areas as opposed to oceanic areas (Blanton, 1991) due to the more rapid response of the shallow waters.

2.5 Storage and Transport of Freshwater Within the Coastal Zone

On reaching the coastal zone freshwater and contaminants are typically retained near to the coast. Transport through and within the coastal zone is subject to advection with the barotropic and baroclinic flow fields and to diffusion. Comparison of advective and diffusive fluxes for the transport of salt within the coastal zone by Blanton, (1986) showed advection to be a more significant process than tidal diffusion.

An analysis of 8 years of salinity and wind data from a region of the inner shelf off the south-eastern United States (Blanton and Atkinson, 1983) was carried out with the aim of assessing the role of the wind in the transport and storage of freshwater within the coastal zone. It was discovered that for low wind speeds loss of freshwater was independent of the wind, however for winds which were both more sustained and strong there was a

correlation between upwelling favourable longshore winds and loss of freshwater from the coastal zone, low salinity surface water being transported offshore by Ekman transport while higher salinity water was transported shoreward near the sea bed.

Analysis of frontal zone response to the longshore wind (Blanton, 1986) found differing adjustment in the inclination of the coastal front to result from opposing wind directions. Under the influence of upwelling favourable winds the front shallowed, low salinity surface water moving outward and reducing the slope. In the case of an opposing wind the front steepened to vertical and freshwater was retained within the coastal zone. Diffusion of freshwater across the front was found to be significantly lower when the front was steep. Application of a numerical model (Blanton *et al.,* 1989) predicted offshore transport of low salinity water during times of upwelling favourable wind stress to be dominated by the advection of lenses of mixed water seaward, providing an efficient method for the export of nearshore water out of the coastal zone.

Lensing can also occur as a result of eddy shedding from fronts. Within the shallow coastal zone frictional forces and bottom stress often prove to be dominant over the Coriolis force, thus altering the balance of forces along the front away from a fully geostrophic situation. This can result in a limiting of the speed and extent of along-front jets and to the generation of eddies, which then control the exchange of materials and energy across the boundary. Eddy shedding from fronts can carry parcels of water and nutrients from one water mass into another. Eddies are therefore important factors in the mixing process.

Use of a steady state analytical model and numerical modelling of the transport of low density coastal zone water by Blanton *et al.,* (1994) confirmed previous findings and highlighted the role of coastal orientation and bathymetry and its relation to wind direction in the loss of freshwater. Variations in the transport of freshwater were largely governed by the wind strength and direction due to direct forcing by wind stress, currents set up by pressure gradients and alterations in the frontal slope due to wind direction.

2.6 Hydrography of the SNSCZ

A large body of work exists in the literature describing the hydrographic and circulatory characteristics of the North Sea as a whole, however observations of the SNSCZ are

scarce. The earliest comprehensive description of the basic characteristics of the Scottish coastal zone was a compilation of early observations collected by the Marine Laboratory, Aberdeen (Craig, 1959) and described tidal and residual circulation and watermasses. In more recent years some attention has been paid to the coastal currents and water structure of the west of Scotland by, for instance, Simpson and Hill, (1986). Work in the area by the Marine Laboratory, Aberdeen (Dooley, 1974a; Turrell and Henderson, 1990; Turrell *et al.*, 1990; Turrell, 1992) has largely focused on the dynamics of Atlantic inflows to the North Sea in offshore waters or on nutrient dynamics in estuaries (*e.g.* Balls, 1992) with only the occasional venture into intermediate coastal zone waters (Dooley, 1971, 1974b, Turrell and Slesser, 1992). To date no review of work on this body of water other than that of Craig has been published.

2.6.1 Basic characteristics of SNSCZ water

The hydrographic characteristics of the SNSCZ in relation to the North Sea as a whole were first described by Laevastu, (1963). The North Sea was divided into a number of geographical regions and their characteristics described based on a review of data available at the time. Lee (1980) updated this description on the basis of later studies. The Scottish Coastal Water region was regarded by Laevastu as extending from east of Orkney down the coast as far south as Flamborough Head, a classification due mainly to the division between rivers flowing to the coast originating in highlands in the north as opposed to the southern lowlands. The region is described as being relatively narrow and occupied by a generally southward residual flow of coastal water of salinity 34-35 which mixes with water of Atlantic origin offshore via the mechanism of localised gyres. Summer surface temperatures reach 12-14 °C and the mean annual temperature range is 7 °C. The coastal water is described as being generally homohaline due to intensive mixing by strong tidal currents except in regions directly affected by runoff but with seasonally occurring vertical salinity gradients offshore, bottom water tending to be more saline than surface.

Monthly mean hydrographic parameters based on data collected by the Marine Laboratory, Aberdeen (Turrell and Slesser, 1992) for a number of regions of the SNSCZ and other areas of the shelf seas around Scotland confirmed the basic salinity and temperature ranges given by Laevastu (1963) for water away from the direct influence of a major freshwater source.

On the basis of multiple observations at stations along a line stretching from the northernmost end of the north-east coast of Scotland north-eastward towards Norway (the EC line) Turrell (1992) produced a hydrographic cross-section of the northern North Sea. A number of distinct watermasses were apparent, including Scottish coastal water, the Fair Isle Current and East Shetland Atlantic Inflow to the east of the coastal zone. Turrell determined that Atlantic water entering the North Sea did not form a current along the Scottish coast, but instead was largely confined to a small number of distinct offshore watermasses.

2.6.2 Thermohaline stratification within the SNSCZ

Average freshwater runoff to the SNSCZ in winter is approximately three times the summer value (Lyons *et al.,* 1993) and as such a much higher degree of haline stratification may be expected in winter than in summer, particularly in areas of high freshwater influence such as St. Andrews Bay. This is out of phase with the incidence of thermal stratification in the summer months which was found by Dooley (1971) to occur off the north-east coast only during summer. The persistence of cold bottom water offshore during summer stratification results in a strong cross-shore near-bed temperature gradient (Dooley, 1983).

Mean inshore salinities in the SNSCZ are slightly higher in summer than in winter (Turrell and Slesser, 1992) due to generally lower levels of runoff, however in the outer coastal zone surface salinities tend to decline a small amount in summer due to the outward spread of diluted water being less inhibited by vertical mixing. Bowden (1950) related salinity levels in the Celtic Sea to the effects of runoff, precipitation and evaporation and showed quantitatively that a summer minimum in salinity was related to decreased evaporation rates over the sea at that time. This being due to the dependence of evaporation on wind speed and sea-air temperature differences, both of which are reduced in summer months. Dooley (1974a) compared Bowden's figures for the Celtic Sea with salinity fluctuations in the North Sea and showed a similar result.

Turrell (1992) stated that the reduction in inshore and offshore salinity levels in North Sea waters in winter is approximately equal but each occur by different mechanisms. Runoff and precipitation increases account for the inshore reduction whilst vertical mixing induced by autumnal gales leads to offshore near-bottom water freshening. A winter decrease in the onshore/offshore density difference is due, therefore to the cooling of

coastal waters rather than a variation in the level of salinity decrease. In Winter the cooling of coastal water decreases the temperature difference between inshore and offshore water to the extent that salinity becomes the controlling factor in the inshore/offshore density gradient.

2.7 Observations of the Residual Circulation of the SNSCZ

Early attempts to deduce the residual current pattern of the North Sea of necessity took a Lagrangian approach, using drift bottles and seabed drifters (*eg.* Fulton, 1897). Observations of salinity distributions made prior to the First World War allowed Bohnecke (1922) to deduce the basic seasonal circulation pattern of the North Sea. Drift bottle studies by Tait (1930a, 1930b, 1931, 1937) in the northern and central North Sea confirmed the basic circulatory pattern and led him to deduce the existence of an anticyclonic eddy system off the Scottish north-east coast centred off Montrose and stretching from Aberdeen down to the mouth of the Tay. The early drift bottle methods used to arrive at this conclusion, the bottles not having drogues or sea anchors, have serious limitations, being highly susceptible to the action of wind on the surface layer and the bottle itself, and also to transport by surface waves (Lee, 1970).

Craig (1959), again using Lagrangian techniques, described a consistent south-westward flow along the north-east coast and explained the eddies postulated by Tait as being an experimental artefact caused by alternating periods of onshore and offshore wind. Dooley (1971) determined that residual flow along the north-east coast is due for the most part to meteorological factors, being associated with either the direct action of the local wind field or to travelling disturbances such as storm surges. He also demonstrated the complexity of coastal wind effects, showing that off the north-east coast the current close inshore is directly affected by wind, but further offshore external forces drive the flow. Depending on which forces are dominant, inshore and offshore currents may be opposed or aligned, leading to the formation of strong horizontal shears between inshore and offshore waters.

Circulation within the coastal zone in the Tay/Forth region can be expected to be significantly modified by the runoff from the Tay, however there is little information in the published literature to verify this. Craig (1959) reported that on a calm day turbid water originating with the Tay estuary can extend six to eight kilometres from the shore in a well defined stream. Low salinity water attributed to the Tay has often been recorded

within the outer Firth of Forth near the north shore after rounding Fifeness. Dooley and Payne (1978) stated that the residual circulation of the Firth of Forth is weak and the main driving mechanism is the wind. The main outflow of low salinity water within the Firth of Forth is usually present at the surface close to the southern shore (Craig, 1959; Dooley and Payne, 1978), making it distinct from water whose origin is the Tay.

2.8 Summary

An attempt has been made in this brief review to indicate the dominant forces behind the movement of water in the coastal zone and the Scottish coastal zone in particular. On the sub-tidal time scales with which this thesis is concerned the circulation may be regarded as consisting of two principal modes: the barotropic, driven mainly by the tides, wind and atmospheric pressure fields, and the baroclinic, resulting from the presence of significant quantities of low salinity water in the coastal zone. In the vicinity of an estuarine plume, such as that of the Tay, the background barotropic circulation will be modified significantly by the presence of low salinity water on a number of spatial and temporal scales.

This thesis describes the results of the analysis of a significant dataset collected off the mouth of the Tay estuary and attempts to describe the residual circulation of St. Andrews Bay in terms of the models of coastal circulation reviewed in this chapter.

Chapter 3

3. The Observational Programme

3.1 Mooring Deployments

During 1993 the Marine Laboratory, Aberdeen deployed current meter moorings within St. Andrews Bay at six sites (M1- M6) on a year-long basis. Geographical locations of the moorings and instrument depths are given in Table 3.1 and locations displayed in Figure 3.1.

A typical mooring configuration is illustrated in Figure 3.2. Each mooring carried two conventional Aandaraa RCM 7 or RCM 4 current meters at a depth of 7-9 m (relative to mean low water spring (mlws) tides) and at a height of 6-7 m above the sea-bed; the exception was M2, the shallowest site, which was fitted with one conventional meter at a depth of 9 m and with an electromagnetic S4 RCM at a depth of 2 m. Each RCM was capable of recording current speed, direction and water temperature for the duration of the deployment while the instruments at a depth of 7-9 m also supplied time-series of salinity. Moorings M1 and M6 carried bottom-mounted Aandaraa water level recorders for the entire study period, while these were added to M2 and M4 in September. M6 was also fitted with a 20 m thermistor chain; unfortunately the chain suffered a fault during the early part of the study leading to the loss of 5 of the 12 channels. The data from the functioning channels was unaffected however, so it was decided to leave the chain in situ.

3.2 Hydrographic Surveys

In addition to the mooring array a series of eight hydrographic surveys were carried out throughout the year along the grid (sections I, J, K and M) shown in Figure 3.1. Profiles of temperature and salinity were recorded at each station using an NBIS Smart CTD. Sea-water samples were collected at selected depths using a pressure triggered rotary sampler and used for calibration of the CTD.

3.3 Primary analysis of moored instrument data

Moored instruments were serviced during the survey cruises at intervals of approximately two months, cruise dates being 7-12 January, 6-10 February, 9-12 March, 1-4 April, 8-13 May, 2-7 July, 10-13 September, 20-25 October and 10-15 December. Due to the logistical problems associated with the servicing of a large mooring array it was not

possible to turn over all the instruments during each cruise. The staggered servicing of the moorings, along with data losses due to instrument malfunction and damage, resulted in a large set of time series which ran concurrently and without interruption only during relatively short periods for a given number of mooring locations. To reduce the difficulties in correlation analysis produced by these staggered records, records obtained from the various instrument deployments were combined to produce longer simultaneous time series where possible. To achieve this it was necessary in a small number of cases to interpolate missing values to cover gaps between deployments; this was done using the unfiltered records to minimise any errors that could occur during this process. In most cases it was necessary to interpolate between 1 and 4 hours of values, however in one case the addition of 17 hours was needed; given the time-scale of variations in the low-frequency sub-tidal flow (upon which attention was focused), lack of apparent sudden changes on either side of the gap and the smoothing effect of filtering an addition of this length was deemed acceptable. Gaps of longer than a day were felt to be too long for interpolation and so the precise length of the time series obtained after sub-division of the long records into approximately two-month periods was largely governed by these breaks.

After addition of the records so as to maximise the length of the available data, the time series, which were recorded at a sampling interval of either 15 or 30 minutes, were low-pass filtered followed by subdivision into common periods of standardised length. The numerical low-pass filter used to remove the effects of diurnal and higher frequency currents is described in Godin (1967) and has 36 weights with a half power point of 72 h (~0.3 cpd). Current velocity records were resolved along local longshore axes derived from consideration of sea-bed contours and mean principal directions of the periodised records, the positive longshore axis was taken to be southward (Table 3.1). The filtered time series thus obtained (periods 1 to 7) form the basic data set of this study. Period lengths are given in Table 3.2. Table 3.3 records which time periods exist for a given mooring position.

3.4 Ancillary data

Hourly wind and atmospheric pressure data recorded at Leuchars, 1km inland of St. Andrews Bay, were supplied by the Met. Office while records from coastal tide gauge stations at Wick, Aberdeen and Leith were supplied by the British Oceanographic Data Centre. Total sea bed pressure (p) at tide gauge stations was computed by addition of atmospheric pressure (p_a) as measured at Leuchars to the pressure due to the water column

calculated using the hydrostatic relation $p = p_a + \rho g \zeta$ where ρ is the average density of seawater, g represents the acceleration due to gravity and ζ is the sea level as recorded by the gauge. For the purposes of the present study absolute values of sea bed pressure were not of interest, so all records had the mean extracted.

Due to the large spatial scale of atmospheric pressure variations the use of atmospheric pressure at Leuchars for the calculation of total pressures at Leith and Aberdeen (40 and 80 km from Leuchars respectively) is acceptable. The adjusted record for Wick cannot be expected to be fully reliable as it lies 360 km from Leuchars, although this distance is still small by the scale of the dominant cyclonic weather systems (~ 2000 km). This record was used only for purposes of comparison within the analysis. Wind and total pressure data were low-pass filtered and divided into period lengths as given in Table 3.2.

3.5 Correlation coefficients

Correlation coefficients are presented throughout according to the method of Sciremmano (1979) after normalisation of the raw correlations by the large-lag standard error, a method which conveys more information than raw correlations by compensating for the interplay of the dominant time scales and length of long time series. Significance levels using this method are 2.6 (99%), 2.0 (95%) and 1.7 (90%).

3.6 Summary

Chapter 3 has presented a description of the observational programme followed during the course of this work. Details have also been presented of the basic analysis performed on the dataset prior to the more detailed analysis described in the remainder of this thesis. The following chapters present the results of this analysis and conclude with a description of the sub-tidal circulation of the St. Andrews Bay area.

Table 3.1. Mooring positions and depths of current meters and water level recorders at mlws. W indicates water level recorder.

Mooring	Position	Local longshore direction (°)	Water depth (m)	Instrument depth (m)
M1	56°31.0'N, 2°31.0'W	225	31	9, 24, 31 (W)
M2	56°22.0'N, 2°38.0'W	170	17	2, 9, 17 (W)
M3	56°22.0'N, 2°30.0'W	180	33	7, 26
M4	56°22.0'N, 2°18.0'W	210	52	9, 46, 52 (W)
M5	56°16.5'N, 2°33.3'W	195	28	7, 21
M6	56°16.3'N, 2°24.0'W	190	52	9, 46, 52 (W)

Table 3.2. Common period lengths of low pass filtered records used in the study.

Period	Start time (h, d, m)	End time (h, d, m)	Length (h)	Length (d)
P1	3, 10, 1	0, 8, 2	694	28.9
P2	1, 8, 2	8, 27, 3	1136	47.3
P3	20, 3, 4	0, 8, 5	821	34.2
P4	0, 10, 5	11, 27, 6	1164	48.5
P5	23, 5, 7	22, 9, 9	1584	66.0
P6	22, 13, 9	21, 18, 10	840	35.0
P7	3, 24, 10	23, 8, 12	1101	45.9

Table 3.3. Low pass filtered time series used in this study. Records available for each period.

Instrument	P1	P2	P3	P4	P5	P6	P7
$M1_1$	C T S	C T S	C T S	C T S	C T S	C T S	C T S
$M1_2$	C T	C T	C^1 T^1	C T	C T	C T	C T
$M1_W$	P T	P T	P T	P T	P T	P T	P T
$M2_1$	-	-	C T	C,T	-	-	-
$M2_2$	C T S	C T S	C T S	C T S	C T S	C T S	C T S
$M2_W$	-	-	-	-	-	P T	P T
$M3_1$	C^2 T^2 S	S	-	-	-	C T S	C T S
$M3_2$	-	-	C T	C T	-	C T	C T
$M4_1$	-	C T S	C T S	-	C T S	C T S	C T S
$M4_2$	-	C T	C T	C T	C T	C T	C T
$M4_W$	-	-	-	-	-	P T	P T
$M5_1$	C T S	C T S	C T S	C T S	C^3 T^3 S^3	-	C T S
$M5_2$	C T	C T	C T	C T	-	-	C T
$M6_1$	-	C T S	C T S	C T S	C T S	C T S	C T S
$M6_2$	-	C T	C T	C T	C T	C T	C T
$M6_W$	-	P T	P T	P T	P T	P T	P T

Instrument order with increasing depth at a given mooring indicated by a subscript, ie. $M3_2$ indicates mooring position 3, lower RCM. A subscript W indicates a sea bed water level recorder.
Record types: C velocity, T temperature, S salinity, P pressure.
Records with a superscript appended were curtailed before the standard period end and finish as follows:
1: 0,21,4 (414 hours); 2: 13,27,1 (420 hours); 3: 1,28,7 (532 hours).

Figure 3.1. Geographical locations of the moorings M1-M6 as deployed in St. Andrews Bay during 1993 (●). The locations of hydrographic stations along lines I, J, K and M are represented by triangles.

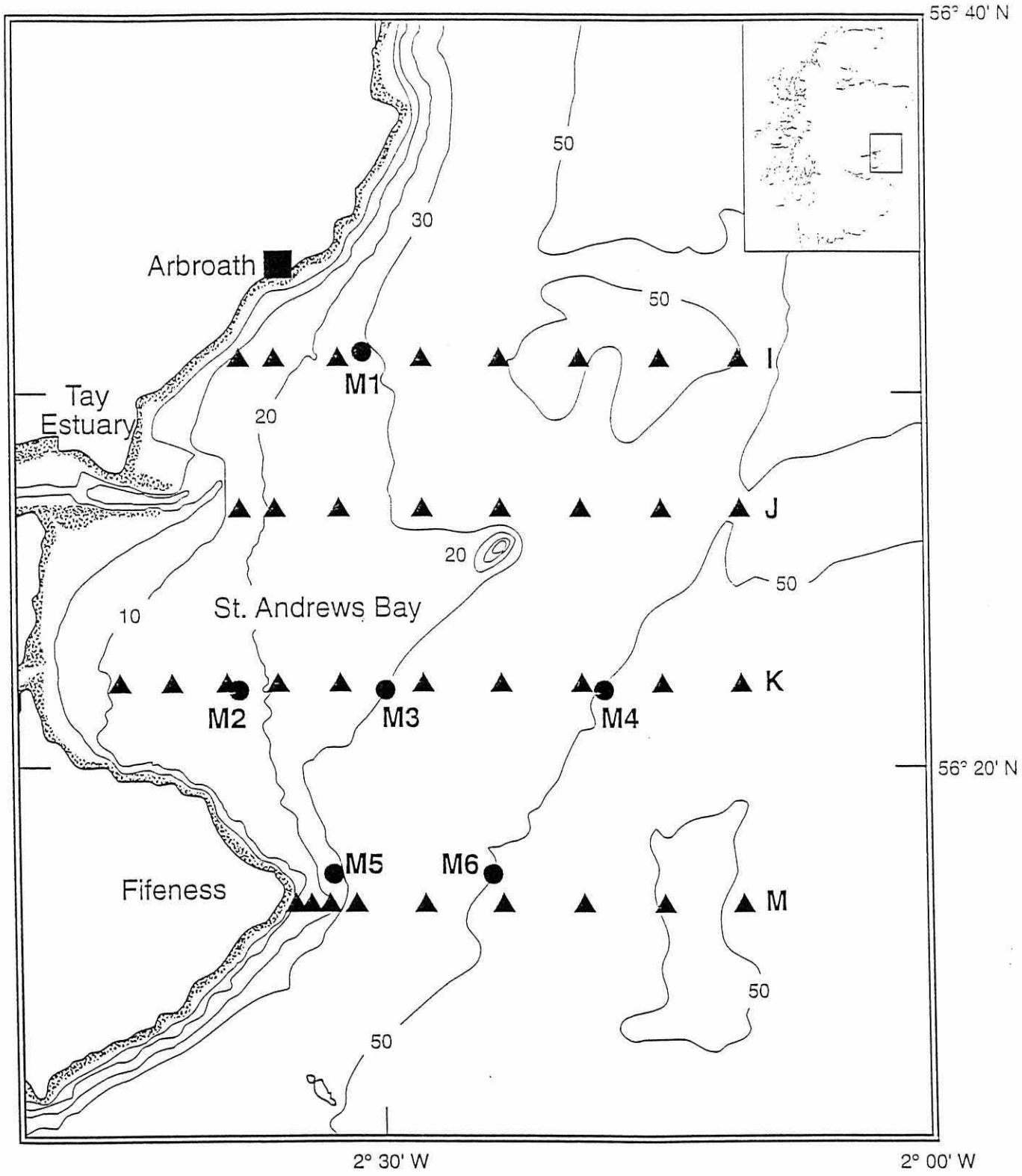

Figure 3.2. Configuration of U-mooring as used in St. Andrews Bay during 1993.

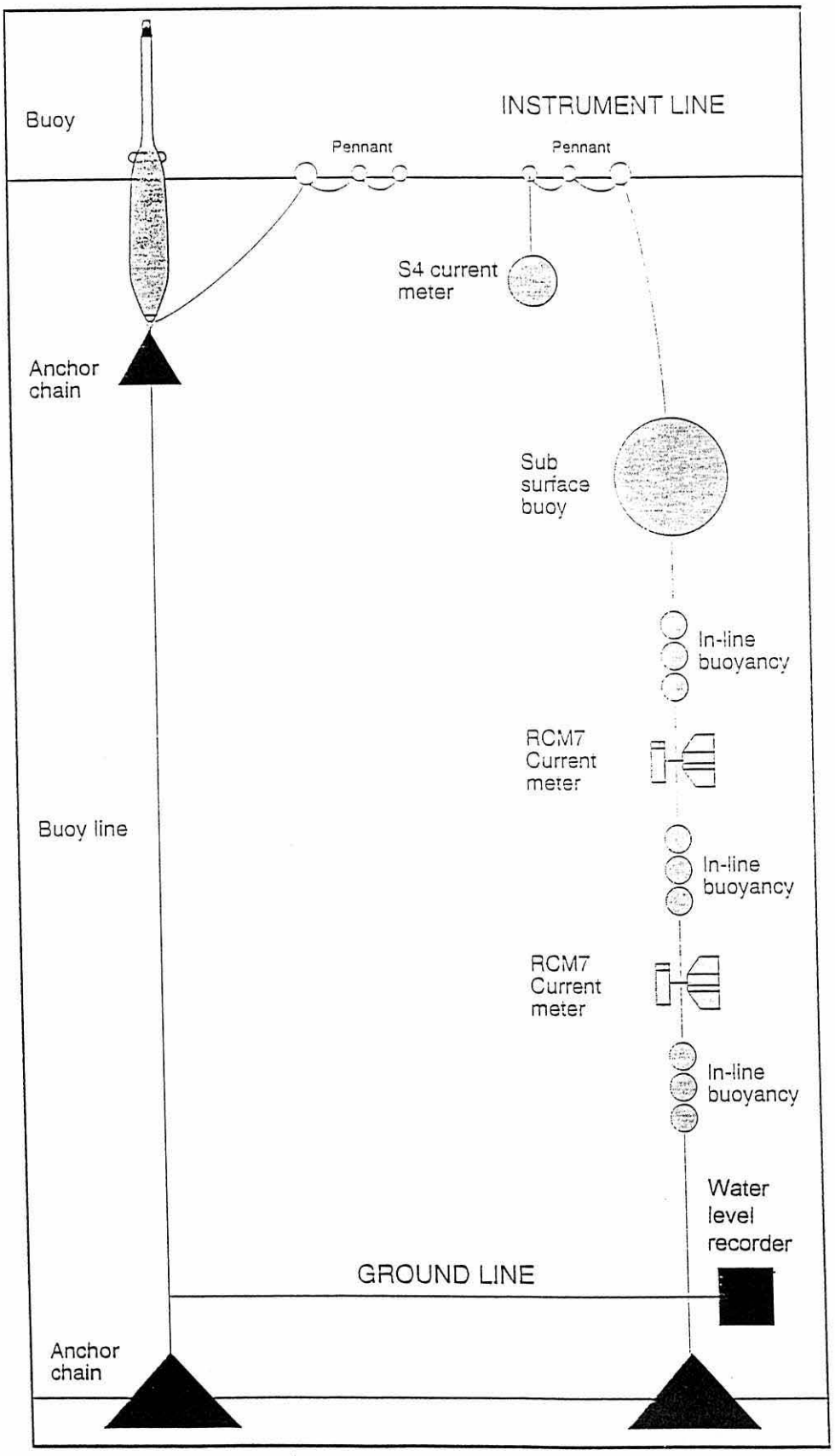

Chapter 4

4. Hydrographic Observations

4.1 The Relationship Between Temperature and Salinity

T-S diagrams for CTD profiles performed during February, March, May, September and October 1993 along lines I, J, K and M are presented in Figure 4.1. The main water mass within the Bay consisted of water of salinity 34 - 34.5. Water within the Bay of salinity lower than 34.0 has its origins within the Firth of Tay as is apparent from the May and September data, when the Firth was also sampled along an extension to line J. It is apparent that mixing of Tay with St. Andrews Bay water followed an approximately linear relation throughout the year. The temperature of both water masses varied seasonally, with the Bay water reaching a minimum in March. Estuarine water can be seen to have warmed at a greater rate than Bay water as summer approached, resulting in an increased slope in the T-S relation, while the inverse was true as winter approached. Vertical thermal stratification within the Bay was apparent during September, with water of salinity 34.3 showing temperature differences of 2 °C. It appears from the September T-S relation that freshwater mixed within the Firth with water drawn from the warmer upper layers of the Bay rather than from the deeper, sub-thermocline waters.

The contrasting distribution of points in the T-S diagrams for September and October suggests that thermal stratification within the Bay largely broke down during the intervening month with the temperature of the reduced salinity water within the Bay dropping sharply.

4.2 The Seasonal Warming and Cooling Cycle

Temperature data was collected throughout the year at M6 using a thermistor chain and supplemented by data from thermistors on the current meters and water level recorder at this location. Figure 4.2 illustrates the variation in the vertical structure of the water column at M6 during 1993. In early March (period 2) the water column was well mixed, with temperatures at the annual minimum value of 5.5 °C (Figure 4.2a). During the spring and summer months temperatures rose, with maxima of 12 °C at 9m and 11.5 °C near the bed (46m) being measured in mid September (period 6) (Figure 4.2b).

The warming of the water column as a whole was gradual, but stepwise increases were also observed. The low-pass filtered record for the RCM and water level recorder mounted thermistors at M6 during period 3 (Figure 4.3a) shows such an increase associated with a mixing event which followed a period of early stratification. This, the first instance of thermal stratification in the vicinity of M6, occurred towards the end of April and was associated with an influx of low salinity water from the Tay (Figure 4.3b). Stepwise increases in surface temperature were typically associated with an influx of freshwater throughout the rising part of the thermal cycle with the inverse being true towards the end of the year (period 7), when water with its origins in the Tay was cooler than the Bay water (Figures 4.4a, 4.4b) and weak inverse thermal stratification events were occasionally observed. This association between the haline and thermal stratification cycles was also typical of the rest of the Bay, being more or less pronounced depending upon the concentration of freshwater within a given area. The final breakdown of the summer thermal stratification in the area of M6 was observed at the start of October (Figure 4.2b).

4.3 Haline Stratification

The haline stratification regime within the Bay and at its northern and southern boundaries was highly variable in detail, being dependant upon distribution of water from the Tay under a variety of wind and runoff conditions. Regionally, however, a number of features could be recognised as consistent throughout the year.

The northern boundary: Section I

Section I, off Arbroath to the north of the mouth of the Firth of Tay, showed little evidence of vertical haline stratification at any time of the year. Figure 4.5, illustrating sectional data collected on the 7th of February, is typical of both the summer and winter situation at this location. Fresher water (<34.3) was evident in this case close to the coast as a small surface feature. Given the strong southerly winds (see for instance Figure 4.17) and high runoff of the previous weeks (Figure 4.10) this lack of a significant quantity of freshwater suggests that water from the Tay is not typically lost from St. Andrews Bay to the north.

The southern boundary: Section M

In contrast section M, the inshore end of which lay approximately 2-3 times as far south of the mouth of the Tay as section I was north of it, typically showed a considerably reduced salinity across the section, with vertical stratification often in evidence. During February (Figure 4.6) salinities were reduced across the entire section at all depths due to the high runoff from the Tay, with a halocline apparent at a depth of approximately 25 m. This suggests that, notwithstanding the prevailing southerly winds of the period, freshwater left St. Andrews Bay primarily to the south after considerable vertical mixing with sea-water. The offshore extent of the reduced salinity water and presence of a halocline indicate that freshwater was also being transported seaward, principally in the upper layers.

Data collected during the March cruise are presented in Figure 4.7 and show the principal features of the distribution of salinity across section M throughout the year. A weak plume was typically observed at approximately 8 km from the shore in 50 m of water. Shoreward of and beneath the plume the water column was typically well mixed due to turbulence associated with the strong currents generated by the presence of the headland of Fifeness. Offshore of the salinity minimum, low salinity water tended to extend further seaward but was restricted to the upper 15 m of the water column due to reduced mixing within the deeper water. The seaward extent of reduced salinity water was less than that observed during the February cruise. This was found to be the usual case throughout the rest of the year, suggesting that offshore transport of freshwater is not likely to be significant during periods that do not feature a high southerly wind and/or high runoff.

The central Bay: Sections J and K

The hydrography of the main Bay area, between the mouth of the Firth and Fifeness, was dominated by thermohaline gradients associated with the Tay plume. The exact offshore extent and depth of the plume varied between cruises. A halocline was typically apparent in the plume region at a depth of approximately 15m, however the steepness of the vertical gradient was highly variable. Table 4.1 presents gradients at the position of vertical gradient maximum for the plume (calculated from Section K data), which was typically found to approximate the 20m sea-bed contour. Stratification within the plume was at its strongest during the February cruise, being almost an order of magnitude greater than during the summer cruises. Indeed during February the plume was highly distinct, with no haline stratification detected seaward of its bounds (Figure 4.8).

Contour plots of surface salinity for the February and July cruises are presented in Figure 4.9. Due to the time taken to cover the hydrographic sampling grid (up to 3 days in poor weather) data for each plot was gathered over a number of semi-diurnal tidal cycles and so is not representative of a "snapshot" of the plume. The figures do however give an indication of the seasonal range of the plume and the associated distribution of reduced-salinity seawater.

4.4 The Effect of the Coriolis Acceleration On the Plume

Calculation of the Kelvin number, K (Equation 2.8), allows an estimation to be made of the extent to which the rotation of the earth acts upon an estuarine or river plume to turn it to flow along the coast (Garvine, 1986). Calculation of K requires knowledge of the depth of the plume at the mouth of the firth as it enters the sea. Such data were only available from the May and September cruises.

Data from the cruise of the 11-12th May gave σ_t values of 21 and 25 at the surface and bottom layers of the water column respectively at the mouth of the firth, resulting in a value for the reduced gravity, g' of 0.039 m s^{-2}. The depth of the plume at the mouth was approximately 10m while the width of the mouth is 4 km, resulting in a Rossby radius of deformation of the order of 5 km and a Kelvin number of 1.6. This suggests that the influence of Coriolis force will act to turn the plume to the south under most circumstances. Runoff at the time of the May cruise was lower than that during winter (Figure 4.10). Data describing the plume depth and vertical density stratification during the high runoff periods of winter are not available, however an estimate of the possible effect of high riverine discharges may still be made. If it is assumed that the plume depth and density of the bottom layer remain the same, but the density of the top layer is reduced to a σ_t value of 15, a K of approximately 1 results. This scenario suggests that the steering effect of the Earth's rotation is reduced when the plume is enhanced by large runoff events. If the depth of the plume were to be increased by the runoff exiting the estuary the value of K would further reduce.

4.5 Seasonal Variations in Freshwater Input

A plot of the time series of the daily mean freshwater discharge from the Tay estuary during 1993 (Figure 4.10) clearly shows the 'event based' nature of riverine freshwater discharge into the coastal zone. Peak daily mean discharges could be over 10 times the

annual mean value of 219 m^3s^{-1}, resulting in a large injection of freshwater into the coastal zone which dropped off on a time scale of 2-10 days. These large events could be expected to lead to considerable changes in the hydrography of St. Andrews Bay and nearby regions of the SNSCZ and possibly to significant changes in the pattern of circulation. An initial indication of the relative importance of the freshwater discharge over a given period (period durations appear in Table 3.2) can be gained by assessing the volume of freshwater reaching the Bay from the Firth of Tay. The values in Table 4.2 were obtained by integration of the time series of daily mean discharges. We see relatively small variation in the volume of water discharged into the Bay between periods ('Total Discharge') except during period 1, when 25% of the 1993 flux of freshwater from the Firth of Tay to the SNSCZ was discharged into St. Andrews Bay. If we take the period length into account and calculate mean discharge rates for each period we see this variation emphasised with the rate of discharge during period 1 an order of magnitude larger than that during period 5. From these calculations, on the basis of buoyancy input alone we could expect a considerably different hydrographic regime to be in place during the winter and summer months.

4.6 Variation in Freshwater Concentrations within St. Andrews Bay

Water of salinity less than 31.5 was only observed during the February cruise (Figure 4.9a). At this time the freshwater discharge of the Firth of Tay was of the order of 500 m^3s^{-1}, over five times as large as during any of the other cruises. During winter and spring the position of the 33.0 isohaline approximated to the 25m isobath across the mouth of the Bay, however during the July and September cruises when runoff to the Bay was below 100 m^3s^{-1} the 33.0 isoline was not apparent within the Bay. It is significant that, paradoxically, water with a salinity in excess of 34.5 was only detected within the region covered by the hydrographic grid during the February cruise. At this time freshwater input to the Bay was at a maximum and was on a gradual decline from the 1993 peak daily mean discharge of 2400 m^3s^{-1} which occurred two weeks previously (Figure 4.10).

The relative amount of freshwater (F_w) in the water column can be estimated from CTD data using

$$F_w = \frac{1}{h} \int_h^0 (S_0 - S) / S_0 \, dz \qquad 4.1$$

where h is depth, S is salinity, S_0 is a base salinity and z is the vertical co-ordinate, positive upward (Blanton *et al*, 1994). If the water column were vertically homogeneous and $S_0 = S$, then $F_W = 0$, *i.e.* there is no freshwater at that location relative to the background salinity. Conversely if $S \rightarrow 0$, then $F_W \rightarrow 1$, *i.e.* the water column consists wholly of fresh water. The vertically integrated formulation used here allows vertical haline stratification to be taken into account. The background salinity S_0 (at which $F_w = 0$) to which freshwater content is referenced was taken to be 34.7, the highest salinity detected throughout the year within the Bay. The freshwater fraction F_w was calculated for all repeats of transects I, J, K and M throughout the year (Figures 4.11-4.14 respectively). The position and strength of the front associated with the boundary between the estuarine plume and more saline offshore water is indicated by the maxima absolute values of dF_w / dy where y is the cross-shelf co-ordinate. This front is most apparent in section K (Figure 4.13) where it can be seen to typically occur at a distance of approximately 12 km from the shore, corresponding to a depth of 25 m. Section J (Figure 4.12) shows the front at a distance of 8 km, also corresponding to a depth of 25 m.

Further from the mouth of the Firth along sections M (Figure 4.14) and I (Figure 4.11) the concentration of freshwater near the coast was much reduced, often being hardly greater than that 20-30 km offshore. It appears that freshwater from the Tay is not held close to the shore as a discrete body beyond the bounds of St. Andrews Bay, being rapidly mixed with seawater with distance from the mouth of the Firth.

Comparisons between the freshwater fractions along sections sampled during February and May prove enlightening. Runoff conditions differed greatly between the two sampling periods, with freshwater discharge from the Tay being six times higher during the February cruise (Figure 4.10) and very high throughout the previous month. A study of Figures 4.11-4.14 however shows the freshwater fraction to be higher during May across all sections; this is particularly apparent in sections J and K. If we study section K alone for the two periods in question, comparing the variations in the freshwater fraction with the salinity difference between surface and bottom waters (Figure 4.15) we see that the water column during February was considerably stratified by the discharge from the Tay, particularly in the region of the plume, while during May the water column was largely vertically well mixed. Thus it seems that when the water within the Bay is vertically well mixed a greater proportion of the river discharge is retained close to shore, even when compared to periods during which far more freshwater enters the Bay as

runoff. In contrast freshwater appears to be efficiently transported away from the Bay in a surface plume during periods in which haline stratification is well established, to the extent that even during periods of very large river discharge little freshwater is found to be retained within the Bay.

4.7 The Flushing Time of St. Andrews Bay

The mixing of river water with seawater, initially occurring within the estuary and Firth and continuing within St. Andrews Bay, leads to an accumulation of freshwater within the Bay. The amount of freshwater retained within the Bay depends largely, as is suggested by consideration of the freshwater fractions, on runoff and wind conditions. The extent to which freshwater is retained within the Bay is of interest because freshwater acts as a tracer for nutrients which enter the Bay from the river water. A simple estimate of flushing time is calculated for freshwater present at the time of each survey.

The simplest estimate of flushing time is to assume that freshwater is removed from the Bay at the same rate as it is being added to by river discharge. This is a generalised method of estimation based on simple conservation of mass considerations and does not involve any assumptions about the freshwater removal process. The flushing time is given by

$$t_F = F/R \qquad 4.2$$

where R is the mean rate of influx of freshwater and F is the total volume of freshwater accumulated in the study area (Ketchum and Keen, 1955). To determine the total volume of freshwater F, the Bay was divided sectionally into strips of volume dV with a width corresponding to the distance between isobaths at 5 m gaps and a length determined by the distance between the I section off Arbroath and the M section off Fifeness. A mean freshwater fraction was calculated for each strip, the total freshwater volume thus being given by

$$F = \sum Fw\, dV \qquad 4.3$$

with the summation being carried out to the 35 m isobath, beyond which $dFw/dy \rightarrow 0$. Flushing times were calculated for each of the five cruise periods for which data were available across all four sections (Table 4.3).

These flushing times should not be regarded as indicative of a physically realistic time scale as the method assumes salinity is in a steady state in the Bay area. They do however provide useful evidence for comparisons between different events when considered along with the total volume of freshwater within the Bay. High runoff events such as occurred at the time of the February cruise (500 m^3s^{-1}) can be associated with low salinities within the Bay as a whole, the freshwater being confined to a thin, surface plume (Figure 4.9a) which, in association with the wind, acts to remove freshwater from the Bay at a rapid rate. This leads to a flushing time an order of magnitude faster (t_F = 3 days) than that calculated during low runoff events (for instance t_F = 50 during the May cruise when runoff was 80 m^3s^{-1}). This suggests that during the winter months the large flux of freshwater and associated contaminants, such as nutrients, reaching the Bay from the estuary may quickly be transported beyond the Bay itself to the south and east. During periods of low runoff however, mixing may be more likely to occur due to the lower level of stratification and wind, and so freshwater and nutrients of riverine origin are more likely to be held within the Bay.

4.8 The Role of the Wind in the Retention of Freshwater in St. Andrews Bay

During the February cruise the local wind blew from the south-west, an upwelling favourable direction in the case of the N.E. coast, with a speed of 5 ms^{-1}. During the May cruise the wind was oppositely directed with a speed of 6 ms^{-1}. If comparisons are made between the freshwater fraction and degree of haline stratification along section M for the February and May cruises (Figure 4.16) we see that during the earlier period low salinity water has been advected offshore in the upper part of the water column while during the May cruise stratification is only apparent within 10 km from the shore.

This result suggests that the orientation of the longshore component of the wind may play a significant part in the flushing of freshwater from St. Andrews Bay or the retention of such water and its associated nutrient load within the Bay. Time series of the freshwater fraction at M1, M2 and M5 based on salinity recorded at the upper RCMs at each site were averaged to give values representative of the entire Bay. Comparison of the time series obtained with the longshore component of the wind stress (Figure 4.17) suggests that southerly winds led to a flushing of the Bay while northerly or low wind periods led to retention. The role of the strong southerly winds of winter in flushing the Bay is emphasised by a regression of wind stress against mean F_W (Figure 4.18).

If the wind stress is compared to the difference in freshwater fraction between the northern site M1 and M5 off Fifeness (Figure 4.19) we see that only very rarely, during strong southerly winds, was there a greater amount of freshwater to the north of the mouth of the Firth. Comparison of Figures 4.19 and 4.10 shows that during the strong southerly winds of January/February a negative longshore F_w gradient was only apparent during the peak discharge event for the year. In this case we can conclude that transport of freshwater from the Bay during southerly wind events is not to the north of the Bay but offshore and in the surface layers of the water column (Figure 4.16).

The role of runoff from the Tay in determining freshwater concentrations within the Bay is complex. Obviously the Tay is the principal source of freshwater within the Bay but it appears that runoff peaks are not necessarily reflected in freshwater concentrations within the Bay due to flushing induced by the wind. Figure 4.20 compares time series of runoff and mean F_w for the Bay. It is obvious that the role of the wind is more significant than that of runoff on a seasonal scale. However, on time scales shorter than seasonal large runoff events do appear to give rise to freshwater concentration peaks above a general seasonal base level, with a lag of the order of 10-12 days. The relationship is, however, sporadic, the influence of the wind being dominant.

4.9 Discussion

It appears from the hydrographic data that variations in temperature and salinity within St. Andrews Bay on a time scale shorter than the seasonal are dominated by the freshwater discharge from the Tay. The exact relationship between discharge variations and temperature and salinity variations is not simple. Stratification over the winter months, being directly due to the presence of low salinity water, was found to be limited to the area of direct influence of the estuarine plume; the near-coast region. During the summer months, however, thermal stratification induced by solar heating acted with haline stratification to give a two-layer regime across much of the Bay. The reduction in runoff during the summer period results in insolation being the dominant contributor to thermohaline stratification within the Bay. The increasing stability of this stratification over the summer months is not only the result of the increasing effect of surface thermal heating. It is also due to the reduction in the incidence of strong winds and hence input of mixing energy to the upper layers of the sea. The balance of forces governing the

seasonal mixing/stratification cycle has been comprehensively described in the work of Simpson (Simpson *et al.*, 1978, 1990, 1991, Simpson and Bowers, 1984).

It has been demonstrated that even during periods of strong southerly wind, freshwater typically left the Bay to the south into the outer Firth of Forth. The degree of offshore transport was related to the wind direction, with southerly winds encouraging seaward movement of freshwater in the upper layers of the water column leading to flushing of the Bay, while winds directed toward the south led to trapping of freshwater within the Bay and a deepening of the halocline, often to the extent of complete vertical homogeneity. The low winds of spring and summer were typically associated with an increase in the amount of freshwater retained within the Bay. During spring, when runoff was still high, flushing times reached a maximum and large amounts of freshwater were stored within the Bay. The freshwater concentration decreased during summer due to the lack of runoff, but did not reach the low levels detected during the strong southerly winds of February.

The relationship between wind direction and flushing of freshwater from a coastal zone has been modelled by Blanton *et al.*, (1989) using a 2-D (cross-shore/depth) time-dependant numerical model. They investigated the effect of local wind regimes on a coastal frontal zone generated by riverine discharge off Savannah. They found a steepening in the frontal zone and a corresponding increase in vertical homogeneity in response to downwelling favourable winds (in the case of the N.E. coast of Scotland, north-easterly) and an increase in stratification accompanied by offshore lensing of coastal water in the surface layers during upwelling favourable winds. Blanton's group studied transport of freshwater in a coastal current along a straight coastline where a large mean runoff from a number of sources was normal. In contrast the present study deals with a comparatively low discharge estuarine plume within a Bay. The same mechanisms appear, however to be in operation in both cases.

The role played by the wind in retaining freshwater within and dispersing it from St. Andrews Bay has significant implications for the fluxing of nutrients and other contaminants from the Bay. During the spring and summer months the high concentrations of freshwater within the Bay are likely to be associated with correspondingly high concentrations of nutrient if a conservative relation between nutrient and salinity is assumed. This is of course unrealistic during the spring and summer months, when primary production reaches a maximum. It does however imply that

production is more likely to be sustained by the introduction of fresh nutrients to the Bay. Likewise we can hypothesise that during winter high-runoff events, nutrients are likely to be exported from the Bay rapidly within the upper layers of the water column, particularly when under the influence of the southerly wind regime typical of that period.

Table 4.1 Maximum vertical salinity gradients across the halocline within the Tay plume calculated from section K data.

Cruise date	dS/dz (m^{-1})
7 Feb	0.180
10 Mar	0.040
11-12 May	0.025
4 July	0.035
12 Sept	0.030
23-24 Oct	0.130

Table 4.2. Mean discharge rate, volume of freshwater discharged during 1993 and volume discharged during each period as a percentage of the annual total.

Period	Period length (whole days)	Mean discharge rate m^3s^{-1}	Total discharge km^3	Percentage of annual total
P1	29	706	1.77	25.6
P2	48	150	0.623	9
P3	35	295	0.892	12.9
P4	49	148	0.628	9.1
P5	66	72	0.409	5.9
P6	35	199	0.603	8.7
P7	45	138	0.535	7.7
1993	365	219	6.915	100

Table 4.3. Total volume of freshwater, mean rate of influx and flushing times of St. Andrews Bay during the periods of the 1993 cruises

Cruise date	F (km^3)	R (m^3s^{-1})	t_F (days)
7 Feb	0.125	500	3
10 Mar	0.202	100	23
11-12 May	0.344	80	50
4 July	0.176	50	41
23-24 Oct	0.283	100	33

Figure 4.1 The relationship between temperature and salinity throughout the Firth of Tay and St. Andrews Bay during 1993. Data from CTD profiles performed along lines I, J, K and M.

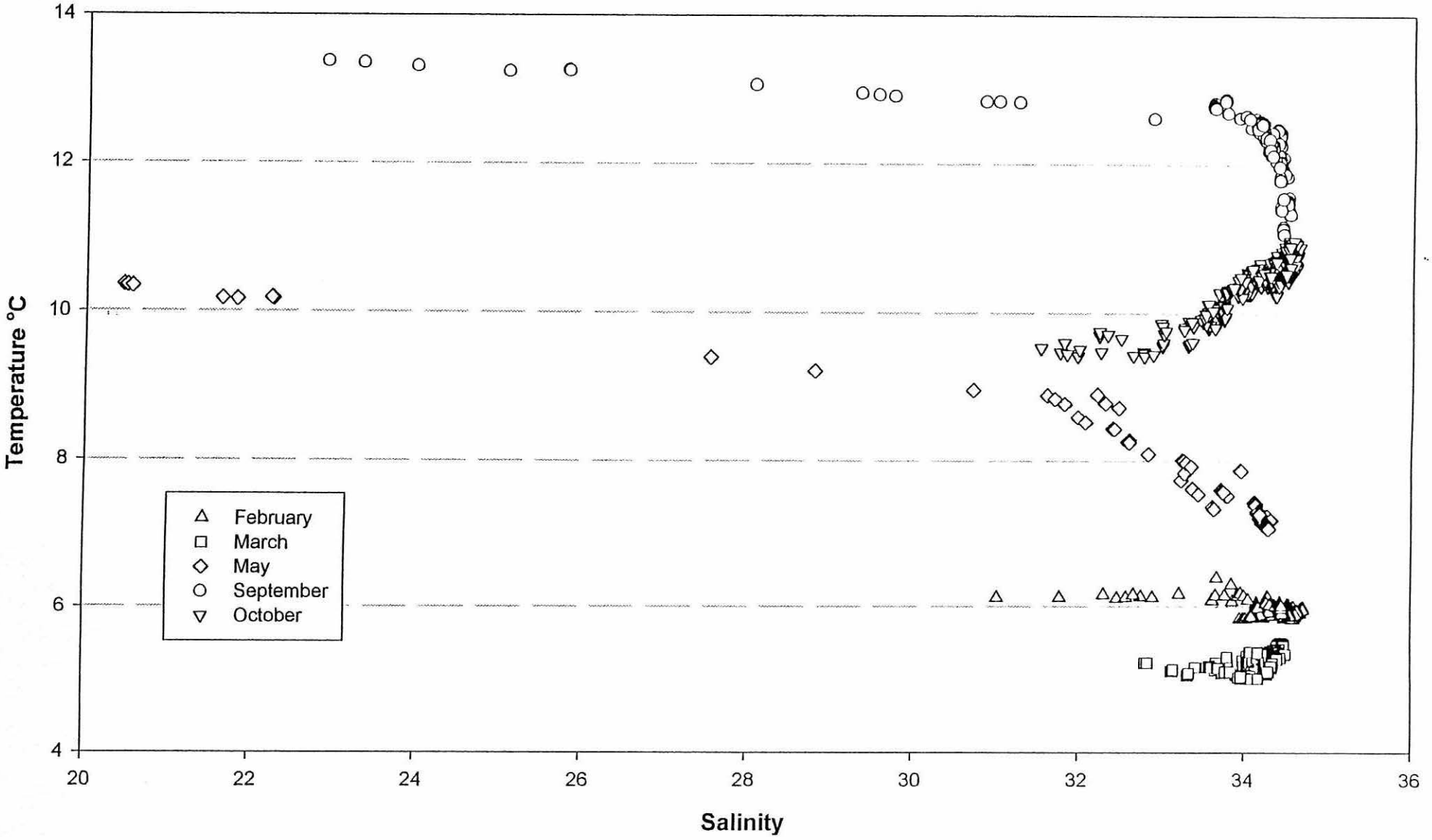

Figure 4.2 Vertical thermal stratification as measured at M6 using a thermistor chain. Each individual plot corresponds to each of the common periods 2-7.

Figure 4.2a Period 2.

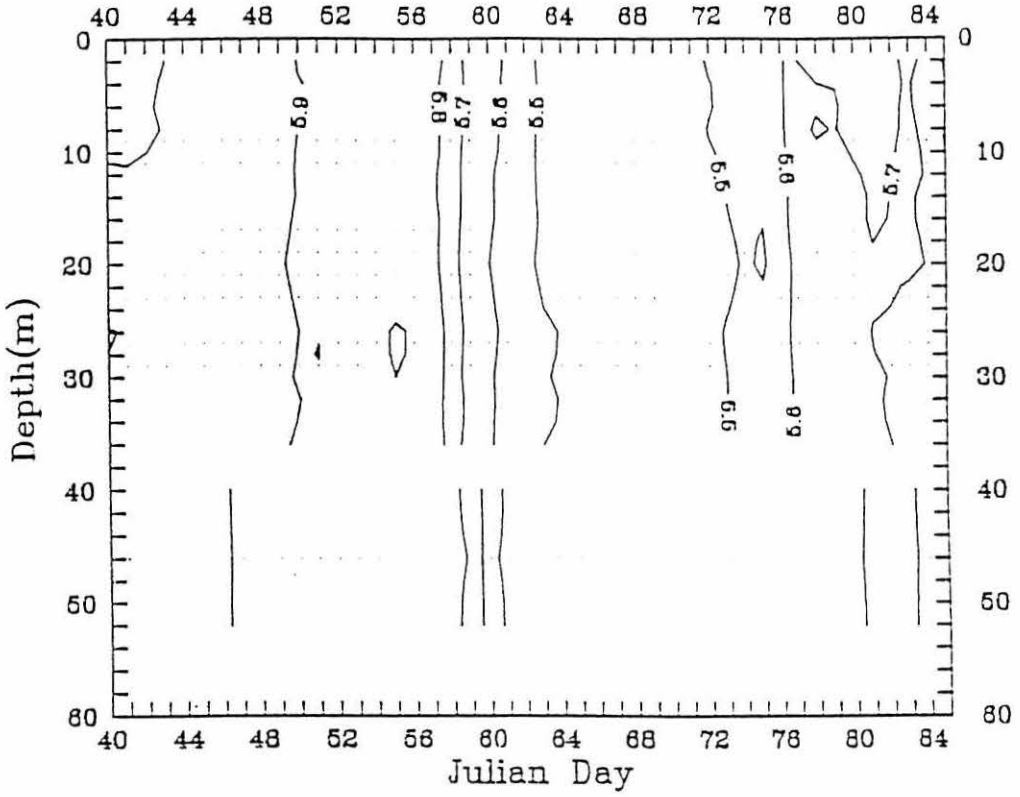

Figure 4.2b Period 6.

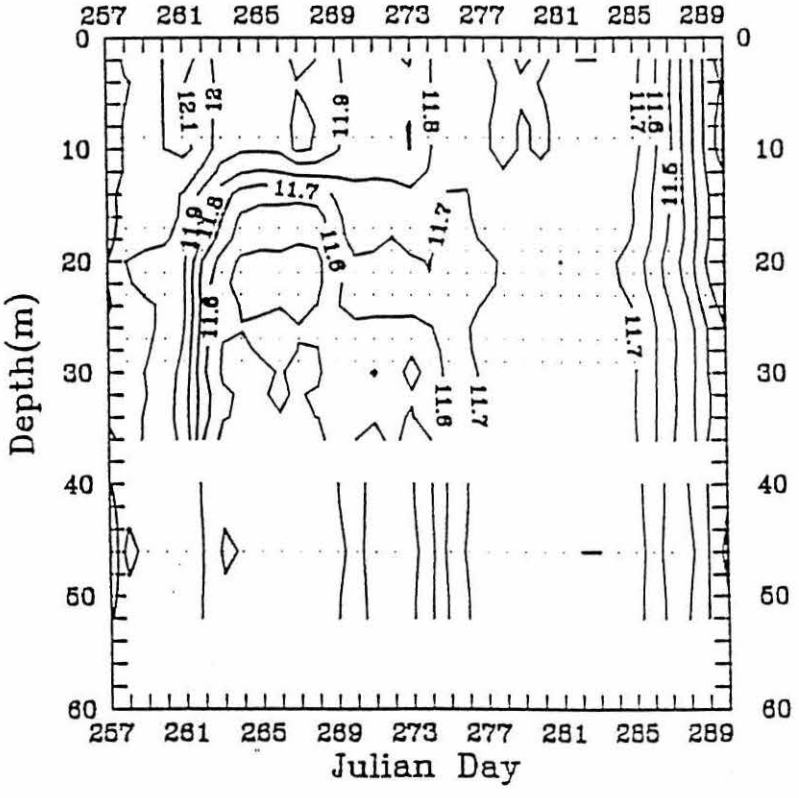

Figure 4.3a Temperature recorded at M6 during period 3 showing the onset of seasonal thermal stratification within the Bay (April 19-26) followed by a mixing event which led to stepwise warming of the deeper waters. Data recorded from thermistors mounted onto an RCM and a water level recorder. Depths 9m (solid line) and bed (52m) (dot-dash line).

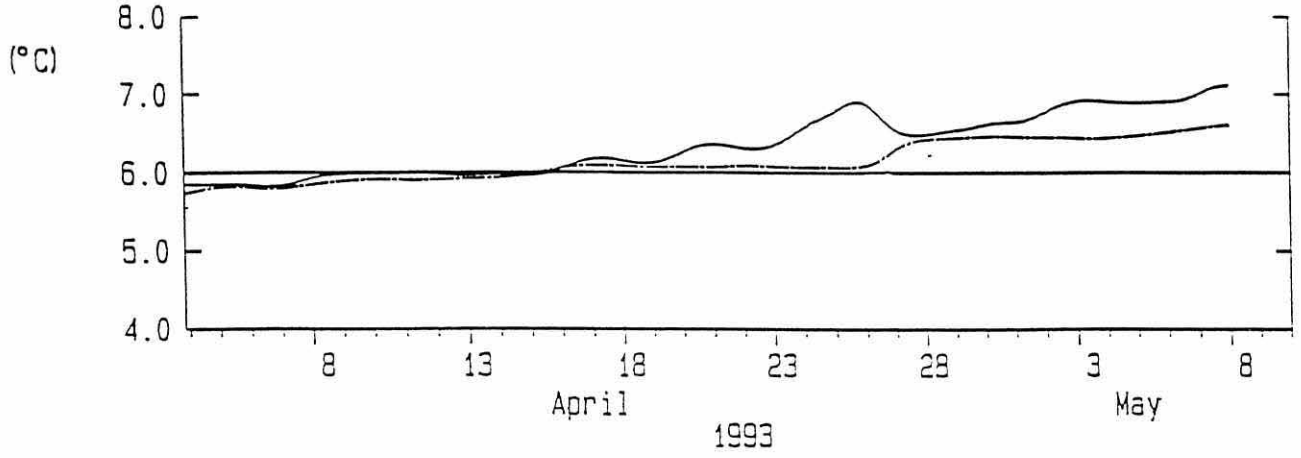

Figure 4.3b Salinity at M6 at a depth of 9m corresponding to the thermal time series of 4.3a The relationship between the influx of low salinity water and the stratification event of April 19-26 is apparent.

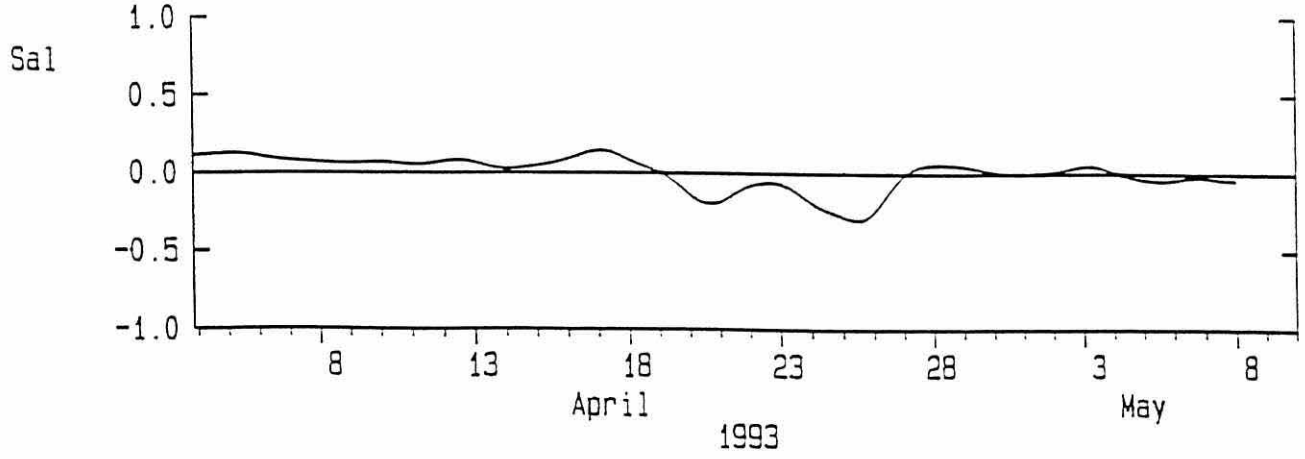

Figure 4.4a Temperature recorded at M6 during period 7 illustrating stepwise decreases in surface temperature towards the end of the year. Weak inverse stratification events associated with an influx of cold low salinity water (Figure 4.5b) can be seen to occur on the 13th of November and the 8th December. Data recorded from thermistors mounted onto an RCM and a water level recorder. Depths 9m (solid line) and bed (52m) (dot-dash line).

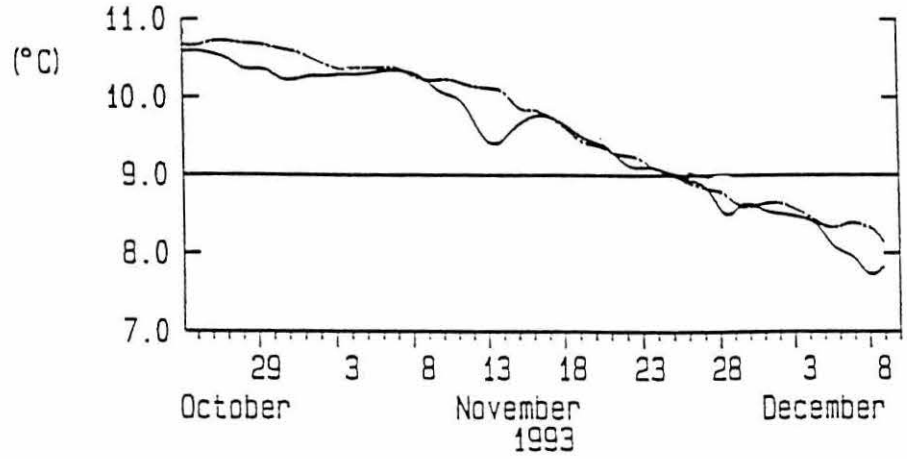

Figure 4.4b Variation from mean salinity at M6 at a depth of 9m corresponding to the thermal time series of 4.4a.

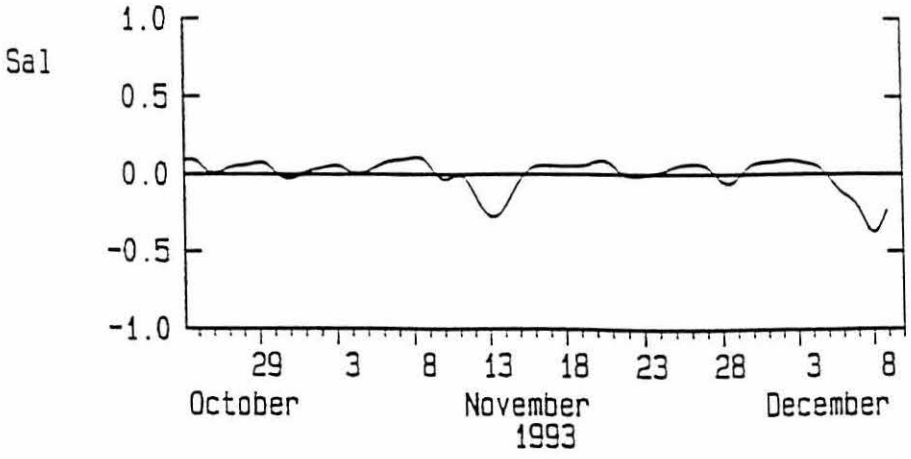

Figure 4.5 The salinity distribution along section I during the February cruise.

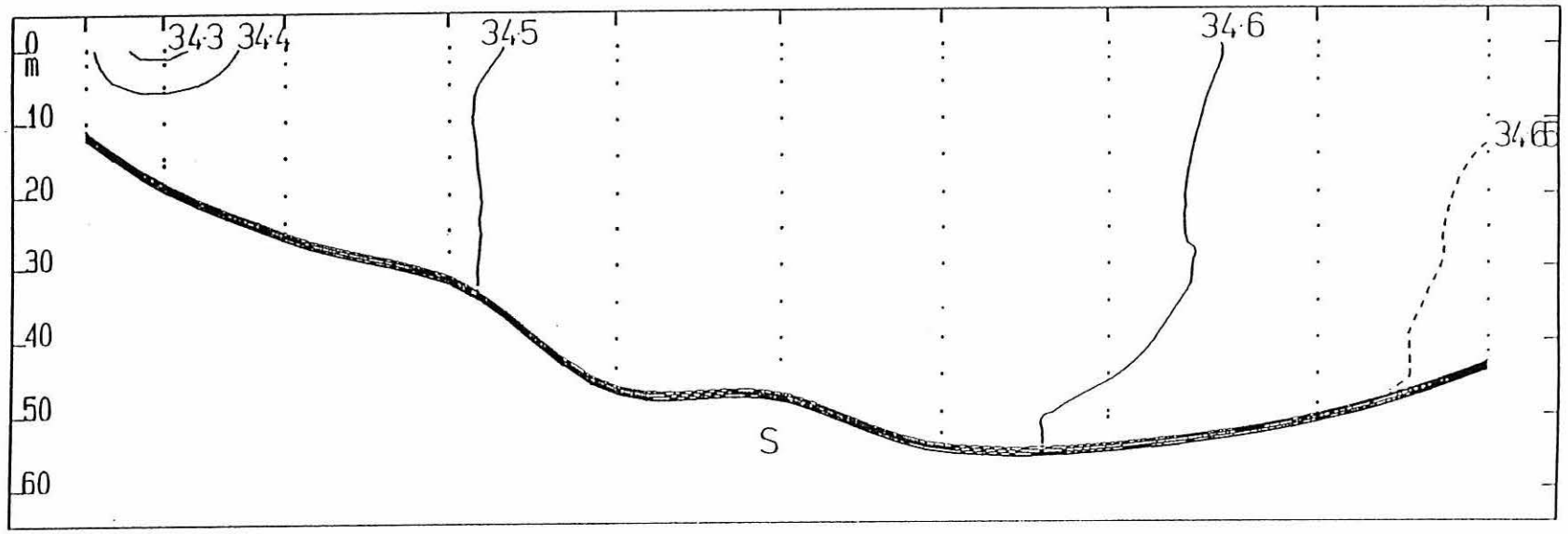

Figure 4.6 The distribution of salinity along section M during the February cruise.

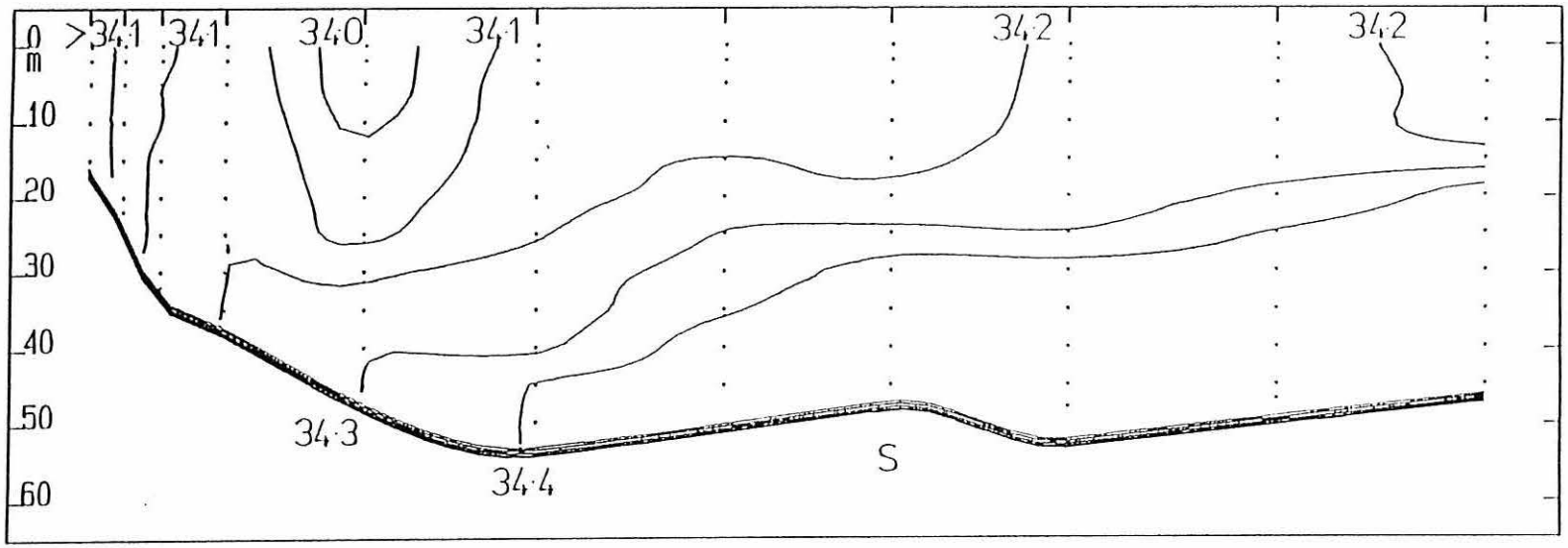

Figure 4.7 The distribution of salinity along section M during the March cruise.

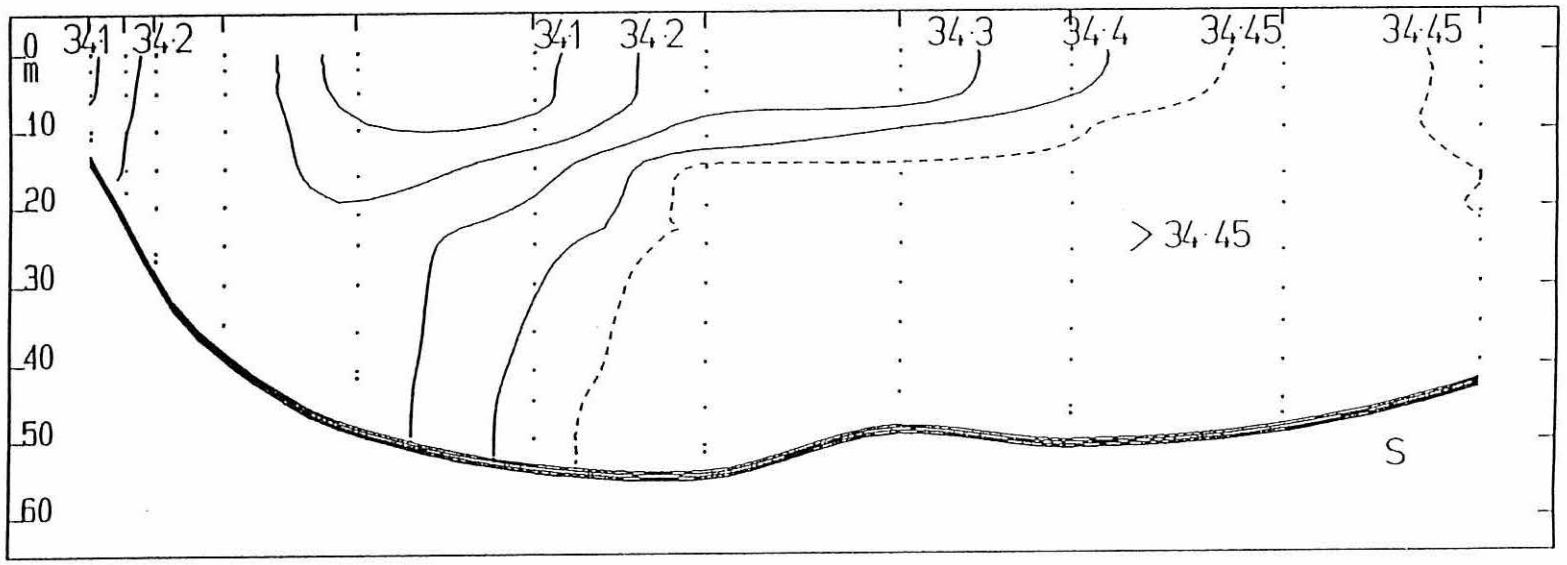

Figure 4.8 The distribution of salinity along section K during the February cruise.

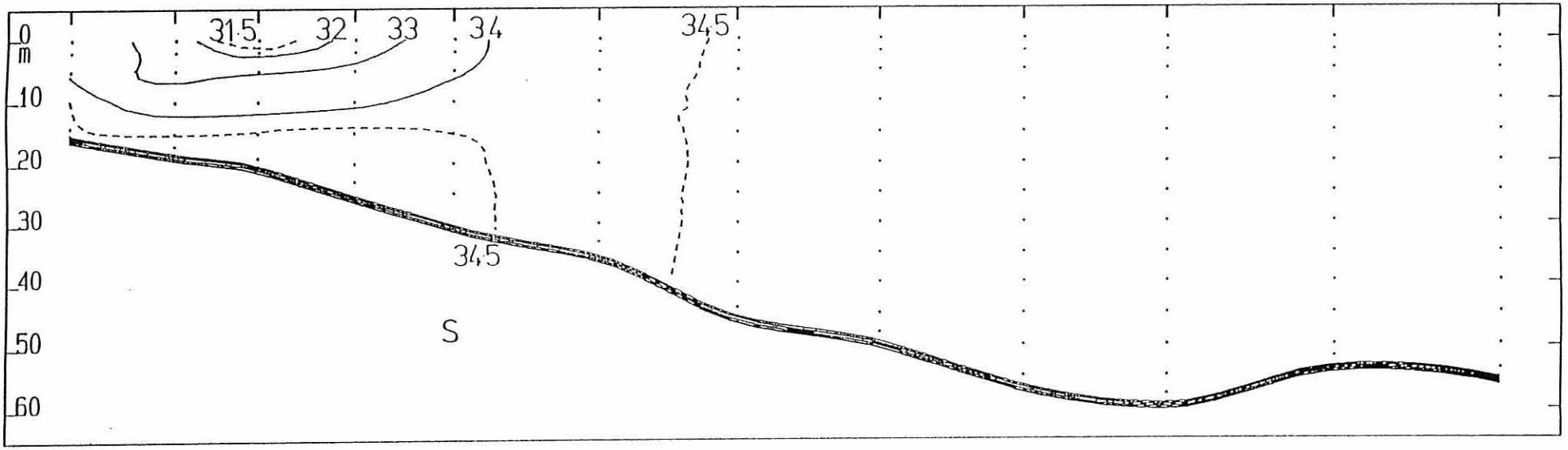

Figure 4.9. Seasonal variations in surface salinity across St. Andrews Bay during 1993. Data compiled from surface observations during the February and July cruises, representative of winter and summer riverine input scenarios respectively.

Figure 4.9a. February. The mean wind at the time of sampling was 5 m s^{-1} from the south-west. River discharge was 500 m^3 s^{-1}.

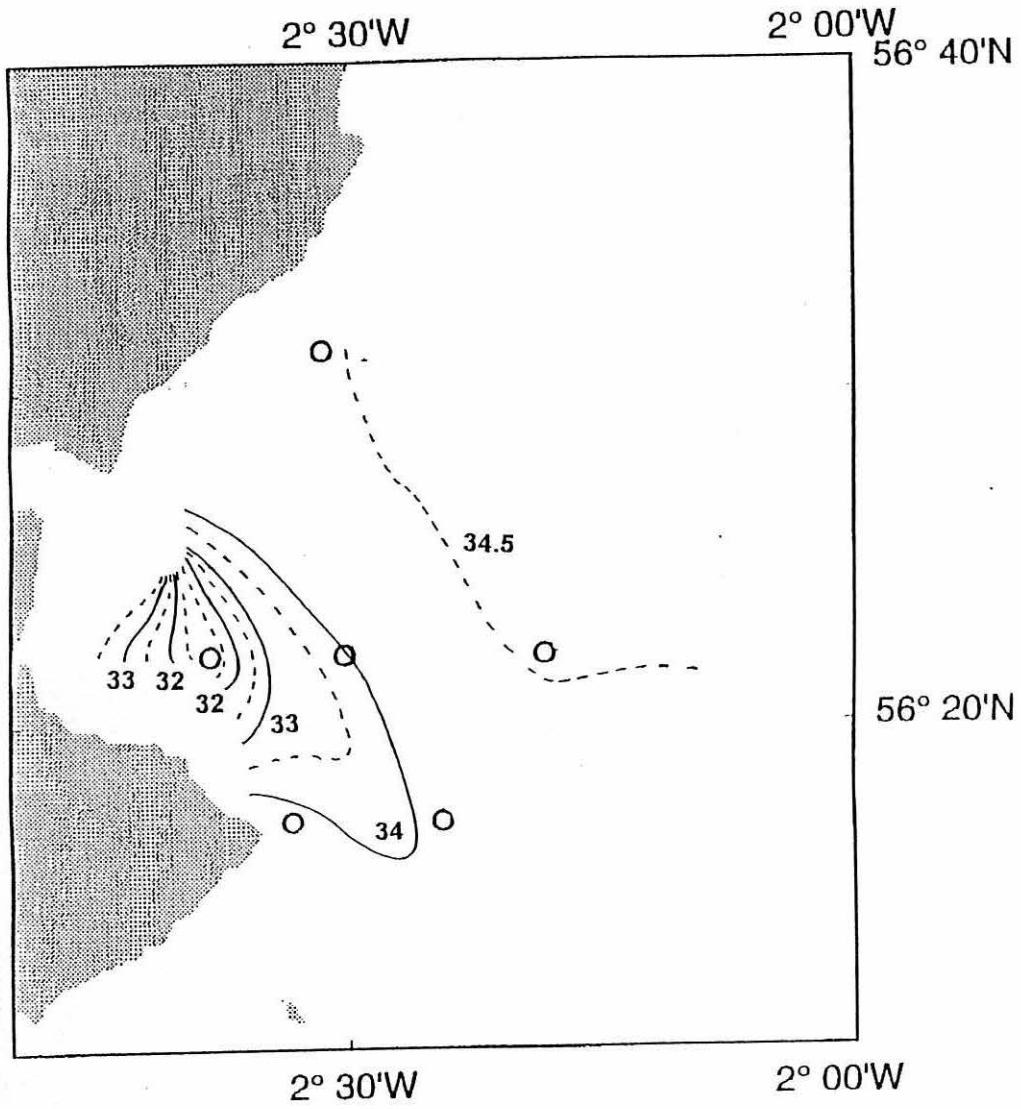

Figure 4.9b. July. The mean wind at the time of sampling was 3-5 m s^{-1} from the west. River discharge was 50 m^3 s^{-1}.

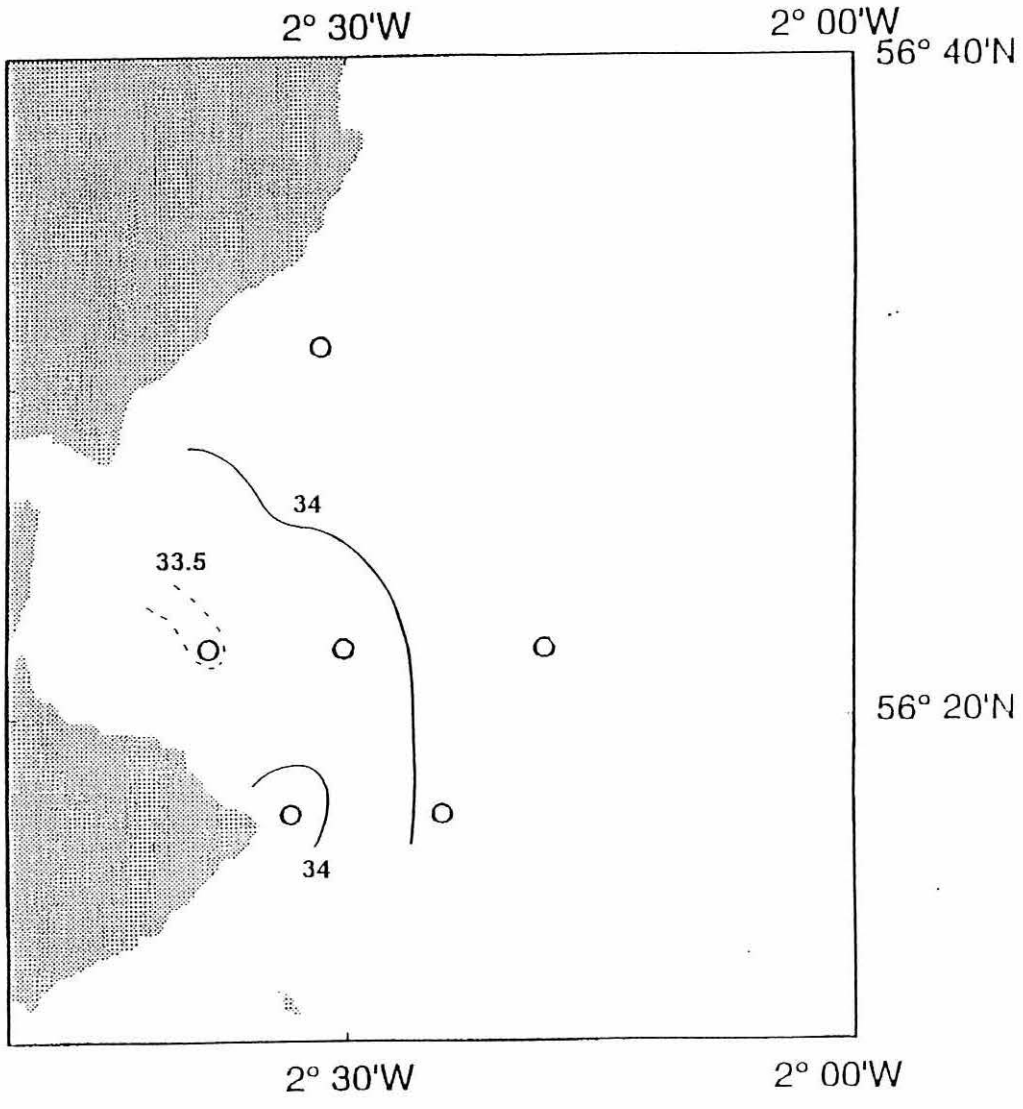

Figure 4.16 Time series of the daily mean discharge of the River Tay during 1993 measured above the tidal limit. Data supplied by Tay RPB.

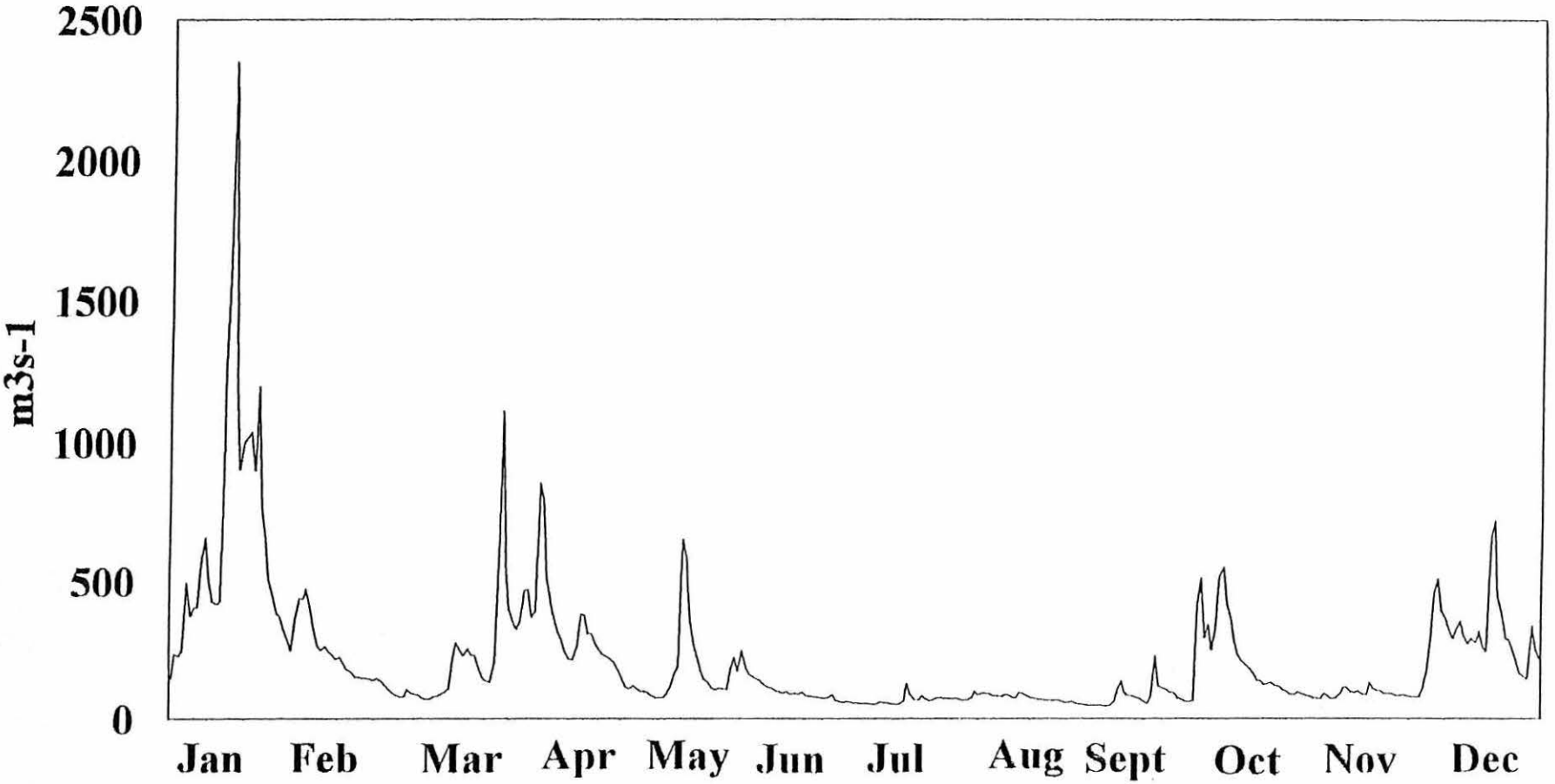

Figure 4.11 Variation throughout the year in the cross-shore distribution of the freshwater fraction (F_w) along section I.

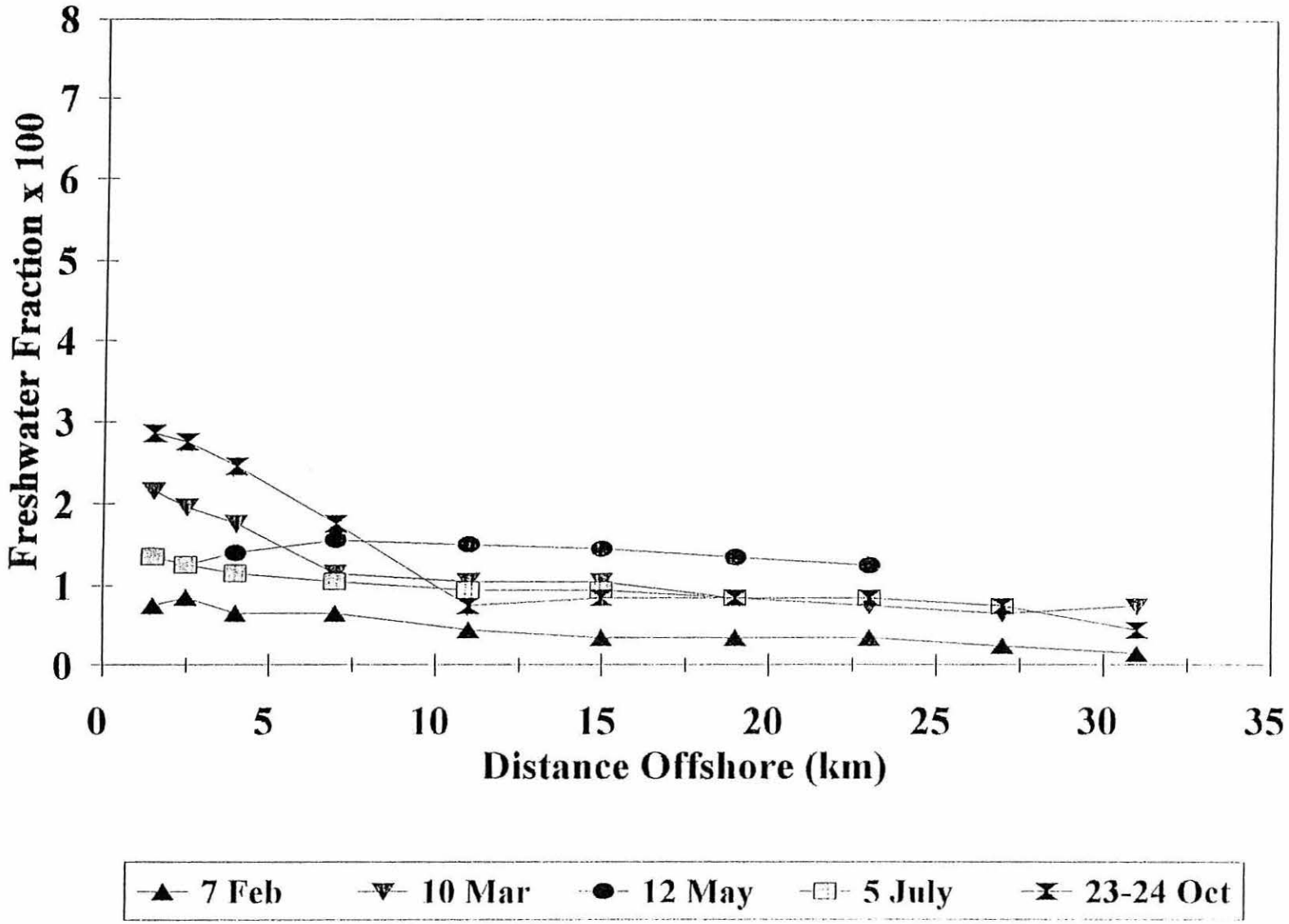

Figure 4.12 Variation throughout the year in the cross-shore distribution of the freshwater fraction (F_w) along section J.

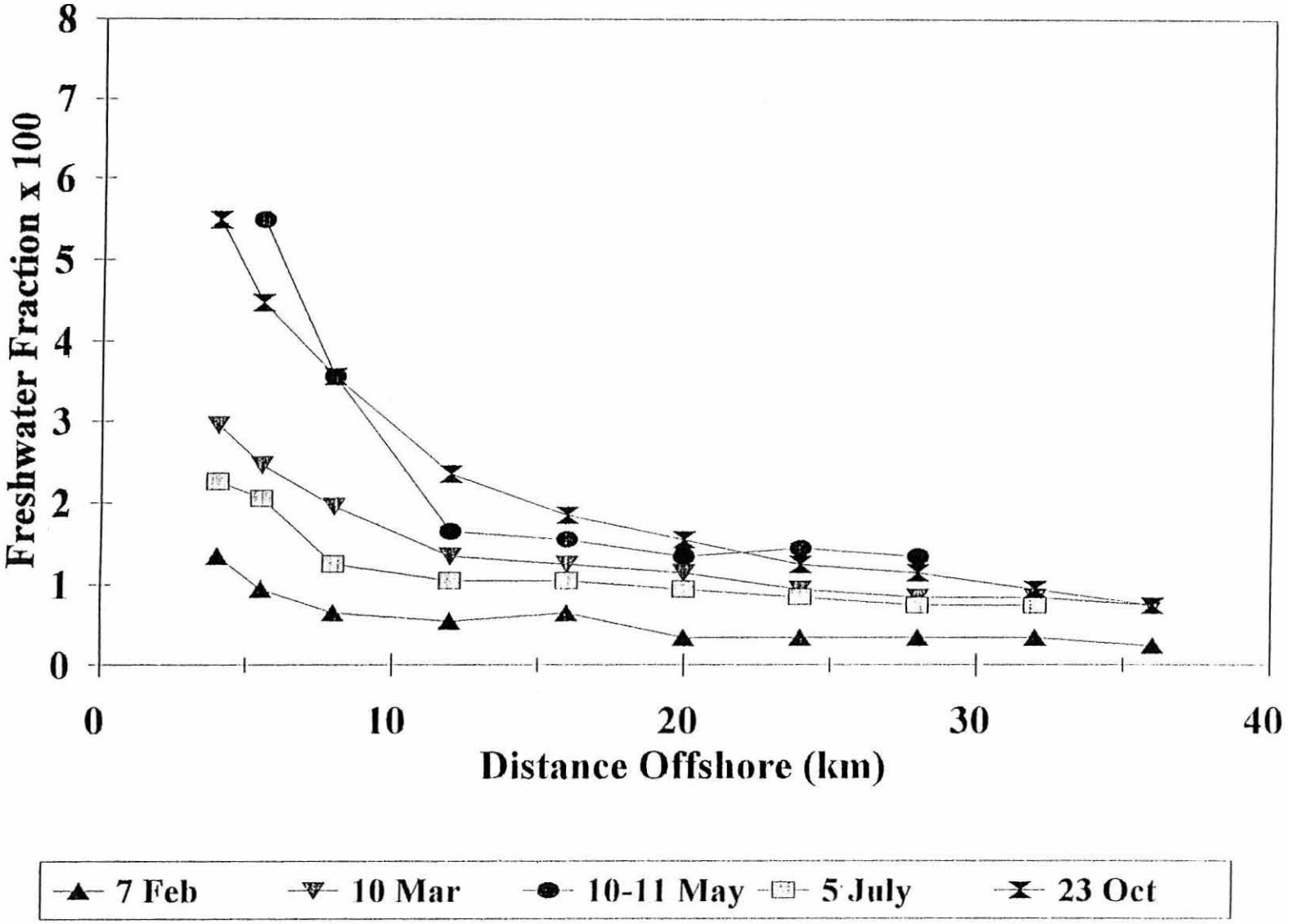

Figure 4.13 Variation throughout the year in the cross-shore distribution of the freshwater fraction (F_w) along section K.

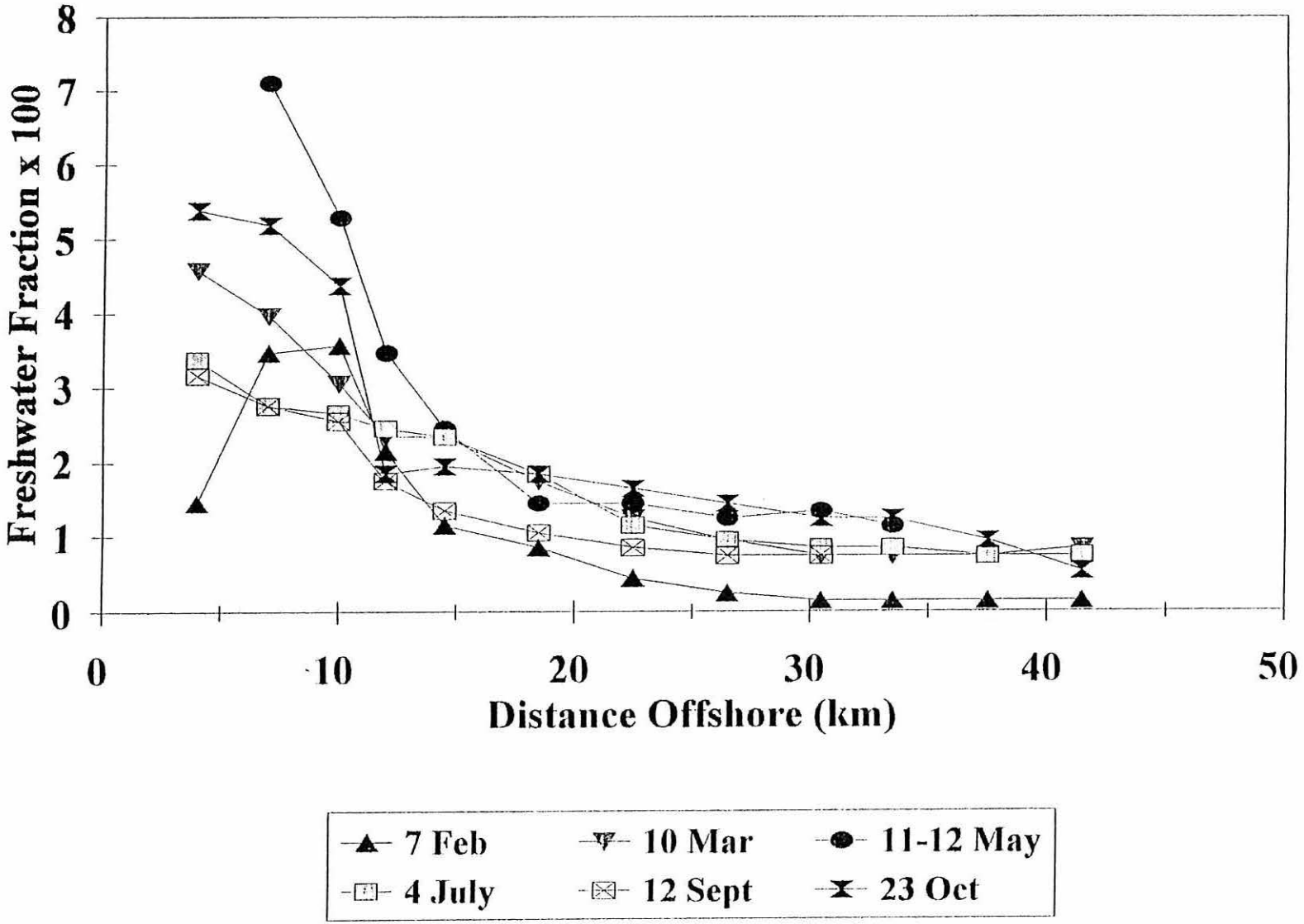

Figure 4.14 Variation throughout the year in the cross-shore distribution of the freshwater fraction (F_w) along section M.

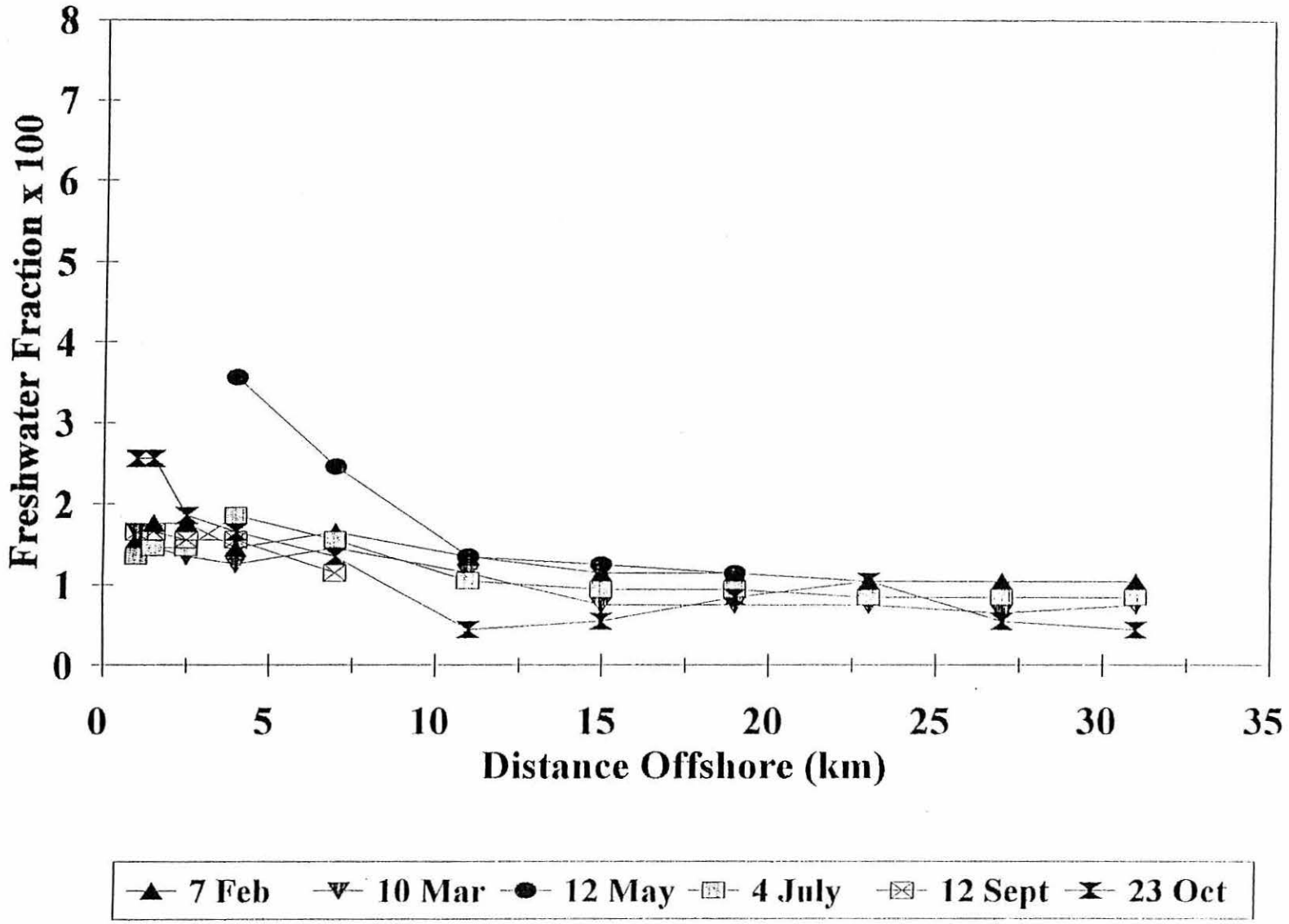

Figure 4.15 A comparison of the cross-shore variation in vertical haline stratification and distribution of freshwater (parameterised by the freshwater fraction, F_w) along section K during February and May. The unbroken line represents F_w while the dashed line represents the vertical difference in salinity between surface and bed.

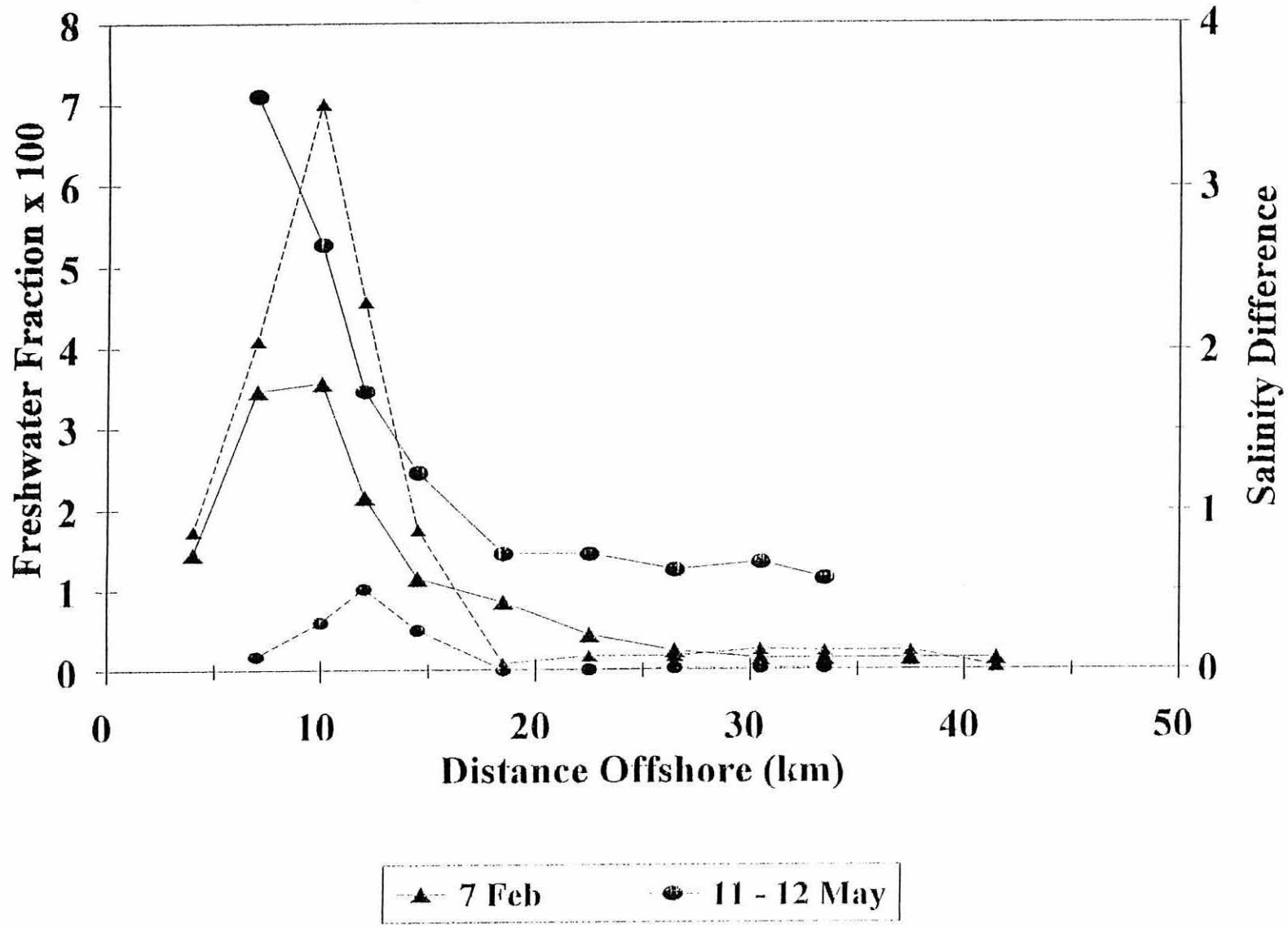

Figure 4.16 A comparison of the cross-shore variation in vertical haline stratification and distribution of freshwater (parameterised by the freshwater fraction, F_w) along section M during February and May. The unbroken line represents F_w while the dashed line represents the vertical difference in salinity between surface and bed.

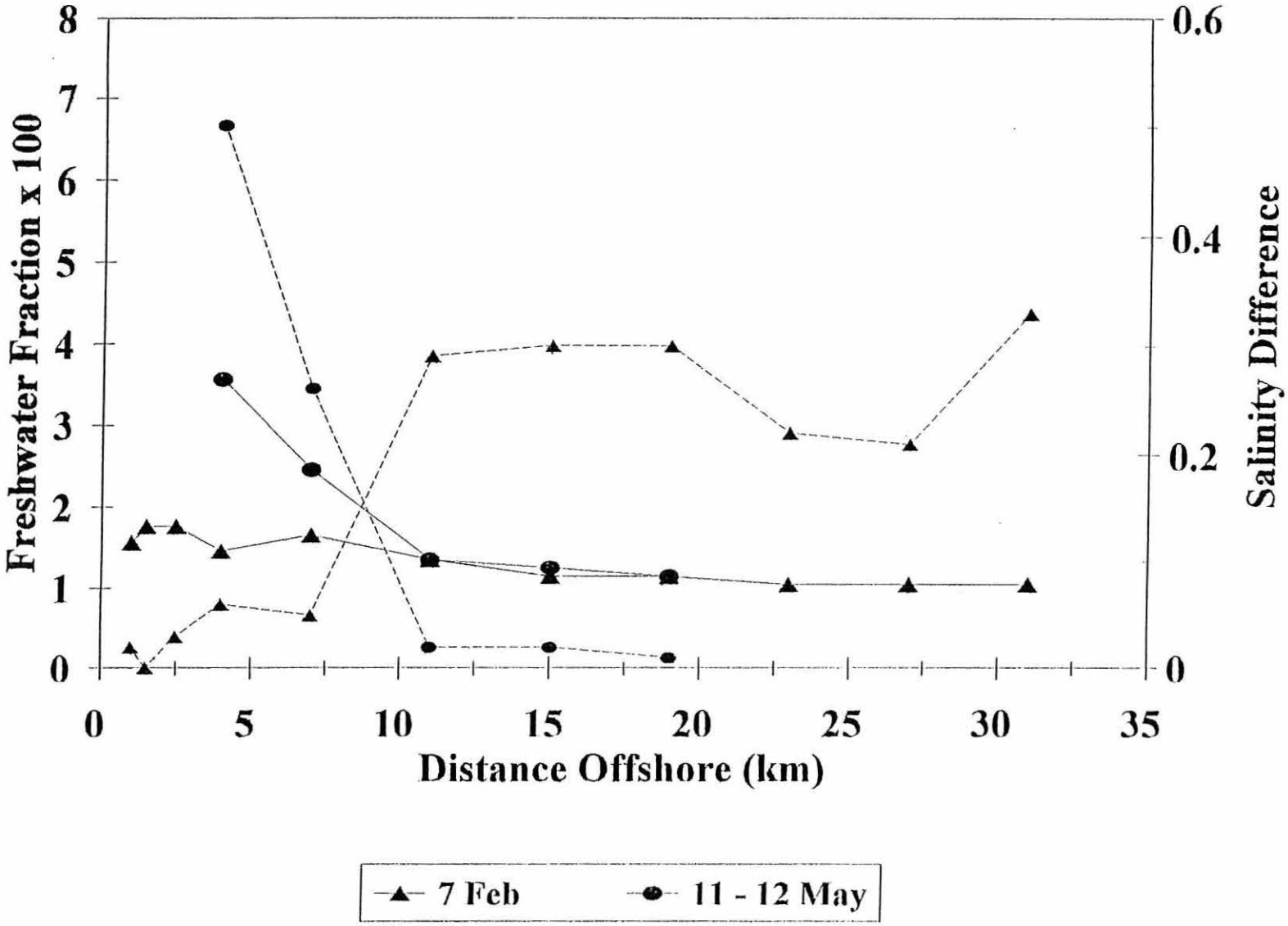

Figure 4.17 Comparison between variations of the mean freshwater fraction (F_w) for St. Andrews Bay, estimated by averaging of the time series of salinity recorded at M1, M2 and M5, and the longshore component of the wind stress during 1993. A positive wind stress corresponds to a wind from the north.

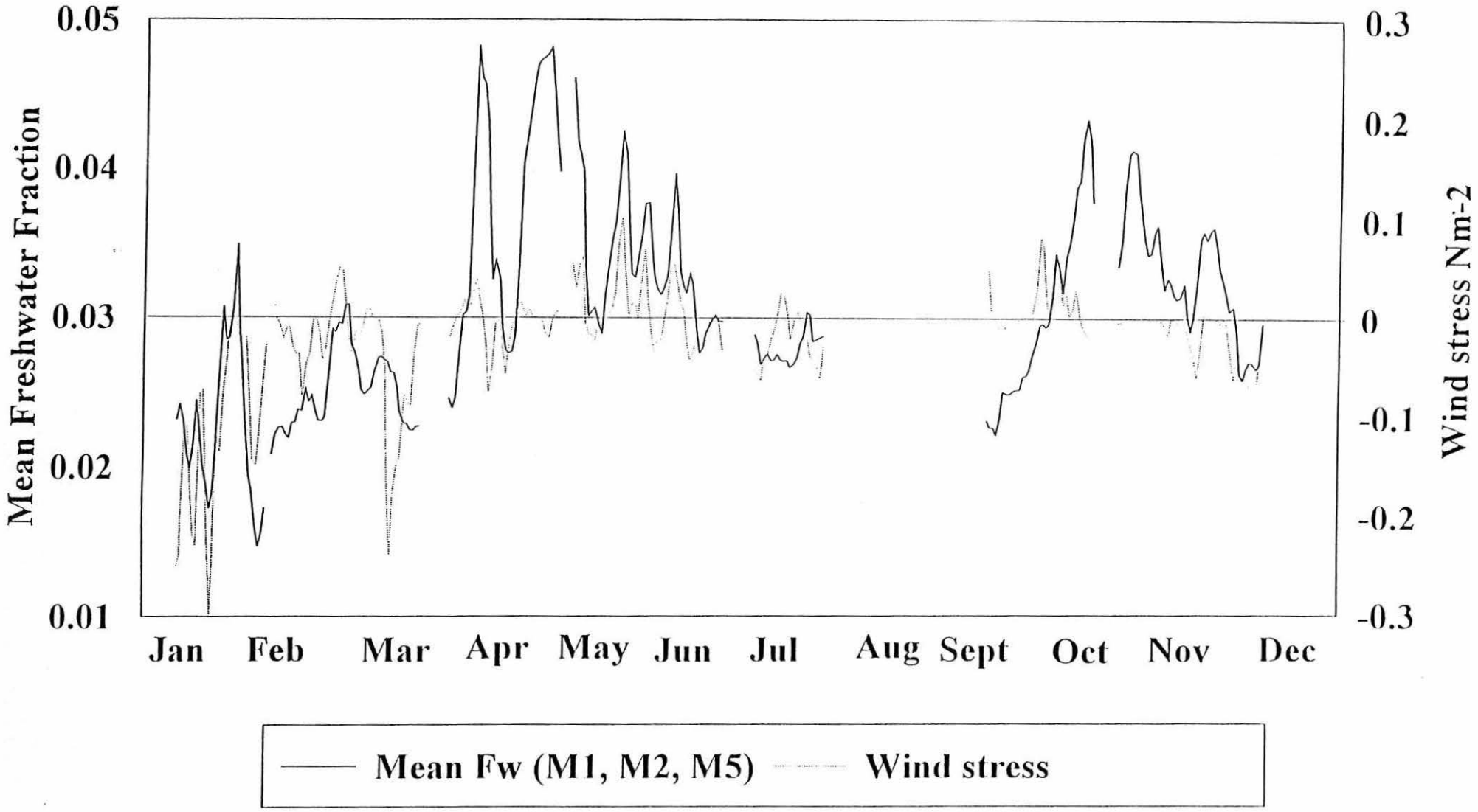

Figure 4.18 A regression of daily mean wind stress against daily mean values of the freshwater fraction (F_w) averaged across St. Andrews Bay (M1, M2, M5). A negative wind stress is generated by a wind blowing from the south.

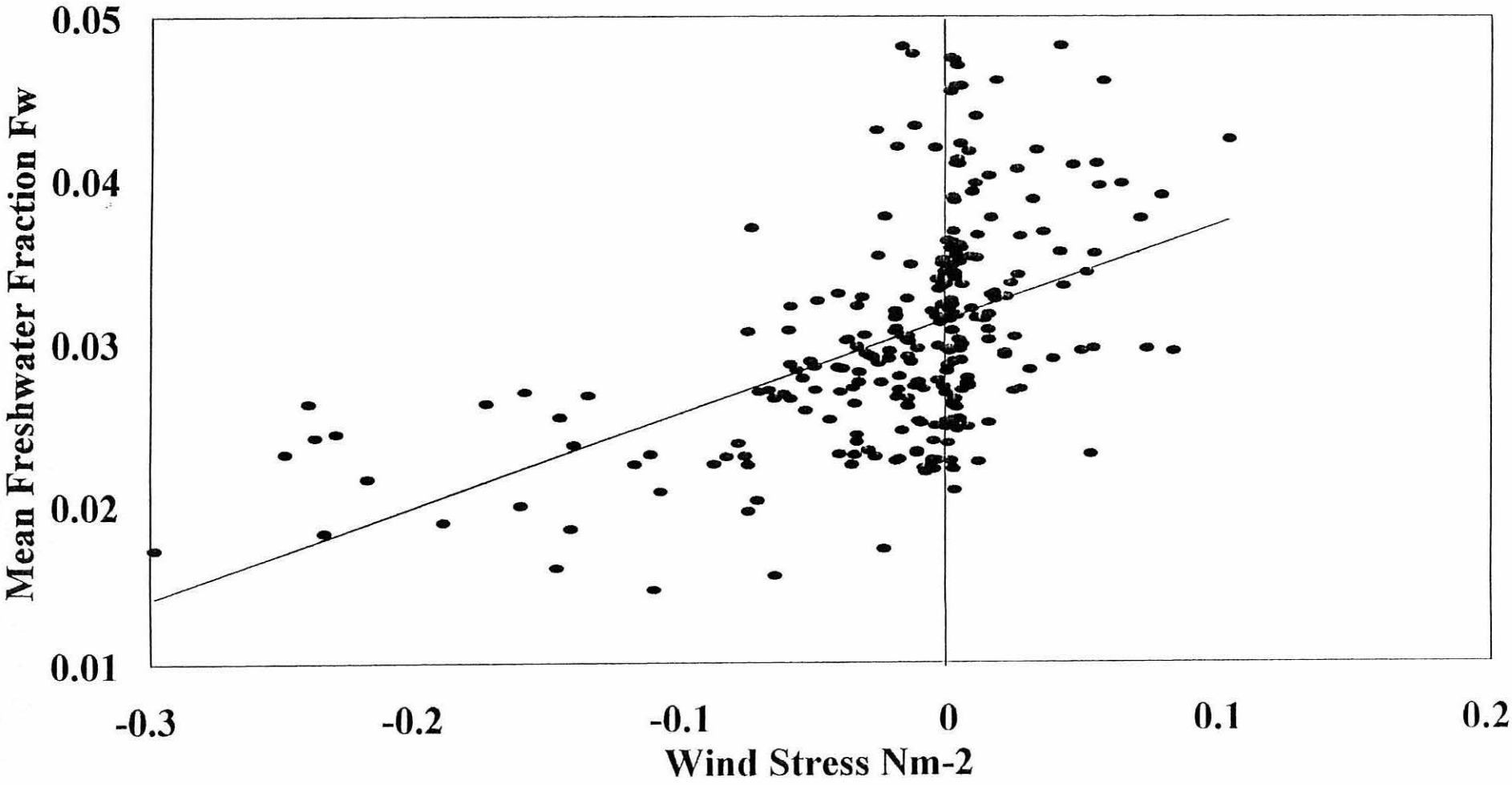

Figure 4.19 Daily mean longshore wind stress and difference in daily mean values of the freshwater fraction (F_w) between the south (M5) and north (M1) of St. Andrews Bay. A negative wind stress is generated by a wind blowing from the south. The plot illustrates the relationship between the orientation of the longshore wind and the freshwater gradient across the Bay.

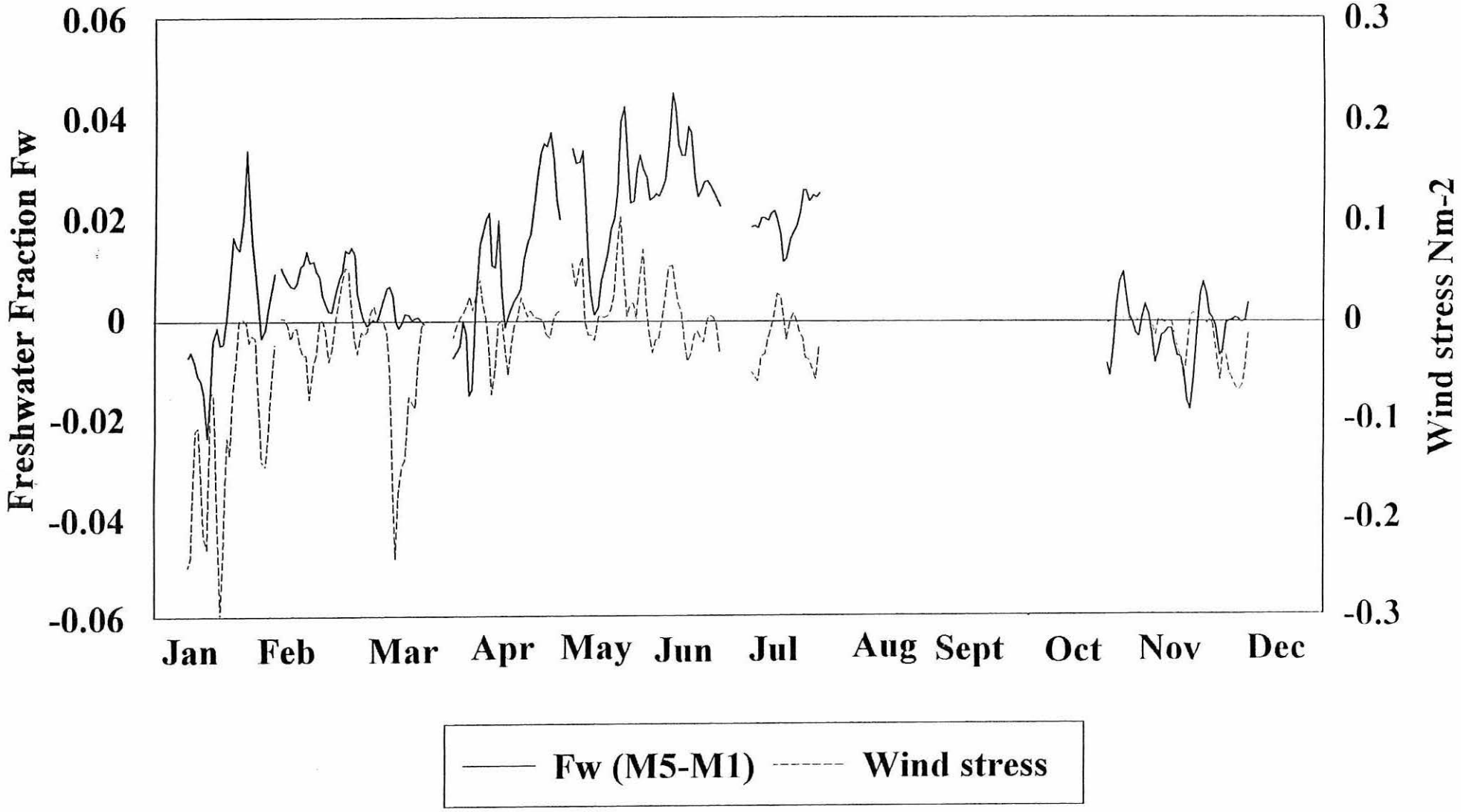

Figure 4.20 Daily mean freshwater discharge as measured above the tidal limit of the River Tay and daily mean values of the freshwater fraction (F_w) averaged across the Bay (M1, M2, M5) during 1993.

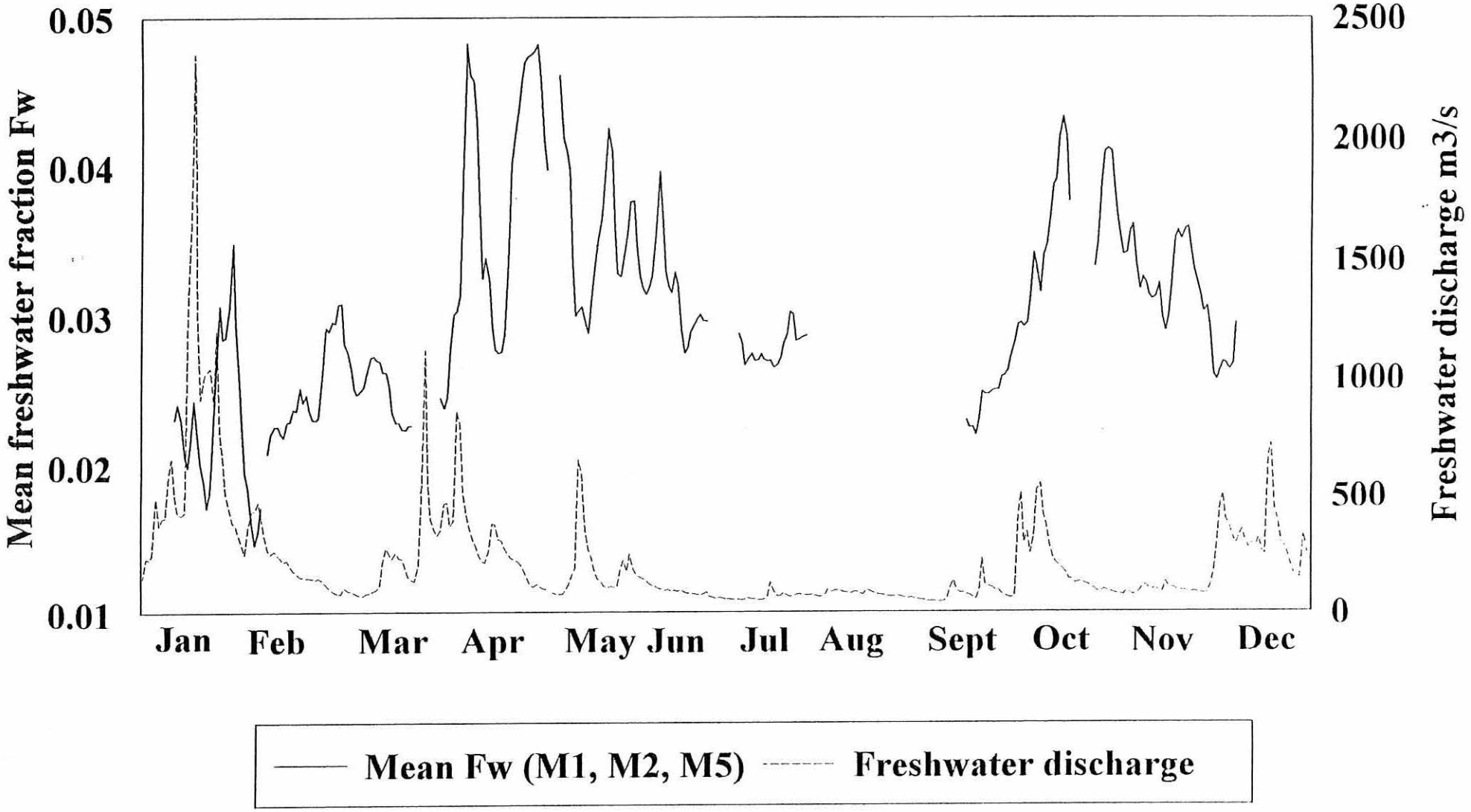

Chapter 5

5. Time Series Observations

5.1 Tidal Currents

North and east components of the longest available unfiltered time series (a minimum of three months), prior to division into periods, from each current meter position were subjected to harmonic analysis. Using the resultant amplitudes and phases of the Cartesian components of each tidal constituent, the amplitudes of the principal and minor axes of the tidal ellipse, the phase lag and orientation of the principal axis were calculated (Pugh, 1987) and are presented for the M_2, S_2 and M_4 constituents in Table 5.1.

Tidal currents in the North Sea are dominated by the semi-diurnal constituent, of which the largest species is the M_2 followed by the S_2 (*e.g.* Howarth, 1990); the S_2:M_2 ratio is stated in a number of sources (Howarth, 1990; Pugh, 1987) to be in the region of 0.3 - 0.4 for the North Sea away from the vicinity of amphidromes; this was found to be largely true of the study area. The amplitude of the M_2 species was typically 2-3 times that of the S_2, being in the region of 30 cm s^{-1} at the depth of the upper instruments rising to 40 cm s^{-1} at M1 and 46 cm s^{-1} at M5 where the presence of the headland of Fifeness could be expected to increase tidal speeds. A reduction in amplitude of 10-20% occurred between upper and lower RCMs accompanied by a phase lag of approximately 20° at the surface with respect to the bottom. The M_2 tide at mooring position M2 was an exception to this with a phase lag of 60° towards the bed, accompanying a drop in amplitude of 40%. The sense of rotation of the tidal ellipse was anticlockwise at all instruments for the main semi-diurnal tides except near the surface at M1 where the ellipse was virtually isotropic.

The orientation of the tidal ellipse was typically along isobath for both the M_2 and S_2 tides with only small variations with depth. The tides at mooring location M2 were an exception however as the ellipse for both semi-diurnal species was rotated 50° clockwise at the lower (mid-depth) instrument into (approximate) alignment with the mouth of the Tay estuary.

Charlton (1980) states that tidal motion within the Tay region consists of a progressive wave travelling southwards offshore while towards and inside the estuary the motion is a quasi-standing wave, leading to a complex tidal circulation between the regimes. It appears that at the sites monitored during this study semi-diurnal water movements were largely associated directly with the travelling wave except below the plume at M2. The differences in amplitude, phase and orientation of the M_2 and S_2 ellipses at the near-bed current meter at M2 (designated as $M2^2$) indicate that the complex tidal circulation observed by Charlton (1980) near the mouth of the estuary and giving rise to residual gyres may extend further south into St. Andrews Bay itself. This is borne out by Charlton *et. al.* (1975) who state that the flood tide gives rise to a large clockwise eddy within St. Andrews Bay.

The M_4 species showed more variability (as a percentage of a mean value) than the main semi-diurnal species but was typically small in comparison to them. However, at M5 the amplitude of the M_4 tide increased to twice its level at the other instruments (~5 cm s^{-1}); this increase in speed may be attributed to curvature of the tidal flow around Fifeness. Enhanced tidal flows around headlands are often associated with vorticity-generated eddies on either side of the headland. In the case of Fifeness a residual anticlockwise flow would be expected in the Bay to the north of the headland, generated during the ebb tide and a reversed circulation to the south generated during the flood. These residuals would be accompanied by an offshore flow near the headland (although the extent of such a flow is difficult to estimate); such a flow has been measured off Portland Bill on the south coast of England (Pingree and Maddock, 1977).

5.2 Sub-Tidal Currents

5.2.1 Initial statistical analysis

After removal of the dominant tidal signal the 61 records, as divided into common periods, (see Tables 3.2 and 3.3 for period lengths and dates) and 7 corresponding time series of wind stress were statistically analysed to determine the mean speed, direction and stability of the record. The stability of a record in Cartesian vector form with components *u(t), v(t)* is given by the ratio of the vector to the scalar mean speed expressed as a percentage, such that a value of 100% is a totally stable flow. The current results are

presented in detail in Table 5.2 with results for the mean wind in Table 5.3 and are illustrated in Figure 5.1.

The variability of the vector series was described by calculation of the statistics of the variance ellipse. If σ_{uu}, σ_{vv} and σ_{uv} are equal to the variances and covariance of the orthogonal components, then the direction of the principal axis of variability is given by ψ where

$$tan\ \psi = (\sigma_{11} - \sigma_{uu})/\sigma_{uv} \qquad 5.1$$

and

$$\sigma_{11} = \tfrac{1}{2}(\sigma_{uu} + \sigma_{vv} + [(\sigma_{uu} - \sigma_{vv})^2 + 4\sigma_{uv}^2]^{\frac{1}{2}}) \qquad 5.2$$

is the maximum variance along the principal axis of variability (Thompson and Pugh, 1986). The variance of the vector component normal to the principal axis of variability is given by

$$\sigma_{22} = (\sigma_{uu} + \sigma_{vv}) - \sigma_{11} \qquad 5.3$$

The principal direction (ψ) is taken for the sake of consistency to be the orientation of the southerly axis of maximum variance. The total variance and standard deviations of the sub-tidal currents and wind stress along the principal and minor axes of variance are presented for all periods in Tables 5.2 and 5.3 respectively and are plotted in Figure 5.2. These results are discussed in the following section.

5.2.2. Observations of the mean current regime

Near-bed flows

The mean circulation 5m above the seabed was directed shoreward throughout the year across the study area. Maximum variability in flow direction was seen at $M5^2$ due to its proximity to the headland of Fifeness; during period 7 the mean near-bed flow was directed offshore to the south-east in line with that measured at a depth of 7m. With the exception of flows at $M1^2$ the mean currents were typically directed into St. Andrews Bay, a regime indicative of an estuarine circulation focused on the mouth of the Firth. Mean currents at $M3^2$, $M4^2$ and $M6^2$ shared many characteristics and showed indications of seasonal variability with reduced speeds during the summer months. The lack of any

increase in stability (typically between 30% and 60%) over winter at these positions suggests that increased runoff during the winter months is unlikely to wholly account for this and the typically higher winds must play a part.

M1[2], to the north of the estuary mouth, showed an extremely stable (70%-95%) near-bed onshore mean flow normal to the coastline, rather than directed toward the Firth mouth, throughout the year (a variation in the onshore angle during period 3 may be a product of the short record length), reaching a maximum of 7 cm s^{-1} during the winter months and a minimum of 4 cm s^{-1} over summer.

Flows at 7-9m

The mean directions of the flows at a depth of 7-9m were generally more variable over the year than those near the bed, however the upper instruments at M3, M4, M5 and M6 typically showed increased stability relative to those near the bed. As for the near-bed flows, currents at M3[1], M4[1] and M6[1] were similar in direction, being largely orientated along topography to the south-west except during period 1 when the flow at M3[1] was directed offshore and normal to the sea-bed bathymetry. The similarity in mean flow characteristics between these three mooring positions indicates that similar forcing was occurring at each position. As was the case for the near-bed flows, currents at M4[1] and M6[1] were aligned, showing the probable influence of topography on the flows as both mooring positions lie on the 50 m bed contour. The mean flow at M4[1] was typically faster than that at M6[1] by up to 100%.

Mean residual currents at M5[1] were generally larger than those observed at any of the other instruments at a comparable depth and were indeed of a similar magnitude to those measured at M2[1] at a depth of only 2m. The maximum mean current of 9.8 cm s^{-1} recorded at any instrument occurred at M5[1] during the summer months (period 4) when both the mean wind speed and runoff were low. The location of the mooring, just off the headland of Fifeness, together with the high degree of stability (typically >80%) suggests the possibility that tidal rectification may be a factor in the generation of these high current speeds, however an alternative explanation lies with geostrophic flows generated by the cross-shore density gradient. Examination of the low-passed records showed no

evidence of a signal at the frequency of the spring/neap cycle, suggesting that the explanation lies with the latter theory. This will be addressed in Chapter 7.

M1[1], along with M3[2], featured some of the lowest mean speeds recorded during the study period (as low as 1.9 cm s^{-1}). The greatest magnitudes and stabilities of flow at M1[1] occurred when the mean wind was from the east leading to the current being directed southward along the coastline during summer and autumn (periods 4 and 6). During period 5 however, a stable (75%) south-going current was apparent while a wind, stable for most of the period, was blowing in the opposite direction.

The mean flow at M2[2] at a depth of 9m (mid-depth at this mooring) showed the characteristics of a bottom return flow driven directly by the outflow from the Tay estuary. The flow was directed northward and typically towards the mouth of the estuary along the 20m bottom contour with a speed of between 4 and 5 cm s^{-1} except during period 1 when the mean speed reached 7 cm s^{-1}.

Flows at 2m

Available records for periods 3 and 4 at M2[1] indicate a strong mean current regime (up to 9 cm s^{-1}) directed toward the south and west over the periods observed.

Summary

For all periods (except periods 1 and 7 at M1[1]) the mean sub-tidal currents at the 7-9 m instruments were directed towards the south, typically along-isobath. The important exception to this was at M2[2] where the mean flow, in common with the near-bed flows at the other moorings, was directed towards the estuary mouth as a return flow beneath the estuarine plume. The stability of the flows at M3[1], M4[1], M5[1] and M6[1] was typically higher than that at the lower instruments on the same moorings and particularly stable flows (>90%) occurred at M4[1] and M5[1]. Tidal rectification could generate consistent residual currents at M5[1] as could the cross-shore density gradient. Numerical modelling of the area would determine the degree to which tidal rectification may be important. Unfortunately, no models of St. Andrews Bay of sufficiently high resolution exist. The very stable high velocity mean currents observed at M4[1], particularly over the summer months, cannot be explained by tidal rectification. Virtual displacement plots indicate

that these highly stable currents are largely unaffected by the wind stress (*e.g.* Figure 5.3), suggesting a baroclinic origin.

The mean circulation at 7-9 m within the study area was directionally stable with a few notable exceptions: Flow at M1[1] was directed northwards during periods 1 and 7 while at M3[1] and M5[1] it was directed seawards. The high mean SW wind during period 1 (τ = 0.122 Nm^{-2}) may explain these flows during this period, while during period 7 strong SE wind events recorded during the latter part of the month may account for the mean northward flow at M1[1].

At M2[1] the flow at a depth of 2m was strong with mean flow to the west and south. The flow appears to have been driven westwards by mean south winds (period 3) and south-westward by easterlies (period 4), responding strongly to variations in the local wind field with enhanced flows in all directions but east.

There was typically a decrease in the speed of the flow with depth at all moorings during periods when such comparisons were possible, except at M1 where the reverse was true. A few exceptions to this general trend were observed at M1 (periods 4 and 6) and at M6 (period 6).

5.2.3 Observations of current variance

The standard deviations of the low passed flows along the principal and minor axes of variability ($\sigma_{11}^{1/2}$ and $\sigma_{22}^{1/2}$), along with the total variance and orientation of the principal axis are presented in Table 5.2 and plotted in Figure 5.2 for each period. The ratio $(\sigma_{22}/\sigma_{11})^{1/2}$ (Table 5.2) is a measure of the polarisation of the flow, with a value of 0 indicating rectilinear flow and a value of 1 isotropic flow.

The axes of maximum variance for the sub-tidal flow at both near bed and upper instruments showed an approximate along isobath alignment throughout the year at M3, M4, M5 and M6; this was also true of the flow at M1[1] and M2[1] for the periods recorded. Variations in the angle of the orientation of the principal axes between upper and lower instruments at M3, M4, M5 and M6 were small. M3 and M4 typically showed clockwise rotation with depth, with a larger rotation apparent at M3 (< 27°) than at M4 (< 2°) during

comparable periods, while M5 and M6 rotated in an anticlockwise manner by up to 21° at M5 and 42° at M6.

The principal axis of variability at $M2^2$ was directed towards the mouth of the estuary for all periods during 1993, while at a depth of 2m the principal axis was aligned north/south, indicating the differing balances of forcing factors at each depth at this location. At $M1^1$ the situation indicated a complex variability in the force balance near the bed, with alignments of the principal axis anywhere between parallel and normal to the shore with no preferred sense of rotation.

Total variance levels at all instruments were typically higher during the winter periods than summer and the pattern of the differing levels between periods was broadly reflected in the wind stress variance (Table 5.3), suggesting the importance of the local wind stress as the primary forcing factor for current variability.

For the periods during which the current meter at $M2^1$ was in place the total variance was up to four times as large at that position than at any other, as would be expected in a wind-driven regime (Table 5.2a). At a depth of 7-9 m the temporal variability in the total variance between periods was found to be very similar for $M4^1$ and $M6^1$, dropping from approximately 45 cm^2s^{-2} during period 2 to 15 cm^2s^{-2} during periods 3 to 5. A similar pattern of variation was apparent at $M3^1$ but with a slightly smaller total variance. At $M2^2$, periods 1 and 2 showed a variance far smaller than that recorded at comparable depths at the other moorings (excepting M1) indicating the probable role of the haline stratification induced by the estuarine plume in inhibiting the downward transfer of energy imparted to the water column via wind stress. During other periods the variance was similar to that at the other sites. Total variance levels 5 m from the sea-bed were in most cases less than those recorded at the upper instruments, but with a number of exceptions, particularly at M1 where the opposite was equally likely to be the case. A notable exception was during periods 6 and 7 when the near bed variance was larger at M4 and M6, this was also the case at M3 during period 6.

The least polarised variance ellipse was found to occur at $M1^2$ during period 1 (0.88). Near-bed flows at this instrument were, in common with $M5^2$, more isotropic throughout

the year than those measured higher in the water column. The opposite was typically true for flows measured at the other moorings. The most consistently rectilinear flow was measured at M4[2] where $(\sigma_{22}/\sigma_{11})^{1/2}$ was typically less than 0.35.

Summary

Variance ellipses throughout the study area were typically aligned with seabed contours throughout the water column, indicating the importance of topographic steering on water movements within the area. The similarity in shape and orientation of the variance ellipses at M3, M4 and M6 suggests the same forcing factors drive flow variations at each site. Deviations from this pattern are notable at two sites in particular. In the first case M1, where variations at the upper meter are aligned with the coast, but those at the near-bed meter indicate the interplay of differing forces, and in the second case M2 where variations in flow are typically aligned with an axis through the mouth of the estuary indicating the effect of the river plume at that site. M5 appears to be largely driven by the same forcing factors as the outer moorings but shows, particularly during period 5, deviations from the general pattern.

5.2.4 Depth-mean currents

Depth mean currents were calculated from the low-pass filtered current records for sites and periods where simultaneous time series were available for two depths, resulting in a set of 27 records. Mean and variance statistics for these records are presented in Table 5.4. The statistics for M2 were strongly biased towards surface flow due to the positioning of both instruments within the upper half of the water column and so records from the instrument at M2[2] at a depth of 9m (mid-depth) were used to approximate the depth-mean flow in all further analyses.

The depth dependence of the currents has been quantified by the ratio β (Table 5.4) after Thompson and Pugh (1986), where

$$\beta = N(\sigma_{11} + \sigma_{22}) / \Sigma (\sigma_{11}(i) + \sigma_{22}(i)) \qquad 5.4$$

such that $\{\sigma_{11}, \sigma_{22}\}$, $\{\sigma_{11}(i), \sigma_{22}(i)$ for $i = 1..N\}$ are the magnitudes of the principal and minor axes of the variance ellipse of the depth mean current and the N series used to form

the depth mean; in all cases for which the depth mean was calculated N = 2. If $\beta = 1$ then the motion is independent of depth, if $\beta = 0$ then the depth mean current is zero.

A seasonal trend in β (Table 5.4) was apparent, with currents typically becoming more independent of depth during the winter months when the lack of thermal stratification and typically stronger winds combine to allow a greater transmission of energy from the upper to the lower water layers. On average over 70% of the variance ($\beta > 0.7$) was related to depth independent motion. However, variations between mooring positions were apparent, with the least dependence on depth being at M4 (81% - 93%) while the most depth dependant mooring was M2, where significant haline stratification due to the estuarine plume was typically present.

5.3 Empirical Orthogonal Function (EOF) Analysis of the Sub-Tidal Data Set

Empirical orthogonal function (EOF) analysis, a technique used widely in meteorology and oceanography (Preisendorfer, 1988; Joliffe, 1990, 1993) to extract dominant patterns (modes) from large multi-component data sets, was applied to the sub-tidal records for each period. The aim of the analysis is to reduce the dimensionality of the data to a number of mutually normal (independent) modes, each of which may account for a percentage of the total variance. In many cases a small subset of these orthogonal modes will account for a large proportion of the total variance and may often be simply interpreted as being associated with a given forcing factor. The correlation matrix, which is effectively derived from the records after standardisation by division by their respective standard deviations, was used in this case. This has the effect of giving all time series equal weight and so removes the dominating effect of variance magnitude which, given the strongly differing variances characteristic of the data set, particularly when records from M2[1] are included (Figure 5.2), could mask important correlations.

Orthogonal components of the low pass filtered current meter records resolved along the principal and minor axes of variance (u and v respectively) were subjected to simultaneous analysis for each period. Records included in the analysis are listed in Table 5.5, incomplete periods were omitted. The percentage of the total variance of the entire data set explained by each of the first four modes (e_1 to e_4) for a given period is given in Table 5.6.

Due to the differing number of records available for each period (Table 5.5) a direct comparison over the year of the percentage of the total variance explained by a given mode can lead to only limited conclusions, however certain trends are apparent. There was some evidence of a seasonal trend with typically 65-75% of the total variance for each period explained by the first three modes, dropping to 55-60% during periods 3 and 4. The first mode accounted for more of the variance during the winter months (Table 5.6).

The mean circulation pattern associated with each mode can be described by taking the values of the eigenvectors (or weights) associated with the u and v records for each instrument to represent the orthogonal components of a vector whose magnitude gives an indication of its significance within a given mode (Thompson and Pugh, 1986). Further information can be gained from this approach by calculation of the proportion of the total variance associated with a given vector using the formula

$$T = (\sigma_{11}\, u_p + \sigma_{22}\, v_p) / (\sigma_{11} + \sigma_{22}) \qquad 5.5$$

where σ_{11} and σ_{22} represent the variance of the current meter record along the principal and minor axes of the variance ellipse and u_p, v_p represent the percentage of the normalised variance explained by a given mode for each record. The vectors u_p and v_p are obtained by multiplication of the eigenvalue by the square of the appropriate weight. This method allows scaling by the variances of the orthogonal components to take into account the differing levels of energy associated with the first two principal directions.

Results

The first mode was expected to consist largely of barotropic variations in the flow field as β (Table 5.4), indicates that on average 70% of current variation in the region was independent of depth. This did indeed appear to be the case with e_1 consisting mostly of variation within a barotropic north/south flow field. This is well illustrated by Figure 5.4a, which describes the first mode for period 7. The vectors are approximately aligned and of similar length at both depths, indicating a circulatory pattern which was similar in direction at all moorings and within which the contribution of the variance at each depth

to the first mode was similar. The value of T attached to each vector lies in the range 50-70 (with the exception of M2 at 44), showing that the majority of the variance of each individual record is associated with the first mode and is similar at each instrument. In contrast the second mode (Figure 5.4b) was less organised with each vector being associated with a smaller proportion of the total variance of each current record.

The barotropic aspect of the flow regime illustrated by Figure 5.4a was not as simple during the summer months. Depth independent variations in flow at the inner mooring positions (M1, M2, M3, M5) were often apparently unrelated to those at the offshore moorings M4 and M6, the dominant barotropic motion being split between the first and second modes. During the summer months, taking period 4 as an example (Figure 5.5), these "inner" and "outer" barotropic motions were split between e_1 and e_2. A greater proportion of the energy for each inner mooring record (T) was associated with depth-independent longshore motions within the first mode than the second (Figure 5.5a), while most of the energy within e_2 was associated with correlated motion at M4 and M6, motion uncorrelated with that at the inner sites (Figure 5.5b). During the winter months however, taking period 7 as an example, the majority of the barotropic motion at M4 and M6 was coherent with that at the inner moorings and contained within e_1 (Figure 5.4a). The second mode also featured independent barotropic motion at M4 and M6 (Figure 5.4b), however it explained less of the total energy (T) than during the summer months.

Summary

The dominance of the barotropic mode of variability within the St. Andrews Bay area is confirmed by the EOF analysis and appears to consist, during the summer months, primarily of two topographically steered modes which can be regarded as "inner" and "outer" regimes. During the winter months this dual regime system appears to become dominated by a single order, which accounts for most of the energy within the system by mutually correlated, barotropic, topographically steered motion. Variability within the barotropic regime is further investigated in Section 5.4.2.

5.4 Wind Forcing

Low pass filtered wind data were converted into wind stress using the relation

$$\tau = \rho_a C_D W_i W \qquad 5.6$$

where the drag coefficient C_D is taken to be 1.2 x 10^{-3} after the formulation by Large and Pond (1981) for wind speeds below 11 m s^{-1}, typically the case over the study area during 1993. Wind stress statistics are presented in Table 5.3.

Strong and stable (Stability factor = 95%) south-westerly winds blew during period 1 resulting in a mean wind stress four times that recorded during periods 3 to 7 (Figure 5.1). The total variance followed largely the same pattern as the mean stress ranging from 0.01 N^2m^{-4} during period 1 to a tenth of that during periods 3, 4 and 5. Typically the principal direction was aligned with the direction of the mean wind. The principal axis of variance was approximately SW-NE throughout all periods except 7 (Figure 5.2). The stability of the wind field showed a seasonal pattern with an increase over the winter months.

Figure 5.6 illustrates, as a percentage of the number of studied days during which the daily mean wind stress exceeded 0.02 Nm^{-2} (~4 m s^{-1}), the variation in orientation of the mean wind field. It is apparent that the vast majority of winds which were strong enough to have a potentially significant forcing effect on the circulation of St. Andrews Bay through stress on the sea surface blew from W-SW, *i.e.* were offshore winds. This effect was even more apparent for days of strong wind, taken to be a wind stress in excess of 0.1 Nm^{-2} or 8 m s^{-1} (Figure 5.7).

5.4.1 Correlations between the sub-tidal circulation and the wind field

The low-passed current records resolved along the axis of maximum variance used in the EOF analysis (positive was taken to be in the direction of the south-going axis) were subjected to a rotational correlation analysis (in 5° steps). The angles and corresponding correlation coefficients for optimum correlation with the wind stress for both zero-lag and lagged correlation maxima (Sciremmano, 1979) were found for current variations both in the principal direction and normal to it. Table 5.7 presents the maximum correlations

between the wind stress and current resolved along the principal axis of the variance ellipse while Table 5.8 presents correlations resolved along the minor axis of variance.

The objective of the correlation analysis was to determine the extent of direct forcing by the wind through the action of wind stress, as opposed to for instance, set-up. Correlations in excess of one day were judged to be unlikely to be due to direct frictional forcing by the wind and to that end the quoted maximum correlation coefficient is for peak correlations between wind and current events up to a lag of 24 hours.

Observations

A strong link between wind stress and current was apparent at all depths, with 86% of the records showing a correlation above the 95% significance level for variations in flow along the principal axis of variance (Table 5.7) and 43% along the minor axis (Table 5.8). An increase in the lag time for maximum correlation was often associated with increasing depth. The correlation results were studied in association with corresponding time series in order to uncover the main characteristics of the wind/current relation at each mooring position.

Time series of current and wind stress are presented in Figures 5.8-5.12 to illustrate various points raised in the text. For the purposes of intercomparison during analysis, presented records were resolved along the local long and cross-shore directions for each mooring position described in Table 3.1.

M1

The longshore current at a depth of 9m showed significant correlations (in excess of 99%) with the wind stress throughout the year with variations in the longshore north-going component of the current being driven by winds from the south and vice-versa (eg Figure 5.8, showing period 4). Significant correlations with the cross-shore flow (Table 5.8) were only apparent during period 2 when north-going longshore winds led to offshore flow at the upper RCM and during periods 3 and 6 when offshore flow was associated with onshore wind events and vice-versa.

Variations in the near-bed flow showed correlations with the wind as high as or higher than those near the surface. Winds with a strong offshore component tended to be associated with a longshore flow to the south and to lead to enhancement of the onshore residual flow while those with an easterly component tended to reduce it (Tables 5.7, 5.8). The southerly component of the prevailing wind tended to drive a north-going longshore flow and again enhance the onshore flow.

M2

At a depth of 2m variations from the mean flow were typically driven by the north/south component of the wind in the same direction.

At the lower instrument (9m) the mean flow directed towards the mouth of the Firth was enhanced by south-westerly winds (Table 5.7) with the flow being forced onshore under the influence of the offshore component of the wind (Figure 5.9). This variability in the estuarine bottom return flow may be explained by postulating an upwelling mechanism forced by the westerly (offshore) component of the wind

M3

The upper instrument at the M3 location showed zero-lag correlations between wind stress and current resolved along the principal axis of variance in excess of 95% for all available periods, while correlations of similar significance occurred at a longer lag time (up to 24 hours) near the sea-bed (Table 5.7). This trend towards longer lags appears to be linked to distance from the coast as it was marked at M4 and M6 at both depths. Significant correlations along the minor axis of variance did not occur at the near surface RCM but were apparent near the bed.

The mean flow was typically to the SW (Figure 5.1) but was reversed during the strong SW winds of period 1. Variations from the mean flow at the upper instrument were either in the direction of the wind or to the right of it (Table 5.7) suggesting an "Ekman" type response to the wind stress. Near the bed the current variations were typically to the left of the wind with minimal lag (Table 5.8) while strong correlations with the wind in an almost parallel direction occurred with a lag of the order of one day (Table 5.7) suggesting the gradual deepening of the wind driven layer with time.

M4

The mean flow at M4 showed great stability at the surface over the summer months and appeared to be disrupted only by the occasional strong winter wind event. The extremely high correlation with wind stress during period 5 (Figure 5.10) shows that, during the summer at least, variations in the SW wind were associated with almost instantaneous variations in the mean south-westward flow. Near-surface variations in longshore flow were reflected in similar variations near the bed (Figure 5.10).

M5

Variations from the typically stable southward flowing mean current at M5 were strongly correlated with the wind at both depths, generally at short lag times (Table 5.7). The mean south-going flow was not wind driven, however, as although enhancement was associated with northerly winds (Figure 5.11), reversal was observed only during strong southerly wind events as occurred during period 1 (when the entire water column was affected) (Figure 5.12). At the upper instrument the water responded to wind events at an angle of between 10° and 40° to the right of the wind direction (Table 5.7).

M6

Although having much in common with M4 the near-surface mean circulation at M6 showed slightly less stability while the near-bed flow was typically onshore. At the upper instrument the mean southward flow was enhanced by winds from the south and south-west (which also typically drove the onshore component of the current) (Tables 5.7, 5.8) and could be blocked or occasionally reversed by winds from the north and east.

Summary

The direct effect of the wind transmitted to the water column via surface stress was obviously of primary importance in forcing water movements in the St. Andrews Bay area during 1993 and accounted for a large proportion of the variance of the current time series at all depths. The extent of this influence is investigated in the next section. The response of the water column to wind stress appears to be complex and variable, even at a single instrument. However application of classical "Ekman" and coastal upwelling type

models may be expected to explain a considerable proportion of the current variability given these observations and such models are applied later in this chapter.

5.4.2 EOF analysis of wind stress and sub-tidal currents

The EOF analysis of section 5.3 was repeated with wind stress vectors included. As expected most of the vector distributions within each mode were broadly similar to those formed in the absence of the wind. The degree of correlation between the wind and the vector distributions reveals the extent to which the wind stress is likely to govern the various circulatory modes. Figures 5.13-5.19 illustrate the distribution of vectors of currents and wind stress for all periods for the first two modes of the analysis.

As found in the previous EOF analysis, during most periods the majority of the variance was associated with aspects of a north/south barotropic flow. The relation of this mode of the circulation of the Bay to the wind appears somewhat variable in the analysis. During periods 1, 4, 6 and 7 (Figures 5.13, 5.16, 5.18 and 5.19) the inner mode identified in the previous analysis was associated with aligned winds blowing along a SW/NE axis. During periods 6 and 7 a single mode of movement was apparent across the entire study area (Figures 5.18, 5.19), taking up the majority of the energy (T) at most of the moorings. During period 6 this mode was associated with the SW/NE wind, however during period 7 the flow pattern appeared to be associated with a strong onshore wind event recorded on the 29th December.

The outer barotropic mode, with which the majority of the variance at M4 and M6 was associated, appears to have been either largely independent of the wind during the spring and summer months (periods 2 and 3, Figures 5.14 and 5.15), or associated in some way with an opposing wind stress (periods 4 and 5, Figures 5.16 and 5.17). During most periods aspects of both scenarios are highlighted in the first two modes.

5.5 Modelling the Steady-State Response

An initial estimate of the steady state response of St. Andrews Bay to local wind forcing was gained by applying the coastal variant of a simple regression model originally proposed by Prandle (1987) and applied by Gmitrowicz and Brown (1993) to a region of strong density gradients off the north-east coast of England. The Coastal Model is based

on the assumption that the current is constrained to flow in a given direction by bottom topography or lateral boundaries. The model uses the angles and lags of maximum correlation calculated during the rotary correlation analysis of section 5.4.1 (Tables 5.7 and 5.8) and follows the simple hypothesis that at the angle and time of maximum response, the current measured is generated solely by the direct effect of the wind stress.

The wind stress τ_c at an angle α to the flow direction (positive anticlockwise) forces a current C_c which at time t is given by

$$C_c(t) = R_c \tau_c (t - L) \qquad 5.7$$

where R_c is the slope of the linear regression between the wind stress and measured current and L is the time lag of current response to wind forcing. The model was applied to flows resolved along both the principal and minor axes of current variability for each instrument and for all periods.

Results

A significant proportion of the total current variability can be explained by wind forcing using only this limited model. The percentage of variability explained (V%, Table 5.9) was found to fluctuate considerably at all instruments between periods with no seasonal modulation apparent, despite the decrease in the variance of the mean wind by a factor of ten between periods 1 and 3.

Comparisons of V% at each depth show little evidence that the percentage of the total variance explained decreases with depth as found by Gmitrowicz and Brown (1993) except at M5. Indeed at M6 the inverse was typically the case while at the other moorings the ratio was variable throughout the year with little indication of seasonal modulation. The same was true of similar comparisons between the variance of flows predicted by the coastal model.

The model was found to fit best at M1 and M5, moorings positioned nearest to the coast and where the sea-bed topography was parallel to the coastline. The percentage of the total current variance explained at these moorings was in excess of 40% when averaged

over the year at M1[1], M1[2] and M5[1] and reached as high as 70% at M1[1] during period 7, where a wind stress of 0.1 Nm^{-2} (corresponding to a wind of 8 m s^{-1}) was predicted to force an longshore current of 11.6 cm s^{-1}. The poorest fit was at M4 and M6. As little as 6% of the variance was explained by this model at M6[1] during period 6, indicating the dominating presence of other forcing factors or an inability of this simple model to describe the response of the water column to wind stress forcing at these outer moorings.

The degree of response to wind stress (given by R_c) along the principal axis was strongly variable at all instrument positions. A depth comparison shows that a wind of a given strength typically forced stronger currents at the upper meters at M1, M2 and M5 while the opposite was true at the outer moorings M4 and M6. The strongest response occurred at M2[1] where a wind stress of 0.1 Nm^{-2} gave rise to currents of up to 35 cm s^{-1} along the principal axis of variability at a depth of 2 m. The minor axis response was in many instances the opposite to that of the principal axis, particularly at M1, M3 and M4, indicating an increase in isotrophism with depth at M1 particularly.

Summary

The simple wind-driven coastal model gives a quantification of the response of the water column to the wind at a given instrument. It is, however, primitive, being based on the assumption of a frictional balance between the surface and bottom stress with no other forcing terms. Its usefulness lies in its ability to highlight the extent of this balance. Where the percentage of variability explained (V%) was high the major driving force on the water column was likely to be a frictionally balanced flow directly driven by wind stress. Where it was low other factors are likely to have been important. The role of wind stress was found to have been important at all mooring positions, but particularly at the inner sites where between a quarter and half of the total variance could be attributed to the direct frictional effect of the wind.

5.6 Depth of the Wind-Driven Layer

The well known theory of wind driven circulation devised by Ekman (Ekman, 1905) declares that under the influence of steady wind stress a turbulent shear layer forms, over which the stress reduces to zero and within which the water column is well mixed. A

similar layer is formed above the sea-bed due to bottom friction. The thickness of these "Ekman layers" (D_E) can be estimated from

$$D_E = 0.4\, u^*/f \qquad 5.8$$

where, for the upper layer $u^* = (\tau/\rho)^{1/2}$ is known as the shear velocity, τ being the wind stress, f the Coriolis parameter (1.22×10^{-4} s^{-1}), and ρ the mean density of the water column. Calculation of D_E for various wind strengths (Table 5.10) shows that for a typical wind of 5 m s^{-1} the Ekman depth would be expected to be approximately 20 m, while for the strongest winds, recorded at 15 m s^{-1} on 21st of January, the entire water column would be influenced by the wind at all sites within the study area.

Stratification due to either surface heating or freshwater input can reduce the depth of this layer, but only by a limited amount (Csanady, 1982). This being the case the inner moorings, at a depth of 30 m or less are likely to be significantly influenced by the wind at all depths for much of the year, while flow at the outer moorings (M4 and M6) would only be directly wind-driven near the bed during unusually strong winds. The influence of the wind-driven layer on circulation and mixing can extend to fill the entire water column at other times than during strong winds if the thickness of the bottom Ekman layer is sufficient to cause an overlap. The thickness of the bottom layer has often been estimated by using the same formula with $u^* = (0.03 - 0.05)\, G$ where G is the geostrophic speed above the boundary layer (*e.g.*, Weatherly *et. al.*, 1980; Dickey and van Leer, 1984), however in shallow water with tidal currents large in comparison to sub-tidal residuals the magnitude of the near-bed tidal flow is likely to be of far greater significance than geostrophic flows in establishing a vertically mixed layer near the sea-bed. Taking an average tidal amplitude of 0.3 m s^{-1} for the area gives an approximation of 30 m for the lower mixed layer. This suggests that flows produced near the bed by coastal up/downwelling due to the conservation of mass at coastal boundaries may not be trapped close to the sea-bed but extend upwards through the water column, resulting in currents generated by wind stress occurring at all levels.

5.7 Seabed Pressure Variations

5.7.1 Year-long records

After low-pass filtering the mean was removed from the atmospheric and total seabed pressure records prior to analysis. Statistics for the records are presented in Table 5.11. The sea level record from the Aberdeen tide gauge ended on 3rd November due to damage, statistics for Aberdeen are therefore based on a filtered record length of 7298 hours while the rest are based on 8690 hours of filtered data. Correlations between both sea level and adjusted seabed pressure and the atmospheric pressure were calculated using the method of Sciremmano (1979) from records edited to match the length of the Aberdeen period and are also presented in Table 5.11.

The total pressures for the year were highly coherent (Figure 5.20) particularly for large events, indicating the relatively large coherence scale of the wind field, while a correlation with atmospheric pressure was only apparent at the Leith site. This may have been a consequence of the differing orientation of the coastline at each site (that at Wick and Aberdeen being aligned SW/NE while that at Leith is approximately E/W within the large embayment of the Firth of Forth) to the wind field which is strongly correlated with the passage of low pressure zones and typically blows from the south-west.

Standard deviations, maxima and minima of the sea level records at each site increased moving northward along the coast showing the increasing influence of variations in the atmospheric pressure field (Table 5.11). The larger maxima than minima indicate the importance of the passage of low-pressure zones across Scotland in raising coastal sea levels. Statistics of the total pressures show largely the same pattern with a reduction in the variance and maximum pressure at each site but an increase in the magnitude of the minimum, producing maxima and minima of the approximately the same order.

EOF analysis of the total coastal pressure field indicated 86% of the variance was accounted for by the first mode, which represented simultaneous raising and lowering of sea level along the coast. The rest of the energy (13%) was in the second mode, which was associated with pivoting of the longshore pressure field.

5.7.2 Seabed pressure records: periods

The total pressure records for the coastal sites were divided into the appropriate periods (1 - 7) and again the mean was removed. Records obtained from the moored, bottom-mounted, water level recorders were low-pass filtered, edited to the appropriate lengths and the means were removed. Statistics for these records are presented in Table 5.12.

Both the standard deviation and maxima of the pressure records showed a clear seasonal decrease in magnitude over the summer months, with the standard deviation falling to 1/2 - 2/3 of its winter (period 1) value at all sites. During the winter months high winds associated with the predominant low-pressure systems generated a succession of storm surges which manifested as coastal pressure maxima, the observed seasonal pattern was associated with this.

5.7.3 EOF analysis of adjusted seabed pressures

Adjusted seabed pressures for each period were submitted to EOF analysis, results are displayed in Table 5.13. Results were in agreement with those obtained from the year-long records, with typically 99% of the variance explained by the first three modes. The major proportion (up to 96% during period 6) being accounted for by the first mode which corresponded to a raising and lowering of sea levels across the entire SNSCZ as indicated by the common sign and magnitude of the eigenvector throughout the sites. The second mode was again regional and typically associated with variations in the longshore pressure gradient, indicated by the change of eigenvector sign moving along the coast, accounting for up to 18% of the variance (period 1). During period 7, however, this process was dominated by a rise in the pressure at M1 and M2 with a corresponding reduction at Leith. Local pressure variations at M1 dominated mode 3 in most of the previous periods. The percentage of the total energy associated with these variations was small, although the proportion of the variance of the M1 records associated with these local effects can be significant. The increased importance in the local mode during period 7 appears to be have been due to two periods of strong (up to 11 ms^{-1}) south-easterly wind between the 15th and 30th of November which led to set-up within the Bay.

The role of storm surges in the generation of mode 1 variations is discussed in the next sub-section. Variations in the longshore pressure gradient as indicated by the second

mode may be associated with the passage of surges but may also be generated by local winds or freshwater input and are of importance to the circulation of the coastal zone. Localised variations in the pressure field appear to be minor under most circumstances although strong onshore winds appear to lead to set-up, particularly within the northern part of St. Andrews Bay.

5.8 The Role of Storm Surges in Forcing Coastal Pressure Variability Within the SNSCZ

Consideration of the results of the EOF analysis (Table 5.13) and the spatial coherence of the total pressure records (Figure 5.20) suggests the vast majority of pressure variations within the SNSCZ occurred simultaneously on a spatial scale far larger than the SNSCZ itself. However applying the formula $c = (g\ D)^{½}$ for the speed of a travelling wave, with D the mean depth, set at 50m gives $c = 22$ m s^{-1}. A storm surge travelling south at this speed would thus take approximately 5 hours to travel the 420 km between Wick and Leith. A comparison of the timing of peak pressures at those sites for the event of 21st of February, for instance (period 2, Figure 5.21), showed the pressure surge took exactly that time to cover the intervening distance.

Comparisons of the plotted pressure with weather charts (Royal Meteorological Society, 1993) showed most observed pressure maxima to be associated with strong winds to the north of Scotland over the shelf edge, the forcing factor for most external storm surges (Heaps, 1969). Analysis of the timing of peak values of major events showed the majority of significant peaks to be associated with externally generated storm surges. Slopes due to storm surges are well known to lead to often dramatic increases in current velocity within coastal zones and as such are likely to be important to the circulation of the study area.

5.9 The Longshore Pressure Gradient

On the basis of the north/south tilting identified as the second mode of the EOF analysis pressure gradient time series were calculated between M6 and Aberdeen (separated by 83 km). These sites were selected as the most appropriate for calculation of the longshore pressure gradient as the intermediate coastline is straight and the separation distance is sufficient to minimise noise due to small-scale local elevations in the sea-surface.

Gradients were also calculated between Leith and Aberdeen (separated by 143 km) and Leith and Wick (separated by 420 km) for purposes of comparison and to determine any differences between the local (M6 - Aberdeen) slope and the larger scale SNSCZ slope. The pressure gradient was calculated for periods 2 to 6 as a pressure record for period 7 was unavailable from Aberdeen and likewise for M6 during period 1. Due to the strong agreement between the sites the period 1 record for Aberdeen-Leith was also used.

Variability in the longshore pressure gradient was found to be highly correlated between sites in all cases (>99%). Figure 5.22 shows gradient time series for period 2 as an example. Slight differences, probably due to coastal orientation, were evident in reduction or enhancement of the sea slope in certain winds. Although no significant local variability was apparent the magnitude of the slope between Leith and Wick was found to be approximately half the value of that between M6 and Aberdeen for slopes in both directions. A possible cause lay in the choice of one coastal and one offshore pressure sensor for the local slope, which means the computed gradient was in fact a combination of longshore and cross-shore gradients. The slope between M6 and Wick (360 km) was calculated for comparison with the Leith-Wick slope; amplitudes were found to be typically very close, indicating that the cross-shore slope was typically of a smaller scale than the longshore gradient and did not alter it to any significant degree. The reduced size of the large scale SNSCZ slope when compared to the local slope is therefore in some way a product of the longshore scale. The influence of coastal length scale and shape is further discussed in Chapter 6.

5.9.1 The relationship between the longshore pressure gradient and the wind

Gradient time series were found to be strongly correlated with the longshore wind throughout the year with a lag of between 0 and 5 hours. The maximum correlation was typically with winds blowing from S-SW (Table 5.14), in the sense that SW winds led to a piling of water to the north, however during period 6 this relation broke down and the correlation was inverted. Visual inspection of the wind stress time series showed that during period 6 the mean SW wind was almost wholly absent, the main features of the pressure gradient record, a pair of large peaks on the 2nd and 8th of October appear to have been due to a storm surge associated with a strong low pressure system which lay to the south-west of England at the start of the month, travelled north briefly before

returning to the south-west on the 5th and weakening on the 8th (Royal Meteorological Society 1993). Also associated with this system was a 0.5 dbar negative surge which peaked on the 7th.

Longshore pressure gradients were converted to sea-surface slopes by application of the gradient hydrostatic relation

$$\frac{\partial p}{\partial x} = \rho g \frac{\partial \zeta}{\partial x} \qquad 5.9$$

which assumes gradients in atmospheric pressure and water density to be small over the study area. As regards density this is not a reasonable assumption within St. Andrews Bay, however over the large spatial scale of the slope (83 km) small scale localised density changes become unimportant.

The strong correlation during both winter (Figure 5.23) and summer (Figure 5.24) months between the longshore wind and longshore sea-surface gradient (Table 5.14), suggests that throughout 1993 the local wind stress was the dominant factor in slope generation and only under unusual circumstances was a significant pressure gradient generated by non-local forcing alone.

If we assume no longshore slope exists in the absence of wind, regression analysis of wind stress against the longshore pressure gradient for periods 1 to 6 suggests that the relation

$$\tau_x = R \frac{\partial \zeta}{\partial x} \qquad 5.10$$

with τ_x in units of Nm^{-2} best fits a value of $R = 12 \times 10^{-4}$ (Table 5.14). A moderate wind of 8 m s^{-1} ($\tau_x = 0.1$ N m^{-2}) could be expected to produce a longshore slope of 8.2×10^{-7}.

5.10 Discussion

The mean flow regime in the St. Andrews Bay region is typical of a coastal estuarine circulation. The mean circulation in the Bay area consists of a landward flow near the sea-bed, converging on the mouth of the Firth within the Bay. Such a regime has been documented for many regions of freshwater influence in coastal zones, for instance in Delaware Bay by Pape and Garvine (1982). The circulation of Delware Bay was modelled by Beardsley and Hart (1978) who predicted a landward near-bed flow toward the estuary from a distance of the order of tens of kilometres. This is a similar scale to that observed in St. Andrews Bay where a distinct mean flow toward the estuary of the order of 4.5 cm s^{-1} (~4 km day^{-1}) was clearly apparent at M4 and M6 at a distance of 30 km.

Near the surface, mean flow was typically longshore and towards the south, with relatively stable flows being a feature of the outer instruments and the instrument off Fifeness in particular. Tidal rectification could produce stable mean flows at M5[1], however the very stable, relatively high velocity mean currents observed at M4[1], particularly over the summer months, cannot be explained by this process. Study of virtual displacement plots indicates that these highly stable mean currents are insensitive to the direction of the wind stress (Figure 5.3), which, along with the increased stability with distance above the sea-bed, suggest a possible baroclinic origin.

Within the plume itself the data return was relatively poor, however the flow appeared to respond strongly to changes in the local wind direction with flow enhancement in all directions but offshore.

Variability in flow direction was strongly steered by the coastal alignment of sea-bed bathymetry at all depths across the study area except near the sea-bed to the north of the Bay (M1) and beneath the plume near the mouth of the Firth (M2), where variability in the cross-shore flow appears to have been particularly significant. The majority of flow variability at all sites was independent of depth, over 70% on average. Depth dependence in the flow decreased moving offshore with currents at the outer sites showing the least depth dependence (M4, 81% - 93%). Near to the mouth of the Firth haline stratification

leads to a dissociation of surface plume and deeper currents and an associated decrease in the percentage of the variance associated with barotropic motion.

The significance of barotropic variations in flow to the circulation of the study region was confirmed by application of EOF analysis to the flow field. The dominance of barotropic motion in the first few orthogonal modes of an EOF analysis has been observed by Thompson and Pugh (1986) in the Celtic Sea and off the Oregon coast by Kundu *et. al.* (1975). Within the area of the SNSCZ off the Firth of Tay two principal modes of barotropic variability were apparent within the current field during the summer months. These opposingly directed "inner" and "outer" regimes appear to be dominated by a single significant barotropic mode of variability during the winter period. Inclusion of the wind stress within the analysis illustrated the linkage between the wind and barotropic modes. The inner mode appeared to be forced directly by a similarly oriented longshore wind, as did the single winter mode. The "outer mode" observed at M4 and M6 during summer appeared to be associated with an oppositely directed wind stress. This opposition suggests that the forcing factor may have been a longshore pressure gradient set up by the longshore wind. The splitting off of an opposing barotropic mode at the shallow inner stations during the winter periods may be attributed to the depth of the wind driven layer reaching the sea-bed, leading to a flow at all depths largely in the direction of the longshore component of the wind. This wind-driven flow would typically oppose a flow driven by the pressure gradient, since this appears to be typically set up by the same wind but in the opposite direction along the coast. An analysis of the depth of wind-driven and near-bed mixed layers using simple Ekman-type models suggested that within the Bay flow at all depths is likely to be influenced directly by the wind throughout the year, whereas seaward of the Bay, in deeper water, the wind-driven layer is likely to extend to the bottom only during strong winds.

Analysis of daily wind data suggest that a significant onshore wind was a relatively unusual event in this area of the SNSCZ during 1993 and so the effects of coastal set-up would not normally be an important factor in driving the mean local circulation. Specific wave orientated studies were not conducted as part of this research program, however on the basis of the evidence of the wind direction and frequency data we may assume effects associated with waves were also likely to be less important than in many coastal areas as

offshore winds have only a very short fetch and so waves of significant size would not normally occur within the Bay. This suggests that wave related effects such as the Stokes drift and modifications to the effects of wind stress via the action of waves on the sea-bed may be less important within St. Andrews Bay than in other, particularly western, coastal regions of the British Isles.

The direct effect of the wind transmitted via friction to the water column was obviously of primary importance in forcing water movements in the St. Andrews Bay area during 1993, accounting for a large proportion of the variance of current time series at all depths. The response of the water column to wind stress appears to be have been complex and variable even at a single instrument. Application of a simple regression-based model gave an assessment of the extent of the local role of the wind stress based on the assumption of a frictional balance between the surface and bottom stress with no other forcing terms. The wind stress was found to have been important at all mooring positions, but particularly at the inner sites where between a quarter and half of the total variance could be attributed to the direct frictional effect of the wind. A significant problem with this simple model was the strong relation between wind stress and the longshore pressure gradient, which leads to anomalous correlations in the model. This is particularly the case in deeper waters where the role of direct forcing by the wind stress is unlikely to have been as significant as close to the shore but the role of the pressure gradient is likely to be of increasing importance.

EOF analysis of the coastal pressure field during 1993 indicated 86% of the variance was accounted for by the first mode which represented apparently simultaneous raising and lowering of sea level along the coast, the rest of the energy being associated with pivoting of the longshore pressure field. Comparisons of the plotted pressure with weather charts (Royal Meteorological Society, 1993) showed most observed pressure maxima to be associated with strong winds to the north of Scotland over the shelf edge, the forcing factor for most external storm surges (Heaps, 1969). Analysis of the timing of peak values for major events showed the majority of significant peaks to be associated with externally generated storm surges

Comparisons between plotted sea-bed and coastal pressure (using the "periodised" records from M6) and the local wind show little evidence of the "classical" relationship between coastal sea level and the local longshore wind as is often described in the literature (*eg.* Csanady, 1981). Many of these accounts however, deal with the North American oceanic coastal boundary where the offshore length scale is large compared to the scale of weather systems and the shelf edge and therefore deep water, is often in close proximity to the shore, which is not the case in the North Sea. Heaps (1969) described and modelled the response of sea levels within the North Sea to spatially variable wind fields finding a regime which can give rise to locally complex effects via the generation of externally generated storm surges which propagate southwards along the Scottish east coast. Dooley (1971), in an analysis of short-term residual variations off Aberdeen, examined an external storm surge which produced an oscillation in the longshore current with a duration of approximately one day. Variations on such a small scale are smoothed out by the low-pass filter and are unlikely to be of significance to the long term flow regime, however given the presence of consistent large weather systems to the north as occurred during period 1 in particular, storm surges may produce an effect of much longer duration. The North Sea, being a largely enclosed shallow basin with a horizontal scale of the same order as cyclonic weather systems, tends to react to a wind field by piling water against the windward coast. In the case of a non-uniform wind field, for instance, strong winds in the southern North Sea or over the shelf north of Scotland, this can lead to an alteration of coastal sea levels unrelated to the local wind within the SNSCZ and to the generation of large scale longshore pressure gradients which will in turn generate a current. Dooley (1971) identified the cause of differently directed longshore residual flows off Aberdeen to be a non-uniform wind field, with offshore flows (15 km from the shore) largely determined by circulations forced by non-local winds and inshore flows (3 km out) by local winds. He does not however suggest a mechanism for this circulation. The examples he gives indicate that the mechanism for the (largely barotropic) offshore flow was a longshore pressure gradient which can be generated by local or non-local winds. Such a gradient will give rise to an longshore residual current opposing the wind which has generated the slope and which will be typically dominated in shallower water close to the shore by the local wind which gives rise to a windward residual flow.

The strong correlation between the longshore wind and longshore sea-surface gradient suggests that during 1993 the local wind stress was the dominant factor in slope generation and only under unusual circumstances was a significant pressure gradient generated by non-local forcing alone. It is apparent that although coastal sea-level is dominated by large scale variations due to set-up associated with externally generated storm surges, the longshore gradients associated with these events are typically smaller than those generated directly by the frictionally balanced local wind stress. The effect of externally generated slopes will therefore be to either enhance or reduce that produced by the locally generated slope. Regression analysis of the relation between wind stress and the longshore slope found a linear relationship with a wind of 8 m s^{-1} giving rise to a slope of 8.2 x 10^{-7} along the Scottish north-east coast, a value comparable to that found by other researchers. Cragg *et. al.* (1983) found a value of 7.5 x 10^{-7} for the West Florida coast while Marmorino (1983) calculated values twice that for the same region and Pettigrew (1980) found a lower value of 3 x 10^{-7} to be valid off Long Island.

Longshore sea-surface gradients can then be regarded as occurring on two principal scales within the SNSCZ. The local scale due to the frictionally balanced local wind stress along a straight coastline and a larger scale of the order of the dimensions of the North Sea associated with the effects of storm surges.

On a smaller scale highly localised reversals in the longshore pressure gradient over scales of the order of 50 km have been reported by Marmorino (1983) off the Florida coast using calculations from closely separated measuring sites. It is difficult to determine if such reversals occur in the region of St. Andrews Bay as, for instruments as closely sited as the water level recorders within the study area (< 30 km), unimportant small amplitude sea-level variations are large enough to act as noise, producing a signal of the same order as that of interest and obscuring it. Such noise was evident in the small-scale time series presented by Marmorino (1983) even at a separation of 70 km. This problem makes measurement of pressure gradients across St. Andrews Bay itself impossible.

Table 5.1. Tidal ellipse data for M_2, S_2 and M_4 tides.
Bearings are standard clockwise from grid north. Sense of rotation of the tidal vector is given as C, clockwise and A, anticlockwise under phase.

RCM	Tidal Component	Major Axis (cm s^{-1})	Minor Axis (cm s^{-1})	Phase (°)	Orientation (°)
M1[1]	M_2	39.2	0.8	206 C	219
	S_2	14.7	0.1	224 C	221
	M_4	1.9	0.9	266 A	106
M1[2]	M_2	31.8	7.3	184 A	215
	S_2	11.1	2.4	221 A	215
	M_4	2.2	1.6	236 A	175
M2[1]	M_2	25.8	2.8	209 A	194
	S_2	8.1	0.4	226 A	189
	M_4	2.6	1.3	302 C	263
M2[2]	M_2	14.4	8.9	148 A	144
	S_2	4.8	3.3	179 A	139
	M_4	0.9	0.1	256 C	93
M3[1]	M_2	29	1.6	206 A	184
	S_2	10.8	0.8	223 A	184
	M_4	1.8	0.4	294 C	208
M3[2]	M_2	25.3	7.8	181 A	190
	S_2	10.1	2.7	226 A	191
	M_4	0.9	0.2	191 A	209
M4[1]	M_2	31.3	1.4	216 A	193
	S_2	14.1	0.5	240 A	194
	M_4	2.5	0.5	275 A	230
M4[2]	M_2	28.7	8	198 A	201
	S_2	10.4	2.9	230 A	200
	M_4	0.8	0.4	247 A	107
M5[1]	M_2	46.3	3.4	200 A	195
	S_2	16	1.4	224 A	198
	M_4	5.6	2.1	212 A	172
M5[2]	M_2	37.8	2.6	195 A	198
	S_2	12.6	0.2	222 A	196
	M_4	4.4	2.3	245 A	194
M6[1]	M_2	29.7	4.6	175 A	184
	S_2	11.5	1.2	212 A	183
	M_4	1.7	0.1	269 C	239
M6[2]	M_2	25.1	13	169 A	196
	S_2	9.4	5.2	191 A	195
	M_4	0.8	0.3	240 A	262

Table 5.2a. Sub-tidal current statistics.

Mean direction (θ) and orientation of principal axis of variance (ψ) are standard clockwise bearings from grid north. The stability of a record in Cartesian vector form is given by the ratio of the vector mean to the scalar mean speed expressed as a percentage, such that 100% is a totally stable flow. Columns headed $\sigma_{11}^{½}$ and $\sigma_{22}^{½}$ give the standard deviation of the record along the principal and minor axes of variance respectively. The right-hand column gives a measure of isotrophy for the sub-tidal flow, with a value of 1 indicating isotropic flow and 0 rectilinear flow.

RCM	Period	Mean speed ($cm\ s^{-1}$)	θ (°)	Stability	Total variance (cm^2s^{-2})	$\sigma_{11}^{½}$ ($cm\ s^{-1}$)	$\sigma_{22}^{½}$ ($cm\ s^{-1}$)	ψ (°)	$(\sigma_{22}/\sigma_{11})^{½}$
M1[1]	1	3.8	25	8	19.5	4.0	1.9	226	0.48
	2	2.9	177	58	7.3	2.4	1.3	242	0.53
	3	1.9	205	26	4.4	1.8	1.0	219	0.55
	4	4.2	240	75	12.5	3.3	1.4	211	0.42
	5	3.0	229	75	6.1	2.2	1.1	233	0.49
	6	5.5	245	67	32.3	5.4	1.8	227	0.34
	7	3.4	6	32	26.2	5.0	1.2	222	0.24
M1[2]	1	6.8	308	90	18.2	3.2	2.8	143	0.88
	2	5.0	304	90	10.1	2.6	1.8	168	0.68
	3	4.1	357	86	5.4	2.0	1.2	249	0.63
	4	3.9	310	71	10.0	2.7	1.6	200	0.58
	5	4.6	309	95	6.9	2.5	0.9	110	0.38
	6	5.2	318	76	15.3	3.3	2.0	198	0.61
	7	4.9	332	80	19.9	4.2	1.5	224	0.35
M2[1]	3	9.4	262	57	86.5	7.5	5.5	179	0.73
	4	7.9	212	47	66.0	7.0	4.1	176	0.58
M2[2]	1	7.2	338	92	26.1	4.9	1.5	155	0.31
	2	4.6	1	84	12.3	3.2	1.5	161	0.47
	3	4.3	14	78	12.8	3.1	1.7	147	0.56
	4	3.3	51	44	12.5	3.1	1.7	147	0.57
	5	4.0	10	83	9.8	2.7	1.7	176	0.62
	6	4.8	37	54	23.3	4.7	1.1	171	0.24
	7	4.4	3	81	20.8	4.1	1.9	152	0.47
M3[1]	1	5.5	106	11	41.0	5.9	2.6	188	0.44
	6	5.0	196	78	17.5	3.7	2.0	170	0.54
	7	4.1	218	52	17.6	3.8	1.8	171	0.47
M3[2]	3	2.6	234	35	8.4	2.7	1.0	188	0.38
	4	2.2	225	47	5.8	2.2	1.0	205	0.46
	6	2.8	295	29	21.0	4.4	1.2	197	0.26
	7	2.8	295	5	12.8	3.3	1.5	191	0.45
M4[1]	2	6.9	206	50	44.8	5.9	3.2	214	0.53
	3	6.0	245	93	13.1	3.2	1.8	219	0.56
	5	7.6	227	92	20.0	3.9	2.2	201	0.57
	6	6.6	237	84	22.1	4.4	1.7	200	0.39
	7	5.1	219	68	21.2	4.3	1.7	205	0.4
M4[2]	2	4.9	312	17	36.0	5.8	1.5	215	0.25
	3	2.9	280	52	8.0	2.6	1.1	209	0.42
	4	3.1	248	40	12.5	3.4	1.0	209	0.29
	5	3.3	283	51	10.6	3.1	1.0	210	0.31
	6	5.2	278	37	30.3	5.3	1.4	202	0.26
	7	4.7	290	54	22.5	4.5	1.5	204	0.32

Table 5.2b. Sub-tidal current statistics.

Mean direction (θ) and orientation of principal axis of variance (ψ) are standard clockwise bearings from grid north.

RCM	Period	Mean speed ($cm\ s^{-1}$)	θ (°)	Stability	Total variance (cm^2s^{-2})	$\sigma_{11}^{½}$ ($cm\ s^{-1}$)	$\sigma_{22}^{½}$ ($cm\ s^{-1}$)	ψ (°)	$(\sigma_{22}/\sigma_{11})^{½}$
M5[1]	1	6.4	109	38	44.4	6.5	1.6	201	0.24
	2	6.7	166	84	19.2	4.0	1.8	204	0.44
	3	8.7	168	96	20.0	4.0	2.0	195	0.48
	4	9.8	159	91	33.8	5.5	1.9	202	0.34
	5	7.0	162	96	8.0	2.4	1.6	144	0.66
	7	5.7	171	73	24.3	4.7	1.3	196	0.28
M5[2]	1	4.3	355	60	18.9	4.0	1.6	191	0.39
	2	3.6	255	52	12.9	3.2	1.6	183	0.5
	3	3.7	228	52	14.2	3.4	1.6	201	0.48
	4	3.4	282	79	5.8	2.1	1.2	185	0.56
	7	3.1	154	1	17.2	3.9	1.3	191	0.32
M6[1]	2	5.8	230	21	44.4	6.3	2.2	192	0.34
	3	4.5	209	78	13.7	3.2	1.9	182	0.6
	4	4.7	206	79	14.4	3.3	1.8	199	0.55
	5	3.9	233	55	16.9	3.8	1.7	221	0.45
	6	4.7	193	67	22.0	4.4	1.7	205	0.38
	7	4.6	224	51	21.3	4.2	2.0	190	0.47
M6[2]	2	5.4	326	69	35.0	5.8	1.4	186	0.24
	3	2.8	297	61	7.2	2.3	1.4	183	0.6
	4	2.6	260	60	7.2	2.3	1.3	189	0.57
	5	2.9	290	64	7.3	2.5	1.1	179	0.45
	6	6.1	292	33	44.1	6.4	1.8	181	0.29
	7	4.3	301	47	23.7	4.6	1.7	186	0.36

Table 5.3. Wind stress (τ) statistics.

Mean direction (θ) and orientation of principal axis of variance (ψ) are standard clockwise bearings from grid north. θ given as angle wind blows to (*ie.* in the same sense as currents). The stability of a record in Cartesian vector form is given by the ratio of the vector mean to the scalar mean speed expressed as a percentage, such that 100% is a totally stable flow. Columns headed $\sigma_{11}^{½}$ and $\sigma_{22}^{½}$ give the standard deviation of the record along the principal and minor axes of variance respectively. The right-hand column gives a measure of isotrophy for the sub-tidal flow, with a value of 1 indicating isotropic flow and 0 rectilinear flow.

Period	τ (Nm^{-2})	θ (°)	Stability	Total variance (N^2m^{-4})	$\sigma_{11}^{½}$ (Nm^{-2})	$\sigma_{22}^{½}$ (Nm^{-2})	ψ (°)	$(\sigma_{11}/\sigma_{22})^{½}$
1	0.122	54	95	0.0100	0.088	0.047	228	0.53
2	0.051	75	77	0.0044	0.063	0.020	248	0.32
3	0.024	347	39	0.0010	0.028	0.014	263	0.5
4	0.029	247	39	0.0014	0.036	0.010	237	0.28
5	0.031	65	51	0.0015	0.037	0.010	254	0.26
6	0.029	248	46	0.0017	0.035	0.023	251	0.66
7	0.029	7	76	0.0020	0.038	0.022	154	0.57

Table 5.4. Depth Mean Current Statistics.

Mean direction (θ) and orientation of principal axis of variance (ψ) are standard clockwise bearings from grid north. β represents the depth dependance of the flow (see text) such that a value of 1 indicates that the motion is independant of depth, a value of 0 that the depth-mean current is zero. Columns headed $\sigma_{11}^{1/2}$ and $\sigma_{22}^{1/2}$ give the standard deviation of the record along the principal and minor axes of variance respectively

Mooring	Period	Mean speed ($cm\ s^{-1}$)	θ (°)	Total variance ($cm^2 s^{-2}$)	$\sigma_{11}^{1/2}$ ($cm\ s^{-1}$)	$\sigma_{22}^{1/2}$ ($cm\ s^{-1}$)	ψ (°)	β
M1	1	4.3	311	11.6	3.1	1.5	205	0.62
	2	2.7	284	5.4	1.9	1.3	213	0.62
	3	2.5	2	2.8	1.4	0.9	245	0.58
	4	3.6	272	9.3	2.9	1.1	204	0.83
	5	3.0	284	3.8	1.6	1.0	93	0.58
	6	4.8	283	17.7	3.8	1.8	215	0.75
	7	3.7	339	21.0	4.5	1.0	222	0.91
M2	3	4.6	299	22.7	4.1	2.4	164	0.46
	4	4.4	200	24.3	4.5	2.0	173	0.62
M3	6	3.8	190	13.6	3.6	1.0	190	0.71
	7	2.9	221	11.9	3.3	1.1	183	0.78
M4	2	5.5	220	37.4	5.8	2.0	214	0.93
	3	4.0	252	8.6	2.7	1.1	209	0.82
	5	4.8	237	12.4	3.2	1.4	205	0.81
	6	5.3	247	22.5	4.6	1.3	202	0.86
	7	4.5	248	19.6	4.2	1.3	205	0.90
M5	1	4.6	50	28.0	5.1	1.4	196	0.88
	2	4.2	185	13.5	3.4	1.3	193	0.84
	3	4.9	179	9.6	3.0	0.9	190	0.56
	4	4.3	176	13.4	3.6	0.8	197	0.68
	7	3.8	171	17.9	4.1	1.1	193	0.86
M6	2	5.1	307	35.9	5.9	1.1	189	0.90
	3	3.0	235	7.9	2.5	1.2	185	0.75
	4	3.1	222	7.2	2.5	1.1	195	0.67
	5	3.1	259	9.0	2.8	1.0	205	0.74
	6	4.6	227	26.6	5.1	1.0	190	0.80
	7	4.0	259	18.9	4.2	1.1	189	0.84

Table 5.5. Low pass filtered current meter records included in the EOF analysis.

Period	$M1^1$	$M1^2$	$M2^1$	$M2^2$	$M3^1$	$M3^2$	$M4^1$	$M4^2$	$M5^1$	$M5^2$	$M6^1$	$M6^2$
1	*	*		*					*	*		
2	*	*		*			*	*	*	*	*	*
3	*		*	*		*	*	*	*	*	*	*
4	*	*	*	*		*		*	*	*	*	*
5	*	*		*			*	*			*	*
6	*	*		*	*	*	*	*			*	*
7	*	*		*	*	*	*	*	*	*	*	*

Table 5.6. Percentage of the variance of the total dataset for each period explained by the first four eigenmodes.

Period	e_1	e_2	e_3	e_4
1	40	20	15	10
2	25	23	19	8
3	24	15	14	10
4	29	20	12	9
5	32	23	12	9
6	35	19	13	9
7	36	16	14	10

Table 5.7a. Correlations between wind stress and sub-tidal currents resolved along the principal axis of variability, positive to south.

Only correlations in excess of 90% significance are presented (coefficient of 1.70), a correlation coefficient of 2.00 is 95% significant, a coefficient of 2.60 is 99% significant (Sciremmanno 1979). Data are presented for maximum normalised zero lag (n.z.l.) correlations and maximum lagged correlations (up to 24 hours). α is the optimum angle of correlation of the wind stress with the current, given firstly as the angle between wind and current ($-180 < \alpha \leq 180$), such that positive is a response to the right of the wind, and secondly as a standard bearing from grid north (wind blowing to).

RCM	Period	Maximum n. z. l.	α (°)	Degrees freedom	Maximum correlation	Lag (h)	α (°)	Degrees freedom
M1[1]	1	2.76	40, 188	19	2.76	0	40, 186	19
	2	2.60	70, 172	29	2.60	0	70, 172	29
	3	3.12	60, 159	28	3.15	3	60, 159	28
	4	4.33	35, 176	33	4.51	9	35, 176	33
	5	3.51	175, 58	41	3.51	0	175, 58	41
	6	2.89	55, 172	18	3.01	9	50, 177	19
	7	4.12	90, 132	25	4.31	8	95, 127	25
M1[2]	1	2.61	-60, 203	19	3.41	21	-50, 193	19
	2	3.56	-35, 203	28	4.64	24	-45, 213	28
	3	2.03	-115, 4	14	2.03	0	-115, 4	14
	4	4.11	25, 175	34	4.41	11	20, 180	34
	5	3.53	160, 310	41	3.53	0	160, 310	41
	6	2.96	15, 183	23	3.15	8	10, 188	23
	7	3.46	105, 119	27	4.07	14	105, 119	27
M2[1]	3	3.36	10, 169	27	3.36	0	10, 169	27
	4	3.12	15, 161	35	3.41	15	15, 161	35
M2[2]	1	2.78	-80, 235	21	2.79	2	-80, 235	21
	2	4.05	-95, 256	29	4.11	8	-90, 251	29
	3	2.72	-90, 237	23	2.72	0	-90, 237	23
	4	4.02	-40, 187	34	4.03	2	-35, 182	34
	5	2.31	-140, 315	45	3.24	24	-155, 331	47
	6	2.98	-35, 206	21	2.98	0	-35, 206	21
	7	3.31	10, 142	26	3.60	10	10, 142	26
M3[1]	1	2.14	25, 163	12	2.39	18	30, 158	12
	6	2.55	-10, 180	23	2.56	3	-10, 270	23
	7	2.99	80, 91	21	3.22	12	80, 91	21
M3[2]	3	ns	-	-	2.50	24	-150, 338	27
	4	1.98	20, 185	35	3.57	24	35, 170	36
	6	2.84	-30, 227	19	3.00	13	-40, 237	18
	7	1.96	90, 101	27	2.15	11	95, 96	27
M4[1]	2	1.99	-135, 349	29	3.44	24	-125, 339	30
	3	ns	-	-	ns	-	-	-
	5	5.03	130, 71	42	5.04	1	130, 71	42
	6	ns	-	-	ns	-	-	-
	7	ns	-	-	1.78	24	145, 60	20
M4[2]	2	2.06	-145, 0	29	3.02	24	-130, 345	30
	3	ns	-	-	2.73	24	-135, 344	27
	4	1.77	-125, 334	37	1.77	0	-125, 334	37
	5	2.83	-150, 0	43	3.29	22	-150, 0	43
	6	ns	-	-	1.85	24	-90, 342	15
	7	1.84	145, 59	19	2.32	24	155, 49	20

Table 5.7b.

RCM	Period	Maximum n. z. l.	α (°)	Degrees freedom	Maximum correlation	Lag (h)	α (°)	Degrees freedom
M5[1]	1	2.93	15, 186	19	2.97	5	15, 186	19
	2	4.31	10, 194	28	4.31	0	10, 194	28
	3	2.74	15, 180	24	2.74	0	15, 180	24
	4	4.31	40, 162	36	4.42	6	40, 162	36
	5	3.02	25, 119	15	3.02	0	25, 119	15
	7	2.77	40, 156	26	2.77	2	45, 151	26
M5[2]	1	2.52	10, 181	20	2.61	8	15, 176	20
	2	3.69	-70, 250	29	3.69	0	-70, 250	29
	3	2.04	-60, 261	23	2.78	24	-120, 321	24
	4	3.89	-5, 190	34	4.43	14	0, 185	35
	7	2.28	85, 106	24	2.32	4	85, 106	24
M6[1]	2	1.98	140, 52	29	2.14	24	-150, 342	30
	3	1.85	70, 112	26	1.85	0	70, 112	26
	4	2.10	-110, 309	32	2.10	0	-110, 309	32
	5	3.00	-180, 41	40	3.17	14	-170, 31	40
	6	ns	-	-	ns	-	-	-
	7	ns	-	-	1.75	24	140, 50	20
M6[2]	2	ns	-	-	2.54	24	-150, 336	30
	3	ns	-	-	2.14	24	-160, 343	26
	4	2.05	-145, 284	36	2.05	0	-145, 334	36
	5	3.19	-180, 359	42	3.70	23	-180, 359	42
	6	1.78	-90, 271	16	2.12	24	-120, 301	14
	7	ns	-	-	ns	-	-	-

Table 5.8a. Correlations between wind stress and sub-tidal currents resolved along the minor axis of variability, positive offshore.

Only correlations in excess of 90% significance are presented (coefficient of 1.70), a correlation coefficient of 2.00 is 95% significant, a coefficient of 2.60 is 99% significant (Sciremmanno 1979). Data are presented for maximum normalised zero lag (n.z.l.) correlations and maximum lagged correlations (up to 24 hours). α is the optimum angle of correlation of the wind stress with the current, given firstly as the angle between wind and current ($-180 < \alpha \leq 180$), such that positive is a response to the right of the wind, and secondly as a standard bearing from grid north (wind blowing to).

RCM	Period	Maximum n. z. l.	α (°)	Degrees freedom	Maximum correlation	Lag (h)	α (°)	Degrees freedom
M1[1]	1	ns	-	-	ns	-	-	-
	2	2.29	100, 52	29	2.29	0	100, 52	29
	3	2.33	-175, 304	25	2.39	6	-170, 309	25
	4	ns	-	-	ns	-	-	-
	5	ns	-	-	ns	-	-	-
	6	2.20	-95, 232	21	2.20	0	-95, 232	21
	7	ns	-	-	ns	-	-	-
M1[2]	1	ns	-	-	1.71	24	155, 258	21
	2	ns	-	-	1.70	24	-75,153	31
	3	2.76	-85, 244	13	2.76	1	-80, 249	13
	4	2.79	-25, 135	32	2.83	7	-30,140	33
	5	2.50	10, 10	47	3.18	19	20,0	49
	6	2.03	-160, 268	18	2.03	0	-160, 268	18
	7	ns	-	-	ns	-	-	-
M2[1]	3	2.89	25, 64	22	2.89	0	25, 64	22
	4	ns	-	-	1.97	24	-60, 146	36
M2[2]	1	ns	-	-	ns	-	-	-
	2	2.61	110, 321	33	2.61	0	110, 321	33
	3	ns	-	-	ns	-	-	-
	4	ns	-	-	1.95	24	55, 2	34
	5	3.53	-100, 186	46	3.53	0	-100, 186	46
	6	1.99	-110, 191	29	1.99	0	-110, 191	29
	7	2.00	-160, 222	20	2.14	14	-160, 222	20
M3[1]	1	ns	-	-	ns	-	-	-
	6	ns	-	-	ns	-	-	-
	7	ns	-	-	ns	-	-	-
M3[2]	3	2.41	-100, 198	26	2.41	0	-100, 198	26
	4	2.77	-50, 165	38	2.77	0	-50, 165	38
	6	1.74	-100, 207	29	1.74	0	-100, 207	29
	7	2.65	-120, 221	22	2.92	16	-115, 216	23
M4[1]	2	4.14	40, 84	28	4.16	4	50, 74	28
	3	ns	-	-	3.13	24	175, 314	25
	5	ns	-	-	ns	-	-	-
	6	ns	-	-	ns	-	-	-
	7	2.64	30, 85	21	2.69	7	30, 85	21
M4[2]	2	ns	-	-	ns	-	-	-
	3	ns	-	-	ns	-	-	-
	4	1.78	-45, 164	38	1.78	1	-45, 164	38
	5	2.82	170, 310	44	2.82	0	170, 310	44
	6	1.73	-110,222	21	1.73	0	-110, 222	21
	7	1.91	-30, 144	26	1.92	2	-30,144	26

Table 5.8b.

RCM	Period	Maximum n. z. l.	α (°)	Degrees freedom	Maximum correlation	Lag (h)	α (°)	Degrees freedom
M5[1]	1	ns	-	-	2.55	24	70, 41	20
	2	ns	-	-	ns	-	-	-
	3	ns	-	-	ns	-	-	-
	4	1.78	-25, 137	33	1.95	13	-30, 142	34
	5	ns	-	-	1.89	11	70, 344	18
	7	ns	-	-	ns	-	-	-
M5[2]	1	ns	-	-	ns	-	-	-
	2	2.30	140, 313	31	2.30	0	140, 313	31
	3	1.84	-140, 251	24	1.88	7	-130, 241	24
	4	2.05	-85, 180	37	2.05	0	-85, 180	37
	7	ns	-	-	ns	-	-	-
M6[1]	2	2.36	80, 22	30	2.36	0	80, 22	30
	3	1.92	95, 357	25	1.92	0	95, 357	25
	4	ns	-	-	2.12	24	150, 319	35
	5	ns	-	-	ns	-	-	-
	6	ns	-	-	ns	-	-	-
	7	2.19	45, 55	23	2.19	0	45, 55	23
M6[2]	2	ns	-	-	ns	-	-	-
	3	1.83	-75, 168	27	1.83	0	-75, 168	27
	4	3.49	-80, 179	36	3.53	5	-75, 174	37
	5	2.93	140, 309	45	3.05	14	135, 314	46
	6	3.44	-90, 181	22	3.44	0	-90,181	22
	7	2.52	-80, 176	24	2.78	17	-70, 166	25

Table 5.9a. Relationships between currents (in m s^{-1}) and local wind stress (Nm^{-2}) for the Coastal Model.

R_c is the slope of the regression between wind stress and current, $\sigma_{c11}{}^{½}$ and $\sigma_{c22}{}^{½}$ are the standard deviations of the current vector time series (in the direction of the principal and minor axes of variance) as predicted by the model, while V% gives the percentage of the variance of the original, observed, current time series explained by the model.

RCM	Period	Principal axis R_c ($x10^2$)	Principal axis $\sigma_{c11}{}^{½}$ (m s^{-1})	Principal axis V%	Minor axis R_c ($x10^2$)	Minor axis $\sigma_{c11}{}^{½}$ (m s^{-1})	Minor axis V%
M1[1]	1	33	2.5	34	8	0.7	2
	2	47	1.2	18	9	0.6	4
	3	69	1.1	26	20	0.5	5
	4	150	2.6	52	21	0.2	1
	5	35	1.2	24	26	0.3	1
	6	160	3.6	44	26	0.9	2
	7	116	4.3	70	9	0.3	<1
M1[2]	1	29	2.5	34	13	1.1	6
	2	45	2.3	53	26	0.6	3
	3	63	1	19	28	0.9	17
	4	122	2	41	63	0.8	6
	5	67	1.3	26	32	0.4	3
	6	88	2.2	31	28	0.9	6
	7	98	3.3	56	3	0.1	<1
M2[1]	3	329	4.7	26	123	3.4	13
	4	352	4	24	134	1.3	3
M2[2]	1	34	3	34	9	0.5	1
	2	40	2.5	50	25	0.7	4
	3	67	1.8	25	30	0.5	2
	4	107	2.1	36	27	0.6	3
	5	113	1.2	15	53	0.9	8
	6	102	3	39	15	0.4	1
	7	77	2.9	41	38	0.9	4
M3[1]	1	62	4.1	40	15	1.1	3
	6	79	1.9	21	17	0.4	1
	7	101	2.7	40	21	0.5	1
M32	3	81	1.3	19	27	0.5	3
	4	79	1.3	29	32	0.5	4
	6	92	3	43	12	0.4	1
	7	46	1.3	14	38	1	7
M4[1]	2	144	3.4	25	39	2.5	14
	3	64	0.9	7	51	1.1	9
	5	83	3	46	45	0.5	1
	6	60	1.6	11	6	0.1	<1
	7	64	1.5	11	40	1	5
M4[2]	2	151	3.3	29	15	0.3	<1
	3	91	1.3	22	6	0.2	<1
	4	92	1	8	21	0.3	1
	5	123	1.6	25	18	0.4	2
	6	71	2.4	18	16	0.5	1
	7	109	2.4	26	16	0.6	2

Table 5.9b.

RCM	Period	Principal axis R_c ($x10^2$)	Principal axis $\sigma_{c11}^{1/2}$ ($m\ s^{-1}$)	Principal axis V%	Minor axis R_c ($x10^2$)	Minor axis $\sigma_{c11}^{1/2}$ ($m\ s^{-1}$)	Minor axis V%
M5[1]	1	58	4.4	43	10	0.9	2
	2	81	3.3	56	6	0.3	1
	3	150	2.2	24	14	0.3	1
	4	308	4.1	49	59	0.6	1
	5	69	1.9	43	76	0.7	6
	7	67	2.6	27	17	0.4	1
M5[2]	1	32	2.3	29	5	0.4	1
	2	35	2.2	38	21	0.7	4
	3	96	1.9	25	2	0.6	3
	4	69	1.6	43	19	0.4	3
	7	61	1.9	20	10	0.4	<1
M6[1]	2	110	2.5	14	21	1	2
	3	45	1.2	10	50	0.7	4
	4	95	1.2	10	61	0.7	3
	5	73	2	23	20	0.4	1
	6	32	1	5	21	0.5	1
	7	61	1.4	9	41	0.9	4
M6[2]	2	133	2.7	21	9	0.4	<1
	3	63	1	13	33	0.5	3
	4	75	0.8	9	38	0.8	9
	5	115	1.5	29	24	0.5	4
	6	93	3.1	22	54	1.3	4
	7	27	0.9	3	26	0.9	4

Table 5.10. The depth of the wind-driven layer as predicted by the theoretical "Ekman" relation.

Wind speed ($m\ s^{-1}$)	2	4	6	8	10	12	14	16	18	20
Layer depth (m)	8	16	24	32	40	48	56	65	73	81

Table 5.11. Statistics of sea level (S.L.) and total pressure (T.P.) recorded at coastal tide gauges.

Maxima and minima are relative to the mean value. $\sigma^{1/2}$ is the standard deviation, Corr. a.p. is the coefficient of the correlation with atmospheric pressure where values of 1.7, 2.0 and 2.6 represent significance levels of 90%, 95% and 99% respectively.

	S.L. $\sigma^{1/2}$ (m)	S.L. max (m)	S.L min (m)	S.L. Corr. a.p.	T.P. $\sigma^{1/2}$ (dbar)	T.P. max (dbar)	T.P. min (dbar)	T.P. Corr. a.p.
Wick	0.17	0.74	-0.38	-4.45	0.13	0.45	-0.44	0.30
Aberdeen	0.15	0.60	-0.31	-4.61	0.11	0.41	-0.33	1.26
Leith	0.11	0.37	-0.28	-5.11	0.09	0.35	-0.38	3.59

Table 5.12. Coastal and water level recorder pressure statistics (in dbar).
Maxima and minima are relative to the mean value for the period. Superscripts (W) signify water level recorders deployed in St. Andrews Bay.

Instrument	Period	$\sigma^{1/2}$	Maximum	Minimum
Wick	1	0.139	0.251	-0.273
	2	0.123	0.230	-0.251
	3	0.069	0.198	-0.109
	4	0.084	0.146	-0.229
	5	0.044	0.126	-0.101
	6	0.126	0.279	-0.392
	7	0.080	0.216	-0.210
Aberdeen	1	0.116	0.264	-0.257
	2	0.113	0.264	-0.193
	3	0.071	0.157	-0.172
	4	0.074	0.121	-0.255
	5	0.042	0.087	-0.118
	6	0.099	0.216	-0.332
Leith	1	0.099	0.219	-0.239
	2	0.090	0.333	-0.152
	3	0.066	0.097	-0.190
	4	0.066	0.114	-0.303
	5	0.054	0.110	-0.135
	6	0.103	0.162	-0.348
	7	0.071	0.131	-0.245
M1^{W}	1	0.107	0.212	-0.203
	2	0.092	0.299	-0.170
	3	0.090	0.150	-0.233
	4	0.068	0.131	-0.268
	5	0.078	0.135	-0.204
	6	0.115	0.203	-0.359
	7	0.253	0.484	-0.310
M2^{W}	6	0.111	0.189	-0.354
	7	0.196	0.311	-0.274
M4^{W}	6	0.118	0.224	-0.373
	7	0.066	0.121	-0.199
M6^{W}	2	0.105	0.336	-0.156
	3	0.070	0.137	-0.181
	4	0.071	0.135	-0.288
	5	0.050	0.101	-0.137
	6	0.119	0.217	-0.378
	7	0.069	0.125	-0.195

Table 5.13. Summary of EOF analyses of sub-tidal total sea pressure variations.

The first figure in columns 4-10 is the eigenvector corresponding to a given mode, the figure in brackets is the percentage variance explained for each record. The total variance explained by each mode appears in column 2.

Period	Mode	Total variance (%)	Wick	Aberdeen	M1	M2	M4	M6	Leith
1	1	80	-0.46 (68)	-0.53 (91)	-0.53 (90)	*	*	*	-0.47 (71)
	2	18	0.65 (30)	0.30 (6)	-0.32 (7)	*	*	*	-0.62 (27)
	3	1	-0.24 (<1)	0.56 (1)	-0.70 (2)	*	*	*	-0.38 (1)
2	1	85	-0.41 (70)	-0.48 (97)	-0.43 (77)	*	*	-0.47 (96)	-0.45 (86)
	2	9	0.79 (29)	0.20 (2)	-0.38 (7)	*	*	-0.16 (1)	-0.41 (8)
	3	5	0.13 (<1)	-0.12 (<1)	0.82 (16)	*	*	-0.30 (2)	-0.45 (5)
3	1	90	-0.40 (71)	-0.47 (99)	-0.46 (93)	*	*	-0.47 (98)	-0.45 (89)
	2	8	0.83 (29)	0.11 (<1)	-0.20 (2)	*	*	-0.17 (1)	-0.47 (9)
	3	1	0.00 (0)	-0.24 (<1)	0.87 (5)	*	*	-0.31 (1)	-0.31 (1)
4	1	91	-0.42 (79)	-0.46 (97)	-0.47 (99)	*	*	-0.47 (99)	-0.43 (83)
	2	8	0.72 (21)	0.21 (2)	-0.11 (<1)	*	*	-0.15 (1)	-0.64 (17)
	3	<1	-0.55 (1)	0.68 (1)	0.07 (<1)	*	*	0.16 (<1)	-0.45 (<1)
5	1	87	-0.39 (68)	-0.47 (95)	-0.45 (90)	*	*	-0.47 (96)	-0.45 (86)
	2	10	0.80 (32)	0.19 (2)	-0.18 (2)	*	*	-0.23 (3)	-0.49 (12)
	3	2	0.07 (<1)	-0.40 (2)	0.85 (8)	*	*	-0.26 (1)	-0.23 (1)
6	1	96	-0.36 (89)	-0.38 (95)	-0.38 (99)	-0.38 (99)	-0.38 (99)	-0.38 (99)	-0.37 (93)
	2	2	-0.76 (9)	0.15 (<1)	-0.23 (1)	-0.05 (<1)	0.16 (<1)	0.16 (<1)	0.55 (5)
	3	1	0.37 (1)	0.63 (3)	-0.56 (2)	-0.31 (1)	-0.14 (<1)	-0.10 (<1)	0.15 (<1)
7	1	56	-0.37 (46)	*	-0.26 (23)	-0.35 (42)	-0.48 (78)	-0.53 (95)	-0.40 (53)
	2	31	0.05 (1)	*	0.63 (74)	0.53 (54)	-0.32 (19)	-0.07 (1)	-0.46 (40)
	3	11	0.92 (53)	*	-0.17 (2)	-0.17 (2)	-0.08 (<1)	-0.19 (2)	-0.24 (4)

Table 5.14 Standard deviations and maximum correlations with the wind stress for the longshore sea surface gradient.

$\sigma^{1/4}$ $\delta\varsigma$ /δx represents the standard deviation of the longshore gradient. Correlations are given using the method of Sciremammamo (1979) with hourly lags bracketed, angles are for wind blowing to and are given as standard bearings from grid north. R is the slope of the regression line between the daily mean gradient (x 10^7)and an alongshore wind resolved along a bearing of 225° from grid north, the orientation of the coastline between St. Andrews Bay and Aberdeen.

Period	1	2	3	4	5	6
$\sigma^{1/4}$ $\delta\varsigma$ /δx x 10^7	6.12	3.67	1.69	2.24	2.02	4.29
Max. corr. with wind stress	3.66 (3)	4.43 (5)	3.43 (11)	4.91 (0)	5.66 (0)	3.34 (20)
Angle of max. corr (°)	30	355	10	45	15	245
R x 10^{-4}	13.4	10.9	9.1	12.6	12.6	-3.7

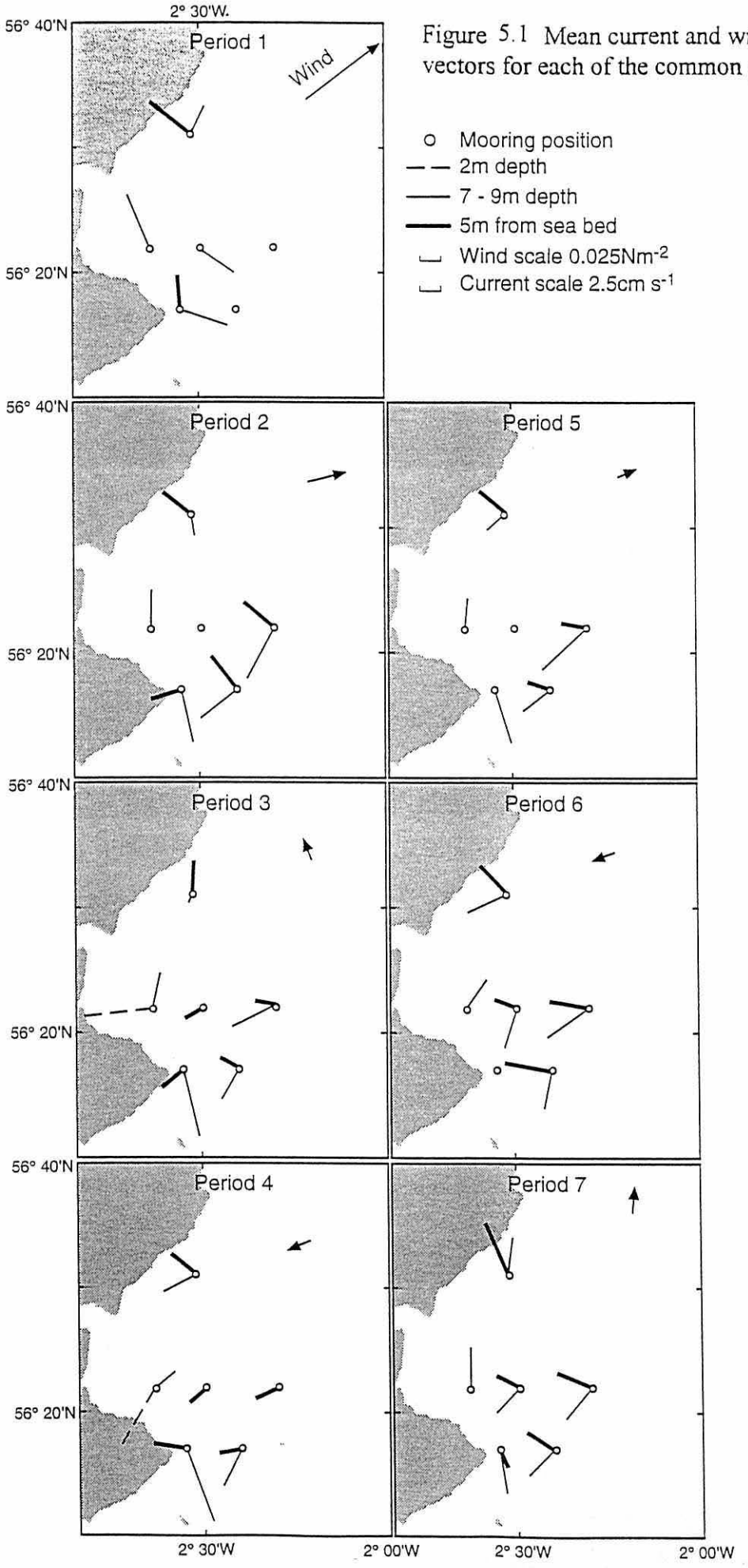

Figure 5.1 Mean current and wind residual vectors for each of the common periods

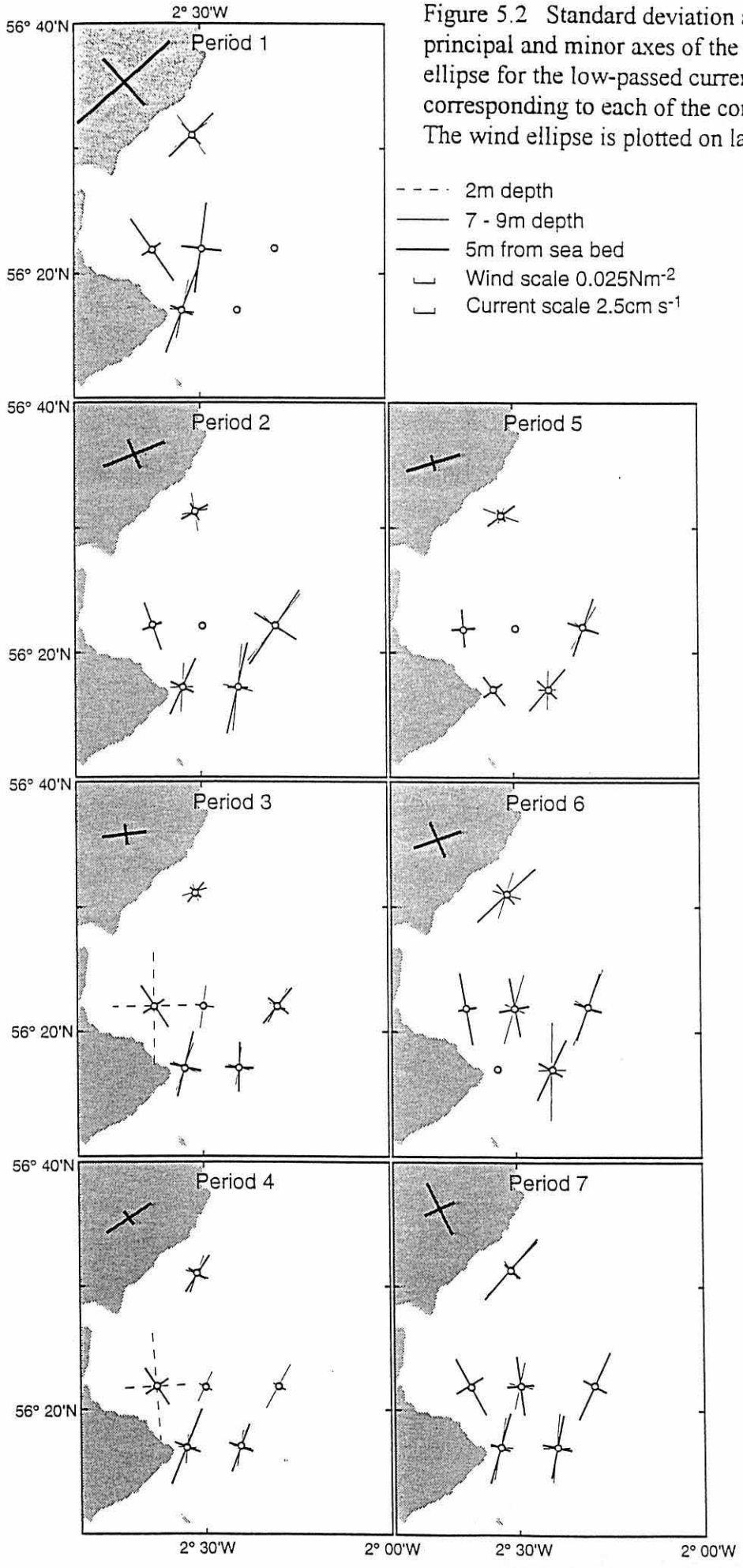

Figure 5.2 Standard deviation along the principal and minor axes of the variance ellipse for the low-passed current records corresponding to each of the common periods. The wind ellipse is plotted on land.

Figure 5.3a Virtual displacement plot for the low-passed flow during period 3 measured at M4[1]. Dashes are at 5 day intervals from the start of the record.

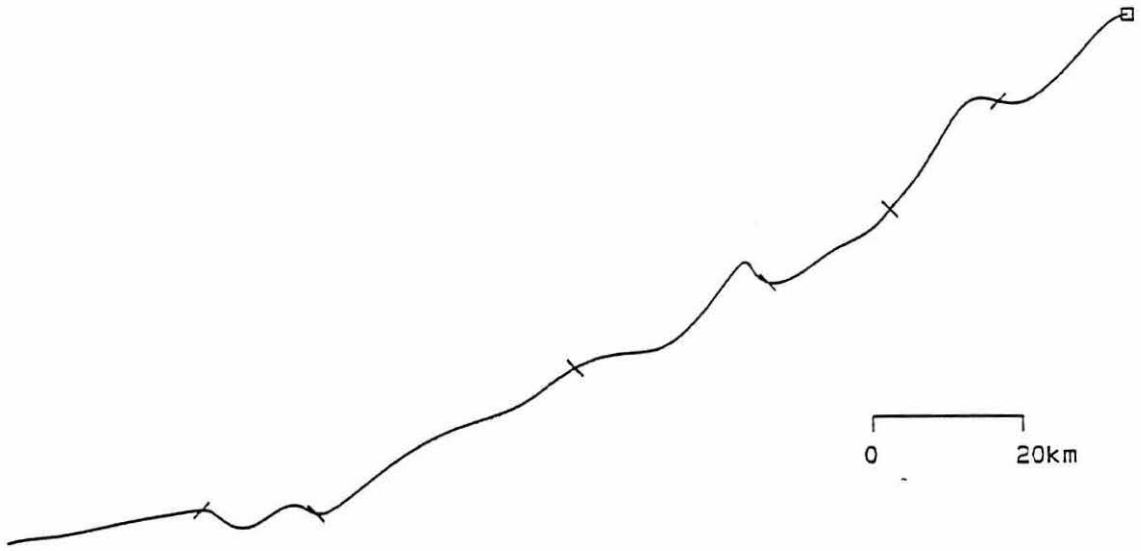

Figure 5.3b Virtual displacement plot for the low-passed wind during period 3. dashes are at 5 day intervals from the start of the record.

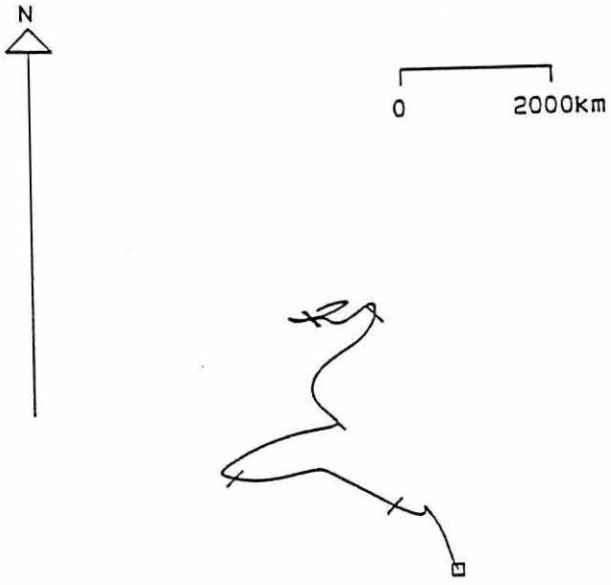

Figure 5.4 Current vectors representing the circulatory pattern corresponding to the first and second empirical modes (e_1 and e_2) of the residual circulation of St. Andrews Bay during winter (period 7). The relative length of a vector indicates the relative importance of variability at a given RCM within the mode. The orientation of the vector shows the direction of movement within the mode. T is given as a figure next to each vector and quantifies the proportion of the total variance of the record at a given RCM associated with each mode.

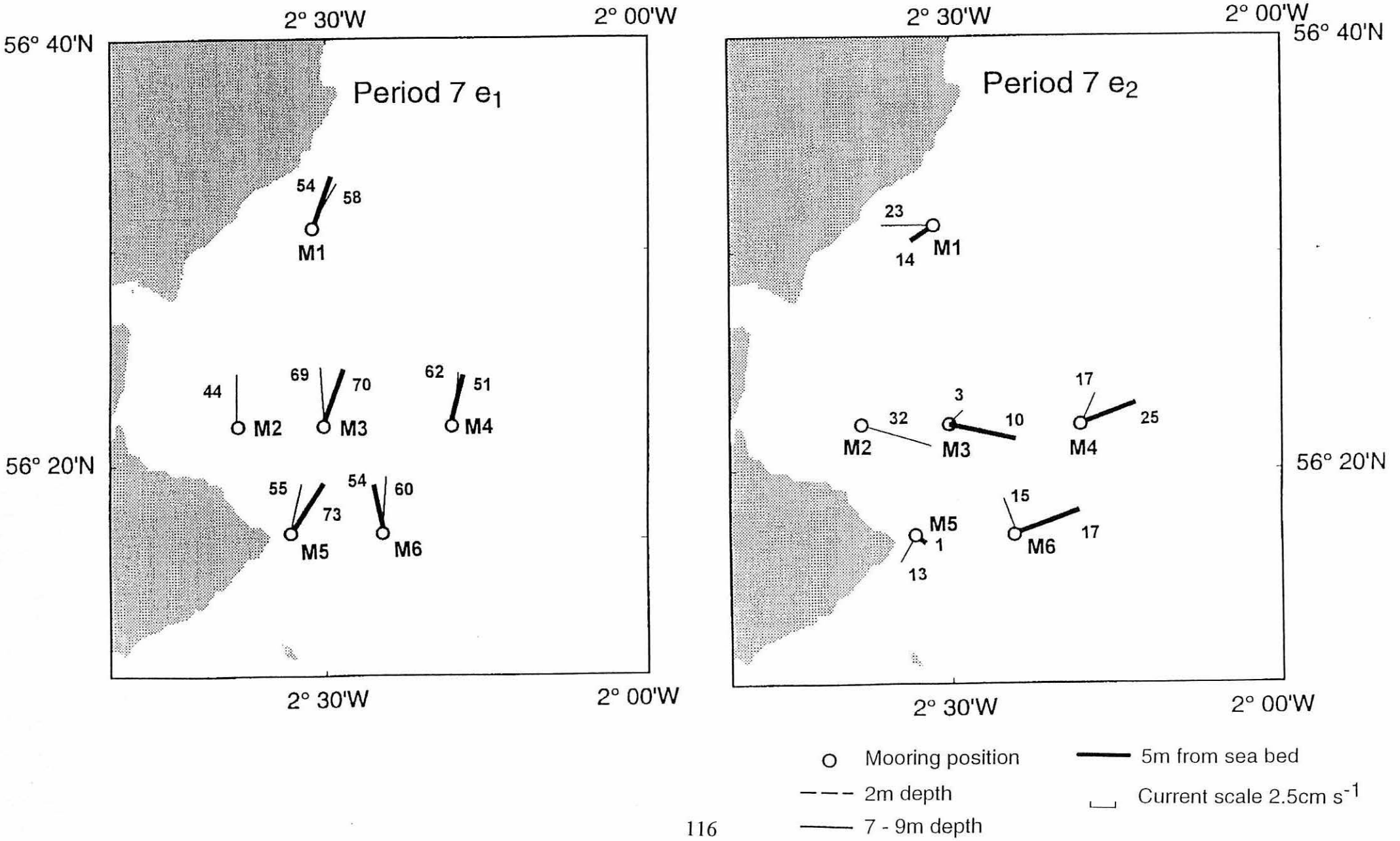

Figure 5.5 Current vectors representing the circulatory pattern corresponding to the first and second empirical modes (e_1 and e_2) of the residual circulation of St. Andrews Bay during summer (period 4). The relative length of a vector indicates the relative importance of variability at a given RCM within the mode. The orientation of the vector shows the direction of movement within the mode. *T* is given as a figure next to each vector and quantifies the proportion of the total variance of the record at a given RCM associated with each mode.

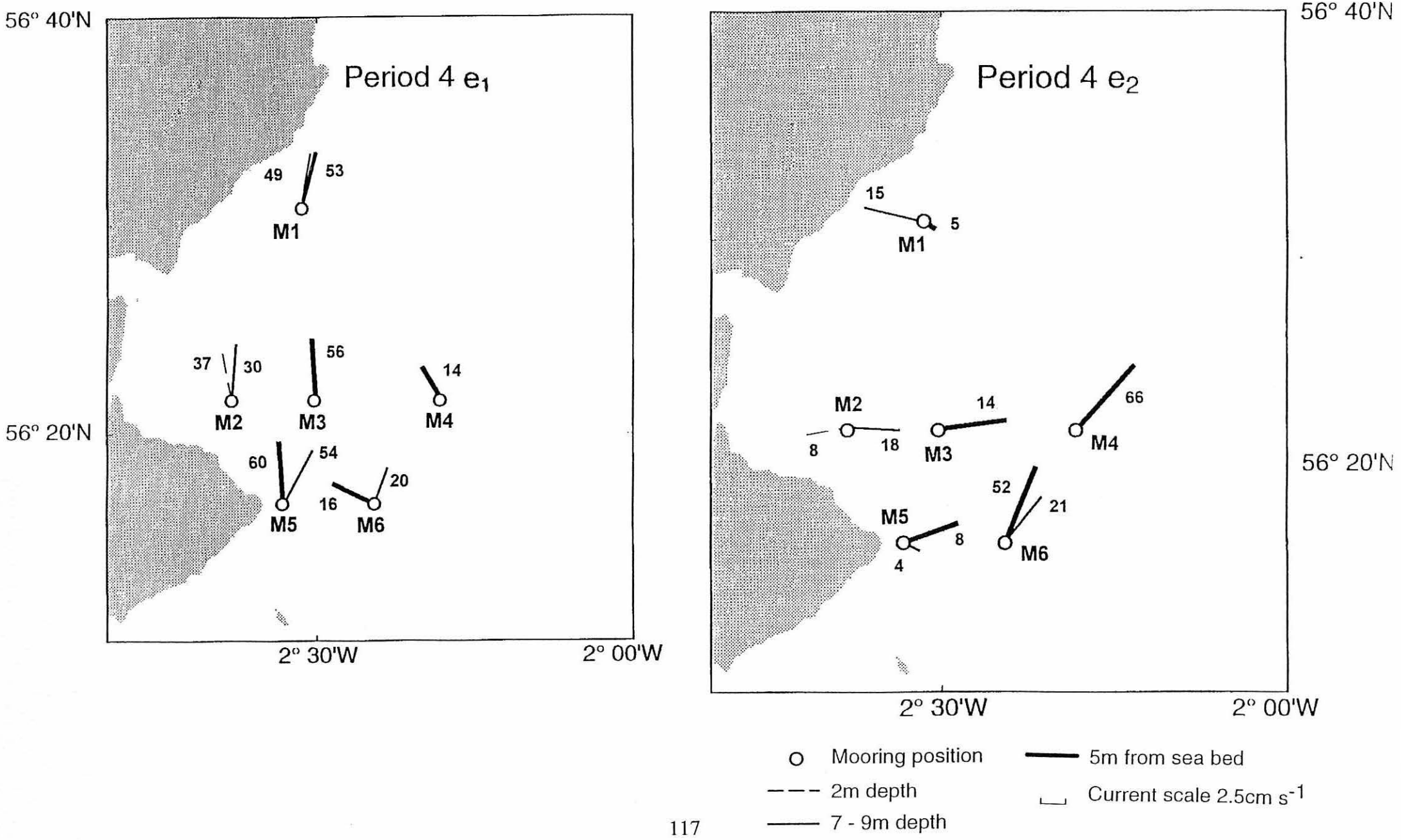

Figure 5.6 Number of days of wind *towards* a given direction as a percentage of the total number of days with a daily mean wind stress in excess of 0.02 Nm^{-2} (wind speed > 3.6 m s^{-1}).

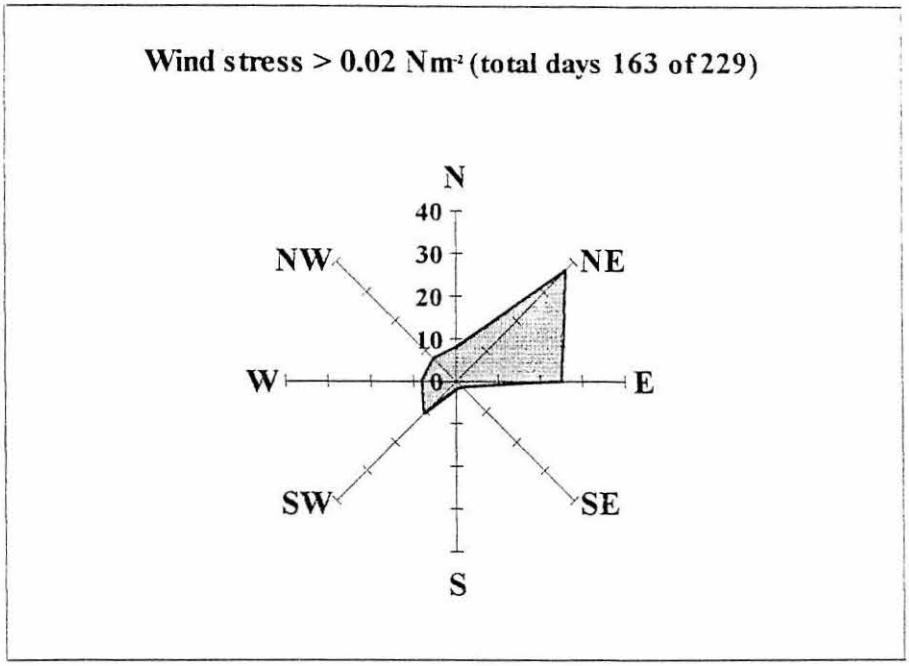

Figure 5.7 Number of days of wind *towards* a given direction as a percentage of the total number of days with a wind stress in excess of 0.1 Nm^{-2} (wind speed 8 m s^{-1}).

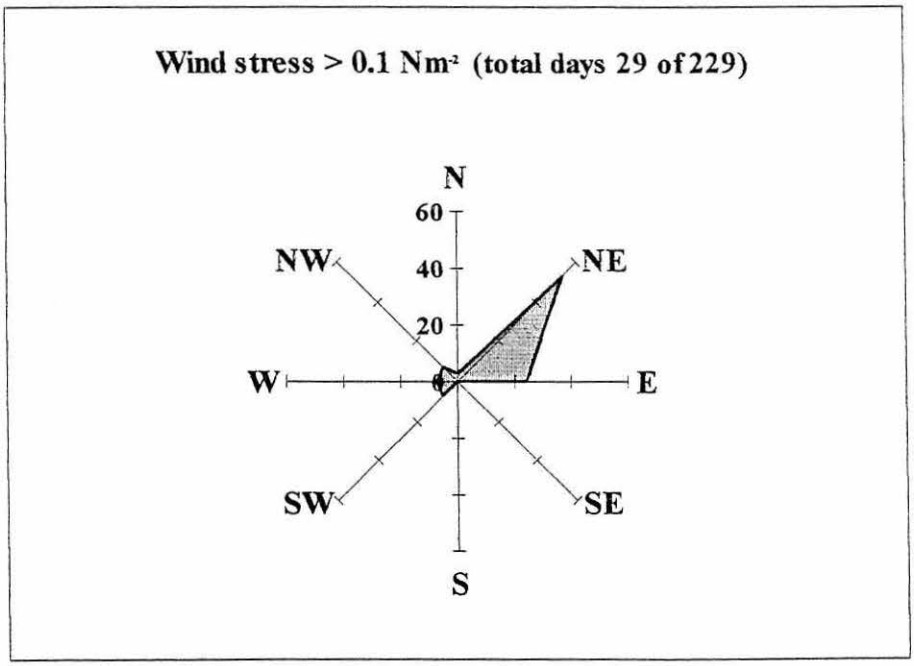

Figure 5.8. Low passed time series of longshore wind stress and flow, M1, period 4.
Time series were resolved along the local longshore axis of variability (south positive) (Table 3.1). Wind stress is represented by a dotted line, current at a depth of 9m by a solid line and at a depth of 24m by a dashed line.

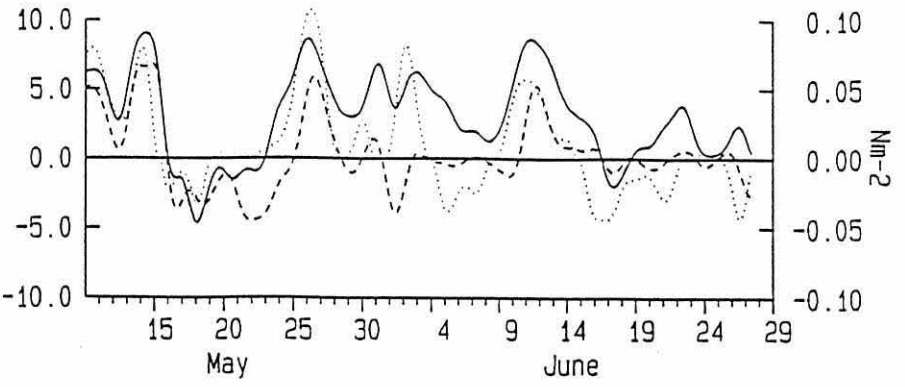

Figure 5.9. Low passed time series of cross-shore wind stress and flow, M2, period 1.
Time series were resolved along the local cross-shore axis of variability (offshore positive) (Table 3.1). Wind stress is represented by a dotted line, current at a depth of 9m by a dashed line.

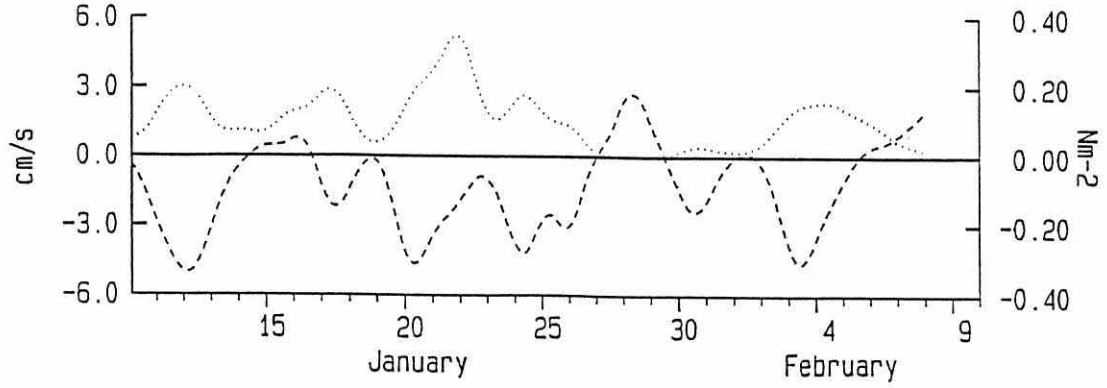

Figure 5.10. Low passed time series of longshore wind stress and flow, M4, period 5.
Time series were resolved along the local longshore axis of variability (south positive) (Table 3.1). Wind stress is represented by a dotted line, current at a depth of 9m by a solid line and at a depth of 46m by a dashed line.

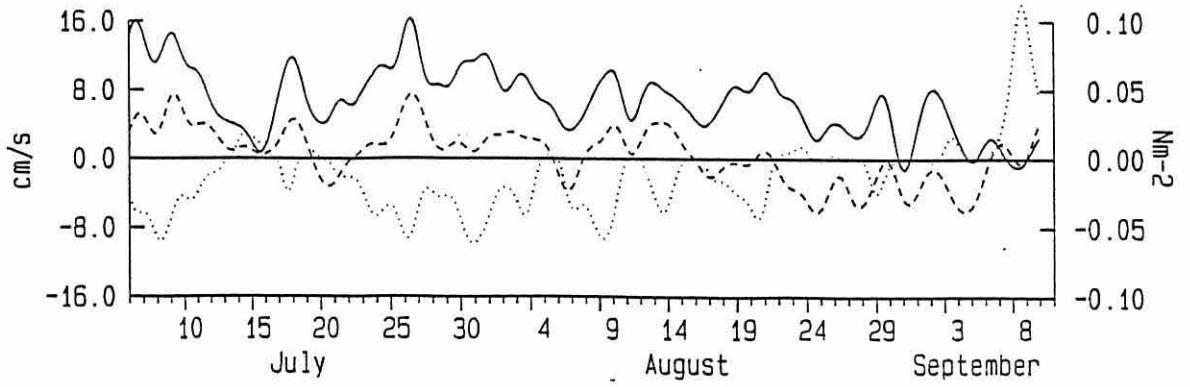

Figure 5.11. Low passed time series of longshore wind stress and flow, M5, period 4.
Time series were resolved along the local longshore axis of variability (south positive) (Table 3.1). Wind stress is represented by a dotted line, current at a depth of 7m by a solid line and at a depth of 21m by a dashed line.

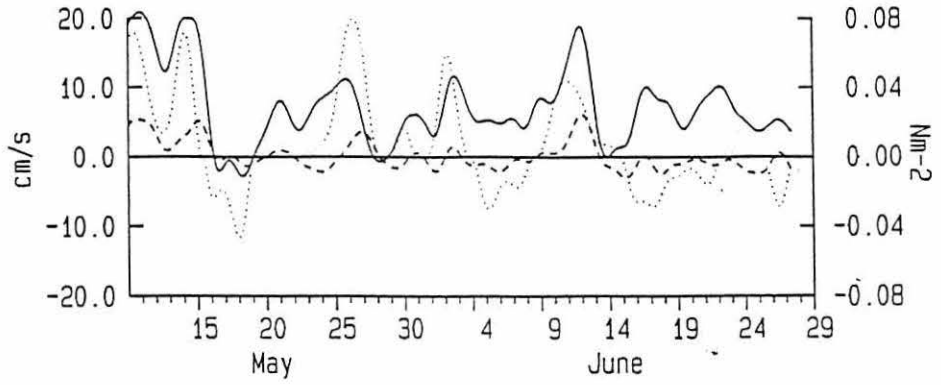

Figure 5.12. Low passed time series of longshore wind stress and flow, M5, period 1.
Time series were resolved along the local longshore axis of variability (south positive) (Table 3.1). Wind stress is represented by a dotted line, current at a depth of 7m by a solid line and at a depth of 21m by a dashed line.

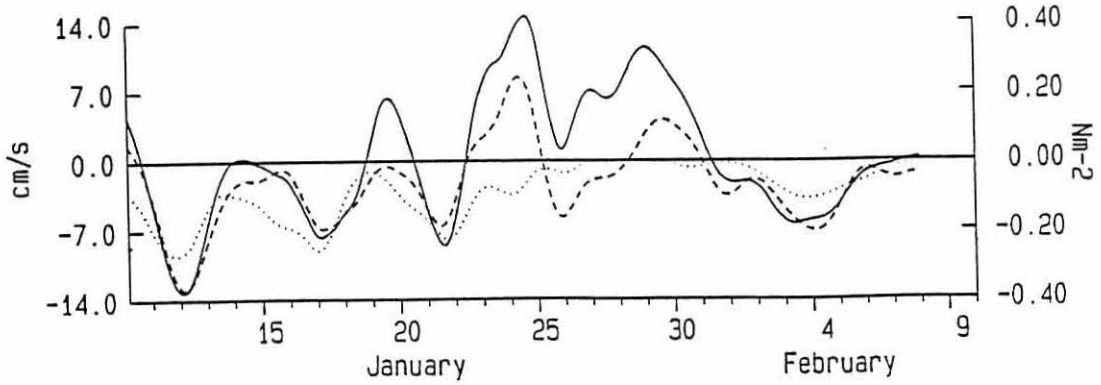

Figure 5.13 Current and wind stress vectors corresponding to the first 2 modes (e_1 and e_2) of the EOF analysis of period 1 data. The length of a given vector relative to the other vectors in the mode indicates the relative importance of variability at a given RCM to the mode. The orientation of the vector shows the direction of movement within the mode. The wind vector is plotted on land.

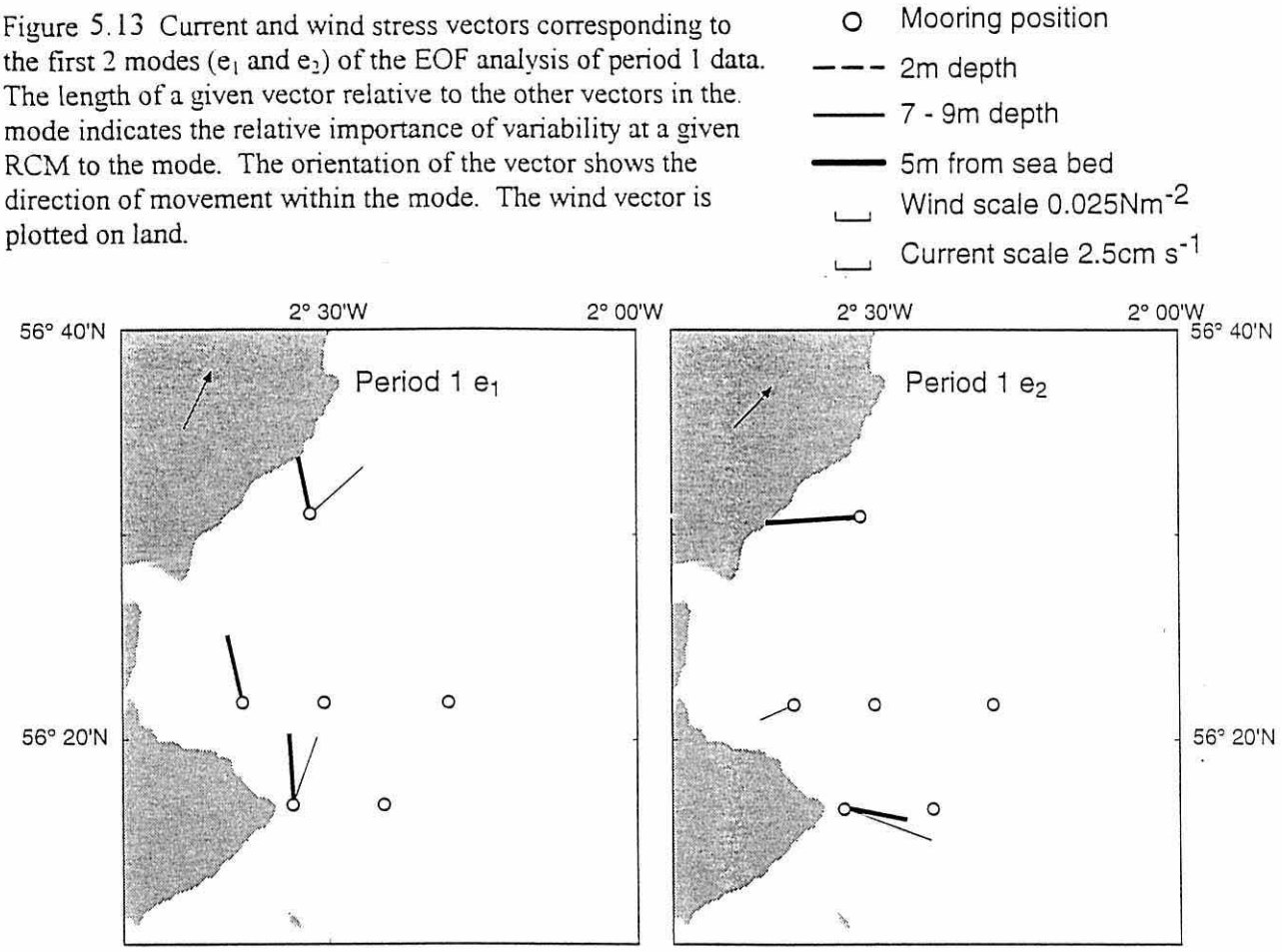

Figure 5.14 Current and wind stress vectors corresponding to the first 2 modes (e_1 and e_2) of the EOF analysis of period 2 data.

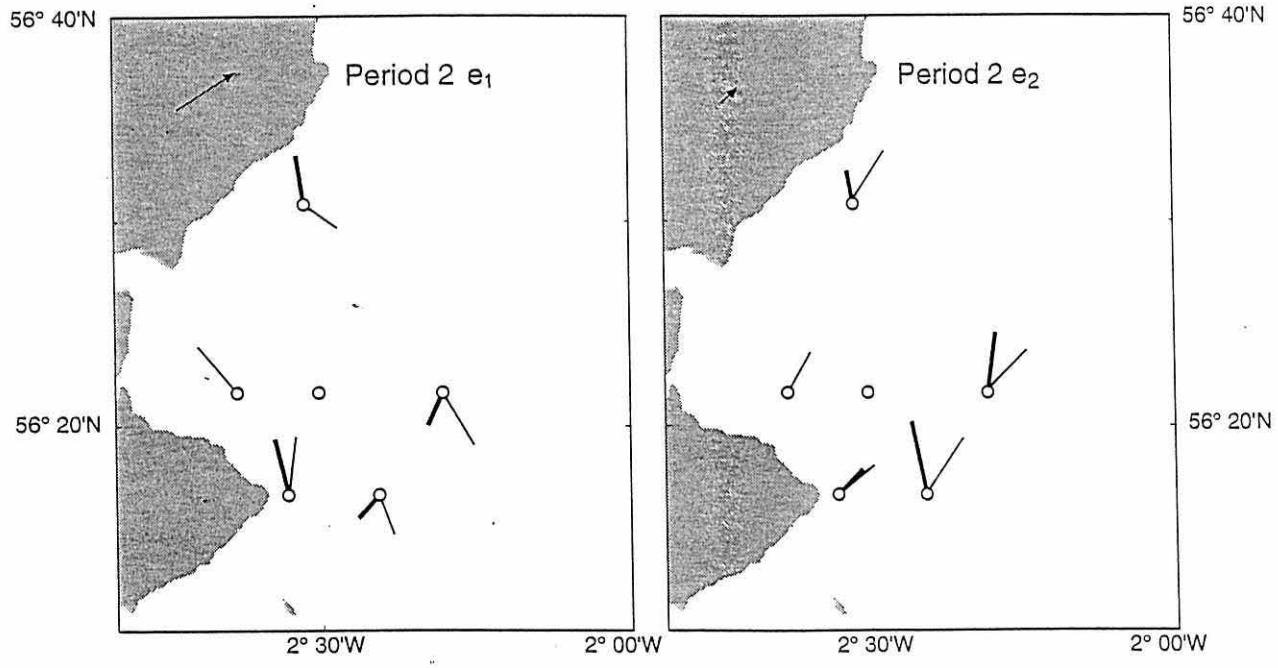

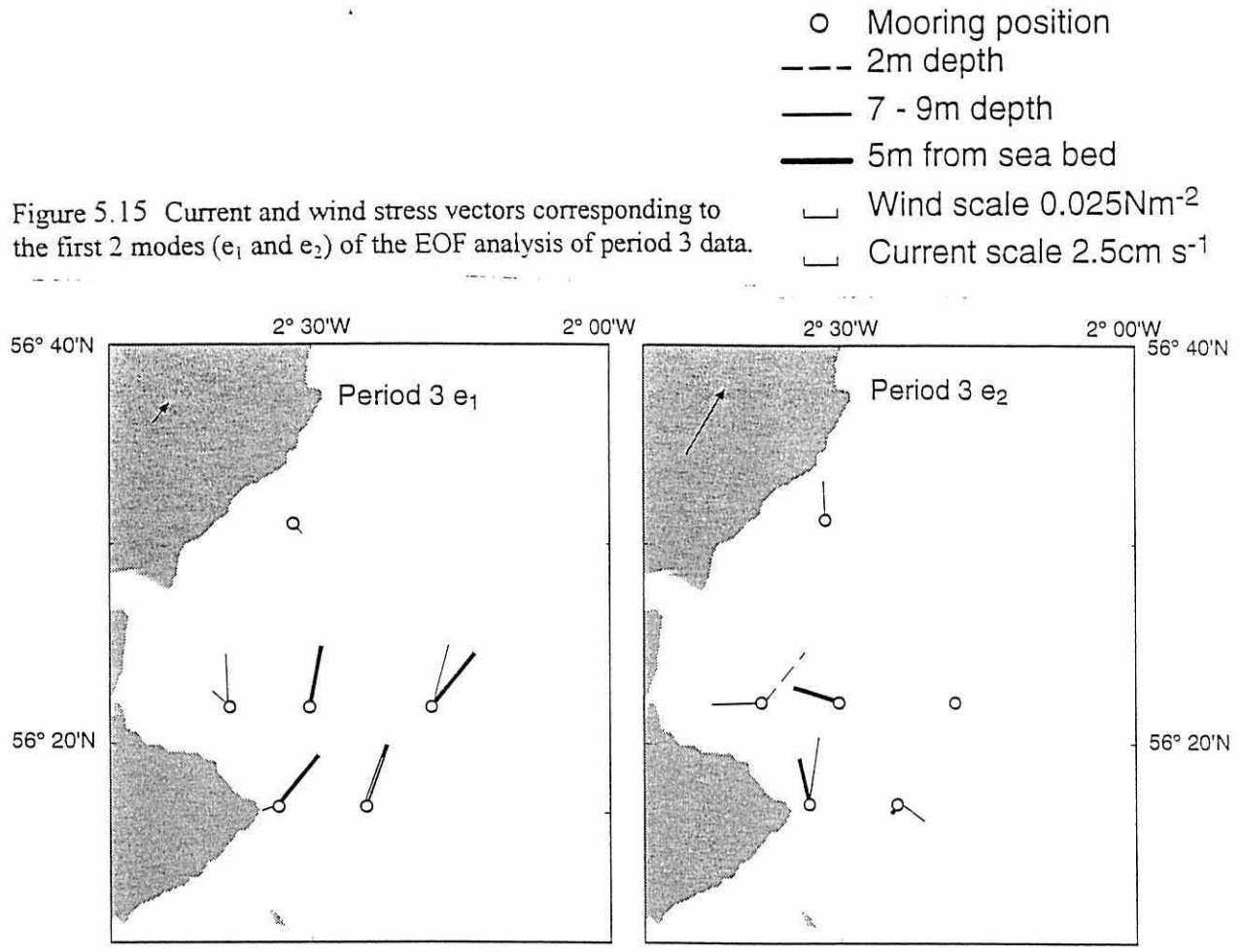

Figure 5.15 Current and wind stress vectors corresponding to the first 2 modes (e_1 and e_2) of the EOF analysis of period 3 data.

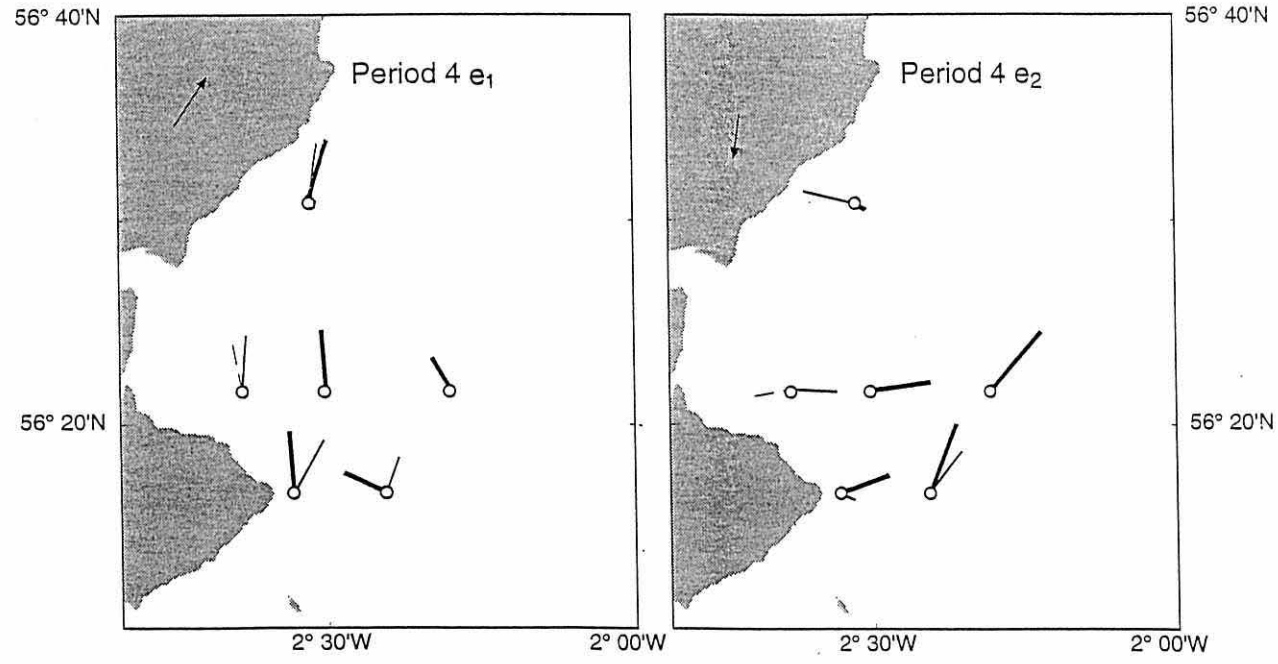

Figure 5.16 Current and wind stress vectors corresponding to the first 2 modes (e_1 and e_2) of the EOF analysis of period 4 data.

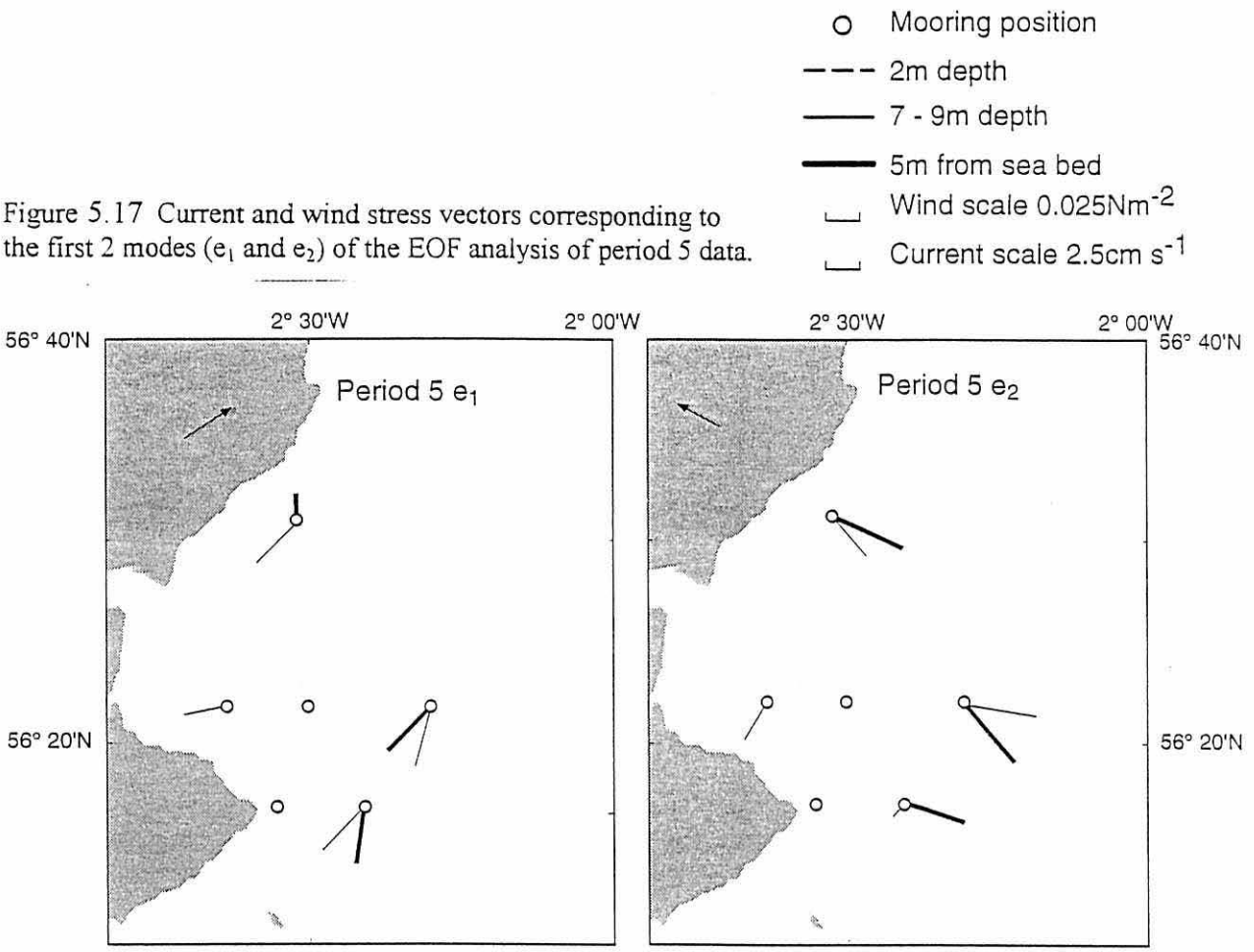

Figure 5.17 Current and wind stress vectors corresponding to the first 2 modes (e_1 and e_2) of the EOF analysis of period 5 data.

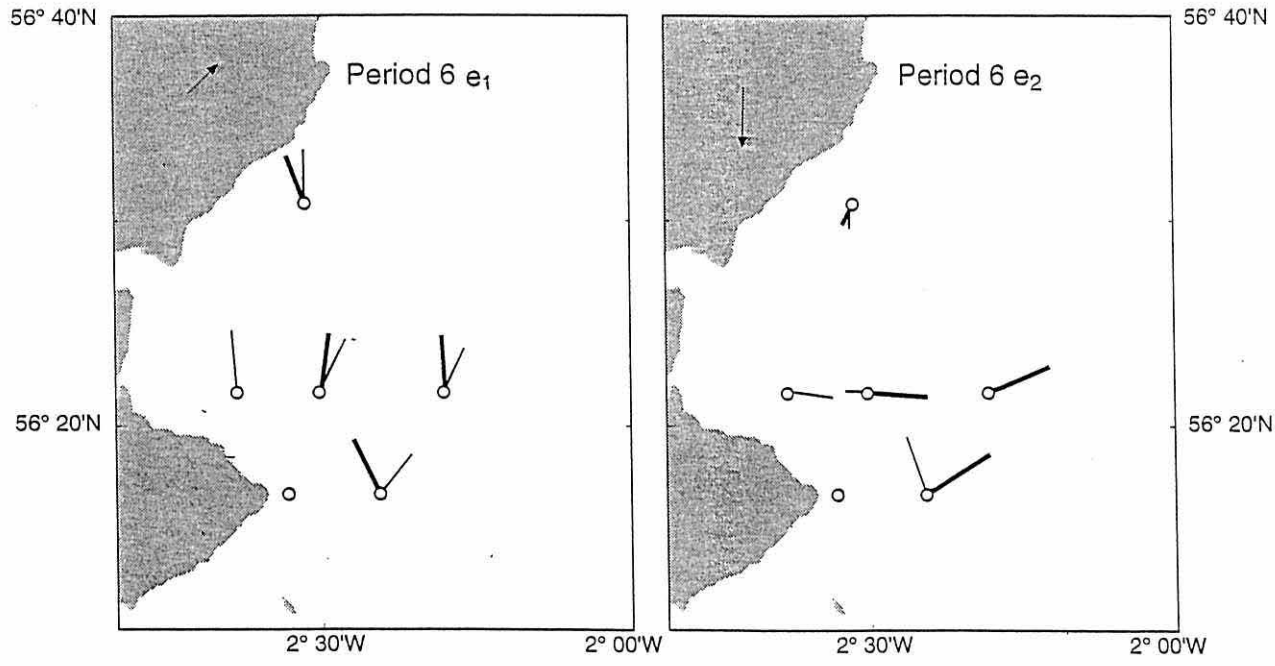

Figure 5.18 Current and wind stress vectors corresponding to the first 2 modes (e_1 and e_2) of the EOF analysis of period 6 data.

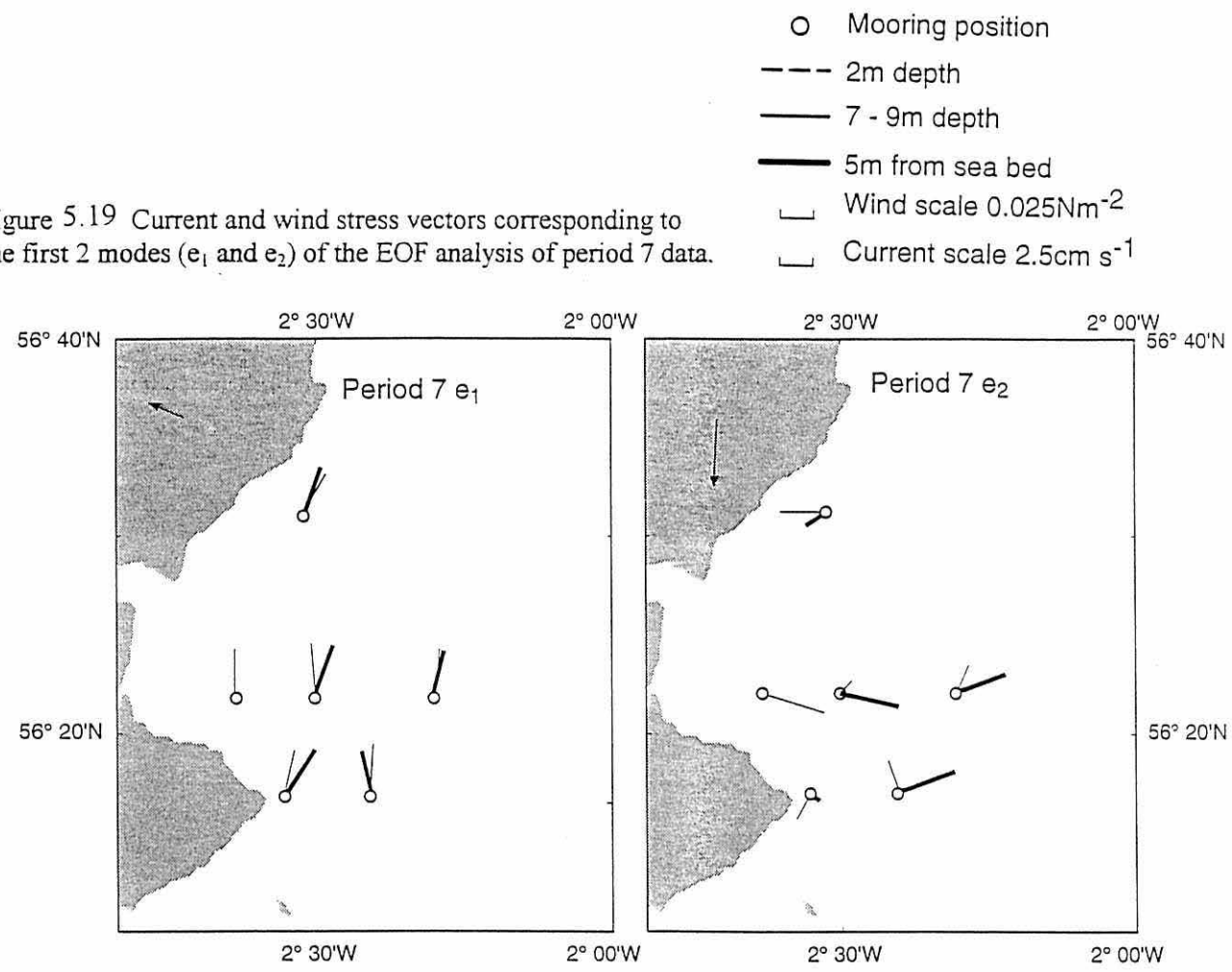

Figure 5.19 Current and wind stress vectors corresponding to the first 2 modes (e_1 and e_2) of the EOF analysis of period 7 data.

Figure 5.20 Variation of total seabed pressure from the mean (in dbar) at Wick, Aberdeen and Leith (moving downwards on the plot). The value for Wick is increased by 0.5 dbar while that for Leith is reduced by 0.5 dbar for purposes of clarity. Total pressure = atmospheric pressure + sea level as measured by coastal tide gauges.

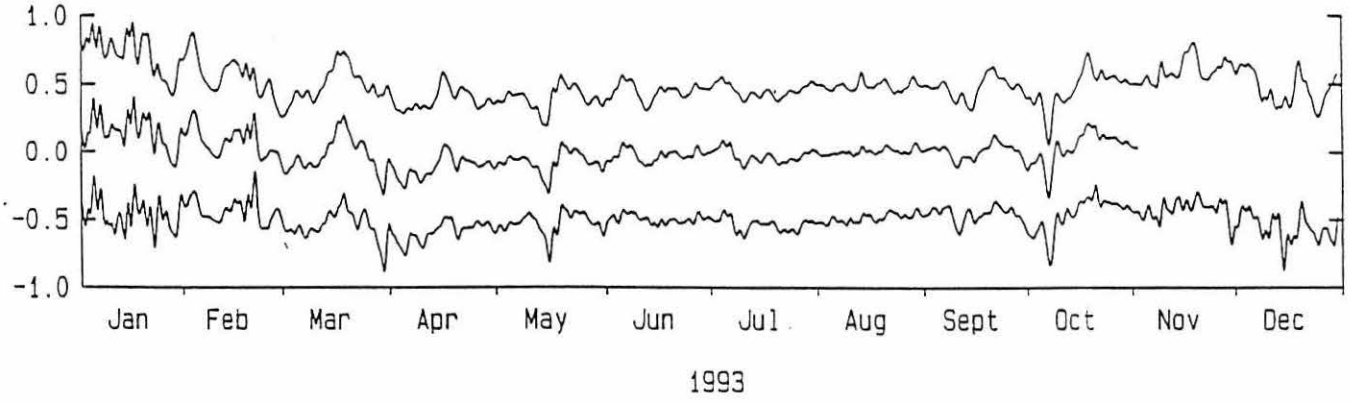

Figure 5.21 Variation of total seabed pressure from the mean (in dbar) moving southward along the coast during period 2 showing the progression of a storm surge into the North Sea.

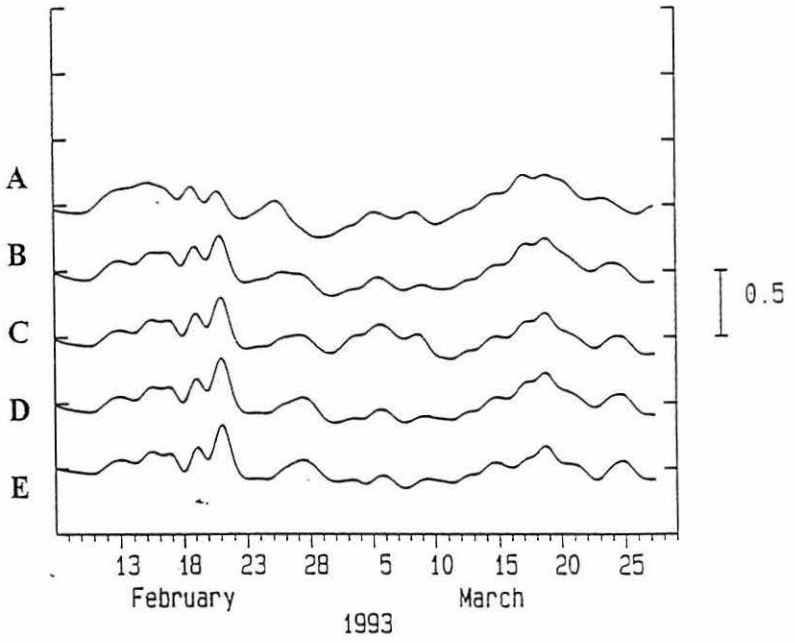

A: WICK
B: ABERDEEN
C: M1
D: M6
E: LEITH

Figure 5.22 Comparison of time series of variation about the mean for the longshore pressure gradient measured between various locations along the Scottish north-east coast during period 2. The high degree of correlation is apparent.

A. M6 - Wick
B. Leith - Wick
C. Leith - Aberdeen
D. M6 - Aberdeen

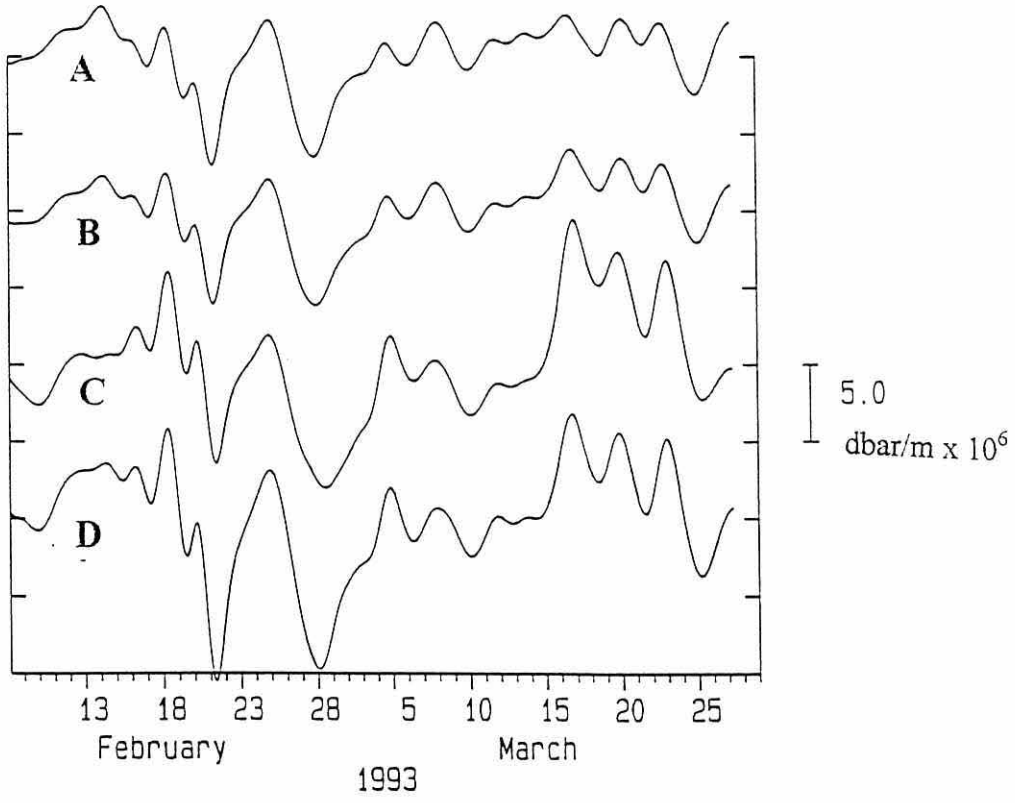

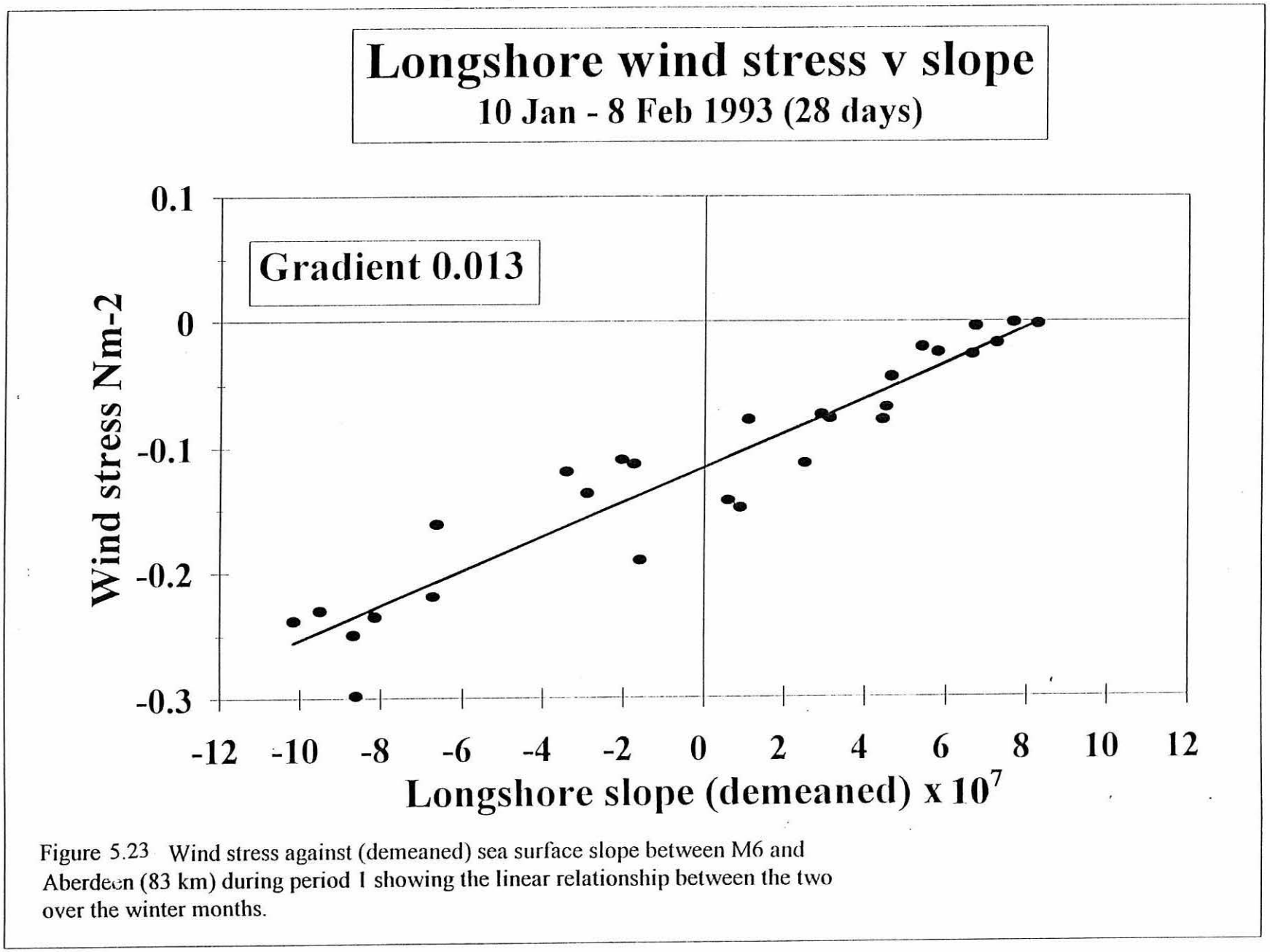

Figure 5.23 Wind stress against (demeaned) sea surface slope between M6 and Aberdeen (83 km) during period 1 showing the linear relationship between the two over the winter months.

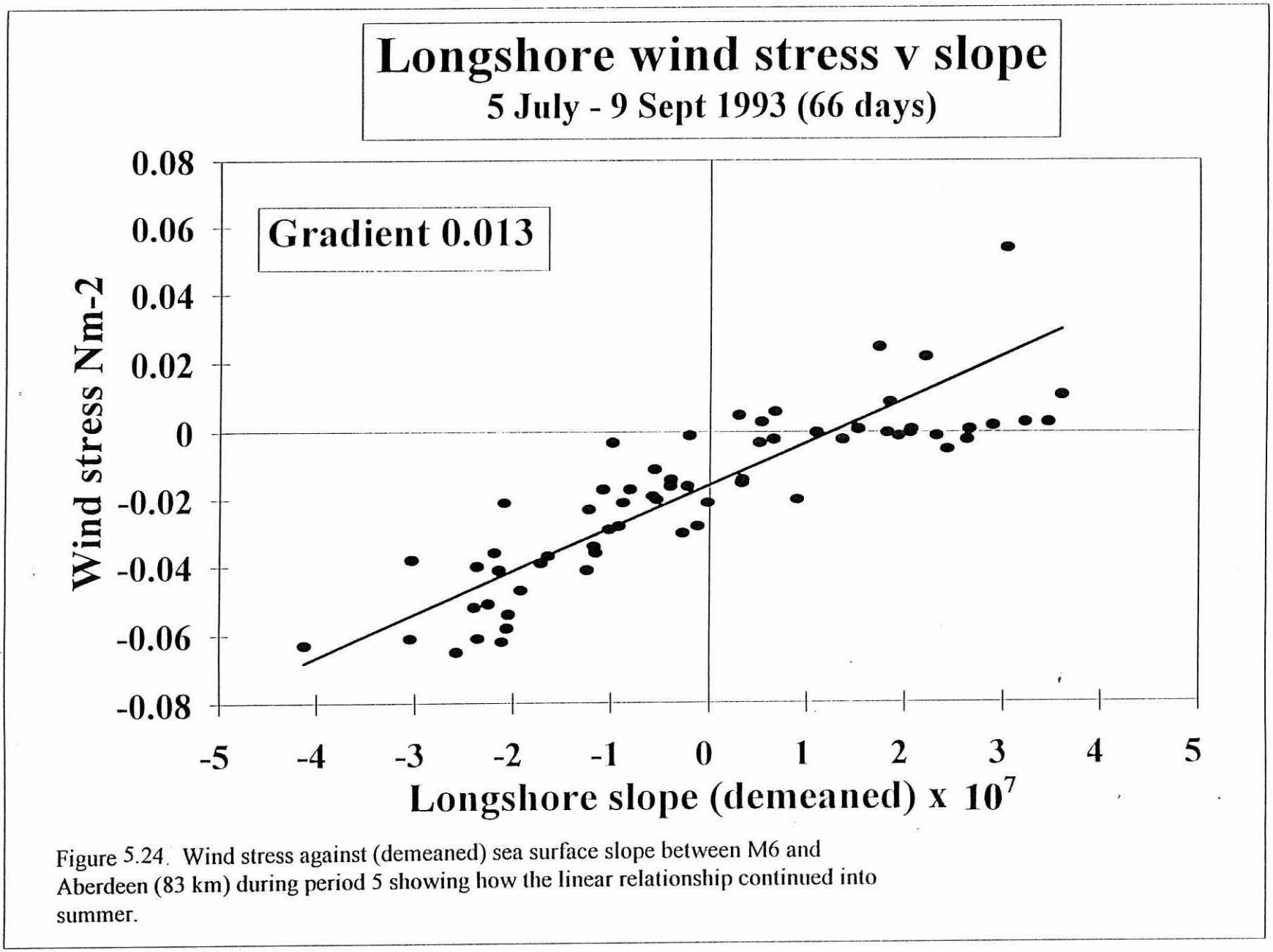

Figure 5.24. Wind stress against (demeaned) sea surface slope between M6 and Aberdeen (83 km) during period 5 showing how the linear relationship continued into summer.

Chapter 6

6. The Longshore Momentum Balance

6.1 The Longshore Momentum Equation

On the basis of the value of β (Table 5.4), and the results of the EOF analysis it is apparent that the majority of the variance in flow at any mooring position was independent of depth and topographically steered. The data suggest the direct effect of the local wind stress and variations in the wind-forced longshore pressure gradient to be major driving factors in the sub-tidal circulation within the study area, the pressure gradient being dominant in deeper water and vice-versa. Confirmation of the extent of the roles played by these factors in relation to other potential forcing factors in driving the barotropic circulation within the coastal zone can be gained by calculating the terms of the linearised longshore depth-meaned horizontal momentum equation which can be written

$$\frac{\partial u}{\partial t} - fv = -\frac{1}{\rho}\frac{\partial p}{\partial x} + \frac{(\tau_{sx} - \tau_{bx})}{\rho h} \qquad 6.1$$

for an orthogonal co-ordinate system with x longshore and positive to the south and y positive in an offshore direction. $\frac{\partial u}{\partial t}$ represents the local acceleration, fv the Coriolis acceleration, $\frac{\partial p}{\partial x}$ is the longshore pressure gradient, τ_{sx} represents the longshore surface stress and τ_{bx} stress due to bottom friction. The density of seawater (ρ) was taken to have a constant value of 1025 kg m^{-3} for the purposes of this formulation. Terms of the equation have units of m s^{-2}.

6.2 Parameterisation of the Terms of the Momentum Balance

Bottom friction

Under circumstances where tidal streams dominate subtidal currents, the bottom friction term, typically parameterised as quadratic, can be linearised (Csanady, 1976; Scott and Csanady, 1976; Winant and Beardsley, 1979) such that

$$\frac{\tau_{bx}}{\rho h} = \frac{ru}{h} \qquad 6.2$$

where r is an appropriate coefficient of friction. This coefficient has usually been determined by workers by assuming a steady-state balance between wind and bottom stress. In which case, using (6.2) we obtain

$$\rho r u = \tau_{sx} \qquad 6.3$$

In shallow waters (~30m) Winant and Beardsley (1979) found r to be in the region of 5 x 10^{-4} m s^{-1} which is in agreement with values calculated by Huyer *et. al.* (1978) for shelf waters off Oregon. Scott and Csanady (1976) found values of approximately 15 x 10^{-4} m s^{-1} off Long Island, slightly more than the value of 10 x 10^{-4} m s^{-1} calculated for 60m of water in the same region by Noble *et. al.* (1983). From the results of the Coastal Model of Section 5.5 (Table 5.9) r was calculated for the study area. The coefficient r is related to R_c (Equation 5.7) by

$$r = (\rho R_c)^{-1} \qquad 6.4$$

Values covered the range 3 - 30 x 10^{-4} m s^{-1}. Selecting only values for which the correlation between wind and current was high (V% > 40) narrows the range to give a value of approximately 10 x 10^{-4} m s^{-1} for r, in agreement with other sources. There are potential inaccuracies in using a parameterisation of this type in a region where the magnitude of oscillatory tidal currents typically exceeds that of the sub-tidal residuals generated by the wind. This problem was addressed by Heaps (1978) who derived a

formula for r, which is tidally variant and suitable for coastal regions where tidal ellipses are largely degenerate. r is given by

$$r = \frac{4kU}{\pi} \qquad 6.5$$

where U is the tidal amplitude and $k = 2.5 \times 10^{-3}$ is the usual bottom drag coefficient in a tidal regime assuming a quadratic drag law (Hill and Simpson, 1988). For St. Andrews Bay, with a typical amplitude of the M_2 constituent of 30 cm s^{-1} this formulation gives $r = 10 \times 10^{-4}$ m s^{-1} which is of the same order as values derived from the wind/bottom stress regressions. This tidal formulation was used in the momentum balance calculations at each mooring site with locally determined values for the M_2 tide. The term was calculated using the depth mean flow except in the case of mooring M2 where the measured current at mid-depth was used.

Pressure gradient

The estimation of the longshore gradient utilised in this parameterisation took into account only variations in the sea-surface slope due to forcing factors on the scale of the north-east coast, with the Aberdeen - St. Andrews Bay gradient being used in the calculations. Localised pressure gradients due to horizontal density variations are likely to be important in the region directly influenced by the Tay plume and the equation should contain a term to represent the effects of such gradients. Slopes produced in this way are, however, likely to be highly complex in the region of the plume and the inclusion of such a term would complicate the picture considerably. To that end, localised baroclinic effects have been ignored in this analysis and are separately dealt with in Chapter 7.

Wind stress

The wind stress term used in this form of the momentum equation ($\frac{\tau_{sx}}{\rho h}$) varies inversely with depth, representing the diminishing effect of the wind on the depth mean circulation in deeper water.

The Coriolis term

fv was estimated using the depth-averaged cross-isobath flow at each mooring with $f = 1.21 \times 10^{-4}$ s^{-1}.

Local acceleration

Time series of the local acceleration $\frac{\partial u}{\partial t}$ were estimated from the depth mean current series using a centred difference scheme with a one hour step.

This formulation of the momentum equation neglects non-linear advective terms as being small in relation to the other terms. Calculation of the Rossby number $\varepsilon = u_0 / fL_y$ (*e.g.*, Allen and Smith, 1981) where u_0 is a characteristic streamwise velocity ($u_0 = 5$ cm s^{-1}) and L_y is a characteristic cross-shelf scale, say 10 km, gives $\varepsilon = 0.05$, far less than one, indicating that the non-linear terms due to the subtidal flow are unlikely to be important. Csanady (1975) shows that even in cases where $\varepsilon > 1$ the momentum flux due to non-linear terms typically modifies the longshore flow significantly only within a few kilometres of the shore.

Time series of the five terms of the linearised momentum equation were calculated for each mooring position and period; standard deviations of each term are presented in Table 6.1. An examination of the percentage of the variance of each term taken up by the first empirical mode of an EOF analysis of the five terms was used to obtain an indication of the significance of each term to the momentum balance (Table 6.2), as was visual inspection of the time series.

6.3 Results: The Significance of Individual Terms to the Momentum Balance

Local acceleration

The local acceleration was found to be everywhere the smallest term in the balance (Table 6.1), the typically low contribution to the first empirical mode (Table 6.2) indicating a low degree of correlation with the other terms. These results suggest that the local acceleration was not a significant factor in the circulation of the St. Andrews Bay area during 1993.

Coriolis acceleration

The Coriolis term was found to be of a significant size in all cases ($\sigma^{½}$ 1-3 x 10^{-6} m s^{-2}), however the contribution of the term to the first mode of the EOF analysis was erratic both spatially and temporally (Table 6.2). This was particularly apparent on visual inspection of the time series (not included here due to space limitations). In similar studies the Coriolis acceleration has often been found to be the largest term but poorly correlated with other terms in the balance, see for instance Allen and Smith (1981) in a study of circulation off the Oregon coast. Lentz and Winant (1986) have pointed out that for cross-isobath flow values of the order of those observed here (~1-3 cm s^{-1}) a significant proportion of the record may be due to instrument noise, leading to a "false" value. The most likely explanation for the poor correlation lies, however, in the poor resolution of the depth-averaged cross-shore flow by a two-instrument mooring. It is probable that the Coriolis acceleration does play some role in driving the circulation. For instance Amin (1988) observed significant values off the north east coast of England (again poorly correlated with other terms in the momentum equation) while Murray (1975) found it to be significant even within 1 km of the coast. However, potential noise due to the errors outlined above makes it difficult to establish the true extent of the effect. It appears from the data (Tables 6.2 and 6.3) that the Coriolis term may have been occasionally significant at the inner moorings M1 and M2 where onshore near-bed flows dominated the cross-shore circulation.

Pressure gradient

During all periods the pressure gradient was the dominant term in the equation, with a standard deviation of 2-6 x 10^{-6} m s^{-2} (Table 6.1) and an average of 75% of the variance explained by the first empirical mode (Table 6.2). The dominance of the pressure gradient term can be seen in Figures 6.1 and 6.2 which show time series plots of bottom stress, pressure gradient and wind stress terms. Figure 6.1 illustrates data collected at M1 during period 1when south-westerly longshore winds were dominant. Figure 6.2 shows data from M4, period 2 and illustrates a pair of significant pressure events peaking on the 21st and 28th of February.

Wind stress

The standard deviation of this term was of a significant magnitude, particularly at the inner sites and during the windier periods as would be expected (e.g. Figure 6.1). However, even at the shallowest site (M2) its magnitude amounted to only half that of the pressure gradient (Table 6.1 and Figure 6.3). Consideration of the first empirical mode shows an average of 70% of the wind variance explained, with the highest values observed at M5 (Table 6.2).

Bottom friction

The bottom stress term was typically of a similar amplitude to that of the wind stress (Table 6.1 and e.g. Figure 6.2). A significant proportion of the variance of this term was explained in the majority of cases by the first empirical mode (Table 6.2), however, the erratic contribution of the Coriolis term to that mode was also a feature of this term.

6.4 Balancing the Momentum Equation

On the basis of the results of the statistical and EOF analyses it appears that, although subject to a high degree of local variation, the barotropic longshore momentum balance of the St. Andrews Bay area can be largely explained as a quasi-steady, frictionally controlled, interplay between the direct effects of wind stress and the longshore pressure gradient, which, at least during 1993, was largely generated by the local longshore wind and/or a similarly directed wind field over the northern North Sea. In most cases the majority of the contribution to the first empirical mode was from the wind stress and pressure gradient terms (Table 6.2). Such a relation can be represented by Equation 6.6.

$$\frac{ru}{h} = -\frac{1}{\rho}\frac{\partial p}{\partial x} + \frac{\tau_{sx}}{\rho h} \qquad 6.6$$

Comparisons between correlations of wind (**C**) and pressure gradient (**B**) terms with the bottom stress term (**A**), which is proportional to the depth-meaned current, for a given period (Table 6.3) show clearly that at the inner moorings the wind stress (**C**) is dominant in driving the flow (correlation coefficient positive) (Figure 6.4) with the pressure gradient (**B**) dominant at the outer moorings (Figure 6.2). Study of Figures 6.1-6.4, for example, indicates that in the majority of cases peaks in the friction term can be attributed

to either one or the other forcing factor. However, a simple addition of the wind and pressure gradient terms of the time series (terms **B** + **C**) as in Equation 6.6 (Table 6.3) typically results in a domination of the balance by the pressure gradient in most cases by virtue of its large magnitude, even where a clear link between wind and current is apparent (e.g. Figure 6.5).

Clearly the simple balance of terms as described in Equation 6.6 fails to describe the dynamical balance between the terms adequately, particularly at the inner sites. The individual terms of Equation 6.6 were subjected to regression analysis to determine the ratio between the pressure and wind terms required for the optimal fit to the bottom stress term. The results for all periods except period 6 were found to be consistent, with the pressure gradient term (**B**) requiring division by a factor of approximately three to balance the wind stress term, the variation consistent throughout the year at a given mooring.

Correlation coefficients were calculated (Sciremammano, 1979) between time series of the bottom stress term (**A**) and the sum of the pressure gradient and wind stress terms (**B** + **C**). These coefficients are compared in Table 6.3 with similarly calculated coefficients in which the pressure gradient term was divided by three (**B/3** + **C**) and with the Coriolis term (**D**) added to both formulations.

6.4.1 Results

Division of the pressure gradient term by a factor of three improved the correlation of the summed pressure gradient and wind stress terms with the bottom stress term in 60% of all cases (Table 6.3) and reduced the amplitude of the joint pressure and wind term to a comparable level to that of the bottom stress term. Figure 6.6 shows the time series of terms **A** and (**B/3** + **C**) for M1, period 4 and can be compared with Figures 6.4 and 6.5. The improvement in fit to the bottom stress was clearest at the shallower mooring sites (exemplified by M1 and M5) where wind stress was most important, while at M4 and M6, where the depth-mean flow was largely driven by the pressure gradient, the improvement in correlation, if any, was typically small. The improvement in amplitude matching was, however, significant. In only one case (M1 period 5, when the pressure gradient was dominant) did the reduced pressure gradient lead to a significant de-correlation between the terms of the balance. Addition of the Coriolis term to either **B** + **C** or **B/3** + **C** tended

to reduce the correlation in most cases, however at M1 and M6 some improvement was noted.

6.5 Summary

It appears from the results of the correlation analyses that the contribution of the Coriolis term is less important than the contributions of the wind and pressure gradient terms. Although potentially significant, the poor resolution of the cross-shore flow introduces a considerable source of error to this term.

The apparent excess in the pressure gradient term is difficult to explain. A significant source of error lies in the omission of density gradients from the pressure term in the balance, but the inclusion of a term to represent the action of density gradients within the study area is not likely to correct the pressure gradient excess in most cases as what is required is an approximately linear decrease in the gradient. The specific role of local density gradients in driving the baroclinic circulation of the area is dealt with in the next chapter. Further study of the depth averaged flow is unlikely to reveal the source of the imbalance, a depth-dependant analysis of the relation between the measured currents and wind may reveal more.

An assumption has been made in requiring a decrease in the pressure gradient term to balance the momentum equation, it would seem to be equally possible if not more likely that the wind stress is underestimated. The agreement in the magnitude of the coefficient of friction (r) calculated by the tidal formulation and via wind stress/current regressions lends confidence, however, to the magnitude of the wind stress term. It is of course possible that the land-based wind is less than that within the Bay. However the measuring station is less than 1km from the shore and with the coastal location of the moorings not too much variation would be expected.

Additional confirmation in the required reduction of the pressure gradient can be gained by a comparison of the measured near-bed flow and the flow predicted using Equation 6.6 with the wind set to zero during a period of low wind but significant pressure gradient. Such an event occurred on February 21st . The measured change in current velocity from the start of the event to its peak at M4 was 27.5 cm s^{-1} (Figure 6.2). Using equation 6.6

with the wind stress term set to zero and the pressure gradient as measured predicts a current speed of 83 cm s^{-1}, three times larger than that observed. This suggests that the pressure gradient acting in and around St. Andrews Bay is considerably smaller than, but correlated with that measured along the north-east coast.

A perspective on the relation between the two terms can be gained by applying a set of equations derived by Csanady (1981) describing the relationships between the longshore wind stress and longshore pressure gradient generated by it to the measured data. Csanady provided a comprehensive conceptual framework to explain coastal circulation regimes in which the longshore pressure gradient plays an important part in his Arrested Topographic Wave (Csanady, 1978a) and Shelf Circulation Cell (Csanady, 1981) models.

If the wind stress acting along a section of coastline is modelled as a periodic forcing such that

$$F_x = (\tau/\rho)\cos kx \qquad 6.7$$

where k represents the longshore wavenumber, then the longshore slope is given by $\frac{\partial \zeta}{\partial x}$ where

$$\frac{\partial \zeta}{\partial x} = \left(\frac{k\tau}{\rho g}\right)\left(\frac{fL_y}{r}\right) \qquad 6.8$$

and the longshore and cross-shore scales, L_x and L_y are given by

$$L_x = \frac{2\pi}{k}, L_y = \left(\frac{2r}{fks}\right)^{1/2} \qquad 6.9$$

From 6.8 and the second of 6.9 we get

$$\frac{\partial \zeta}{\partial x} = \left(\frac{\tau}{\rho g}\right)\left(\frac{2fk}{rs}\right)^{1/2} \qquad 6.10$$

For a wind of 8 m s^{-1} we have the following:

Longshore wind stress $\tau = 0.1 Nm^{-2}$

Density $\rho = 1025$ kg m^{-3}

Coriolis parameter $f = 1.21 \times 10^{-4}$ s^{-1}

Coefficient of friction $r = 10^{-3}$ ms^{-1}

Cross-shore sea-bed slope $s = 10^{-2}$

Longshore scale $L_x = 150$ km

Which, from 6.10, gives a longshore slope of 3×10^{-7} for the coast between the Moray Firth and the Firth of Forth. This is approximately a third of the measured gradient for such a wind strength and is that which is required to satisfy the momentum balance. This result may be fortuitous as the value is rather sensitive to the magnitude of the cross-shore slope which is taken at its mean value along the north-east coast. In the immediate vicinity of St. Andrews Bay the slope is considerably less. The result does suggest however, that the slope due to the direct effect of the wind on the north-east coastal zone may be that which is effective in driving flow within and near St. Andrews Bay and the larger measured slope is enhanced by that generated by the large scale wind field over the northern North Sea.

A frictionally controlled momentum balance between pressure gradient and wind stress has been described for the Scottish west coast by Hill and Simpson (1988). They found however, that longshore pressure gradients and wind stress tended to act sympathetically, with the pressure gradients typically having their origin in non-local winds associated with the passage of small low-pressure systems near and across the British Isles. This does not appear to be typical of the SNSCZ, where the pressure gradient and wind stress act to oppose each other and the pressure gradient appears to be strongly correlated with the local wind field.

In summary although the wind stress term in the momentum equation fails to balance the pressure gradient term by a factor of approximately three across the study area, it is clear from the data and EOF analyses that an approximate balance does actually exist. The wind stress was the dominant forcing factor for variability in the depth mean flow inshore

while the longshore pressure gradient dominated in deeper waters. This relation between wind stress and the longshore pressure gradient in association with the results of the scale analysis suggests the dominant barotropic circulatory regime may be somewhat analogous to a shelf circulation cell as described by Csanady (1981) with a longshore scale of the same order as that of the north-east coast of Scotland (~ 150 km).

Table 6.1. Standard deviations ($\sigma^{1/2}$ x 10^6 m s^{-2}) of the terms of the longshore momentum equation (Equation 6.1).

From left to right columns represent the local acceleration, Coriolis acceleration, pressure gradient, wind stress and bottom stress.

Mooring	Period	u_t	fv	$-p_x/\rho$	$\tau_{sx}/\rho h$	$\tau_{bx}/\rho h$
M1	1	0.40	2.05	6.00	2.77	1.21
	2	0.24	1.60	3.60	1.85	0.78
	4	0.26	1.75	2.20	1.10	1.10
	5	0.14	1.72	1.98	1.03	0.55
	6	0.36	2.25	4.20	1.04	1.55
	7	0.49	1.24	-	0.76	1.83
M2	1	0.60	2.32	6.00	3.50	1.33
	2	0.32	1.88	3.60	1.35	0.88
	3	0.35	2.44	1.66	0.82	0.83
	4	0.29	2.45	2.20	0.95	0.81
	5	0.29	2.03	1.98	0.59	0.74
	6	0.36	1.36	4.20	1.33	1.32
	7	0.45	2.75	-	2.04	1.11
M3	6	0.30	1.38	4.20	0.72	1.19
	7	0.38	1.41	-	1.06	1.10
M4	2	0.59	2.49	3.60	0.97	1.27
	3	0.38	1.36	1.66	0.39	0.60
	5	0.30	1.73	1.98	0.51	0.71
	6	0.32	1.75	4.20	0.57	0.99
	7	0.42	1.65	-	0.53	0.93
M5	1	0.61	1.69	6.00	2.73	2.81
	2	0.34	1.63	3.60	1.44	1.88
	3	0.34	1.09	1.66	0.60	1.63
	4	0.39	1.01	2.20	0.95	1.96
	7	0.47	1.35	-	1.13	2.25
M6	2	0.58	1.35	3.60	0.71	1.18
	3	0.33	1.46	1.66	0.30	0.51
	4	0.26	1.33	2.20	0.47	0.49
	5	0.19	1.51	1.98	0.34	0.54
	6	0.32	1.26	4.20	0.49	1.01
	7	0.44	1.35	-	0.63	0.84

Table 6.2. Percentage of the normalised variance of each term explained by the first empirical mode of the EOF analysis of terms of the momentum equation (Equation 6.1).

Mooring	Period	u_t	fv	$-p_x/\rho$	$\tau_{sx}/\rho h$	$\tau_{bx}/\rho h$
M1	1	4	49	82	81	25
	2	1	22	53	69	23
	4	5	63	74	85	64
	5	0	44	75	80	62
	6	16	67	56	69	35
M2	1	7	53	77	67	46
	2	7	22	76	67	56
	3	12	53	52	35	21
	4	9	42	70	75	66
	5	0	66	75	61	1
	6	1	0	65	45	79
M3	6	4	54	71	36	79
M4	2	11	23	89	72	39
	3	37	14	79	61	2
	5	5	3	94	78	78
	6	1	36	77	32	68
M5	1	0	4	86	94	58
	2	0	3	70	90	69
	3	5	26	52	83	48
	4	1	3	80	86	69
M6	2	12	19	88	65	44
	3	31	43	72	49	11
	4	1	23	85	85	1
	5	1	55	89	72	62
	6	3	27	74	46	45

Table 6.3. Normalised maximum correlation coefficients between the bottom stress term and other terms and combinations of terms in the longshore momentum equation .

A correlation coefficient of 1.70 indicates 90% significance, 2.00 indicates 95% and 2.60 indicates 99% (Sciremmano 1979). Lags (hours) are bracketed.

In both Table 6.3 and the chapter text the various terms of the momentum equation are represented as follows

A bottom stress
B pressure gradient
C wind stress
D Coriolis acceleration
E local acceleration

Mooring	Period	B	C	B + C	B + C+ D	B/3 + C	B/3 + C + D
M1	1	-1.11 (17)	1.19 (0)	-0.40 (0)	-0.89 (35)	1.69 (0)	2.15 (0)
	2	-1.26 (50)	3.14 (43)	2.07 (12)	2.34 (13)	3.59 (24)	2.79 (23)
	4	-2.74 (22)	3.77 (12)	-2.20 (50)	2.47 (0)	3.60 (7)	3.43 (0)
	5	3.13 (1)	-2.99 (0)	2.52 (5)	-1.45 (41)	-1.54 (0)	-2.34 (0)
	6	1.80 (1)	1.96 (15)	1.90 (6)	1.88 (10)	2.01 (10)	1.86 (13)
M2	1	-2.02 (0)	2.00 (11)	0.43 (50)	1.17 (26)	1.69 (19)	3.24 (14)
	2	-2.75 (50)	1.98 (13)	-2.65 (40)	-1.30 (42)	0.98 (50)	2.41 (17)
	3	1.64 (50)	-1.82 (50)	0.81 (50)	1.95 (9)	0.27 (6)	1.85 (3)
	4	-2.94 (6)	3.63 (8)	-1.99 (4)	0.71 (8)	1.66 (10)	2.48 (7)
	5	0.00 (0)	-1.51 (39)	-0.53 (42)	-1.58 (50)	-1.55 (40)	-1.43 (50)
	6	2.43 (11)	1.94 (0)	2.69 (0)	2.56 (0)	2.77 (0)	2.19 (0)
M3	6	2.62 (2)	2.41 (2)	2.80 (2)	2.62 (0)	2.98 (2)	1.71 (0)
M4	2	3.74 (15)	-1.51 (3)	4.10 (16)	2.61 (16)	3.66 (19)	0.71 (18)
	3	1.32 (15)	-0.79 (35)	1.39 (14)	1.24 (15)	1.25 (12)	0.78 (15)
	5	4.75 (12)	-3.64 (8)	4.79 (13)	3.72 (14)	3.67 (16)	1.61 (16)
	6	2.80 (9)	0.53 (0)	2.68 (9)	2.80 (7)	2.43 (10)	2.44 (3)
M5	1	-1.93 (0)	2.58 (4)	-1.36 (0)	-1.25 (0)	3.65 (11)	1.97 (17)
	2	-2.17 (0)	3.23 (0)	-1.06 (0)	-0.78 (0)	2.45 (2)	1.86 (24)
	3	-1.06 (0)	2.28 (0)	-0.26 (0)	0.75 (12)	1.74 (0)	1.61 (9)
	4	-2.97 (8)	3.66 (7)	-2.08 (11)	-1.94 (0)	2.28 (6)	0.55 (14)
M6	2	3.25 (13)	-1.36 (5)	3.51 (14)	3.44 (14)	3.73 (15)	2.72 (15)
	3	1.44 (11)	-1.23 (31)	1.45 (10)	1.69 (13)	1.34 (7)	1.57 (15)
	4	-0.66 (0)	2.01 (50)	-0.73 (0)	0.46 (29)	0.69 (33)	1.31 (38)
	5	3.97 (21)	-2.75 (24)	4.07 (21)	2.96 (23)	4.14 (20)	-1.78 (0)
	6	2.72 (7)	0.32 (0)	2.60 (6)	2.37 (8)	2.36 (3)	1.68 (9)

Figure 6.1. Time series of terms of the depth-averaged longshore momentum equation (Equation 6.6) for M1 during period 1.
Term **A** represents bottom stress, term **B** the longshore pressure gradient, term **C** the wind stress term. Positive is southgoing. Vertical axis units are m s^{-2} x 10^{6}. **A** (solid line), **B** (dotted line), **C** (dashed line).

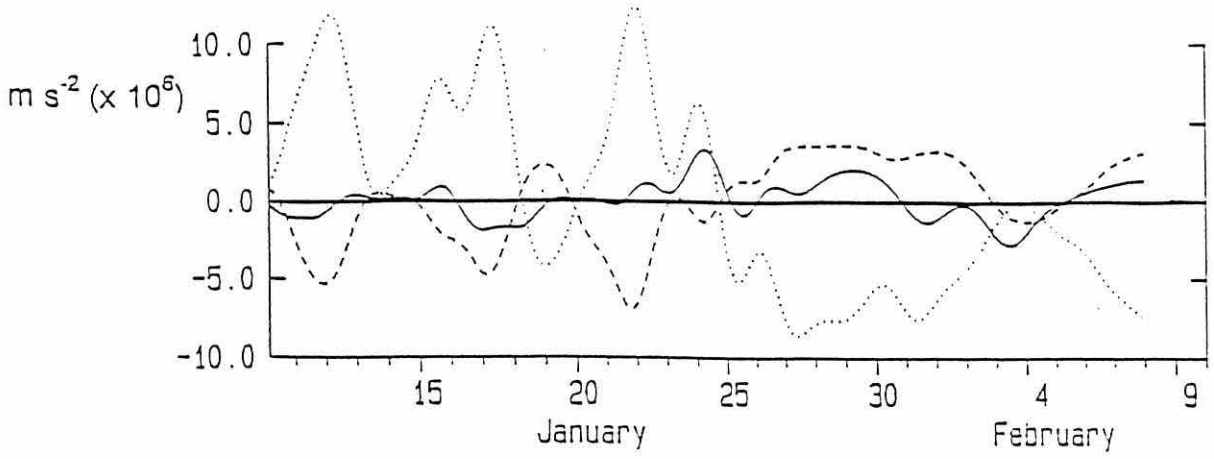

Figure 6.2. Time series of terms of the depth-averaged longshore momentum equation (Equation 6.6) for M4 during period 2.
Term **A** represents bottom stress, term **B** the longshore pressure gradient, term **C** the wind stress term. Positive is southgoing. Vertical axis units are m s^{-2} x 10^{6}. **A** (solid line), **B** (dotted line), **C** (dashed line).

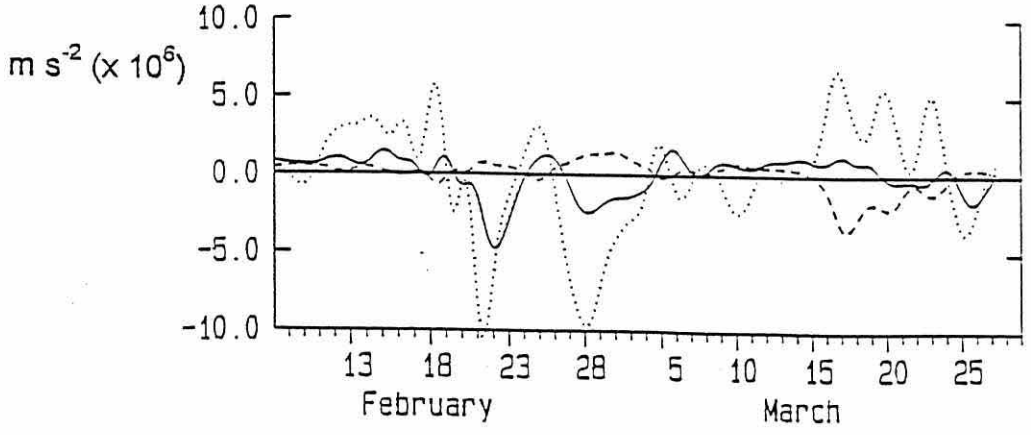

Figure 6.3. Time series of terms of the depth-averaged longshore momentum equation (Equation 6.6) for M2 during period 1.
Term **A** represents bottom stress, term **B** the longshore pressure gradient, term **C** the wind stress term. Positive is southgoing. Vertical axis units are m s^{-2} x 10^{6}. **A** (solid line), **B** (dotted line), **C** (dashed line).

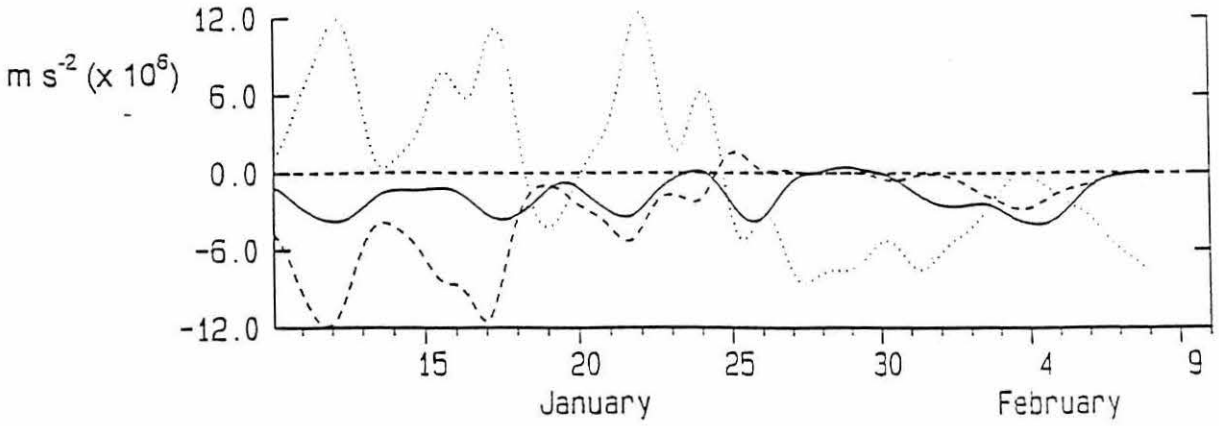

Figure 6.4. Time series of terms of the depth-averaged longshore momentum equation (Equation 6.6) for M1 during period 4.
Term **A** represents bottom stress, term **B** the longshore pressure gradient, term **C** the wind stress term. Positive is southgoing. Vertical axis units are m s^{-2} x 10^{6}. **A** (solid line), **B** (dotted line), **C** (dashed line).

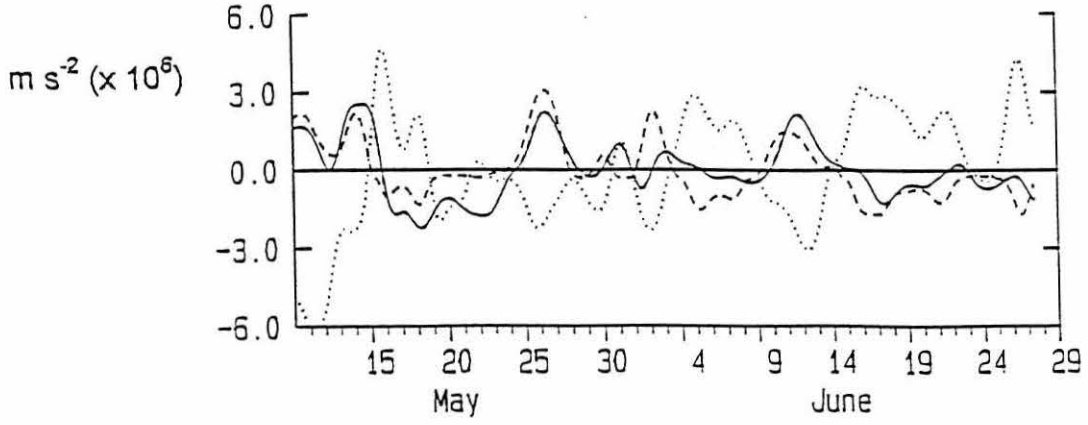

Figure 6.5. Time series of terms of the depth-averaged longshore momentum equation (Equation 6.6) for M1 during period 4.
Term **A** represents bottom stress, term **B** the longshore pressure gradient, term **C** the wind stress term. Positive is southgoing. Vertical axis units are m s^{-2} x 10^{6}. **A** (solid line), **B+C** (dotted line).

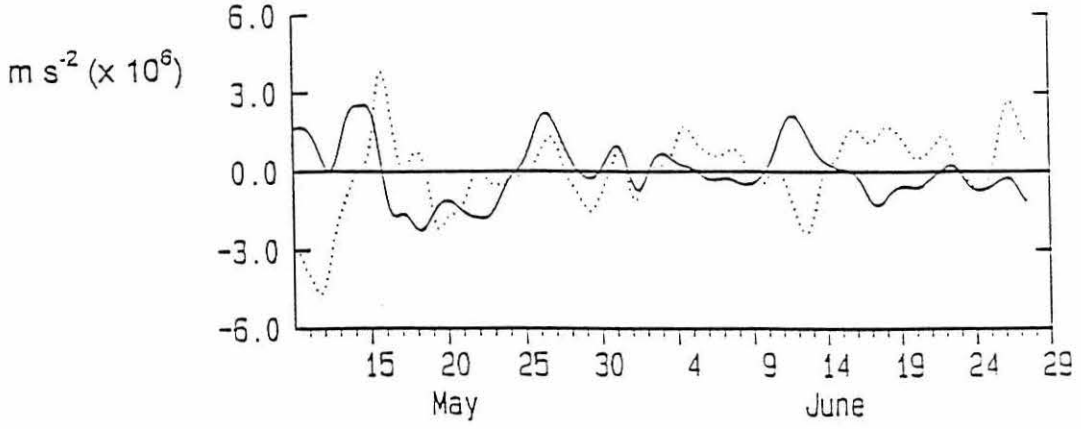

Figure 6.6. Time series of terms of the depth-averaged longshore momentum equation (Equation 6.6) for M1 during period 4.
Term **A** represents bottom stress, term **B** the longshore pressure gradient, term **C** the wind stress term. Positive is southgoing. Vertical axis units are m s^{-2} x 10^{6}. **A** (solid line), **B/3+C** (dotted line).

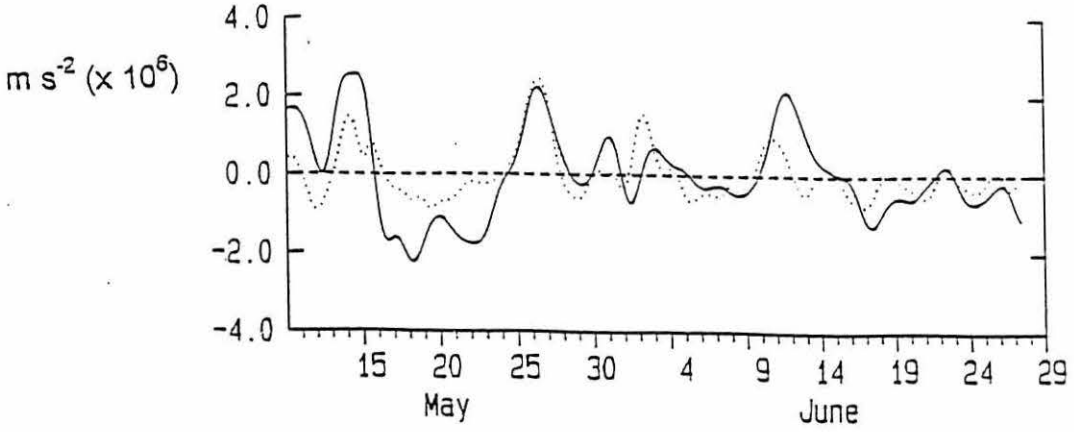

Chapter 7

7. Baroclinic Circulation

7.1 Introduction

Although the majority of the variability within the longshore sub-tidal flow can be explained by examining the interplay between bottom friction and the wind and longshore pressure gradient terms of the momentum equation, a significant proportion of the flow variance and, particularly, the mean flow cannot be accounted for in this way. This is of course to be expected: as shown in Chapter 4, the freshwater outflow from the Firth of Tay dominates the hydrography of St. Andrews Bay and it would be most unusual indeed if the strong density gradients associated with the estuarine plume did not lead to the superimposition of a baroclinic circulatory regime upon the previously described barotropic circulation of the bay.

7.2 Frontally Generated, Tidal-Scale Geostrophic Flows

In order to achieve an estimate of the significance of baroclinic flows within St. Andrews Bay the "thermal wind" equation was applied to the transect data. The thermal wind model assumes surface and bottom friction to be unimportant, which is obviously unrealistic as it has already been determined that both wind stress and bed friction are important in driving the circulation of the bay. The model was not, however, applied in an attempt to achieve a closure of the dynamical balance, but to attempt to determine the potential relative importance of baroclinic flows at various points within the study area.

The thermal wind model predicts the geostrophic velocity shear in the longshore direction to be given by Equation. 7.1

$$\frac{\partial u}{\partial z} = \frac{g}{\rho_0 f}\frac{\partial \rho}{\partial y} \qquad 7.1$$

where g is the acceleration due to gravity, f the Coriolis parameter ($1.21 \times 10^{-4}\ s^{-1}$), $\frac{\partial \rho}{\partial y}$ the cross-shore density gradient and ρ_0 a typical average seawater density, taken to be 1025 kg m^{-3}.

The thermal wind model was initially applied using the cross-shelf density distributions determined during each cruise for sections I, J, K and M. Stepwise integration of Equation 7.1, assuming zero velocity at the seabed, resulted in predictions of geostrophic current velocity of up to 30 cm s^{-1} (south-going) associated with the plume front near the surface. Figures 7.1a and b show predicted geostrophic current velocities through transect J during the May cruise and the associated density structure. The peak predicted velocities can be seen to occur near the surface at the region of maximum density gradient. The wind had been consistently directed towards the south-west for almost a week at the time of sampling, leading to trapping of freshwater within the bay and a steepening of the isohalines. During the period the inner stations were manned the tide was at its northernmost excursion.

Figure 7.2a shows predictions for section K during February, and again the associated density structure is shown in Figure 7.2b. In contrast to the previous example, at this time the plume was limited to the upper half of the water column in water of 20m depth and was not held against the shore (Figure 4.8 illustrates the salinity structure at this time). Surface geostrophic flows are predicted along both the offshore and shoreward edges of the plume, with rotation of frontal jets about the plume in a clockwise direction. This result suggests that during periods when the plume is not held against the shore, *i.e.* during south-westerly winds, detachment of the plume may lead to the generation of strong northward directed geostrophic flows shoreward of the plume, transporting water back toward the mouth of the Firth.

The amount of significant information that can be gained using data from the transects is limited however and can be misleading if not interpreted with care. Transect data collected using a CTD from a single boat is inherently non-synoptic. In an area which shows strong local density variability on a tidal time scale due to the movement of an estuarine plume such as St. Andrews Bay, the density structure represented in the

transects can only be regarded as approximate. The frontal zones associated with the plume are likely to alter shape and position significantly during the performance of a single transect (section K, for instance, typically took 4 hours to complete). This can lead to sharpening or broadening of the density fronts as an artefact of the sampling process and in turn to the prediction of frontally generated currents that may or may not actually exist. To test the applicability of the thermal wind model to the sub-tidal circulation within St. Andrews Bay the predicted shear at the mooring locations was compared to the actual measured shear derived from low-pass filtered current meter records at the appropriate sampling times, where such data existed. Figure 7.3 summarises the comparisons. The results of the test are inconclusive as the majority of points show only a low shear level, however where a significant shear was detected the trend is indicative of the presence of geostrophic currents within the bay.

The main concerns of this study lie with the sub-tidal flow regime. Predictions of geostrophic currents derived from transect data can tell us very little about such flows as tidal time-scale density field variations due to the presence of the Tay plume mask longer time scale processes. To determine the likely significance of the sub-tidal geostrophic circulation, density data from the moored instruments were used.

7.3 The Sub-Tidal Geostrophic Circulation: The "Thermal Wind" Approach

In order to investigate the role of geostrophic currents on a sub-tidal time scale it is necessary to be able to calculate cross-shore density gradients from the time series gathered by the moored instruments. This was only possible in a limited number of cases as the calculation requires simultaneous records from two moorings on a line normal to the shore. The relative positions of each mooring meant that it was not possible to calculate such gradients for M1. Gradients between pairs of mooring sites were calculated for the other cases where simultaneous time series existed.

The density gradient between each pair of moorings was calculated using time series obtained at the upper RCM as conductivity cells were only in place at that level. Geostrophic shears calculated from this data using Equation 7.1 can be equated to the velocity at the depth of the upper instrument if it is assumed that the flow at the sea-bed has a zero contribution from the geostrophic flow and the difference in flow (shear)

between the upper RCM and the lower is solely due to geostrophy. The predicted shears were subjected to correlation analysis (Sciremammano, 1979) with the low-passed velocity shear measured at a specified mooring (Table 7.1). A positive value for the correlation coefficient implies that a positive shear (flow directed southward) is directly correlated with a density gradient that is positive in the offshore direction.

The degree of correlation reveals significant variability at all but mooring 5. There appears to be a significant relationship between the geostrophic flow predicted from the M4 - M3 gradient and the shear at M3 particularly during period 7 (>95%), however at the same time there is also a significant inverse relationship with the predicted shear inshore of the mooring (from the M3 - M2 density gradient) (also >95%). As the predicted geostrophic flow is linearly related to the density gradient between pairs of mooring positions this suggests that the reduced salinity water does not spread to give a gradual cross-bay gradient when the watermass moves offshore, but separates from the coast. This results in a positive density gradient offshore of M3 and its inverse shoreward, suggesting the possibility of a significant geostrophic flow being directed northward in the inshore region during periods when the freshwater plume is separated from the shore. This is well illustrated by Figure 7.4, which shows the relationship between the two salinity gradients shoreward and seaward of M3 during period 7. The solid line indicates the relationship if the gradients were of the same magnitude on both sides of M3. This situation was not evident during period 6 (Table 7.1).

The slight but consistent deviation from the line in Figure 7.4 may suggest that the gradient shoreward of M3 was consistently steeper than the seaward gradient, at least throughout period 7. However, when the salinity gradient was positive inshore (between M3 and M2), suggesting the low salinity water was held close to the coast, the offshore gradient approximated a constant value of approximately -3×10^{-5} m^{-1}. It is most unlikely that salinity rose in the vicinity of M3 before dropping again offshore, so the offshore gradient should have been either positive or zero. The most sensible conclusion is therefore that during period 7 the conductivity cell at M3 recorded values with a small but consistent positive error.

The significant degree of correlation between the near-surface shear flow at M3 and the predicted geostrophic flow during period 7 in addition to the correlation during period 6, which is less significant but still in excess of >90%, suggest a geostrophic component to the sub-tidal flow at this site. Unfortunately it was not possible to calculate a shear at M2 for a period for which a corresponding density gradient was available, so it is difficult to determine the existence of northward-directed shear flows generated by the inshore gradient.

It should be borne in mind that the density gradient between two points in an area such as this, in the region of influence of a significant freshwater plume, is not smoothly varying. Across the frontal edge of the plume the gradient will be considerably steeper than on either side. Any flow generated by this front will be localised and may not be detected by moored instrumentation at all, even if the density gradient is. The predicted baroclinic flow due to the gradient between the two moorings assumes a smoothly varying density field. Given this assumption the true geostrophic velocity field is likely to be in excess of that predicted in the vicinity of a front and less or even absent beyond the influence of the frontal region. Given this fact and the mobile nature of the freshwater mass, as discussed earlier, we can only hope to get a significant correlation between predicted and observed shears if the mooring is positioned in the vicinity of a relatively stable density field. This appeared to be the case in the vicinity of M5.

7.3.1 Geostrophic shear off Fifeness

Four periods of simultaneous time series were collected at M5 and M6. Examination of the correlation coefficients between the predicted geostrophic flows between M5 and M6 and the current shear at M6 show no significant or consistent correlation. At M5 however, the predicted geostrophic shears are correlated with the observed difference between flows at the upper and lower instruments at a probability in excess of 90% during all four periods and in excess of 95% during three of them. During period 2 the correlation is in excess of 99% (Table 7.1). This suggests that flow around Fifeness is significantly influenced by the presence of freshwater from the Tay which leads to the generation of consistent geostrophic flows around the headland.

Due to the strong tidal currents associated with the headland (Table 6.1) the watercolumn typically remains vertically mixed from the shore out to approximately the 35m isobath throughout the year. As a consequence of this mixing area smooth density gradients are typical off Fifeness. This results in salinity, as measured at M5[1], acting as a good indicator of the intensity of the density gradient between M5 and M6 (Figure 7.5). Variations in the salinity gradient off Fifeness are dominated by fluctuations in inshore salinity, salinity as measured at $M6_1$ being relatively stable over time periods of less than the seasonal cycle. This is illustrated by comparing the range of values of the standard deviation for salinity at M5[1] with those at M6[1] (Table 7.2). Comparison of the mean salinities for each period shows them to be identical at the two moorings, with simultaneous variation in the mean between periods apparent, suggesting that mixing of freshwater at the southern end of St. Andrews Bay over sub-tidal timescales modulates the "background" salinity concentration for some distance offshore on seasonal timescales.

Figures 7.6a-d illustrate the degree of correlation between the vertical shear as measured at M5 during periods 2, 3, 4 and 7 and the geostrophic shear predicted by the thermal wind equation. The amplitude of the predicted shear closely agrees with that measured during all periods for which data were available. During all periods the majority of observed events were mirrored in the predicted shears. This is particularly the case during period 2 (Figure 7.6a), when both the amplitude and observed features of the record show a remarkable degree of agreement with predicted values. This level of agreement suggests that the sub-tidal flow and density fields around Fifeness approximate to geostrophic equilibrium, particularly during the winter months when high runoff is usual.

7.4 Estimation of the Mean Density-Driven Circulation

An estimation of the mean density-driven component of the longshore flow at a given instrument was attempted by calculation of the intercept of the multiple linear regression relation between the longshore flow, the longshore wind stress and the longshore pressure gradient using data for the entire year (Table 7.3) and also during each period (Table 7.4). The intercept value then corresponds to the flow velocity when the wind and pressure gradient have a value of zero. Given the previously established relationship between cross-shore salinity gradients and wind strength and direction there is some error implicit

in this method of estimation. An increase in southerly wind velocity will tend to lead to a reduction in the intensity of the density gradients and so a reduction in the speed of the geostrophic flows and vice versa for wind from the north. Given this proviso the intercept flow velocity has been used to estimate the contribution of the density driven flow. The calculation was performed for all velocity records using the longshore component of the current time series, with the dependant variables being the longshore component of the wind stress and the longshore pressure gradient terms as calculated for use in the momentum balance equation.

7.4.1 Intercept results

A clear difference can be seen between the intercept values as calculated for the upper and lower full-year records in Table 7.3. In all cases except M2 intercept values calculated using data from the lower instruments are far smaller than the upper and in most cases not significantly different to zero. In the vicinity of M2 the result suggests a significant density driven flow to the north at mid-depth. This is borne out by the individual period results presented in Table 7.4, in which the M2 intercept values are consistently negative, indicating northward flows.

At the upper instruments the higher positive values are suggestive of significant southward directed flows throughout the year, with the strongest currents being at M5 (Table 7.3). The consistent nature of the southward-directed flows near the surface at all locations is confirmed when the records are broken down into periods (Table 7.4); no negative intercepts were calculated during any part of the year. Significant seasonal variability is apparent at M5 and to a lesser extent M1, while M4 shows a more stable regime.

7.4.2 Mean values of the resolved flow field

The long-term mean flow field is often quoted as being representative of the density-driven circulation. Averaging of the current records over a period of approximately a month (or greater) should result in removal of synoptic scale signals such as the wind and longshore pressure gradient as set up by the wind, from the current records, leaving the average flow due to long-term density effects. However, if the wind for instance, is largely directionally invariant over the averaging period, it will obviously contribute to

the mean flow and enhance or reduce the signal due to the effects of density. Comparison of the intercept values as calculated from the multiple regressions and the mean values of the actual measured current should indicate the extent to which the mean flow is representative of the long-term density driven circulation within St. Andrews Bay, as represented by the intercept values.

Mean values of the annual mean longshore and cross-shore flow as measured at each instrument are presented in Table 7.5. Means for each period appear in Table 7.6.

The distribution apparent across the intercept values is also apparent for the annual mean longshore velocities. The pattern is again confirmed for the period means presented in Table 7.6. Figure 7.7 shows the distribution of the period mean longshore velocities plotted against the intercept values, the solid line represents a perfect 1:1 match. It is apparent that there is a very good agreement between the two sets of values, with the intercept values, representing the density driven flow, closely approximating the mean longshore velocities. This indicates that the long term mean velocity can reasonably be regarded as approximating the mean density-driven flow within St. Andrews Bay throughout the year.

7.5 Modelling the Density Driven Circulation

It cannot be stated categorically that the circulation represented by the mean flow or by the intercept values represents the density driven circulation, however the agreement between the data strongly suggests that this is the case. A degree of confirmation of the role of the long-term density driven circulation within the bay can be achieved by applying a model of a simplified coastal density regime. The model used was developed by Heaps (1972) and is described fully in Appendix A.

The model simulates the steady state density currents throughout the water column produced by a constant discharge of water q from one or more sources. The discharge is treated as originating from a line source and q is given as being per unit length of coastline. As well as a value for q the model requires as input values for the cross-shore density gradient term (as $\frac{1}{\rho_0}\frac{\partial \rho}{\partial y}$) and a suitable value for the eddy viscosity N_z.

The model treats a simple case in which the coastline is regarded as being straight and infinitely long with the freshwater discharge evenly distributed along it. It is, however, suitable as an approximation to the long-term density flow, for which the movement of the estuarine plume can be disregarded to some extent, as can the effects of the wind. If constant values for the cross-shore density gradient term, freshwater discharge and eddy viscosity are used for all water column depths for which it is run, the model output can be used to study the effect of variations in the water column depth on the density current profiles.

7.5.1 Calculation of input parameters

Single input parameters representative of St. Andrews Bay as a whole were used in the model runs. A value for q, the freshwater discharge per unit length was arrived at by division of a mean winter discharge rate of 450 $m^3 s^{-1}$ (average of periods 1 and 2, Table 4.2) by the length of the back of the bay, 22.5 km, giving q to be 0.12 $m^2 s^{-1}$.

The eddy viscosity was parameterised in terms of the amplitude of the tidal velocity following the formula (Heaps and Jones, 1987)

$$Nz = \tfrac{1}{2} K(a_T^2 + b_T^2) \qquad 7.2$$

where a_T and b_T represent the semi-major and semi-minor M_2 tidal velocities and K is a constant with a value of 0.2 s^{-1}. Using M_2 tidal velocities derived from harmonic analysis of current records from the various instruments a range of values of N_z were determined (Table 7.7). These values were used to determine a range of values for the term b, such that $b = kH/N_z$, where k is a linear friction coefficient with a value of 2 x 10^{-3}. A representative value for b of 5 was chosen for use in the model.

A vertically averaged cross-shore density gradient term $(\frac{1}{\rho_0}\frac{\partial \rho}{\partial y})$ corresponding to each mooring position was determined from the sectional data sets discussed in Chapter 4 when possible. On the basis of the results presented in Table 7.8 a representative global value of 2.5 x 10^{-8} m^{-1} was chosen.

7.5.2 Results

The model was run using the above parameters for total depths of 33 and 52m, corresponding to the water column depths at the locations of M3 and M4/M6 respectively, the results appear in Figures 7.8 and 7.9. Longshore flow (u) is well replicated by the model, particularly in water column depths corresponding to the location of M4 (Figure 7.9). Cross-shore flow (v) also appears to be closely reproduced near the sea-bed for both locations, however near surface values are not in agreement. This is perhaps unsurprising given the uncertainties associated with the measurement of cross-shore components of flow.

It seems therefore that many of the features of the long-term flow regime in the bay can be successfully reproduced by a simple steady-state density-driven model. This suggests that the mean flow is driven largely by a density gradient which results from the storage of freshwater within the bay over long timescales.

7.5.3 Application of the model to sub-tidal flow off Fifeness

Application of the thermal wind equations has shown (Section 7.3.1) that a strong relation between the density field and current shear exists off Fifeness. The model was run using the time series of the low-passed density gradient to which the thermal wind equations were applied previously.

Running the model with the parameter values outlined above resulted in a poor fit to observations. The value assigned to q was kept constant, it was therefore necessary to alter the value of the eddy viscosity through the term b. The best fit was produced using a b value of 55, corresponding to an eddy viscosity of 0.001 $m^2 s^{-3}$, smaller values of the eddy viscosity producing current speeds far in excess of those observed and larger values of N_z resulting in too small a shear. For period 4 an eddy viscosity value of 0.003 $m^2 s^{-3}$ (b = 20) was required for an optimal fit. Application of Equation 7.2 using observed values of the M_2 tide results in a value for N_z of 0.025 $m^2 s^{-3}$ and a corresponding b value of 2.5, an eddy viscosity 25 times larger than that required for most of the year. A reduced value for the eddy viscosity in the model is appropriate if some vertical stratification is present (Heaps, 1972). Given that the Fifeness model runs were concerned with the replication of

shear flow structure on daily time scales rather than the long-term average scenario used previously, a reduction of the value for eddy viscosity due to stratification may well be appropriate.

Figures 7.10-7.13 show the results of the modelling as applied to the low-passed shear at M5 for periods 2, 3, 4 and 7. The agreement between the modelled and measured shear is good, giving confidence in the ability of the model to replicate density driven flows off Fifeness. For an eddy viscosity of 0.001 $m^2 s^{-3}$ the model closely agreed with the results of the thermal wind equation as applied in section 7.3.1, which thus appeared to provide the best fit. Adjustment of the eddy viscosity to 0.003 $m^2 s^{-3}$ allowed the fit to be improved over that of the thermal wind predictions during period 4.

7.5.4 Modelling of mean flows off Fifeness

As an aid to the eventual calculation of fluxes (Chapter 8) the model was used to calculate a range of profiles of flow velocity at a water column depth corresponding to that of the M5 site. The eddy viscosity value was held constant at 0.001 $m^2 s^{-3}$ while the model was run using a range of mean seasonal density gradients. The gradient terms were calculated by applying the linear relation between salinity at M5[1] and the cross-shore density gradient (as $\frac{1}{\rho_0}\frac{\partial \rho}{\partial y}$) (Figure 7.5) to mean salinity values for each season, derived by meaning the salinity time series at M5[1] over periods 1 and 2 for Winter, 3 and 4 for Spring, 5 for Summer and 7 for Autumn (Table 7.9). Figure 7.14 illustrates the variation in predicted longshore velocity profiles resulting from the model runs. The model predicts an approximate increase in surface longshore velocity, directed southwards, of 1.6 cm s^{-1} per 10^{-5} kg m^{-2} increase in the cross-shore density gradient ($\frac{\partial \rho}{\partial y}$).

Longshore flow velocity values corresponding to the various seasonal mean density gradients were used in the calculation of longshore fluxes in Chapter 8.

7.6 Summary

The contribution of the baroclinic circulation to the flow field of St. Andrews Bay is complex, being highly variable on a number of temporal and spatial scales. An accurate

determination of the direct role of the estuarine plume is not within the scope of this study. In order for such an assessment to be achieved deployment of a large number of drogues at a wide range of depths would be necessary to determine variability in the Lagrangian flow field. The main aim of this study is the identification of the principal factors driving the sub-tidal circulation of St. Andrews Bay and to that end analysis has been concentrated on longer-term variability in the flow field.

It is however possible to identify certain trends in the baroclinic circulation on a tidal time scale, particularly the likely presence of south-going geostrophic jets associated with the seaward front of the plume and the inverse at the landward edge of the plume during periods when separation from the land can occur. The thermal wind model suggests that during south-westerly winds when the plume is forced seaward there is essentially a clockwise circulation around the edges of the plume. The scale of these jets is unlikely to be significant with regard to fluxes of nutrients or freshwater into or out of the Bay, however, given the narrowness of the fronts when compared to the scale of the Bay as a whole and their tidal-scale variability.

More significant is the sub-tidal baroclinic circulation. The correlation between the density field and the local low-passed velocity was found to be variable over the Bay as a whole. This is to be expected given the uncertainties associated with the calculation of density gradients, in particular the averaging out of frontal zones between the two positions at which data were available for the calculations. In addition the assumption of geostrophic balance implied in the use of the thermal wind model is unlikely to be accurate at all locations and times. Despite these points a high degree of correlation is apparent at certain locations. The clockwise gyre predicted to exist within the Bay at certain times by the tidal time-scale analysis appears to also exist on a sub-tidal scale. This suggests that during southerly winds refluxing of partially mixed water landward of the core of the plume back toward the mouth of the Firth may occur. This may have a significant influence on the efficiency of the flushing of contaminants from the Firth and the Bay, leading to an increase in the residence time of nutrients within the inner Bay and Firth of Tay.

Although baroclinic flow within the Bay itself appears to have been variable and difficult to identify during 1993, flow around the headland of Fifeness was remarkably consistent. A highly significant correlation exists between geostrophic flows predicted by both the thermal wind model and the more complex model of Heaps (1972) suggesting the flow to be largely in geostrophic balance throughout the year. The success in modelling the flow field in this area is likely to have been due to the largely well mixed nature of the water column in the locality of the headland, a product of the strong tidal currents, which will serve to eliminate fronts in the area of M5.

Values for the mean density driven flow derived from multiple regression of the flow field, longshore wind stress and longshore pressure gradient correlate well with the mean velocity field at the majority of locations and sampling periods. This suggests that the mean density driven flow can be regarded as a close approximation to the long-term mean flow field and is the main driving force of the long-term circulation of the Bay.

Table 7.1. The correlation between the vertical velocity shear measured at a given mooring and the cross-shore density gradient calculated between the upper RCM at pairs of moorings.

Correlation calculations follow the method of Sciremmano (1979) where coefficents of 1.7, 2.0 and 2.6 represent significance levels of 90%, 95% and 99% respectively.

Mooring (shear)	Period	Density gradient moorings	Correlation coefficient
M3	6	M4, M3	1.87
M3	6	M3, M2	1.12
M3	7	M4, M3	2.47
M3	7	M3, M2	-2.10
M4	6	M4, M3	0.94
M4	7	M4, M3	-0.14
M5	2	M6, M5	3.28
M5	3	M6, M5	2.23
M5	4	M6, M5	1.78
M5	7	M6, M5	2.33
M6	2	M6, M5	-0.09
M6	3	M6, M5	1.23
M6	4	M6, M5	1.75
M6	7	M6, M5	-1.95

Table 7.2. Mean and standard deviation of time series of salinity as measured at M5 and M6 for the common periods.

RCM	Period	Mean Salinity	$\sigma^{1/2}$
M5[1]	1	34.1	0.4
M5[1]	2	34.0	0.2
M5[1]	3	33.4	0.5
M5[1]	4	33.3	0.3
M5[1]	5	33.6	0.1
M5[1]	7	33.8	0.2
M6[1]	2	34.0	0.1
M6[1]	3	33.4	0.1
M6[1]	4	33.3	0.1
M6[1]	7	33.8	0.1

Table 7.3. Intercept values resulting from the multiple regression equation between the longshore component of velocity and the longshore wind stress and pressure gradient. Full year records.

RCM (upper)	Intercept value (cm s^{-1})	Standard error (cm s^{-1})	RCM (lower)	Intercept value (cm s^{-1})	Standard error (cm s^{-1})
$M1^1$	2.4	0.2	$M1^2$	0.5	0.2
$M2^1$	2.4	0.6	$M2^2$	-2.5	0.2
$M3^1$	3.7	0.5	$M3^2$	0.8	0.2
$M4^1$	5.1	0.3	$M4^2$	0.5	0.2
$M5^1$	7.0	0.3	$M5^2$	1.1	0.2
$M6^1$	2.4	0.3	$M6^2$	-0.5	0.2

Table 7.4. Intercept values resulting from the multiple regression equation between the longshore component of velocity and the longshore wind stress and pressure gradient. Individual periods.

RCM (upper)	Period	Intercept value (cm s^{-1})	Standard error (cm s^{-1})	RCM (lower)	Period	Intercept value (cm s^{-1})	Standard error (cm s^{-1})
$M1^1$	1	4.8	2.6	$M1^2$	1	3.7	2.2
$M1^1$	2	1.9	0.4	$M1^2$	2	1.8	0.3
$M1^1$	3	0.4	0.3				
$M1^1$	4	2.1	0.3	$M1^2$	4	-0.4	0.3
$M1^1$	5	2.2	0.3	$M1^2$	5	0.0	0.2
$M1^1$	6	3.2	1.0	$M1^2$	6	-0.5	0.5
				$M2^2$	1	-5.9	1.5
				$M2^2$	2	-3.7	0.4
$M2^1$	3	3.2	1.2	$M2^2$	3	-3.1	0.5
$M2^1$	4	2.2	0.9	$M2^2$	4	-0.8	0.3
				$M2^2$	5	-3.3	0.3
				$M2^2$	6	-1.8	0.6
				$M3^2$	3	0.6	0.6
				$M3^2$	4	0.5	0.3
$M3^1$	6	3.7	0.5	$M3^2$	6	1.1	0.5
$M4^1$	2	4.5	0.8	$M4^2$	2	0.5	0.8
$M4^1$	3	4.5	0.6	$M4^2$	3	0.7	0.5
				$M4^2$	4	1.2	0.5
$M4^1$	5	6.3	0.4	$M4^2$	5	1.4	0.3
$M4^1$	6	5.4	0.6	$M4^2$	6	1.4	0.7
$M5^1$	1	14.7	3.3	$M5^2$	1	7.0	2.2
$M5^1$	2	6.7	0.4	$M5^2$	2	2.0	0.4
$M5^1$	3	8.5	0.7	$M5^2$	3	2.2	0.7
$M5^1$	4	6.3	0.7	$M5^2$	4	-0.2	0.2
$M6^1$	2	1.6	0.9	$M6^2$	2	-1.5	0.8
$M6^1$	3	3.4	0.6	$M6^2$	3	-0.5	0.5
$M6^1$	4	3.5	0.5	$M6^2$	4	0.7	0.4
$M6^1$	5	2.3	0.4	$M6^2$	5	1.9	0.3
$M6^1$	6	3.7	0.5	$M6^2$	6	0.4	0.8

Table 7.5. Annual mean values of longshore and cross-shore velocity from 1993 data (standard deviation shown in brackets).

RCM (upper)	Longshore flow u (cm s^{-1})	Cross-shore flow v (cm s^{-1})	RCM (lower)	Longshore flow u (cm s^{-1})	Cross-shore flow v (cm s^{-1})
$M1^1$	1.8 (3.4)	-0.1 (1.6)	$M1^2$	0.4 (2.2)	-4.2 (2.5)
$M2^1$	1.5 (7.1)	-3.7 (4.9)	$M2^2$	-3.0 (3.7)	0.9 (1.9)
$M3^1$	4.0 (3.2)	-0.9 (1.7)	$M3^2$	0.8 (2.9)	-0.5 (1.3)
$M4^1$	5.1 (4.5)	-1.7 (2.6)	$M4^2$	0.5 (4.1)	-1.3 (1.3)
$M5^1$	5.2 (5.4)	3.7 (2.2)	$M5^2$	0.2 (3.3)	-1.7 (1.7)
$M6^1$	2.4 (4.2)	-1.0 (2.1)	$M6^2$	-0.6 (4.1)	-1.9 (1.5)

Table 7.6. Mean values of longshore and cross-shore velocity for the individual periods (standard deviation shown in brackets).

RCM (upper)	Period	Longshore flow u (cm s^{-1})	Cross-shore flow v (cm s^{-1})	RCM (lower)	Period	Longshore flow u (cm s^{-1})	Cross-shore flow v (cm s^{-1})
$M1^1$	1	-0.3 (3.8)	-0.1 (1.8)	$M1^2$	1	0.7 (2.7)	-6.1 (3.1)
$M1^1$	2	1.0 (2.2)	1.3 (1.4)	$M1^2$	2	0.8 (2.0)	-4.4 (2.4)
$M1^1$	3	0.5 (1.7)	0.1 (1.0)				
$M1^1$	4	3.0 (3.1)	-0.8 (1.5)	$M1^2$	4	0.2 (2.4)	-2.7 (1.8)
$M1^1$	5	2.3 (2.2)	-0.2 (1.1)	$M1^2$	5	0.4 (1.3)	-4.4 (2.2)
$M1^1$	6	3.5 (5.3)	-1.2 (1.8)	$M1^2$	6	-0.3 (3.0)	-3.9 (2.3)
				$M2^2$	1	-6.5 (4.5)	-1.4 (1.8)
				$M2^2$	2	-3.8 (3.0)	0.7 (1.5)
$M2^1$	3	-0.2 (7.0)	-5.4 (5.4)	$M2^2$	3	-3.1 (2.8)	1.4 (1.9)
$M2^1$	4	2.7 (6.8)	-2.5 (4.0)	$M2^2$	4	-0.7 (2.8)	1.2 (1.9)
				$M2^2$	5	-3.2 (2.4)	1.1 (1.6)
				$M2^2$	6	-1.6 (4.5)	1.8 (1.0)
				$M3^2$	3	0.5 (2.5)	-0.7 (1.0)
				$M3^2$	4	0.7 (2.0)	-0.7 (1.2)
$M3^1$	6	4.0 (3.2)	-0.9 (1.7)	$M3^2$	6	1.3 (4.1)	0.1 (1.6)
$M4^1$	2	3.4 (5.7)	0.3 (3.1)	$M4^2$	2	-0.2 (5.6)	-0.8 (1.5)
$M4^1$	3	4.5 (2.9)	-3.2 (1.8)	$M4^2$	3	0.5 (2.5)	-1.4 (1.1)
				$M4^2$	4	0.9 (3.3)	-0.8 (1.0)
$M4^1$	5	6.8 (3.7)	-2.0 (2.2)	$M4^2$	5	0.5 (3.1)	-1.6 (0.9)
$M4^1$	6	4.9 (4.3)	-2.4 (1.7)	$M4^2$	6	0.9 (5.1)	-1.8 (1.5)
$M5^1$	1	0.2 (6.2)	2.4 (1.6)	$M5^2$	1	-2.4 (3.8)	-0.9 (1.5)
$M5^1$	2	4.9 (3.9)	2.7 (1.8)	$M5^2$	2	0.9 (3.0)	-1.6 (1.7)
$M5^1$	3	7.4 (3.9)	3.7 (1.9)	$M5^2$	3	1.6 (3.3)	-1.0 (1.6)
$M5^1$	4	7.0 (5.0)	5.3 (1.9)	$M5^2$	4	0.1 (1.9)	-2.7 (1.2)
$M6^1$	2	1.0 (6.1)	-0.8 (2.1)	$M6^2$	2	-2.7 (5.6)	-2.6 (1.4)
$M6^1$	3	3.3 (3.0)	-1.2 (1.9)	$M6^2$	3	-0.5 (2.2)	-1.6 (1.3)
$M6^1$	4	3.5 (3.2)	-1.0 (1.8)	$M6^2$	4	0.5 (2.3)	-1.5 (1.3)
$M6^1$	5	1.6 (3.3)	-1.5 (2.3)	$M6^2$	5	-0.3 (2.4)	-1.8 (1.1)
$M6^1$	6	3.2 (4.2)	-0.2 (1.9)	$M6^2$	6	-0.2 (6.1)	-1.9 (2.0)

Table 7.7. Values of the eddy viscosity (N_z) due to the near-bed M_2 tide at a selection of mooring locations and corresponding values of the term b (Appendix A).

Mooring	Nz (m^2s^{-3})	b ($m^{-1}s^3$)
M1	1.6E-2	4.0
M3	1.6E-2	4.0
M4	1.0E-2	10.0
M5	2.5E-2	2.5
M6	1.0E-2	10.0

Table 7.8. Values of the cross-shore density gradient term $(\frac{1}{\rho_0}\frac{\partial \rho}{\partial y})$ (m^{-1} x 10^8) in the vicinity of the mooring locations during each transect.

Cruise	M1	M3	M4	M5	M6
February	0.7	-	1.5	-	1.6
March	2.5	-	2.0	2.5	2.5
May	2.5	-	-	-	3.3
July	2.4	1.6	1.6	-	5.0
September	-	-	2.5	-	-
October	3.0	1.0	1.0	-	1.6

Table 7.9. Mean seasonal salinity at M5[1] and corresponding values of the cross-shore density gradient term $\frac{1}{\rho_0}\frac{\partial \rho}{\partial y}$.

	Mean salinity	$\frac{1}{\rho_0}\frac{\partial \rho}{\partial y}$ (m^{-1}x 10^8)
Winter	34.1	1
Spring	33.3	7
Summer	33.6	5
Autumn	33.8	3

Figure 7.1a Geostrophic current velocities predicted using the thermal wind equation from density data measured along section J during the May cruise. Positive values indicate southward velocities (cm s^{-1}).

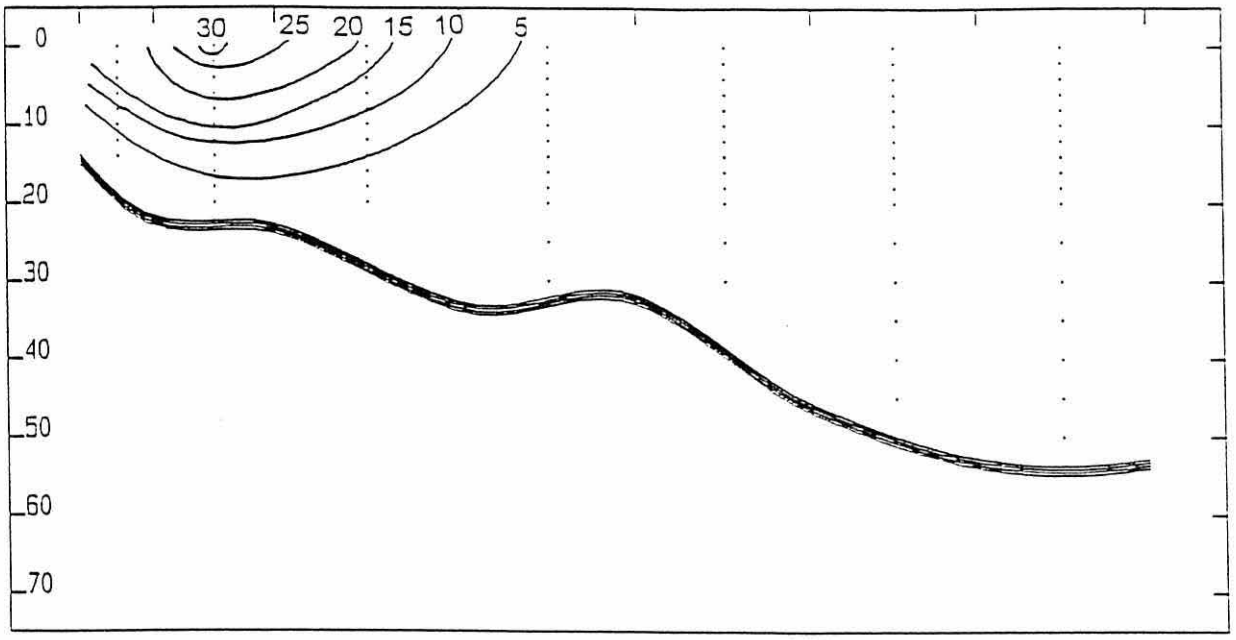

Figure 7.1b Cross-shore density structure (σ_t) measured along section J during the May cruise.

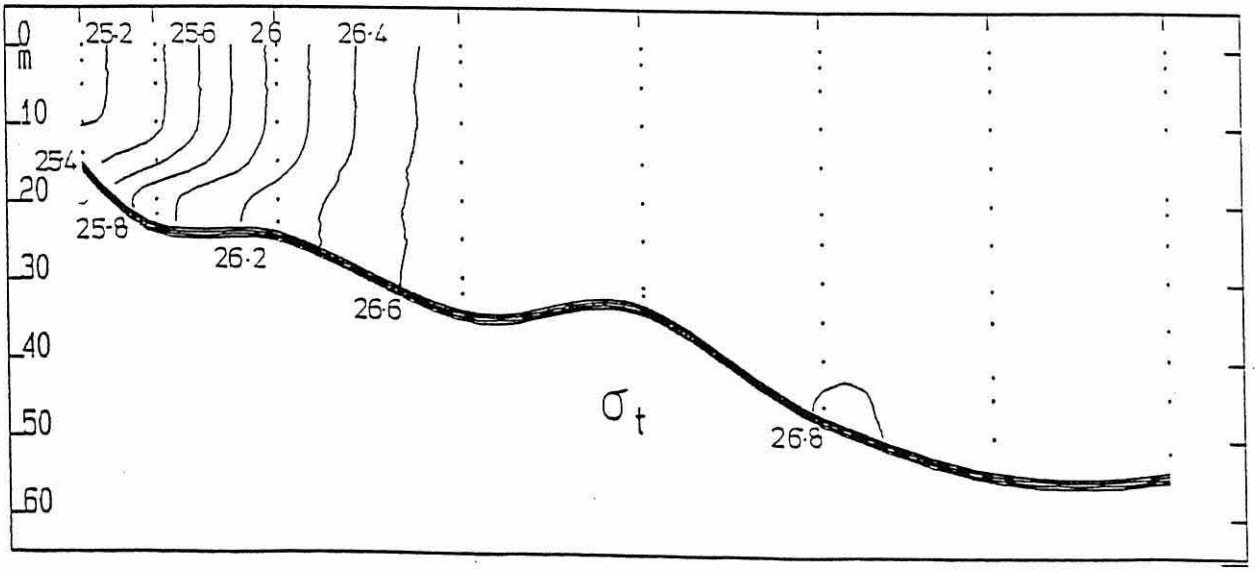

Figure 7.2a Geostrophic current velocities predicted using the thermal wind equation from density data measured along section K during the February cruise. Positive values indicate southward velocities (cm s^{-1}).

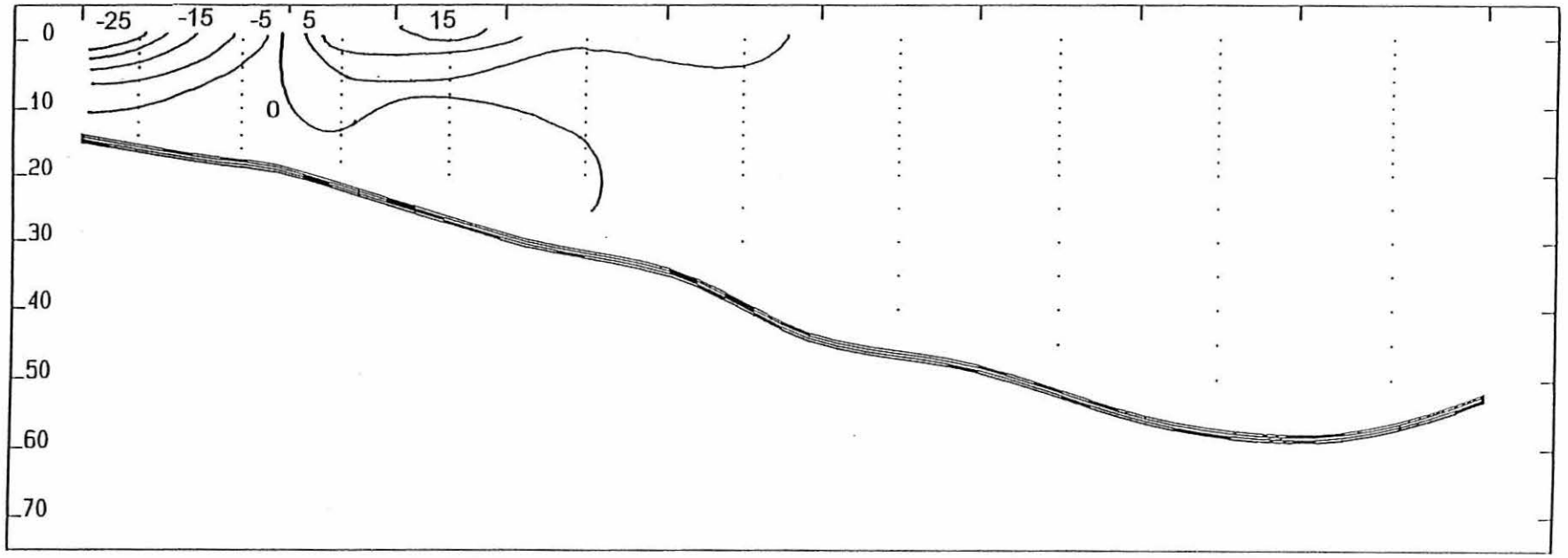

Figure 7.2b Cross-shore density structure (σ_t) measured along section K during the February cruise.

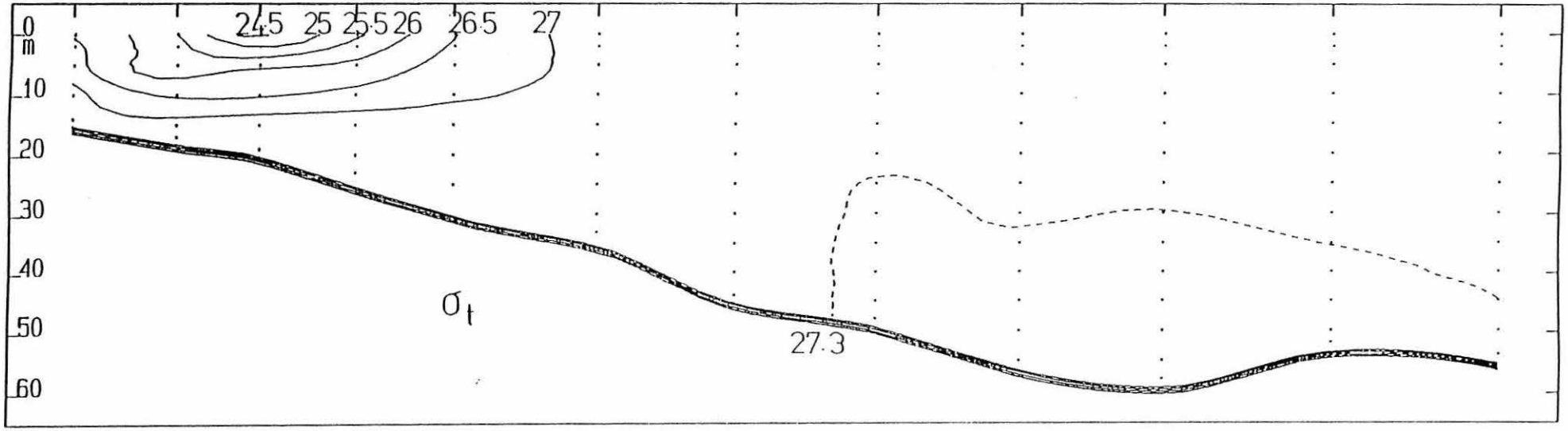

Figure 7.3 Vertical current shear in the vicinity of the mooring locations calculated from transect data using the thermal wind model plotted against the shear as calculated from velocities measured by the moored RCMs. The straight line represents the perfect fit.

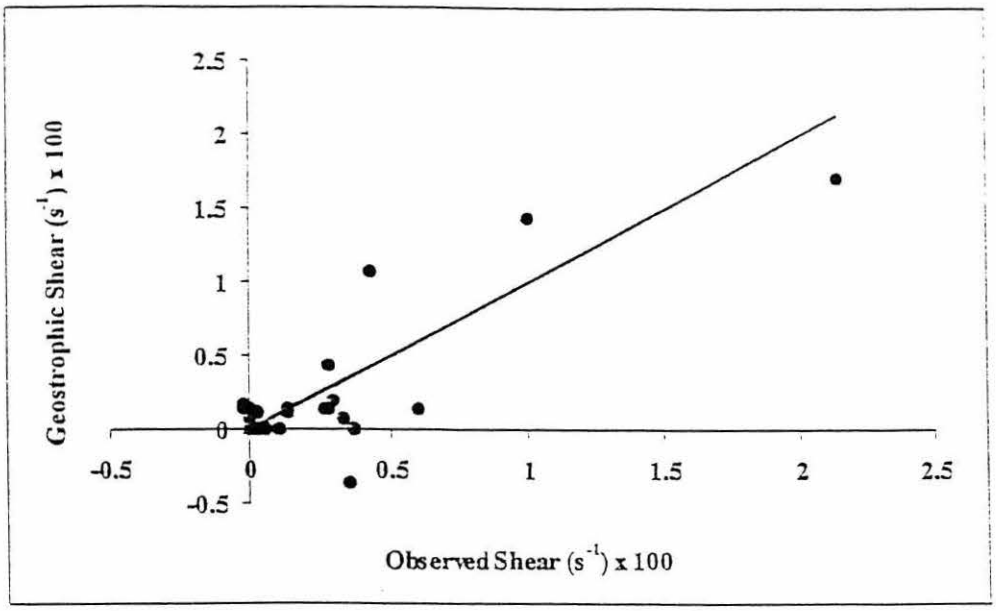

Figure 7.4 The daily mean cross-shore salinity gradient measured between M4[1] and M3[1] during period 7 against that measured between M3[1] and M2[2]. The line represents the relationship if the gradient were symmetrical about M3. Positive values indicate salinity increasing offshore.

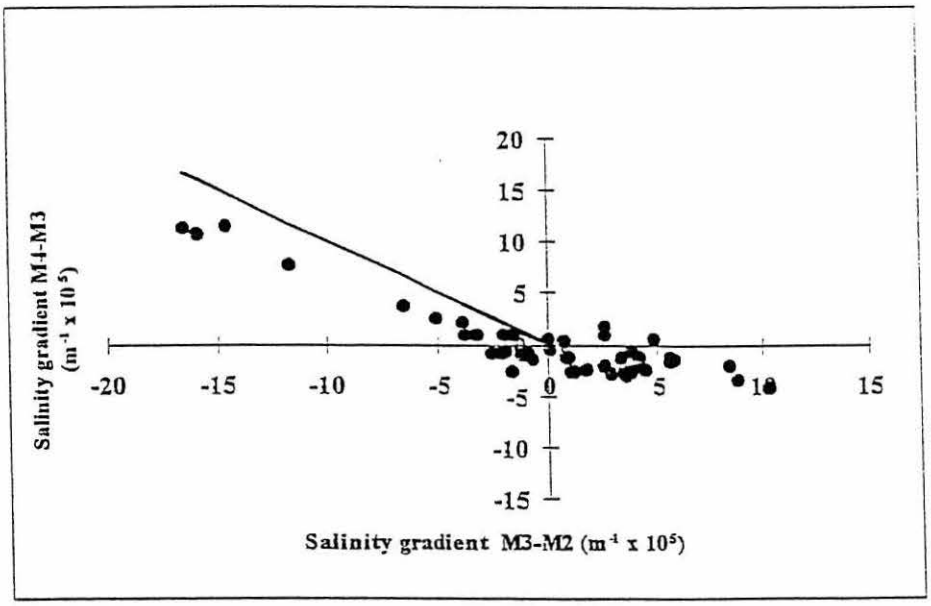

Figure 7.5 The linear relationship between daily mean salinity as measured at $M5^1$ and the daily mean cross-shore density gradient term $\frac{1}{\rho_0}\frac{\partial \rho}{\partial y}$ ($M5^1$-$M6^1$) off Fifeness as calculated from the low-pass filtered time series.

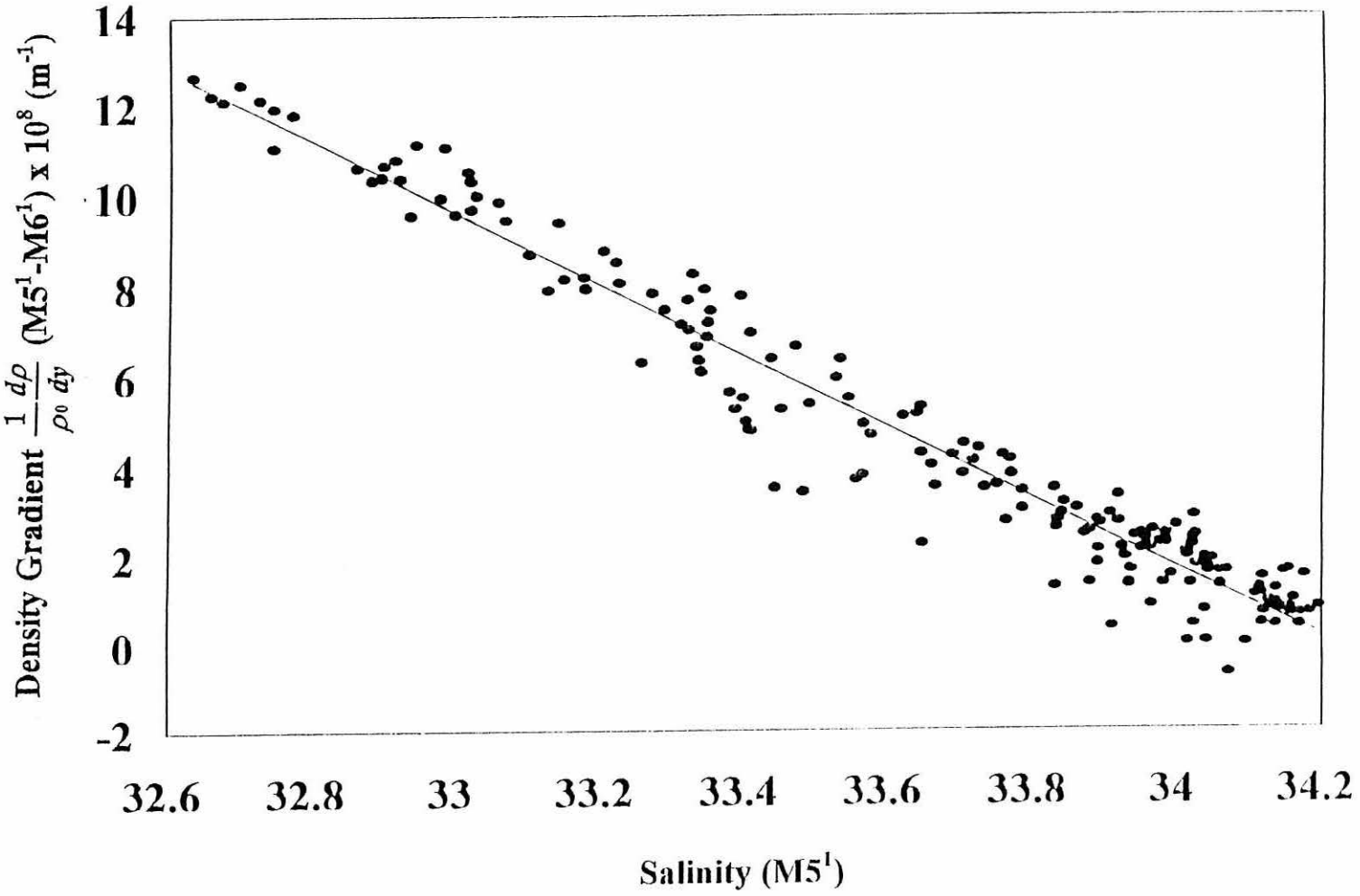

Figure 7.6 Measured vertical shear in (low-pass) longshore velocity between the upper and lower RCMs at M5 (solid line) and the corresponding vertical velocity shear as predicted by the thermal wind equation from density measurements at M5' and M6' (dashed line).

Figure 7.6a Period 2

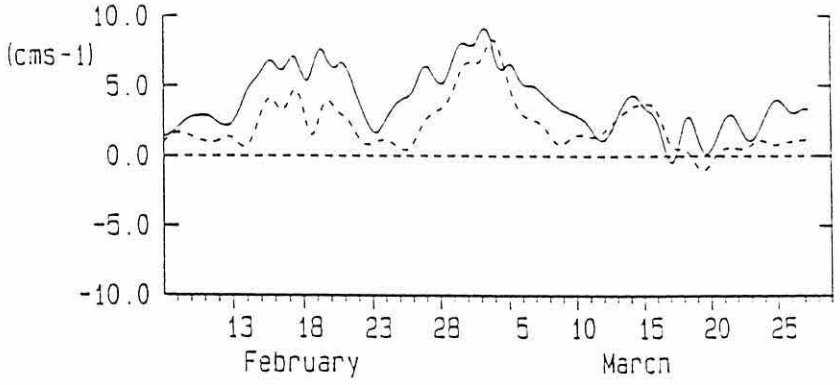

Figure 7.6b Period 3

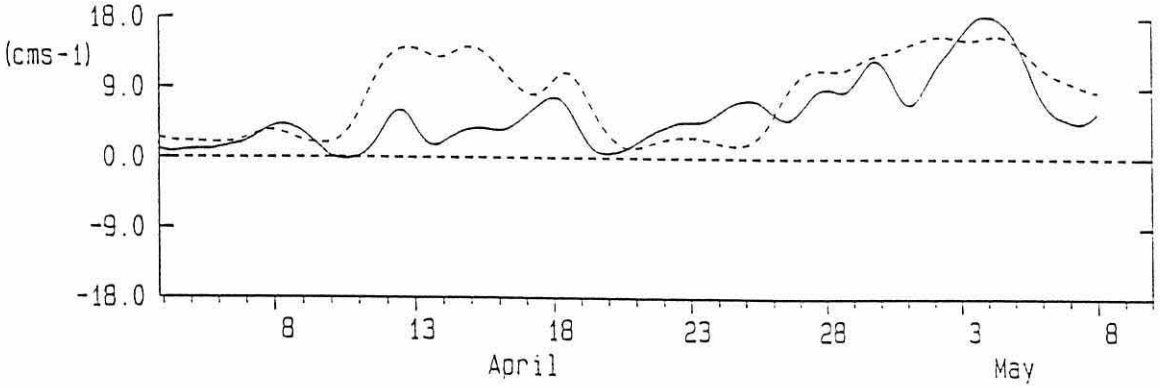

Figure 7.6c Period 4

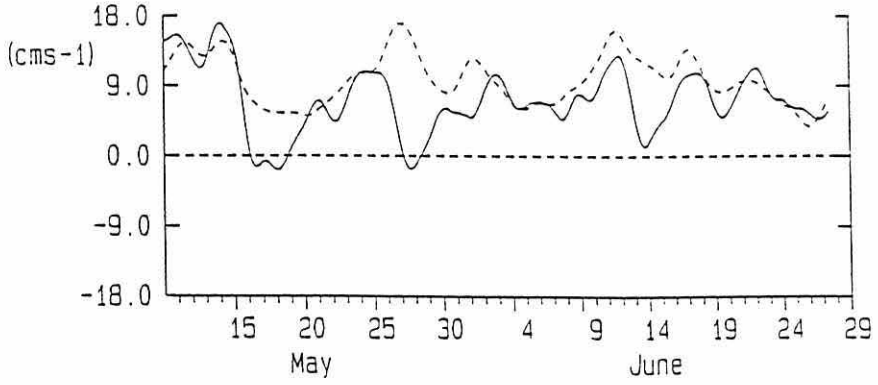

Figure 7.6d Period 7

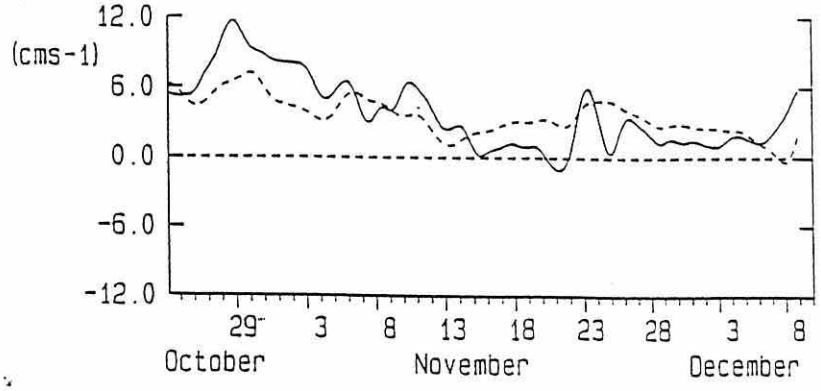

Figure 7.7 The relationship between the intercepts of the regression equation for the longshore velocity against wind stress and pressure gradient for each common period and the means over each common period of the longshore velocities as measured at each instrument. The solid line represents a perfect match.

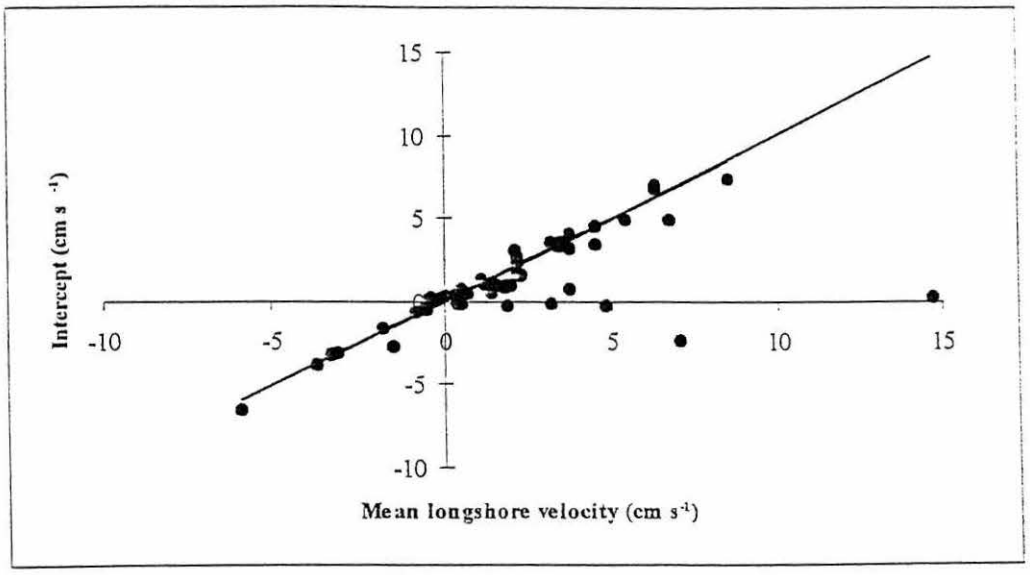

Figure 7.8 Predictions of depth-varying density-driven longshore (u) and cross-shore (v) velocity corresponding to a water column depth of 33m using the model of Heaps (1972) with b =5. The results are compared with the annually averaged values of the current components as measured at M3.

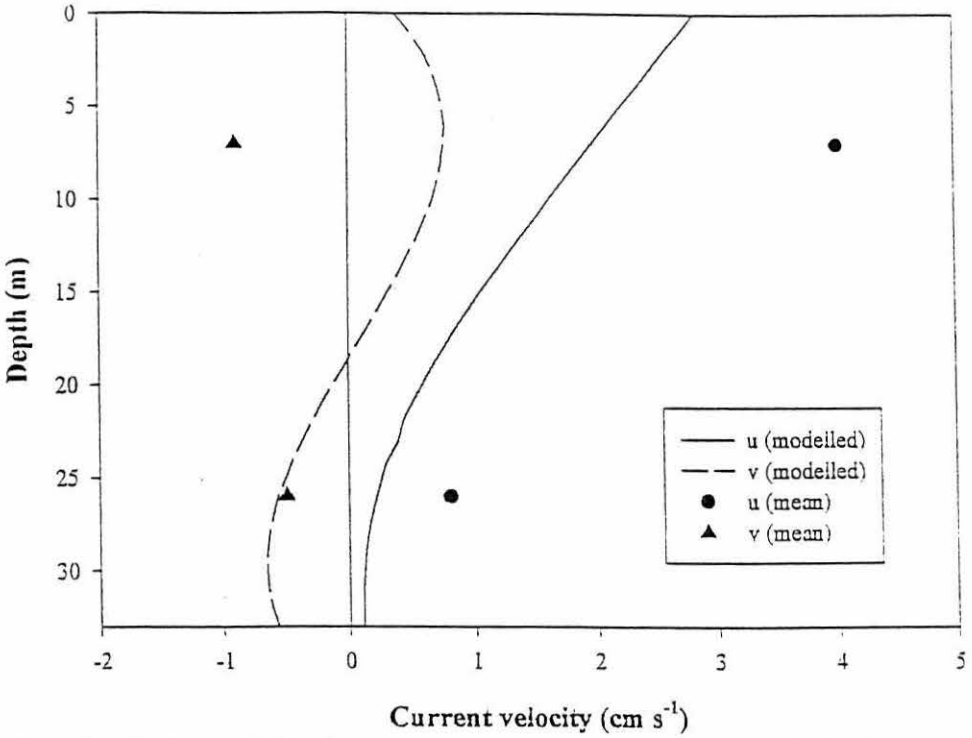

Figure 7.9 Predictions of depth-varying density-driven longshore (u) and cross-shore (v) velocity corresponding to a water column depth of 52m using the model of Heaps (1972) with b =5. The results are compared with the annually averaged values of the current components as measured at M4.

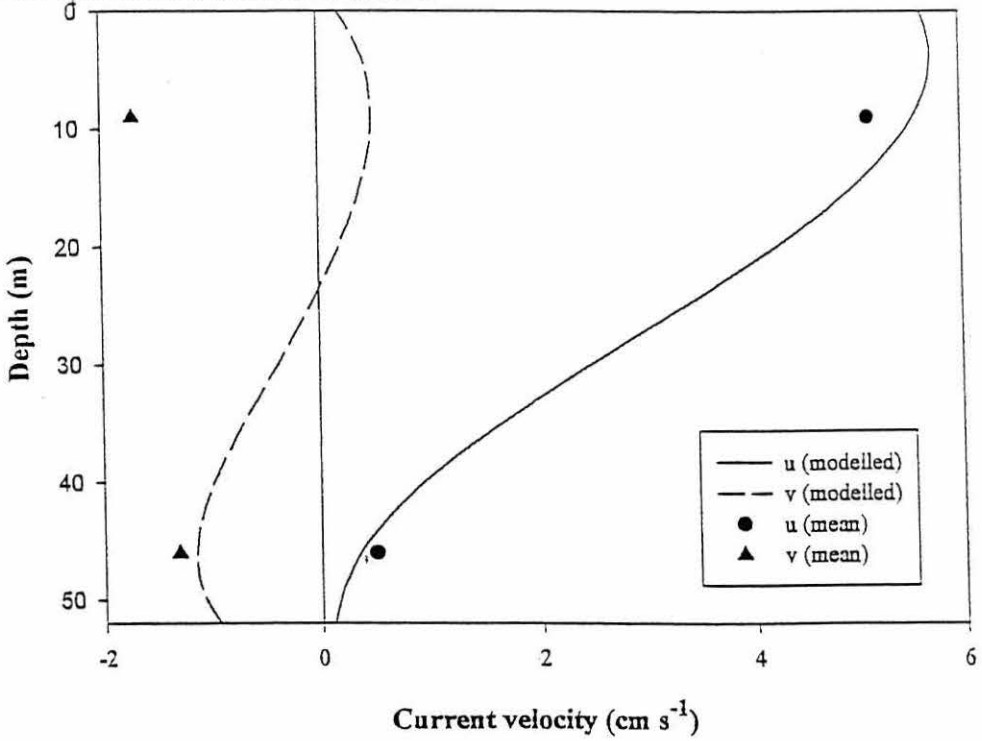

Figure 7.10 Vertical shear as predicted by the model of Heaps (1972) corresponding to and compared with the vertical shear in the longshore flow as measured between the upper and lower instruments (u^1-u^2) at M5 during period 2. Optimal fit required a b value of 55, corresponding to an eddy viscosity (N_z) of 0.001 m^2s^{-3}.

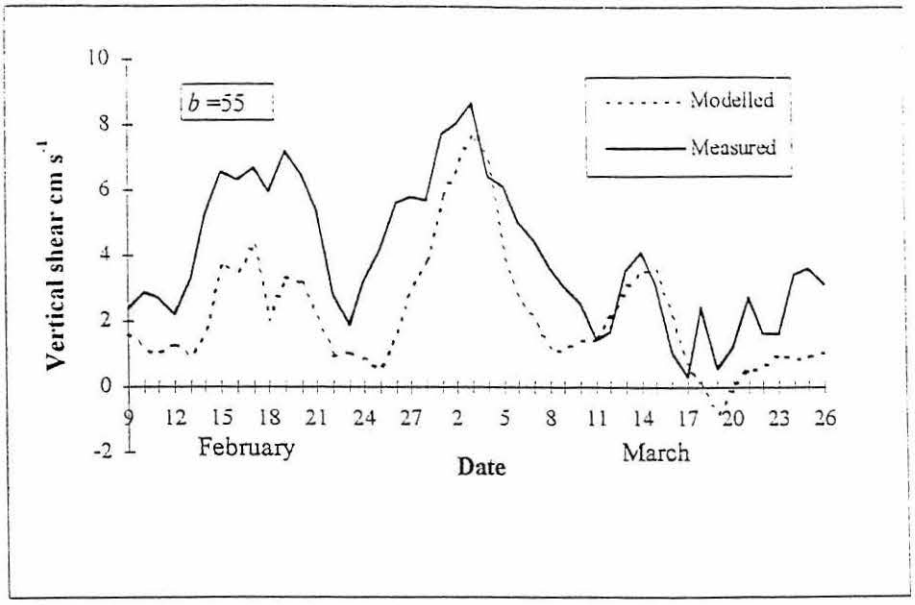

Figure 7.11 Vertical shear as predicted by the model of Heaps (1972) corresponding to and compared with the vertical shear in the longshore flow as measured between the upper and lower instruments (u^1-u^2) at M5 during period 3. Optimal fit required a b value of 55, corresponding to an eddy viscosity (N_z) of 0.001 m^2s^{-3}.

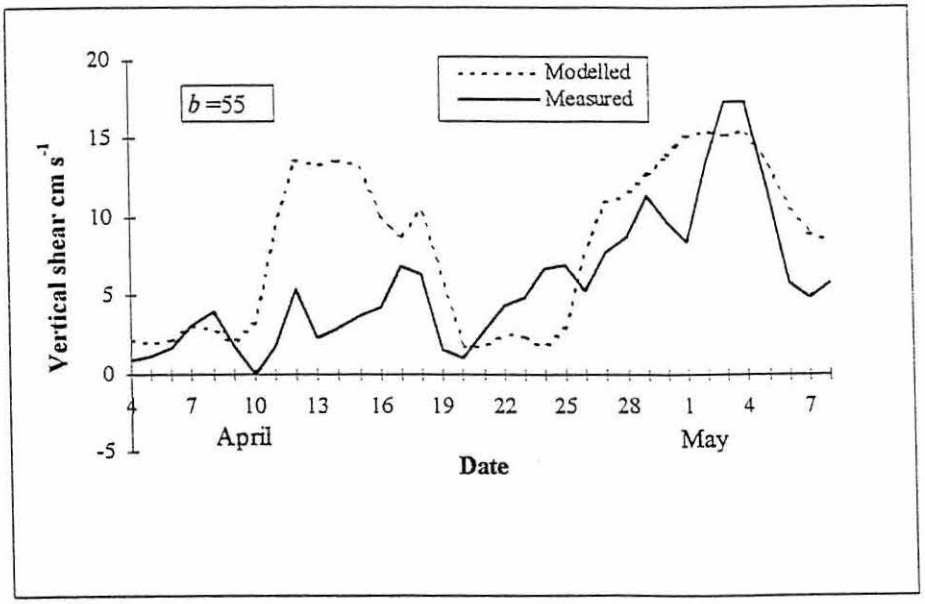

Figure 7.12 Vertical shear as predicted by the model of Heaps (1972) corresponding to and compared with the vertical shear in the longshore flow as measured between the upper and lower instruments (u^1-u^2) at M5 during period 4. Optimal fit required a b value of 20, corresponding to an eddy viscosity (N_z) of 0.003 m^2s^{-3}.

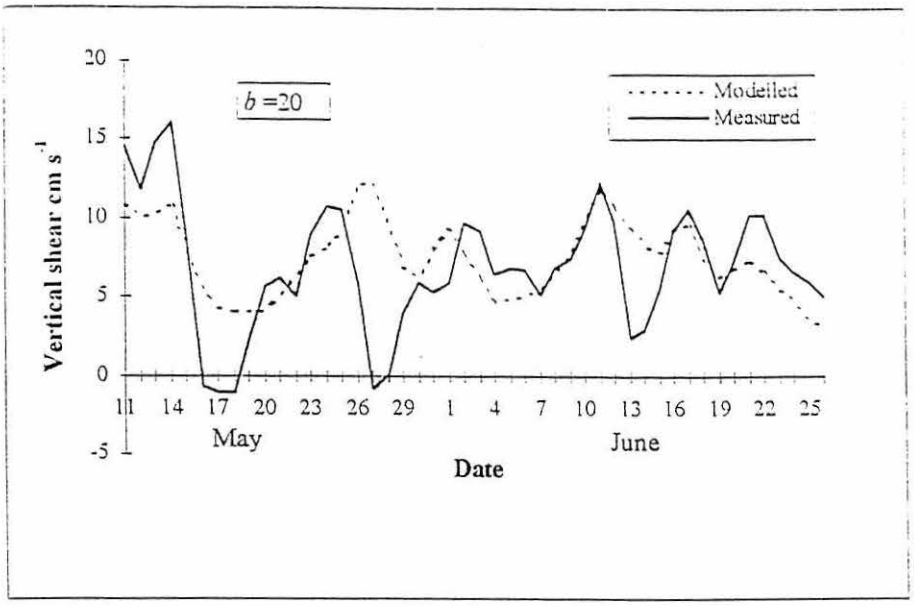

Figure 7.13 Vertical shear as predicted by the model of Heaps (1972) corresponding to and compared with the vertical shear in the longshore flow as measured between the upper and lower instruments (u^1-u^2) at M5 during period 7. Optimal fit required a b value of 55, corresponding to an eddy viscosity (N_z) of 0.001 m^2s^{-3}.

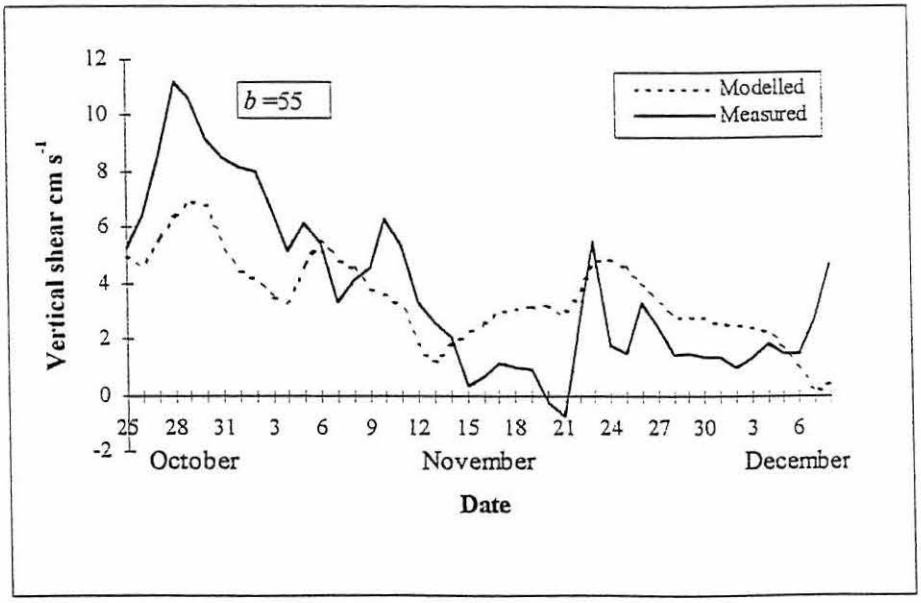

Figure 7.14 Vertical profiles of depth-dependant density driven longshore flow for cross-shore density gradients representative of winter, spring, summer and autumn.
Water column depth 28m (M5), b=55

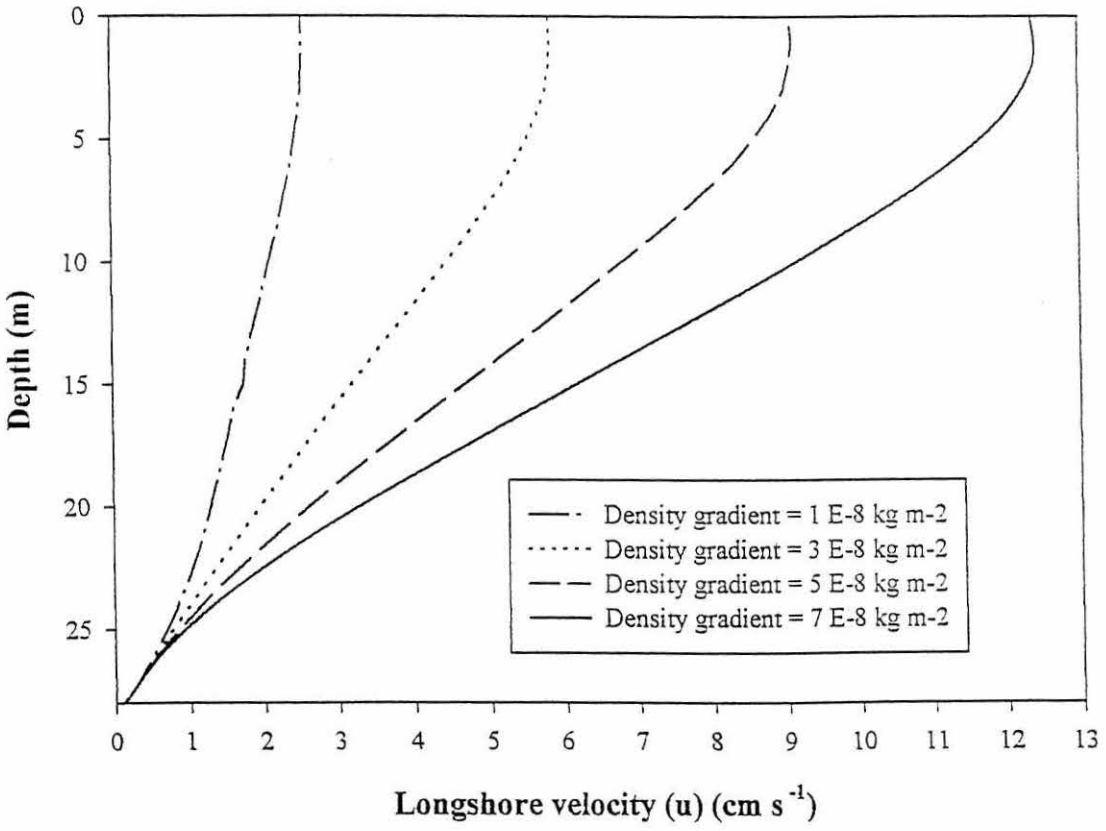

Chapter 8

8. Seasonal Mean Fluxes of Freshwater Through St. Andrews Bay

Estimates of seasonal mean advective fluxes of freshwater through the coastal zone in the St. Andrews Bay area have been attempted using mean data derived in earlier chapters. The approach taken has been to place a "black box" boundary at the outer limits of the Bay through which seasonal fluxes have been calculated (Figure 8.1). The northern and southern faces of the box are normal to the coast, the southern face being defined by line M of the hydrographic cruises, on which lay moorings M5 and M6 to the south. The northern face crosses line I at mooring M1. The outer edge of the box runs north-south and approximates to the 35m isobath.

The outer box limit was chosen using the knowledge that the response of the flow field to the balance between the wind and pressure gradient typically reverses between the 28m (M1) and 52m (M4, M6) isobaths, which implies that a line of zero flow for the depth averaged barotropic circulation will occur somewhere between. As calculated in Chapter 6, balancing the longshore momentum equation for St. Andrews Bay requires the division of the measured north-east coast pressure gradient by a factor of three. If u is set to zero in Equation 6.6 to represent the situation at the hypothetical isobath at which the wind stress and pressure gradient balance we arrive at

$$\tau_{sx} = h\frac{\partial p}{\partial x} \qquad 8.1$$

which equates to Equation 5.10 via the hydrostatic relation (Equation 5.9) using the wind and pressure gradient as measured to give a value of 12m for h ($h = R/\rho g$). However, if the pressure gradient is corrected by a factor of three as is required by the momentum balance, we reach a value of 36m for the isobath at which no barotropic motion occurs. This value was rounded to 35m and used as the outer limit for the coastal box.

The box faces were idealised into simple shapes for ease of calculation, the dimensions of which were calculated using Admiralty charts. The coastline to the north and south of the Bay shelves relatively smoothly, making the assumption of smooth slopes reasonable.

The box was divided into two layers vertically at 20m, taken to approximate to the average depth of the pycnocline in Summer. The dimensions of the box faces are illustrated in Figure 8.2.

In many cases in the literature the calculation of volume fluxes is accomplished by assigning a vertical plane, or face, for which data provided by a current meter are assumed representative. Examples of such an approach can be seen in, for instance Turrell *et al.* (1990), Turrell and Henderson (1990), Blanton *et al.* (1994) and Morris *et al.* (1995). Flux estimates calculated using this method are subject to considerable error as the assumption that the flow measured at the instrument is representative of the flow over a possibly broad area is not necessarily realistic. The error can be reduced by the use of a finer instrument grid, however the cost of such coverage is normally prohibitive, so fluxes must be estimated using the available data. For the present study a mixture of measured and modelled mean flows were used. This methodology was adopted in an attempt to arrive at a value for the mean flow which is more representative for the upper and lower faces than the flow arrived at by averaging the current meter records.

The work of Chapter 7 showed that the correlation between the flow at a given instrument meaned over a period, and the density driven flow as represented by the intercept value of the regression equation for the longshore flow, wind stress and pressure gradient, was good, showing that the density driven flow approximated the mean flow. Following from this, as described in Chapter 7, the model of Heaps (1972) was used to calculate vertical longshore velocity distributions for a range of typical seasonal density distributions corresponding to the location of M5. The velocities predicted by this method were vertically meaned over two "bins", the upper 20m and the rest of the water column, to give representative values for the upper and lower faces (Table 8.1).

At the southern boundary of the box a modelling approach was possible as density gradients between M5 and M6 could be calculated. For the northern face of the box the presence of only a single instrument meant that mean density gradients could not be determined. It was therefore necessary to use mean flows calculated from observational data in the calculation of fluxes through the northern boundary of the box. Consideration of the period mean flows (Table 7.6) showed an obvious seasonal signal to be absent, the principal pattern being the larger longshore velocities at the upper instrument and very small mean velocities near the bed. This, in combination with the fact that the standard

deviation was of the same order of magnitude as the mean itself, obscuring the annual variations, suggested that the use of a seasonally varying velocity was not justified at the northern boundary. The annual mean longshore velocities of 1.8 and 0.4 cm s^{-1} at the M1 instruments and associated standard deviations (Table 7.5) were therefore adopted for all the seasonal flux calculations. Velocity values used in the flux calculations are summarised in Table 8.2.

There is a significant uncertainty attached to the assumption that the flow through the north and south faces is uniform across each face. In the case of the southern boundary variability about the mean has been estimated by calculation of the standard deviation of the model results, taking the results at one metre depth intervals. It should be noted that the calculation of fluxes is intended purely as a means of coarse estimation of the relative magnitudes of the fluxes through each face and from the estuary and care must be attached to the interpretation of the results.

8.1 Fluxes of Seawater

Seasonal volume fluxes of water through the box can be described by the equation

$$Q_C = Q_F + Q_N - Q_S \qquad 8.2$$

such that Q_F represents the flux into the box from the Tay, Q_N and Q_S represent the flux into the box from the north and the flux out of the box to the south respectively. If the fluxes through the north and south faces are regarded as fully describing longshore transport, by conservation of volume the imbalance between these fluxes must be ascribed to cross-shore transport, the flux being given by Q_C. The flux values for the north and south faces are the sum of the values derived for the upper and lower boxes, which were obtained by multiplication of the mean longshore velocity by the area of the box. The box areas are given in Figure 8.2 while the velocities and resulting flux values used appear in Table 8.3. The freshwater fluxes from the Tay are the seasonally meaned discharges during 1993.

8.1.1 Results

The large standard deviation attached to the flux values, particularly through the northern boundary, mean that possible conclusions drawn from the calculations of this section are limited. However, on the basis of the mean values the results of the estimation of fluxes

suggest that only during the winter period did a mean flux of seawater occur through the offshore wall of the box. Examination of the standard deviation values suggests, however, that even this gross conclusion is uncertain.

Given the size of the longshore fluxes it is apparent that the volume flux balance is not sensitive to the rate of riverine input, at least on seasonal timescales. Since a constant input from the north has been applied, the flux balance is totally dependant on changes in the extent of the flux through the southern face of the box. During winter this flux was minimised due to the limitation of freshwater to the surface layer, leading to a weak cross-shore density gradient throughout the rest of the water column and therefore a weak baroclinic flow below the plume. This situation has been identified previously as being due, at least in part, to strong winds from the south which promote offshore flow and a shallowing of the pycnocline. It appears, therefore, that the promotion of an offshore flux of water by southerly winds occurs not only as the result of an "Ekman type" mechanism and an upwelling style offshore movement of freshwater, but also as the result of the weakening of the normal south-going geostrophic flow by the limitation of freshwater to the upper layers.

The results of the calculations suggest that under the weaker winds of summer or during periods of northerly wind, water must be drawn landward from offshore to supplement that pumped southward past Fifeness by the strong geostrophic flows at the southerly end of St. Andrews Bay. If we calculate the mean cross-shore flow speed required to provide the largest seasonal flux of 0.4 $km^3 d^{-1}$ (4700 $m^3 s^{-1}$) during spring we arrive at a figure of 0.6 cm s^{-1} (standard deviation 1.4 cm s^{-1}); velocities of this magnitude can be described as diffusive. If the onshore flow did not occur throughout the water column, as is likely, but was limited to the deeper layers, the weak but consistent mean onshore velocities measured throughout the study at the outer instruments could easily supply the required onshore flux.

8.2 Fluxes of Freshwater

Using the same seasonal flow, velocity fluxes of freshwater through the faces of the box were calculated. The mean freshwater content of the seawater passing through the northern and southern faces each season was estimated by averaging the time series of salinity collected at the upper instruments at M1 and M5 and then calculating the mean freshwater fraction across the face for the period, using the relation presented in Equation

4.1, with the base salinity again taken to be 34.7. Data from periods 1 and 2 were meaned to give the average winter salinity, spring was given by periods 3 and 4, summer by 5 and 6 and autumn by 7. Data was not available from period 6 for M5, the summer average is therefore represented by period 5 alone. The mean salinities and freshwater fractions appear in Table 8.4. Mean rates of freshwater flux (Q') through the faces are calculated by multiplication of the flux of seawater through each face (Table 8.3) by the freshwater fraction (Table 8.4), the percentage freshwater divided by 100, and appear in Table 8.5.

8.2.1 Results

Resulting mean fluxes are again associated with standard deviations of large size. The values for the northern boundary are again approximately twice those of the mean, making firm conclusions difficult to make. The mean fluxes do suggest an enhanced export of freshwater through the southern boundary into the outer Firth of Forth as compared to the input of freshwater to the box through its northern limit throughout the spring and summer, but an approximate balance during autumn and winter. Seasonal fluxes of freshwater through the northern face of the box are directed southward into the box with the mean flow field. The lack of a significant source of freshwater for some distance to the north of the Tay suggests that the majority of freshwater entering the box through the northern boundary originated in the Tay itself, being transported northward against the mean flow mainly by wind events.

Fluxes were dominated during winter and autumn by the riverine input of freshwater. During these seasons higher mean salinities were in evidence at the southern boundary of the box, a situation which reduced the mean south-going vertically meaned flux resulting in an excess of freshwater within the flux box. As the vertically meaned salinity at the southern boundary was higher during these seasons and the average transport through both northern and southern faces was directed towards the south, it appears unlikely that low salinity water was being stored within the Bay over seasonal timescales. If this had been the case lower salinities would have been detected at M5. It appears therefore that the excess must leave the box in some way. Transport offshore through the outer face of the box is only likely to occur under the influence of southerly winds, which indeed dominate over the winter period. As shown in Chapter 4 southerly winds act to enhance stratification. It seems likely, given evidence from hydrographic observations of the water column during the February high runoff period discussed earlier (Chapter 4) that freshwater during the winter and autumn periods is transported out of the box as a shallow

plume. Offshore transport will be enhanced by the southerly winds but significant transport through the southern boundary is likely at the surface. Such a flux does not appear in the present estimation as the surface plume was not resolved by the moored instrumentation.

It appears therefore, that during autumn and winter, fluxes of freshwater from the bay occur principally in the surface layers of the water column. But, during the spring and summer months the dominant mode of transport is via geostrophic currents which, due to more complete mixing of freshwater with seawater, transport stored freshwater from the bay throughout the water column.

8.4 Summary

Mean seasonal fluxes of seawater and freshwater through St. Andrews Bay have been calculated. Transport on seasonal time scales has been determined to be governed by the mean density driven circulation of the Bay and is directed towards the south, into the outer Firth of Forth. Consideration of the magnitude of the fluxes thus derived, in association with the knowledge of the behaviour of freshwater within the Bay derived from previous chapters suggests the approach adopted here is insufficient to describe accurately fluxes of freshwater from the box due to the importance of the estuarine plume in winter. The plume was limited, during winter conditions, typified by high runoff south-westerly winds, to a thin layer which was unresolved by the moored instrumentation. Excess of freshwater within the Bay predicted by the flux balance is thought more likely to have exited the box with the plume rather than in the offshore direction required by the "box model" for conservation of mass.

The flux calculations suggest that during the winter months transport from the box is dominated by the plume due to the limitation of freshwater to the upper layers which results in a diminished density-driven flow throughout the rest of the water column. During summer, however, geostrophic currents driven by the vertically mixed, cross-shore density gradient act to pump water southward, past Fifeness. During the summer months an onshore flux of seawater is required to balance the southward flow of water. This compensatory onshore flux is thought to occur near the seabed as part of the estuarine bottom return flow.

Table 8.1. Mean seasonal density-driven longshore flows (cm s^{-1}) corresponding to the upper (S^T) and lower (S^B) faces of the southern boundary of the flux box. Flows calculated using the model of Heaps (1972). Standard deviations from the mean appear in brackets.

	Velocity S^T cm s^{-1}	Velocity S^B cm s^{-1}
Winter	2.0 (0.3)	0.8 (0.4)
Spring	8.7 (3.1)	1.5 (1.1)
Summer	6.5 (2.3)	1.2 (1.1)
Autumn	4.3 (1.3)	1.0 (0.7)

Table 8.2. Longshore velocities (standard deviation, in brackets) assigned to the upper and lower faces of the flux box.

	Velocity S^T cm s^{-1}	Velocity S^B cm s^{-1}	Velocity N^T cm s^{-1}	Velocity N^B cm s^{-1}
Winter	2.0 (0.3)	0.8 (0.4)	1.8 (3.4)	0.4 (2.2)
Spring	8.7 (3.1)	1.5 (1.1)	1.8 (3.4)	0.4 (2.2)
Summer	6.5 (2.3)	1.2 (1.1)	1.8 (3.4)	0.4 (2.2)
Autumn	4.3 (1.3)	1.0 (0.7)	1.8 (3.4)	0.4 (2.2)

Table 8.3. Estimated resulting mean seasonal fluxes (**Q**) of seawater (and associated standard deviation, in brackets) based on the values of Table 8.2. Flux subscripts refer to southern face (**S**), northern face (**N**), freshwater input (**F**) and excess or deficit (**C**).

	Q_S $km^3\ d^{-1}$	Q_N $km^3\ d^{-1}$	Q_F $km^3\ d^{-1}$	Q_C $km^3\ d^{-1}$
Winter	0.18 (0.03)	0.31 (0.67)	0.03 (0.04)	0.16 (0.41)
Spring	0.73 (0.28)	0.31 (0.67)	0.02 (0.02)	-0.40 (0.96)
Summer	0.55 (0.21)	0.31 (0.67)	0.01 (0.01)	-0.23 (0.55)
Autumn	0.37 (0.12)	0.31 (0.67)	0.02 (0.02)	-0.04 (0.10)

Table 8.4. Seasonal mean salinity and mean percentage freshwater for the north and south faces of the box (standard deviation in brackets).

	S		N	
	Mean salinity	**Percentage freshwater**	**Mean salinity**	**Percentage freshwater**
Winter	34.1 (0.3)	1.8 (0.8)	34.2 (0.1)	1.5 (0.2)
Spring	33.3 (0.4)	4.0 (1.1)	34.0 (0.1)	2.0 (0.3)
Summer	33.6 (0.2)	3.1 (0.5)	34.2 (0.1)	1.5 (0.2)
Autumn	33.8 (0.2)	2.5 (0.5)	33.8 (0.2)	2.7 (0.6)

Table 8.5. Seasonal fluxes of freshwater through the faces of the box (standard deviation in brackets). Suffix are as for Table 8.3. All values x 10^3.

	Q'_S $km^3\ d^{-1}$	Q'_N $km^3\ d^{-1}$	Q'_F $km^3\ d^{-1}$	Q'_C $km^3\ d^{-1}$
Winter	3 (1)	4 (9)	33 (37)	34 (86)
Spring	29 (14)	6 (13)	18 (16)	-5 (11)
Summer	17 (7)	4 (9)	7 (7)	-6 (15)
Autumn	10 (4)	9 (19)	19 (15)	18 (41)

Figure 8.1. Boundaries of the box used in the calculation of fluxes through St. Andrews Bay.

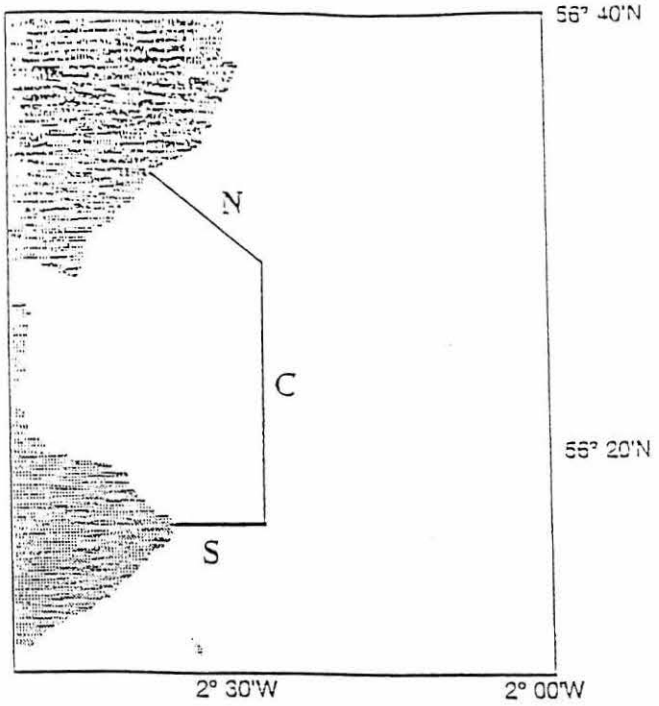

Figure 8.2. Flux box dimensions. **N**, **S** and **C** represent north, south and offshore faces respectively, with the suffix **T** and **B** representing upper and lower sections respectively. The positions of the RCMs on M1 and M5 relative to the face dimensions are indicated by circles.

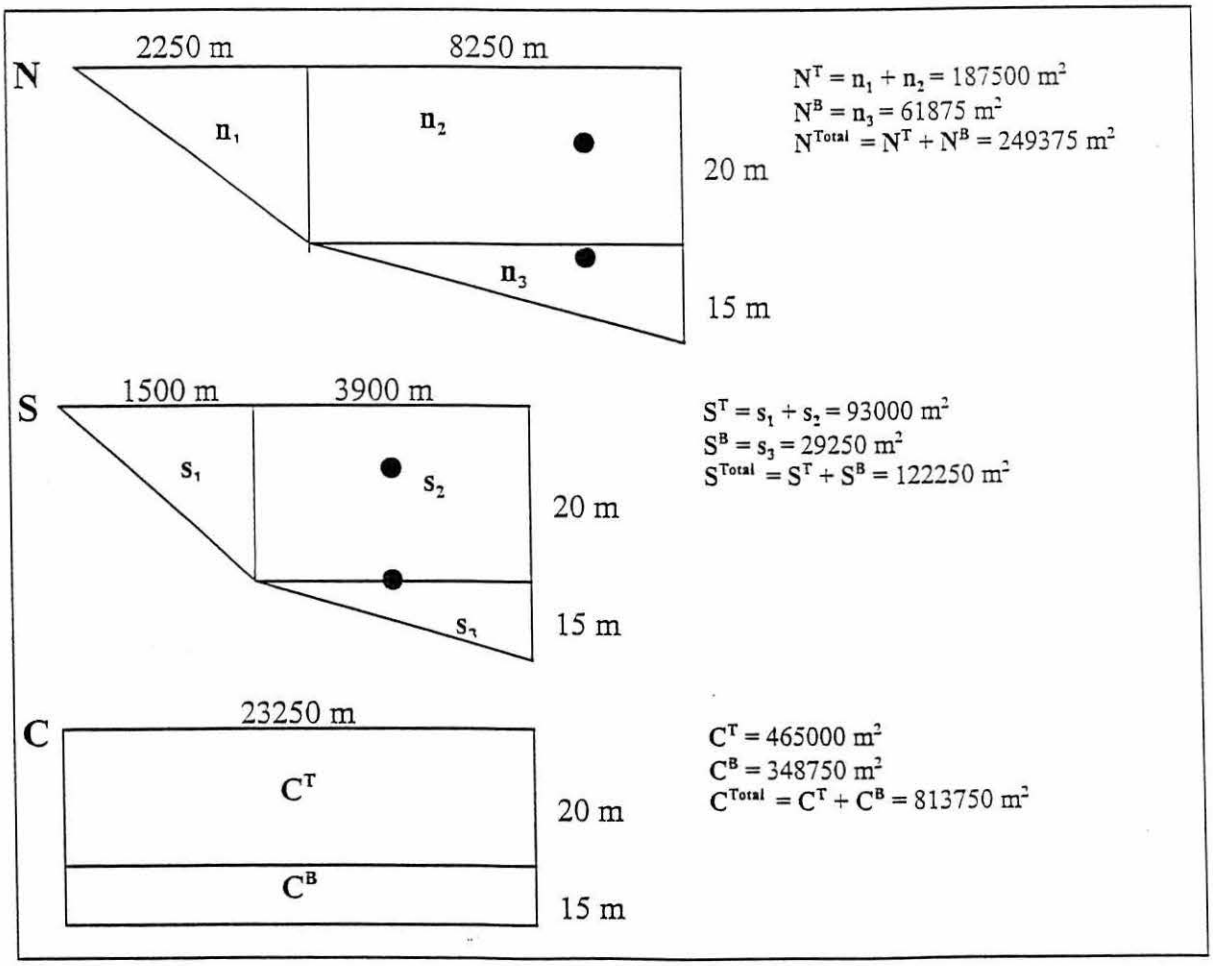

Chapter 9

9. Conclusions

9.1 Summary and Conclusions

Using a unique dataset collected over the course of a year with the aid of both moored and ship-mounted instrumentation the principal features of the hydrography and circulation of St. Andrews Bay, Scotland, have been determined. The transport of both fresh and seawater through the Bay area has been found to be complex, with circulatory patterns governed by the interaction of a range of factors. The most significant on a sub-tidal time scales have been found to be the action of cross-shore density gradients in forcing baroclinic flows and the action of the wind, both direct and indirect through the setting up of opposing longshore pressure gradients. The principal conclusions of the study are summarised below.

1. Variations in temperature and salinity over time scales of the order of days or weeks were dominated by the freshwater discharge from the Tay. Over longer, monthly or seasonal time scales, temperature and salinity respond to seasonal-scale variations in solar heating and runoff. Stratification during winter is restricted to the area of the estuarine plume. Over summer, insolation and runoff act together to stratify most of the Bay. The reduction in the incidence of strong winds during summer allows thermohaline stratification to become established within the Bay.

2. Even during periods of strong southerly wind freshwater typically left the Bay to the south. The role of the Coriolis acceleration was found to be significant in turning the plume southward towards Fifeness. Southerly winds were found to lead to a reduction in gradient of the isopycnals, resulting in a shallow plume and encouraging offshore spreading and flushing of the Bay. Winds directed toward the south resulted in steepening of the isopycnal lines and vertical homogeneity, resulting in the trapping of freshwater within the Bay. During summer the low winds were associated with decreased mean salinities within the Bay.

3. Variability in the low-pass filtered flows was typically barotropic and aligned with the coast at all depths with over 70% of variability at all mooring sites independent of depth. Exceptions to this were near the bed to the north of the Bay and beneath the plume, where cross-shore flow variability was particularly significant. Depth dependence in the circulation became more pronounced as the coast was approached with de-coupling of the plume and lower waters near the mouth of the Firth.

4. During winter the barotropic flow field was dominated by a single mode, with flows aligned with the coast at all locations across the Bay. During summer, however, the longshore barotropic mode split into opposing inner and outer modes. The single mode of winter and the inner mode of summer were found to be associated with an aligned longshore wind. It is suggested that the dominance of this mode during winter may be attributed to the increased strength and duration of the longshore wind over the winter months.

5. Application of a simple regression based wind-driven model of the longshore flow revealed the local longshore wind to account for a significant proportion of the current variance at all locations. The wind was particularly important at the shallower inner sites.

6. The local longshore wind was found to be the dominant factor in the generation of the longshore sea surface slope along the north-east coast. The longshore slope was found to be strongly correlated with the wind and to act so as to oppose it. The outer barotropic mode observed during the summer months could therefore be explained as being due to the action of such a slope. This was verified by calculation of the terms of the barotropic longshore momentum balance.

7. Variability in the sub-tidal circulation within the Bay region was found to be dominated by the interaction of the wind stress, bed stress and the longshore pressure gradient as set up by the wind. In inshore waters the action of the wind was dominant. In the deeper waters of the outer Bay the pressure gradient dominated.

8. The local acceleration was found to be insignificant compared to the other terms in the momentum equation. The Coriolis term was found to be of a significant size, but to be

uncorrelated with the other terms. This is thought to have been largely due to the poor resolution of the cross-shore flow.

9. Although a significant relationship was apparent between the three principal terms of the momentum equation, a global reduction in the pressure gradient to approximately one third of its calculated magnitude was required to reach a balance. It is unclear why such a reduction was necessary. Application of a conceptual model using measured wind data resulted in the calculation of a longshore slope of a magnitude in agreement with the required reduction. This suggests that the slope due to the direct effect of the local wind on the north-east coast may be that which is effective in driving the flow in the St. Andrews Bay area while the larger slope which is measured along the coast is enhanced by the non-local wind field over the North Sea

10. The sub-tidal baroclinic circulation of the Bay was complex and highly variable, both spatially and temporally. Near the bed an onshore flow was a consistent feature throughout the Bay. On both tidal and sub-tidal time scales a clockwise circulation appeared to be a common feature of the Bay, particularly during the dominant southerly winds.

11. Flow around the headland of Fifeness to the south was a consistent feature of the circulation of the Bay. Application of the thermal wind equation and the model of Heaps (1972) using time-series of measured cross-shore density gradients showed strong correlations with the measured vertical shear and agreement in amplitude, suggesting that the baroclinic flow around Fifeness is in approximate geostrophic balance and driven by the cross-shore density gradient which is typically vertically homogenous due to tidal mixing.

12. Comparisons between the long-term mean flow field and the residual of regressions between the longshore flow field, wind stress and pressure gradient suggest that long-term flow within the Bay is driven by density. This was confirmed by application of Heaps (1972) model.

13. Calculation of fluxes of freshwater using a "black box" approach resulted in significant potential offshore fluxes through the open boundary if a balance were to be achieved. It is suggested that fluxes were unlikely to be wholly offshore but to a large extent to

the south as a surface plume, the discrepancy being largely due to an inadequacy in the initial description of the box which did not specifically represent the plume. The plume is thought to be the dominant pathway for south-going transport of freshwater during the winter months. During summer transport to the south was achieved by pumping by geostrophic flows around Fifeness which required an onshore flux of water for mass balance to be achieved.

9.2 Discussion and Suggestions For Future Work

An initial description has been presented of the hydrography and circulation of the St. Andrews Bay region. The work described in this thesis is principally concerned with the determination of the principal components of the Eulerian flow field on sub-tidal time scales. The circulation of the Bay over tidal timescales has not been described. The work described is intended to form a first step towards the calculation of fluxes of nutrient through the Bay. Nutrient fluxes are not presented here but will be presented at a later date in the open literature.

The principal findings of the work programme are listed in Section 9.1 and need not be repeated here. This thesis should be regarded as presenting a first description of the circulation of a little studied and complex region. Very little work exists in the scientific literature concerning the sub-tidal circulation of estuarine plume zones on in shelf seas. A significant body of work has resulted from research carried out in the United States and is reviewed in Chapter 2. However, the estuaries described commonly empty into areas in which the shelf is relatively narrow. This results in an enhanced oceanic influence on the circulation of the plume zone as compared to that seen in British seas.

It is apparent from the results that the circulation of the St. Andrews Bay area is dominated by differing mechanisms on different timescales. At frequencies of approximately weekly the circulation is principally barotropic beyond the immediate influence of the estuarine plume. The barotropic flow is driven principally by the local wind field and the longshore pressure gradient. Limitations in the accuracy with which water levels can be measured by the instrumentation make detailed investigation of the local pressure gradient field difficult. Resolution of the questions raised regarding the difference between the measured and modelled longshore pressure gradient were therefore not possible in this work.

On longer timescales the circulation appears to be principally dominated by the local density gradients resulting from the retention of freshwater issuing from the Tay into the Bay. Freshwater retention and the behaviour of the plume itself is strongly regulated by the orientation of the windfield. During the winter months, when runoff rates are enhanced, the plume appears to become the principal vector by which freshwater is removed from the Bay. This is not the case during the low-runoff summer months.

In conclusion this thesis proposes a seasonally varying conceptual model of the circulation of St. Andrews Bay. The various modes of circulation described by the model being governed by the wind and freshwater inputs from the Tay, either directly or indirectly. There are a number of areas in which further research would add to the knowledge of this area arrived at through this work.

An analysis of the circulation of the Bay area over individual spring and neap tidal periods would be a useful corollary to the present study. Much work has been done in recent years on circulatory and mixing processes in Regions of Freshwater Influence (ROFIs) such as the plume of the River Rhine (Simpson *et al* 1993) showing the formation and breakdown of periodic stratification over tidal cycles to be important to vertical mixing processes. Application of the techniques and models developed in the course of such studies to the area of influence of the Tay plume may add considerably to the understanding gained in the course of this study. It would be possible to use the unique dataset collected during the current work to calibrate tidally-resolving models of mixing within the Bay.

Further work on the Tay plume itself would fill the gap in the description of the circulation of St. Andrews Bay which resulted from poor resolution of the upper layers of the water column. There are problems with measurement in the upper layers using conventional current meters due to aliasing by wave action. Attempts to resolve the surface flow by the installation of electromagnetic S4 current meters at M2 at a depth of 2m resulted in the loss of two instruments at considerable expense. It is unclear whether the instruments were stolen, lost due to collisions with boats or detached as the mooring wire wore through due to continuous wave action, however any future study must take into account all of these factors. In addition adequate resolution of a rapidly changing environment such as a large estuarine plume using moored instrumentation requires a

large array of instruments. More useful information about the plume dynamics and the eventual destination of plume water on rounding Fifeness may be achieved by the use of Lagrangian methods, such as drogues, which can be tailored to float at whatever depth is required for the study.

Resolution of the uncertainty attached to the actual value of the longshore pressure gradient generated by the longshore wind could be achieved by use of a two-dimensional numerical model on varying spatial scales. Modelling of the residual pressure field under a south-westerly wind across the entire SNSCZ would give pressure gradients along different stretches of coast corresponding to different wind speeds. The use of a fine-scale model on the Bay area would show any local reductions in gradient within the Bay while the use of a model on the scale of the entire North Sea (with an appropriate wind field) would reveal the influence of the large-scale wind field on sea-surface slopes along the Scottish coast. Such models should also adequately replicate the balance between wind and pressure gradient in the local area allowing confirmation of the seasonally varying conceptual model proposed in this thesis.

References

Admiralty Chart 190 (1978). *Hydrographer of the Navy. Montrose to Fifeness.*

Allen, J.S. and R.L. Smith (1981). On the dynamics of wind-driven shelf currents. *Phil. Trans. R. Soc. Lond. A* **302**:617-634.

Amin, M. (1988). Spatial variations of mean sea level of the North Sea off the east coast of Britain. *Cont. Shelf Res.* **8**(9):1087-1106.

Aure, J., E. Svendsen, F. Rey and H.R. Skjoldal (1990). The Jutland current: Nutrients and physical oceanographic conditions in late autumn 1989. *ICES Report: CM 1990, C35.*

Balls, P.W. (1992). Nutrient behaviour in two contrasting Scottish estuaries, the Forth and Tay. *Oceanologica Acta* **15**:261-277.

Beardsley, R.C. and J. Hart (1978). A simple theoretical model for the flow of an estuary onto a continental shelf. *J. Geophys. Res.* **83**:873-883.

Blanton, J.O. (1981). Ocean currents along a nearshore frontal zone on the continental shelf of the southeastern U.S.. *J. Phys. Oceanogr.* **11**:1627-1637.

Blanton, J.O. (1986). Coastal frontal zones as barriers to offshore fluxes of contaminants. *Rapp. P. -v. Reun. Cons. Int. Explor. Mer.* **186**:18-30.

Blanton, J.O. (1991). Circulation processes along oceanic margins in relation to materiel fluxes. In: 'Ocean Margin Processes in Global Change.' Eds. R.F.C. Mantoura, J. -M. Martin and R. Wollast. J.Wiley & Sons, pp. 145-163.

Blanton, J.O. and L.P. Atkinson (1983). Transport and fate of river discharge on the continental shelf of the southeastern United States. *J. Geophys. Res.* **88**:4730-4738.

Blanton, J.O., L-Y. Oyey, J. Amft and T.N. Lee (1989). Advection of momentum and buoyancy in a coastal frontal zone. *J. Phys. Oceanogr.* **19**:98-115.

Blanton, J.O., F. Werner, C. Kim, L. Atkinson, T. Lee and D. Savidge (1994). Transport and fate of low-density water in a coastal frontal zone. *Cont. Shelf Res.* **14**(4):401-427.

Böhnecke, G. (1922). Saltzgehalt und Strömungen der Nordsee. *Veröff. Inst. f. Meeresckunde, Univ. Berlin, N.F. A. 10.*

Bowden, K.F. (1950). Processes affecting the salinity of the Irish Sea. *Mon. Not. R. Astron. Soc., Geophys. Suppl.* **6**(2):63-90.

Bowden, K.F. (1983). 'Physical Oceanography of Coastal Waters.' Ellis Horwood, 302 pp.

Bowden, K.F., L.A. Fairbairn and P. Hughes (1959). The distribution of shearing stresses in a tidal current. *Geophys. J.*, **2**: 288-305.

Bowman, M.J. and R.L. Iverson (1977). Estuarine and plume fronts. In: 'Oceanic Fronts in Coastal Processes.' Eds. M.J. Bowman and W.E. Esaias. Springer-Verlag, pp. 87-104.

Broche, P. and P. Forget (1992). Has the influence of surface waves on wind stress to be accounted for in modelling the coastal circulation. *Est., Coast. and Shelf Sci.* **35**:347-351.

Bumpus, D.F. (1965). Residual drift along the bottom of the continental shelf in the Middle Atlantic Bight area. *Limnol. and Oceanogr., Suppl. to 10, R50-R53.*

Charlton, J.A. (1980). The tidal circulation and flushing capability of the outer Tay estuary. *Proc. R. Soc. Edin. (B)* **78**:533-546.

Charlton, J.A., W. McNicoll and J.R. West (1975). Tidal and freshwater induced circulation in the Tay estuary. *Proc. R. Soc. Edin. (B)* **75**:11-27.

Chase, R.R.P. (1979). The coastal longshore pressure gradient: Temporal variations and driving mechanisms. *J. Geophys. Res.* **84**(C8):4898-4904.

Cragg, J., W. Sturges and G. Mitchum (1983). Wind-induced surface slopes on the West Florida shelf. *J. Phys. Oceanogr.*, **13**: 2201-2212.

Craig, R.E. (1959). The hydrography of Scottish coastal waters. *Scottish Home Dept., Marine Res. 2, HMSO.*

Csanady, G.T. (1971). On the equilibrium shape of the thermocline in a shore zone. *J. Phys. Oceanogr.* **1**:263-270.

Csanady, G.T. (1975). Lateral momentum flux in boundary currents. *J. Phys. Oceanogr.* **5**:705-717.

Csanady, G.T. (1976). Mean circulation in shallow seas. *J. Geophys. Res.* **81**(30):5389-5399.

Csanady, G.T. (1978a). The arrested topographic wave. *J. Phys. Oceanogr.* **8**:47-62.

Csanady, G.T. (1978b). Wind effects on surface to bottom fronts. *J. Geophys. Res.* **83**:4633-4640.

Csanady, G.T. (1981). Shelf circulation cells. *Phil. Trans. R. Soc. Lond. A* **302**:515-530.

Csanady, G.T. (1982). 'Circulation in the Coastal Ocean.' Boston: D.Reidel Publ. Co., 279 pp.

Davies, A.M. (1980). Application of the Galerkin method to the formulation of a three-dimensional non-linear hydrodynamic numerical sea model. *App. Math. Modelling* **4**:245-256.

Davies, A.M. (1982). Meteorologically induced circulation on the north west European continental shelf: From a three-dimensional numerical model. *Oceanologica Acta* **5**:269-280.

Department of the Environment (DOE) (1987). Quality status of the North Sea. *Second International Conference on the Protection of the North Sea, London.*

Dickey, T.D. and J.C. van Leer (1984). Observations and simulation of a bottom Ekman layer on a continental shelf. *J. Geophys. Res.*, **89**:1983-1988.

Dooley, H.D. (1971). Some mechanisms for the generation of residual current flow off the Scottish east coast. *Dtch. Hydrogr. Z.* **24**:268-283.

Dooley, H.D. (1974a). Hypotheses concerning the circulation of the northern North Sea. *J. Cons. Int. Explor. Mer.* **36**:54-61.

Dooley, H.D. (1974b). A comparison of drogue and current meter measurements in shallow waters. *Rapp. P. -v. Reun. Cons. Int. Explor. Mer.* **167**:225-230.

Dooley, H.D. (1983). Seasonal variability in the position and strength of the Fair Isle current. In: 'North Sea Dynamics.' Eds. J. Sundermann and W. Lenz. Springer-Verlag, Berlin, pp. 108-119.

Dooley, H.D. and R. Payne (1978). Variability of currents and water properties in the outer Firth of Forth. *Dept. of Agriculture and Fisheries for Scotland internal report.*

Ekman, V.W. (1905). On the influence of the Earth's rotation on ocean currents. *Arkiv for Matematik, Astronomi och Fysik,* **2:11**, 52pp.

Fulton, T.W. (1897). The surface currents of the North Sea. *Scottish Geog. Mag. Vol. 13, no. 12.*

Garcia-Soto, C., I. de Madariaga, F. Villate and E. Orvie (1990). Day-to-day variability in the plankton community of a coastal shallow embayment in response to changes in river runoff and water turbulence. *Est. Coast. and Shelf Sci.* **31**:217-229.

Garvine, R.W. (1974). Physical features of the Conneticut River outflow during high discharge. *J. Geophys. Res.* **79**:831-846.

Garvine, R.W. (1986). The role of brackish plumes in open shelf waters. In: 'The Role of Freshwater Outflow in Coastal Marine Ecosystems.' NATO ASI Series, G7. Ed. S. Skreslet. Springer-Verlag, pp. 47-66.

Garvine, R.W. and J.D. Monk (1974). Frontal structure of a river plume. *J. Geophys. Res.* **79**:2251-2259.

Gmitrowicz, E.M. and J. Brown (1993). The variability and forcing of currents within a frontal region off the northeast coast of England. *Cont. Shelf Res.* **13**:863-890.

Godin, G. (1967). The analysis of current observations. *International Hydrographic review,* **44**: 149.

Grant, W.D. and O.S. Madsen (1979). Combined wave and current interaction with a rough bottom. *J. Geophys. Res.* **84**:1797-1808.

Heaps, N.S. (1967). Storm surges. *Oceanogr. Mar. Biol. Ann. Rev.* **5**:11-47.

Heaps, N.S. (1969). A two dimensional numerical model. *Phil. Trans. R. Soc. Lond.* A **1160**:93-137.

Heaps, N.S. (1972). estimation of density currents in the Liverpool Bay area of the Irish Sea. *Geophys. J. R. astr. Soc.*,**80**: 415-432.

Heaps, N.S. (1978). Linearised, vertically integrated equations for residual circulation in coastal seas. *Deutche Hydrographische Zeitschrift*, **31**: 147-169.

Heaps, N.S. (1980). Density currents in a two layered coastal system with application to the Norwegian coastal current. *Geophys. J. Roy. Astro. Soc.* **63**:289-310.

Heaps, N.S. and J.E. Jones (1987). Vertical profiles of wind-induced current. *Institute of Oceanographic Sciences report* **238**, 51pp.

Heathershaw, A.D. (1982). Some observations of currents in shallow water during a storm surge. *Est., Coast. and Shelf Sci.* **14**:635-648.

Hickey, B.M. and P. Hamilton (1980). A spin-up model as a diagnostic tool for interpretation of current and density measurement on the continental shelf of the Pacific north west. *J. Phys. Oceanogr.* **10**:1.

Hill, A.E. and J.H. Simpson (1988). Low-frequency variability of the Scottish coastal current induced by along-shore pressure gradients. *Est., Coast. and Shelf Sci.* **27**:163-180.

Hill, A.E. and J.H. Simpson (1989). On the interaction of thermal and haline fronts: the Islay front revisited. *Est., Coast. and Shelf Sci.* **28**:495-505.

Howarth, M.J. (1990). 'Atlas of tidal elevations and currents around the British Isles.' Department of Energy, Offshore Technology Report, OTH 89 293, 16pp.

Huthnance, J.M. (1983). Sub-tidal motion on the Scottish continental shelf, August-September 1971. *Cont. Shelf Res.* **1** (3):221-236.

Huyer, A., R.L. Smith and E.J.C. Sobey (1978). Seasonal differences in low-frequency current fluctuations over the Oregon continental shelf. *J. Geophys. res.*, **83**: 5077-5089.

Jollife, I.T. (1990). Principal component analysis: A beginners guide 1. Introduction and application. *Weather*, **45**, 375-382.

Jollife, I.T. (1993). Principal component analysis: A beginners guide 2. Pitfalls, myths and extensions. *Weather*, **48**, 246-253.

Kundu, P.K., J.S. Allen and R.L. Smith (1975). Modal decomposition of the velocity field near the Oregon coast. *J. Phys. Oceanogr.* **5**:683-704.

Laevastu, T. (1963). Surface water types of the North Sea and their characteristics. *Serial Atlas of the Marine Environment. Folio 4. Amer. Geogr. Soc., N.Y.*.

Large, W.G. and S. Pond (1981). Open ocean momentum flux measurements in moderate to strong winds. *J. Phys. Oceanogr.* **11**:324-336.

Lee, A. (1970). The currents and water masses of the North Sea. *Oceanogr. Mar. Biol. Ann. Rev.* 8:33-71.

Lee, A.J. (1980). North Sea: Physical Oceanography. In: 'The North-West European Shelf Seas: The Sea Bed and the Sea in Motion II. Physical and Chemical Oceanography and Physical Resources.' Eds. F.T. Banner, M.B. Collins and K.S. Massie. Elsevier, pp. 467-493.

Lentz S.J., and C.D. Winant (1986). Subinertial currents on the southern California shelf. *J. Phys. Oceanogr.*,**16**: 1737-1750.

Lewis, R.E. (1984). Circulation and mixing in estuary outflows. *Cont. Shelf. Res.*, **3**: 201-214.

Lyons, M.G., P.W. Balls and W.R. Turrell (1993). A preliminary study of the relative importance of riverine nutrient inputs to the Scottish North Sea Coastal Zone. *Mar. Poll. Bull.* **26**:620-628.

Marmorino, G.O. (1982). Wind-forced sea level variability along the West Florida Shelf (Winter, 1978). *J. Phys. Oceanogr.* **12**:389-405.

Marmorino, G.O. (1983). Small-scale variations of the wind-driven coastal sea-level response in the West Florida Bight. *J. Phys. Oceanogr.* **13**:93-102.

Mooers, C.N.K., C.N. Flagg and W.C. Boicourt (1977). Prograde and retrograde fronts. In: 'Oceanic Fronts in Coastal Processes.' Eds. M.J. Bowman and W.E. Esaias. Springer-Verlag, pp. 43-57.

Münchow, A. and R.W. Garvine (1993a). Buoyancy and wind forcing of a coastal current. *J. Mar. Res.* **51**:293-322.

Münchow, A. and R.W. Garvine (1993b). Dynamical properties of a buoyancy-driven coastal current. *J. Geophys. Res.* **98**(C11):20063-20077.

Murray, S.P. (1975). Trajectories and speeds of wind-driven currents near the coast. *J. Phys. Oceanogr.* **5**:347-360.

Noble, M., B. Butman and E. Williams (1983). On the longshelf structure and dynamics of sub-tidal currents on the eastern United states continental shelf. *J. Phys. Oceanogr.*,**13**: 2125-2147.

Norcross, J.J. and E.M. Stanley (1967). Inferred surface and bottom drift, June 1963 through October 1965, circulation of shelf waters off the Chesapeake Bight. *Prof. Papers Environ. Sci. Serv. Admin., U.S. Govt.*, 3(2):11-42.

Officer, C.B. (1976). 'Physical Oceanography of Estuaries.' Wiley & Sons, 465 pp..

Pape, E.H. and R.W. Garvine (1982). The subtidal circulation in Delaware Bay and adjacent shelf waters. *J. Geophys. Res.* **87**:7955-7970.

Pettigrew, N.R. (1980). The dynamics and kinematics of the coastal boundary layer off Long Island. PhD thesis, MIT/Woods Hole Oceanographic Institution, 262pp.

Pingree, R.D. and D.K. Griffiths (1978). Tidal fronts on the shelf seas around the British Isles. *J. Geophys. Res.* **83**:4615-4621.

Pingree, R.D. and D.K. Griffiths (1980). Currents driven by a steady uniform wind stress on the shelf seas around the British Isles. *Oceanologica Acta* 3(2):227-236.

Pingree, R.D. and L. Maddock (1977). Tidal eddies and coastal discharge. *J. Mar. Biol. Assn, U.K.* **57**:869-875.

Pingree, R.D., M.J. Bowman and W.E. Esaias (1977). Headland fronts. In: 'Oceanic Fronts in Coastal Processes.' Eds. M.J. Bowman and W.E. Esaias. Springer-Verlag, pp. 78-86.

Prandle, D. (1987). The fine-structure of nearshore tidal and residual circulations revealed by H.F. Radar surface current measurements. *J. Phys. Oceanogr.* **17**: 231-245.

Presendorfer, R.W. (1988). 'Principal component analysis in meteorology and oceanography.' Elsevier, Amsterdam, 425pp.

Proudman, J. and A.T. Doodson (1924). The principal constituents of the tides of the North Sea. *Phil. Trans. Roy. Soc. (A)* **224**:185-219.

Pugh, D.T. (1987). 'Tides, Surges and Mean Sea-Level.' John Wiley and Sons.

Royer, T.C. (1979). On the effect of precipitation and runoff on coastal circulation in the Gulf of Alaska. *J. Phys. Oceanogr.* **9**:555-567.

Schubel, R.J. and D.W. Pritchard (1986). Responses of Upper Chesapeake Bay to variations in discharge of the Susquehanna River. *Estuaries* 9:45-64.

Sciremmano, F. (1979). A suggestion for the presentation of correlations and their significance levels. *J. Phys. Oceanogr.*, **9**: 1273-1276.

Scott, J.T. and G.T. Csanady (1976). Nearshore currents off Long Island. *J. Geophys. Res.* **81**(30):5401-5409.

Shaw, P-T. (1992). Shelf circulation off the Southeast coast of China. *Rev. Aquat. Sci.* **6**:1-28.

Simpson, J.H. and J.R. Hunter (1974). Fronts in the Irish Sea. *Nature* **250**:404-406.

Simpson, J.H. and R.D. Pingree (1977). Shallow sea fronts produced by tidal stirring. In: 'Oceanic Fronts in Coastal Processes.' Eds. M.J. Bowman and W.E. Esaias. Springer-Verlag, pp. 29-42.

Simpson, J.H. and A.E. Hill (1986). The Scottish coastal current. In: 'The Role of Freshwater Outflow in Coastal Marine Ecosystems.' NATO ASI Series, G7. Ed. S. Skreslet. Springer-Verlag, pp. 295-309.

Simpson, J.H., J. Brown, J. Matthews and G. Allen (1990). Tidal straining, density currents and stirring in the control of estuarine stratification. *Estuaries* **13**:125-132.

Simpson, J.H., J. Sharples and T.P. Rippeth (1991). A prescriptive model of stratification induced by freshwater runoff. *Est. Coast. and Shelf Sci.* **33**:23-35.

Simpson, J.H., W.G. Bos, F. Schirmer, A.J. Souza, T.P. Rippeth, S.E. Jones and D. Hydes (1993). Periodic stratification in the Rhine ROFI in the North Sea. *Oceanologica Acta.* **16**: 23-32.

Skreslet, S. (1986). Freshwater outflow in relation to space and time dimensions of complex ecological interactions in coastal waters. In: 'The Role of Freshwater Outflow in Coastal Marine Ecosystems.' NATO ASI Series, G7. Ed. S Skreslet. Springer-Verlag, pp. 3-13.

Tait J.B. (1930a). Fishery board for Scotland. Scientific Investigations 1930 No. 2. HMSO.

Tait J.B. (1930b). Fishery board for Scotland. Scientific Investigations 1930 No. 4. HMSO.

Tait J.B. (1931). Fishery board for Scotland. Scientific Investigations 1931 No. 3. HMSO.

Tait J.B. (1937). Fishery board for Scotland. Scientific Investigations 1937 No. 1. HMSO.

Thompson, K.R. and D.T. Pugh (1986). The subtidal behaviour of the Celtic Sea-II. Currents. *Cont. Shelf Res.* **5**(3):321-346.

Turrell, W.R. (1992). New hypotheses concerning the circulation of the northern North Sea and its relation to North Sea fish stock recruitment. *ICES J. Mar. Sci.* **49**:107-123.

Turrell, W.R. and E.W. Henderson (1990). Transport events within the Fair Isle current during the Autumn Circulation Experiment (ACE). *Est., Coast. and Shelf Sci.* **31**:25-44.

Turrell, W.R. and G. Slesser (1992). Annual cycles of physical, chemical and biological parameters in Scottish waters. *Scottish Fisheries Working Paper No. 5/92. SOAFD.*

Turrell, W.R., E.W. Henderson and G. Slesser (1990). Residual transport within the Fair Isle current observed during the Autumn Circulation Experiment (ACE). *Cont. Shelf Res.* **10**:521-543.

Uncles, R.J. and M.B. Jordan (1979). Residual fluxes of water and salt at two stations in the Severn Estuary. *Est. and Coast. Mar. Sci.* **9**:287-303.

Uncles, R.J., R.C.A. Elliot and S.A. Weston (1985). Observed fluxes of water, salt and suspended sediment in a partly mixed estuary. *Est., Coast. and Shelf Sci.*, **20**: 147-167.

Wang, D.-P. (1979). Low frequency sea level variability in the Middle Atlantic Bight. *J. Mar. Res.*, **37**: 683-697.

Weatherly, G.L., S.L. Blumsack and A. Bird (1980). On the effect of diurnal tidal currents in determining the thickness of the turbulent Ekman bottom boundary layer. *J. Phys. Oceanogr.*, **10**: 297-300.

Winant, C.D. and R.C. Beardsley (1979). A comparison of shallow currents induced by wind stress. *J. Phys. Oceanogr.*,**9**: 218-220.

Woods, A.W. and R.C. Beardsley (1988). On the barotropic discharge of a homgeneous fluid onto the continental shelf. *Cont. Shelf Res.*, **8**: 307-327.

Appendix

Calculation of density driven currents

Consider the steady state motion of a fluid particle adjacent to an infinitely long coastline and in the vicinity of one or more riverine discharges, the depth integrated equations of continuity and motion are given (Heaps 1972) by

$$\int_{-\zeta}^{h} U dz = -q \qquad \text{A1}$$

$$Nz\frac{\partial^2 U}{\partial z^2} = -fV + g(z+\zeta)\frac{1}{\rho}\frac{\partial \rho}{\partial x} + g\frac{\partial \zeta}{\partial x} \qquad \text{A2}$$

$$Nz\frac{\partial^2 V}{\partial z^2} = -fU \qquad \text{A3}$$

where U and V are depth-dependant density currents flowing in a left handed system of cartesian coordinates with z positive downwards. It should be noted that this is not the coordinate system that has been applied to observational data throughout the thesis, it is therefore neccesary to apply a simple coordinate transformation to the final model results in order to put them in the system used previously for resolution of the observational data. If u and v represent the density currents in the desired frame of reference (as used previously), then $u = V$ and $v = -U$.

Nz is a depth mean eddy viscocity, f the Coriolis parameter, g the acceleration due to gravity, ρ the water density, h the depth of the undisturbed water column and ζ the displacement of the sea surface from its undisturbed level (taken to be samll compared to h). q is a constant that denotes the rate of seaward discharge of water per unit length of coastline, representing the riverine input.

Introduction of the complex variable

$$W_D = U + iV \qquad \text{A4}$$

and combining A2 and A3 gives

$$\frac{\partial^2 W_D}{\partial z^2} = \alpha^2 W_D + \frac{g}{Nz}\left[(z+\zeta)\frac{1}{\rho}\frac{\partial \rho}{\partial x} + \frac{\partial \zeta}{\partial x}\right] \qquad \text{A5}$$

$$\text{where } \alpha = (1+i)\pi / D \qquad \text{A6}$$

$$\text{and } D = \pi(2Nz/f)^{1/2} \qquad \text{A7}$$

the latter being the depth of frictional influence.

Assuming zero tangential stress at the surface and a linear bottom friction law gives a general solution to A5 of the form

$$W_D = Ae^{\alpha(z+\zeta)} + Be^{-\alpha(z+\zeta)} + \frac{ig}{f}\left[(z+\zeta)\frac{1}{\rho}\frac{\partial \rho}{\partial x} + \frac{\partial \zeta}{\partial x}\right] \qquad \text{A8}$$

where A and B denote arbitrary constants. A and B may be determined (Heaps 1972) from the boundary conditions and $\frac{\partial \zeta}{\partial x}$ eliminated from the solutions for U and V in terms of the discharge parameter q. Thus from A8

$$U = \frac{gH}{f}(XQ - YP)\left(\frac{1}{\rho}\frac{\partial \rho}{\partial x}\right) + \left(\frac{fq}{k}\right)(MP - LQ)/S \qquad \text{A9}$$

$$V = \frac{gH}{f}(XP + YQ + \Lambda + \eta)\left(\frac{1}{\rho}\frac{\partial \rho}{\partial x}\right) + \left(\frac{fq}{k}\right)(1 - LP - MQ)/S \qquad \text{A10}$$

where k is a linear friction coefficient. The terms in A9 and A10 are defined as follows:

h total depth of water column

z depth

$H = h + \zeta$ (ζ assumed small compared to h)

$Z = z + \zeta$ (ζ assumed small compared to h)

$$\eta = \frac{Z}{H}$$

$$a = \frac{\pi H}{D} \qquad a_1 = a(1-\eta) \qquad a_2 = a\eta$$

$$b = \frac{kH}{Nz}$$

$$\sinh a = \tfrac{1}{2}\left(e^{a} - e^{-a}\right) \qquad \cosh a = \tfrac{1}{2}\left(e^{a} + e^{-a}\right)$$

$$C = a(\sinh a \cos a - \cosh a \sin a) + b\cosh a \cos a$$

$$E = a(\sinh a \cos a + \cosh a \sin a) + b\sinh a \sin a$$

$$L = b\cosh a_2 \cos a_2$$

$$M = b\sinh a_2 \sin a_2$$

$$P = \frac{C}{(C^2 + E^2)} \qquad Q = \frac{E}{(C^2 + E^2)}$$

$$R = P\cosh a \cos a + Q\sinh a \sin a$$

$$S = 1 - Rb$$

$$\Lambda = (R - P - S)/S \qquad \lambda = 1 + b + b\Lambda$$

$$X = \cosh a_1 \cos a_1 + \left(\frac{b}{2a}\right)(\sinh a_1 \cos a_1 + \cosh a_1 \sin a_1) - \lambda \cosh a_2 \cos a_2$$

$$Y = \sinh a_1 \sin a_1 + \left(\frac{b}{2a}\right)(\cosh a_1 \sin a_1 - \sinh a_1 \cos a_1) - \lambda \sinh a_2 \sin a_2$$

Given an appropriate parameterisation of the eddy viscosity Nz the above sequence of equations may be used to evaluate the density current components U and V for different depths z provided that the terms $\frac{1}{\rho}\frac{\partial \rho}{\partial x}$ and $\frac{fq}{k}$ are known. The model was coded into an Excel spreadsheet for use. Values used in the calculations are discussed in the main text.